AUGMENTED HYDROSTATIC EXTRUSION

by

SINNATHAMBY THIRUVARUDCHELVAN B.Sc.(Eng.)

A Thesis submitted for the degree of

Doctor of Philosophy in the University of London

and

The Diploma of Imperial College

JULY 1970

SUMMARY

Billet augmented hydrostatic extrusion process for some metals has been investigated in detail. Hydrodynamic lubrication in the general hydrostatic extrusion process is studied theoretically. A double reduction die has been designed to achieve back tension (or negative billet augmentation) and tested for possible advantages regarding lubrication, reduction in frictional work, and the possibility of extruding brittle materials successfully.

Copper and mild steel billets were extruded by simple hydrostatic extrusion and billet augmented extrusion. The effect of the magnitude of the augmenting stress on friction and lubrication of the die was estimated. The limits of billet augmentation by excessive deformation of the billet, by plastic buckling and by excessive die stresses were analysed.

Hydrodynamic lubrication in the general hydrostatic extrusion process was investigated and the conditions for its existence derived. The fluid pressure, billet augmenting stress and product augmenting stress relationships under these conditions were predicted. A numerical method was formulated for using the computer to analyse the hydrodynamic lubrication process accounting for the 'sinking in' of billets of work hardening materials in hydrostatic extrusion.

A double reduction die designed for promoting hydrodynamic lubrication in hydrostatic extrusion was used for extruding aluminium, copper and a brittle aluminium alloy with different reductions and compared with the pressures necessary for these reductions using a conventional hydrostatic extrusion die. Different fluids were also

used in these tests to assess their role in lubrication. The limitations of the die as regards to leakage and tensile instability of the billet were investigated.

CONTENTS

1. INTRODUCTION

Various aspects of the hydrostatic extrusion process have been investigated in research laboratories all over the world. The aim of these investigations has been to develop hydrostatic extrusion as a viable production process for the cold forming of metals to various shapes. Since the fluid pressure introduces a state of hydrostatic stress in the billet, the simple hydrostatic extrusion process does not take advantage of the strength of the billet or the product, unlike drawing or open die extrusion. Thus there is no limit to the extrusion ratio or to the shape of the billet because of the hydrostatic state of stress in the billet in simple hydrostatic extrusion.

Although simple hydrostatic extrusion has several advantages over conventional cold extrusion [1]* it also has certain inherent disadvantages. In hydrostatic extrusion the container-billet friction found in direct conventional extrusion is eliminated and the presence of high pressure fluid aids in the lubrication of the die-metal interface. However the initial peak in pressure and the subsequent acceleration of the billet to high velocities in simple hydrostatic extrusion makes it difficult to control the process. Also the stick-slip phenomenon found in simple hydrostatic extrusion at low speeds, caused by the compressibility of the fluid etc., is not desirable in a production process.

There are several well established ways [1] of overcoming these undesirable features.

---

* Numbers in the brackets refer to a list of references given on page 98

Product and billet augmented hydrostatic extrusion are two variants of the basic process considered for the extrusion of rods, sections and tubes. In product or billet augmentation where a mechanical force is applied to the product or to the billet to aid the fluid pressure, the velocity instabilities mentioned above are minimized or eliminated and closer control of the process is obtained. These methods also reduce the magnitude of the fluid pressure necessary for extrusion. But there are limits to the magnitude of the augmenting load or stress and thus to the saving in fluid pressure achievable. Some of these limits are derived and determined experimentally while others are discussed, in this thesis.

The application of augmenting stress alters the state of lubrication of the die and the coefficient of friction is expected to change with different augmenting condition. The coefficients of friction in billet augmented extrusion tests are estimated under certain assumptions.

There is a strong possibility of hydrodynamic lubrication in hydrostatic extrusion, associated with large velocities, high pressures and high viscosities, giving low coefficients of friction. A theory of hydrodynamic lubrication for the generalized hydrostatic extrusion process is presented.

A method of promoting hydrodynamic lubrication at low speeds, especially for hard materials and in billet augmentation, is studied using a double reduction die. The principle underlying this die is the introduction of fluid pressure between two reductions so that for all purposes in plastic deformation the intermediate product is in a state of tension. Thus the first reduction is in effect drawing, under all round hydrostatic pressure and the second reduction (the major) is hydrostatic extrusion with back tension.

2. NOTATION

Symbols used in this thesis, unless otherwise defined or redefined in the text, are as follows:

A, A_o	Area of cross section of the bulged billet and the original billet respectively.
a, b	Constants in the expression for extrusion pressure $p_o = a + b \ln R$.
B_1, B, B_2	$e^{-\gamma p_1}$, $e^{-\gamma p}$, $e^{-\gamma p_2}$ respectively in section 4.6.
D_1, D, D_2	Diameter of the billet, deforming zone and the product respectively.
E, Er, Et	Young's modulus, reduced modulus and Tangent modulus respectively of the material extruded.
F_A	Augmenting load.
$f(\alpha)$	$= \frac{1}{\sin^2\alpha}\{1-\cos\alpha\sqrt{1-\frac{11}{12}\sin^2\alpha} + \sqrt{\frac{1}{11.12}} \ln \frac{1+\sqrt{\frac{11}{12}}}{\sqrt{\frac{11}{12}}\cos\alpha + \sqrt{1-\frac{11}{12}\sin^2\alpha}}\}$
G	$\gamma.\sigma$
H	A constant in $\sigma = \sigma_o + (H - \sigma_o)(1 - e^{-n\epsilon})$
h_1, h, h_2, h_3	are the film thicknesses at the inlet of the die, in the deforming zone, at the die throat and at the exit to the die land respectively.
I	Second moment of area of cross-section of the billet.
K	$= D2(1 - \nu)/2E$.
k	Yield shear stress.
l	Length of strut (billet).
L	Length of die land.
n	Index defined in equation $\sigma = \sigma_o + (H - \sigma_o)(1 - e^{-n\epsilon})$

p_1, p, p_2, p_3 Fluid pressure at the inlet to the die, in the deforming zone, at the die throat and the back pressure respectively.

p_A Fluid pressure in augmented extrusion.

P_{CR} Critical buckling load.

p_H, p_R, p_{FD} Components of extrusion pressure due to homogeneous deformation, redundant deformation and friction respectively.

p_o, p_o^* Extrusion pressure in simple hydrostatic extrusion and that for hardened material through extrusion ratio R respectively.

q, q_o Die pressure at any point on the die-metal surface and the mean die pressure respectively.

Q, Q' Lubricant flow rates defined in section 4.6.

r_i, r, r_f The initial, instantaneous and the final radius respectively in the spherical co-ordinate system (r, θ, φ) except in section 4.52.

r Least radius of gyration of cross-section (of the billet = D/4) in section 4.52.

R Extrusion ratio except in section 4.3.

R_1, R_2 Extrusion ratios at the first and second reductions in the double reduction die.

R_i, R, R_f Radius at the die entrance, instantaneous radius and radius at the exit respectively, in section 4.3.

R_o Extrusion ratio of the undeformed billet through die.

S_{CR} Critical stress for buckling.

U_1, U, U_2 Billet, deformation zone and product velocities respectively.

u_r, u_θ, u_φ Velocities of the deforming material in r, θ, φ directions respectively, in section 4.3.

u, w Velocity of the deforming material perpendicular and parallel to the axis respectively.

V Volume of deforming zone.

x_1, x, x_2 Distances along the die from the apex of the die cone of the inlet, instantaneous and the exit respectively in section 4.6.

Z Distance along the axis, defined in section 4.6.

α Die semi-angle.

α_o Optimum die semi-angle.

ε_1, ε_2, ε_3 Redundant strain at entry, strain of homogeneous deformation and redundant strain at exit respectively.

ε Effective strain of bulged billet, except in section 4.6 and effective strain in $\sigma = \sigma_o + (H - \sigma_o)(1 - \varepsilon^{-n\varepsilon})$ in section 4.6.

$\dot{\varepsilon}_r$, $\dot{\varepsilon}_\theta$, $\dot{\varepsilon}_z$ Strain rates in r, θ and z directions in the deformation zone, in section 4.1.

$\dot{\varepsilon}_{rr}$, $\dot{\varepsilon}_{\theta\theta}$, $\dot{\varepsilon}_{\varphi\varphi}$ Strain rates in r, θ and φ directions in the deformation zone, in section 4.3.

$\dot{\varepsilon}_{r\theta}$, $\dot{\varepsilon}_{\theta\varphi}$, $\dot{\varepsilon}_{\varphi r}$ Shear strain rates in (r, θ), (θ, φ), (φ, r) planes in the deformation zone, in section 4.3.

$\dot{\varepsilon}_{rz}$ Strain rate in the (r, z) plane in the deformation zone in section 4.1.

$\dot{\bar{\varepsilon}}$ Effective strain rate (section 4.3 and 4.1), where (1, 2, 3) are replaced by the respective co-ordinate system,

$$= \sqrt{\frac{2}{3}[\dot{\varepsilon}_{11}^{\,2} + \dot{\varepsilon}_{22}^{\,2} + \dot{\varepsilon}_{33}^{\,2} + 2(\dot{\varepsilon}_{12}^{\,2} + \dot{\varepsilon}_{23}^{\,2} + \dot{\varepsilon}_{31}^{\,2})]}$$

where $\dot{\varepsilon}_{12}$, $\dot{\varepsilon}_{23}$ and $\dot{\varepsilon}_{31}$ are tensor shear strain rates.

η_o, η — Viscosity of fluid at atomosheric and at pressure p respectively.

γ — Pressure coefficient of viscosity of the fluid.

$\dot{\lambda}$ — Parameter in the Levy-Mises equations, in section 4.1.

ν — Poisson's ratio of the material extruded.

μ — Coefficient of friction in augmented extrusion.

μ_o — Coefficient of friction associated with optimum die angle in simple hydrostatic extrusion.

σ, $\overline{\sigma}$ — Yield stress of a material.

σ_o — Constant in the equation $\sigma = \sigma_o + (H - \sigma_o)(1 - e^{-n\varepsilon})$, for a work-hardening material.

σ_A — Billet augmenting stress.

σ_m — $= (\sigma_r + \sigma_\theta + \sigma_z)/3$ Hydrostatic component of stress (mean stress), in section 4.1.

$(\sigma_m)_A$ — Mean yield stress for extrusion of the bulged billet through ratio R.

$(\sigma_m)_\varepsilon$ — Mean yield stress at strain ε.

$(\sigma_m)_{\ln R}$ — Mean yield stress for extrusion at a ratio R.

$(\sigma_m)_{\ln R_o + 2\varepsilon}$ — Mean yield stress for the bulged and extruded billet.

σ_p — Product augmenting stress.

σ_r, σ_θ, σ_φ — Stresses in the r, θ and z directions in the deformation zone in section 4.1.

σ_{xb}, σ_{xf} — Back pull stress and drawing or front pull stress respectively in section 4.3.

τ_{rz} — Shear stress in the (r, z) plane of the deformation zone in section 4.1.

ω — Constant of proportionality in proportional billet augmentation, given by $F_A = \omega \cdot p_A \cdot A_o$

3. SURVEY OF LITERATURE

3.1 Simple hydrostatic extrusion

Much attention has been paid in recent years to various aspects of the hydrostatic extrusion process. Substantial experimental results are available for the hydrostatic extrusion of rods, tubes and various sections of a variety of materials including those which are impossible to extrude by the conventional method. The Bulleid Memorial Lectures Volume IIIB (1965) by Pugh [1] record most of the work done up to that time. Some of the important parameters like the extrusion pressure, die angle, extrusion ratio are related by the well known empirical relationships of the form, '$p = a + b \ln R$'. Some phenomena like 'stick-slip', initial pressure peaking and subsequent speed instability [2] etc. have also been investigated and qualitative explanations put forward. Several ways of minimising these undesirable features are available in various experimental equipments [1]. Though some experimental data are available on the effect of different fluids, the role played by the pressure transmitting fluid in the lubrication of the die is not well understood. Dies with conical, spherical and raduised entry shapes have all been used in hydrostatic extrusion [4]. Warm hydrostatic extrusion experiments with certain metals are described in reference [37]. Some workers have been concentrating on die design and the analysis of die stresses [3, 5, 6]. Extensive investigations are going on into various aspects of pressure vessel design for pressures up to 200 T/in^2 [7, 8, 9, 10, 11]. With present-day materials, to achieve these pressures on a commercially feasible basis needs ingenious designs and extensive testing. High pressure

equipment such as intensifiers, valves, pipes, seals, etc. and instrumentation are also being developed by research workers in this field. Prototypes of integrated hydrostatic extrusion presses are also being developed [7, 12]. Another feature of the hydrostatic extrusion process is the possibility of the semi-continuous or intermittent extrusion of long bars. Several versions of this process have been designed and feasibility studies are going on [13, 14, 15, 16]. Properties of hydrostatically extruded products are being investigated at several places, with regard to the U.T.S., yield strength, fatigue strength, hardness variation, surface finish etc. [17, 18, 19, 20]. Very recently, a means of achieving continuous hydrostatic extrusion has been described [74], and a novel process combining hydrostatic extrusion and machining known as 'Hydrospin' is being developed [75].

3.11 Billet augmented hydrostatic extrusion

This process has been developed for the control of hydrostatic extrusion to minimize stick-slip and to prevent the dangerous release of large energy at the completion of extrusion, which often occurs with simple hydrostatic extrusion [1]. However, there are ways of preventing this release of large energy even in simple hydrostatic extrusion, for example by the method of pressure phasing [43] and by fitting a cap to the end of the billet [1]. Moreover in augmented extrusion, the strength of the billet is made use of to reduce the fluid pressure required for extrusion. Proportional billet augmented extrusion in which the augmenting load is proportional to the fluid pressure was first mentioned by Green and Salter [44] and Fig (1) shows the set-up used by them. In this

assembly the upper vessel has a slightly larger bore than that of the lower vessel. The differential punch slides freely in both vessels. In operation, the upper vessel is pushed towards the lower one thus pressuring the fluid in both the vessels which are interconnected by the small drilled hole through the punch. The pressure is therefore the same at each end of the punch and this results in an out-of-balance force which pushes the punch against the back end of the billet. This out-of-balance force augments the fluid pressure already applied to the billet. One important feature is that the fluid is displaced to the upper vessel as extrusion proceeds. At the end of extrusion, practically all the fluid is displaced to a position remote from the die and separated from it by a choke hole thus minimizing any dangerous release of fluid at the end of extrusion. Fig. (2) shows a variation of the above process of augmented extrusion principle applied to long bars.

Thompson analysed the billet augmented extrusion process [45] using the empirical relationship, $p = a + b \ln R$ for simple hydrostatic extrusion. He thus derived a relationship for an approximate bulging limit or instability in billet augmentation. Most of his experiments in bar extrusion [43] were with proportional billet augmentation. The total extrusion pressure was calculated from the fluid pressure presumably using the proportionality based on the areas of the differential punch. He also estimated [43] the fluid pressure-augmenting stress relations based on his mean induced strain theory. This theory, like that of Pugh is based on experimental findings and has little theoretical basis. Thompson in his paper [45] has also shown some forms of augmenting which would be possible with bar and tube extrusions and these are reproduced here in Fig. (3).

Some results of his experiments on the augmented extrusion of tubes were also given in the paper.

3.12 Product augmented hydrostatic extrusion

Product augmenting is relatively easily achieved with hydrostatic extrusion equipment by incorporating a draw bench. This process has been given different names such as 'hydrostatic drawing' etc. by some investigators [40, 46,47, 48]. Among these investigations that of Parsons et al [46] is notable in that they embarked on finding the influence of the parameters involved and the effect of augmenting on lubrication of the die. They measured the mean die pressure using strain gauges mounted on the outside of the die and with the measured extrusion pressure they determined the coefficient of friction. Fig. (4) reproduced from their paper shows the 'total extrusion pressure' versus extrusion stress/drawing stress ratio, for 15°, 30°, 45°, and 60° die angles. These curves show a minimum indicating the variation of friction conditions for different values of this ratio. The variation of coefficient of friction with this ratio is given in Fig. (5).

3.2 Hydrodynamic lubrication

Wistreich [53] used a split die technique to measure the coefficient of friction in wire drawing of copper and obtained low values (around 0.03). Since then various attempts have been made to promote hydrodynamic lubrication in wire-drawing and several theories have been put forward.

3.21 Hydrodynamic lubrication in wire drawing

Christopherson and Naylor [49] working on an idea originally suggested by Cameron used a pressure tube having a small clearance between it and the wire stock and generated fluid pressure at the die by hydrodynamic action. They also put forward an analysis of hydrodynamic lubrication in wire drawing. To satisfy the experimental results they assumed that the wire travelled eccentrically with respect to the tube and calculated the pressure distribution and other parameters on this basis. The validity of this assumption was questioned by later workers on the field. Also, they did not analyse lubrication conditions in the deforming zone. Tattersall [50] considered the deforming zone, but this simple analysis did not take into account several parameters. Osterle and Dixon [51] considered viscous lubrication in wire drawing with a pressure tube. In their analysis they assumed a rigid-work hardening material ($\sigma = \sigma_y + \eta\bar{\epsilon}$). But they neglected the shear stress of the viscous drag and obtained the pressure distribution along the die. Change in viscosity with pressure and temperature increase caused by plastic working was allowed for and the film thickness along the die was obtained. Finally they discussed some of the restrictions on various parameters for hydrodynamic lubrication. Bedi [52] assumed hydrodynamic film thickness variation along the die as (i) exponential (ii) constant and used the principle of minimum entropy production to analyse the hydrodynamics of wire drawing.

3.22 Hydrodynamic lubrication in hydrostatic extrusion

Since there is fluid at high pressure at the billet end in hydrostatic extrusion there is a strong possibility of hydrodynamic lubrication of the die metal interface. Recently there have been attempts to analyse the mechanics of hydrodynamic lubrication in hydrostatic extrusion.

It can be shown easily that the mean die pressure would be smaller than the fluid pressure if $\cot\alpha > \frac{1}{\mu(R - 1)}$ using a simple analysis. Under favourable conditions the fluid may be expected to penetrate the die metal interface. Rozner and Faupel [54] used a simple hydrodynamic analysis for their experiments in hydrostatic extrusion and obtained a parabolic pressure distribution and a mean film thickness of 6×10^{-4} cms, assuming a linear decay of film thickness. The variation of viscosity with pressure etc. was neglected in this analysis.

Hillier [55] analysed the hydrostatic extrusion process with a constant film thickness using the principle of minimum entropy production. In the analysis he used the upper bound solution by Avitzur and defined a modified Sommerfeld number, $N = \frac{\eta U_1}{\sigma \gamma_b}$. Using N and the experimental results of Pugh he showed that his theory agrees well with the experiments. He also obtained optimum die angles for several reductions. However some of the assumptions are not accurate and the variation of viscosity with pressure is neglected. Iyengar and Rice [56] investigated the conditions for the initiation of a fluid film and for sustained hydrodynamic lubrication. They also used a constant viscosity, a pressure distribution due to Sachs [30], and the approximation that $h \alpha D$. They assumed the existence

of a hydrodynamic wedge at the inlet zone which is essential to attain the die pressure at inlet, which is undoubtedly higher than the fluid pressure in the vessel.

The most recent analysis of hydrodynamic lubrication applied to hydrostatic extrusion and wire drawing is by Wilson and Walowit [57]. In this analysis of the generalized hydrostatic extrusion process they considered a rigid-perfectly plastic material accompanied by other assumptions. However in the final result their definition of 'driving stress', $(p_A + \sigma_p - p_3)$ in the present notation does not include σ_A. If the 'driving stress' is to mean the external stress system performing the work per unit volume of the material being deformed, then obviously σ_A, the billet augmenting stress has to be included. Equation 31 of the reference cited is

$$(p_A + \sigma_p - p_3) = 1 + \frac{1}{\gamma} \ln\left[\frac{2(1 - e^{-\gamma(\sigma + \sigma A)})(D^{-3} - D^{-2G})}{3(3 - 2G)} + D^{-2G} \cdot e^{-\gamma(\sigma + \sigma_A)}\right]$$

using the present notation.

If σ_A appears in the left hand side of this equation it can be rewritten as

$(p_A + \sigma_A + \sigma_p - p_3) = \sigma \ln R + p_{FD}$ - equation 24 in section 4.61

which is the usual expression for extrusion pressure or drawing stress in terms of homogeneous and frictional (and redundant) components.

3.3 Theories of axi-symmetric extrusion

Due to the absence of an exact solution for axi-symmetric extrusion, available ones are upper bounds [21, 22, 23, 24, 25, 26, 27, 28, 29], approximate ones [30], quasi-empirical ones [31] or elaborate ones, for example using experimental flow lines by the

"visioplasticity" method [32, 33, 34, 35]. Attempts have been made [25, 36] to include strain rate effects by making use of stress-strain curves at different strain rates.

A numerical analysis of the temperature changes in extrusion through conical dies was given by Altan and Kobayashi [38].

Available upper bounds fall into three categories;

1. Kinematically admissible velocity fields, being assumed to consist of 'triangular' portions with parallel or converging streamlines and conical discontinuities separating them. One, two or even more portions were used by Halling and Mitchell [26], Kobayashi [22] and Adie and Alexander [60]. The work of deformation in these modes was optimized using computer methods, by varying the shapes of the triangular portions.

2. A method mainly due to Lambert and Kobayashi [27, 28] who superimposed several basic kinematically admissible velocity fields with discontinuities to obtain a velocity field without discontinuities. Fig. (6) shows such a superimposition of velocity fields. Using parabolic boundaries for the basic velocity fields and the concept of a flow function they formulated the strain rates etc. in the field and optimized it for minimum extrusion pressure. This method seems to give upper bounds which are better than any other available. Provision is also made for including friction. They found that extrusion pressures for frictionless extrusions with die angles 45^{o}, 60^{o} and 90^{o} follow the usual straight line variation of the form $p_o = a + b \ln R$ as given below.

Die angle	Extrusion pressure, p_o
45^{o}	$p_o = 0.16 + 1.00 \ln R$
60^{o}	$p_o = 0.45 + 0.90 \ln R$
90^{o}	$p_o = 0.70 + 0.85 \ln R$

3. A method due to Avitzur [24], who used the theory of plastic flow through a conical channel by shield [61], but with the addition of spherical discontinuities at the die entrance and exit. The coefficient of friction was also taken into account in an approximate way. This method is described in detail in section 4.3. An improved method using generalized boundaries is given by Zimmerman and Avitzur [73].

3.31 Theories of hydrostatic extrusion

Though the theories cited in the previous sections may be applied to hydrostatic extrusion the features present in hydrostatic extrusion warrent special treatment. Pugh has given an approximate theory of hydrostatic extrusion [31]. The other theories of hydrostatic extrusion are based on hydrodynamic lubrication as discussed earlier. The effects of size in hydrostatic extrusion are discussed in references [39, 40]. Though suggestions are made regarding the size effect the only theoretical explanation by Avitzur [41] based on his theory [23, 24] is apparently not consistent with experimental findings [42]. Also the hydrodynamic theory by Hillier is said to be insufficient to account for this effect. This may be attributed to higher strain rates as the size decreases and to different lubrication conditions. An explanation based on a theory of hydrodynamic lubrication is given in Chapter 6.

4. THEORETICAL WORK

4.1 The basic equations of axi-symmetric extrusion

In axi-symmetric plastic deformation the non-zero components of stress and strain rates are σ_r, σ_θ, σ_z, τ_{rz}, and $\dot{\varepsilon}_r$, $\dot{\varepsilon}_\theta$, $\dot{\varepsilon}_z$, $\dot{\varepsilon}_{rz}$ respectively, referred to the cylindrical polar co-ordinate system (r, θ, z) shown in Fig. (7). The components of velocity are u and w, perpendicular and parallel to the axis respectively. The component in the θ direction is zero and the flow is along the meridian planes.

The strain rates are related to the velocity components as follows.

$$\dot{\varepsilon}_r = \frac{\partial U}{\partial r} \; ; \; \dot{\varepsilon}_\theta = \frac{U}{r} \; ; \; \dot{\varepsilon}_z = \frac{\partial w}{\partial z}$$

$$\dot{\varepsilon}_{rz} = \frac{1}{2}\left(\frac{\partial U}{\partial z} + \frac{\partial w}{\partial r}\right) \qquad 1.$$

The yield criterion of von Mises is given by the equation

$$(\sigma_r - \sigma_\theta)^2 + (\sigma_\theta - \sigma_z)^2 + (\sigma_z - \sigma_r)^2 + 6\,\tau_{rz}^2 = 2\sigma^2 \qquad 2.$$

The Levy-Mises relations of plastic flow are

$$\frac{\dot{\varepsilon}_r}{(\sigma_r - \sigma_m)} = \frac{\dot{\varepsilon}_\theta}{(\sigma_\theta - \sigma_m)} = \frac{\dot{\varepsilon}_z}{(\sigma_z - \sigma_m)} = \frac{\dot{\varepsilon}_{rz}}{\tau_{rz}} = \dot{\lambda} = \frac{3}{2}\,\frac{\dot{\bar{\varepsilon}}}{\sigma} \qquad 3.$$

where $\sigma_m = (\sigma_r + \sigma_\theta + \sigma_z)/3$, the hydrostatic component of stress

$\dot{\lambda}$ = a positive variable parameter in the stress-strain field

$\dot{\bar{\varepsilon}}$ = equivalent strain

$$= \sqrt{\frac{2}{9}\left[(\dot{\varepsilon}_r - \dot{\varepsilon}_\theta)^2 + (\dot{\varepsilon}_\theta - \dot{\varepsilon}_z)^2 + (\dot{\varepsilon}_z - \dot{\varepsilon}_r)^2 + 6\dot{\varepsilon}_{rz}^2\right]} \qquad 4.$$

Equation 3 satisfies volume constancy in plastic flow, (i.e. $\dot{\varepsilon}_r + \dot{\varepsilon}_\theta + \dot{\varepsilon}_z = 0$) automatically for any $\dot{\lambda}$.

From the stress-strain relationship of the material

$$\sigma = H(\dot{\bar{\epsilon}}) \quad \text{by strain hardening hypothesis.} \qquad 5.$$

The equations of equilibrium in the r direction and the axial direction are given by

$$\left.\begin{aligned} &\frac{\partial \sigma_r}{\partial r} + \frac{\partial \tau_{rz}}{\partial z} + \frac{\sigma_r - \sigma_\theta}{r} = 0 \\ &\frac{\partial \sigma_z}{\partial z} + \frac{\partial \tau_{rz}}{\partial r} + \frac{\tau_{rz}}{r} = 0 \end{aligned}\right\} \qquad 6.$$

Equations 1 through 6 contain 7 unknown quantities σ_r, σ_θ, σ_z, τ_{rz}, u, w and $\dot{\lambda}$ and seven independent equations. Thus the solution is unique [63] for a set of boundary conditions. However these equations and the boundary conditions for an extrusion problem make it difficult for an analytical solution to be obtained. The velocity and stress boundary conditions for hydrostatic extrusion with zero friction is given in Fig. (7).

Using extremum principles one can evaluate reasonable upper and lower bounds to the true solution. A lower bound solution is associated with a stress field satisfying the equilibrium equations, the yield criterion and the stress boundary conditions but need not satisfy the kinematic or velocity conditions. Upper bounds are associated with model velocity fields satisfying constancy of volume and the kinematic conditions, but need not satisfy the stress conditions. Upper bounds are relatively easier to formulate and are usually close to experimental observations.

4.2 Theories of axi-symmetric extrusion

In the literature there are technological theories of

extrusion by Sachs [30], Pugh [31], etc. Sachs's theory assumes a simplified deformation pattern and is based on a differential equation of equilibrium, assuming axial and radial directions as principal directions and plane sections remain plane after deformation. This theory allows for friction but not for redundant deformation and is found to be inaccurate for large die angles and reductions. Pugh's theory [31], described below, is for hydrostatic extrusion where the friction is small and it allows for friction and redundant work in an approximate way.

4.21 An approximate theory of hydrostatic extrusion (By Pugh)

The hydrostatic extrusion pressure is given by;

$$p = p_H + p_R + p_{FD}$$

where p_H, p_R and p_{FD} are the components of work due to homogeneous deformation, redundant shearing concentrated at discontinuities at the die entrance and exit and the frictional resistance respectively per unit volume of material extruded. It can be easily shown that the redundant work expended for a spherical boundary at the die entrance or exit is

$$p_{R1} = k \left(\frac{\alpha}{\sin^2\alpha} - \cot \alpha\right)$$

or $p_{R1} = \frac{4k}{3}(\tan \alpha/2)$ for an optimum conical boundary at the entrance or exit to the die, where k is the yield shear stress. For a parabolic boundary, Fig. (8) the expression for p_{R1} is derived in appendix II and optimised on a computer. The values of dimensionless p_{R1} with various die angles are given in Table (1). Also the values for spherical and optimum conical boundaries are given in the table for comparison. Values of p_{R1}/k are plotted for various die angles and compared with the

curves for other boundaries in Fig. (9). It is easily seen that the optimum parabolic boundary gives the lowest p_{R1} for all the boundaries considered.

Continuing with Pugh's theory he converts p_{R1} into a redundant strain at entry using Tresca's yield criterion ($\sigma = 2k$), thus

$$\frac{p_{R1}}{\sigma} = \frac{1}{2}\left(\frac{\alpha}{\sin^2\alpha} - \cot\alpha\right) = \epsilon_1 .$$

When σ is variable $p_{R1} = \int_0^{\epsilon_1} \sigma d\epsilon$

Once the material has changed direction by redundant shearing at the entrance it undergoes a homogeneous deformation given by

$$p_H = \int_{\epsilon_1}^{\epsilon_2} \sigma d\epsilon \quad \text{where } \epsilon_2 = \epsilon_1 + \ln R$$

Similarly to condition at the entrance it can be shown that at exit the material undergoes change in direction with redundant strain ϵ_1 thus

$$p_{R2} = \int_{\epsilon_2}^{\epsilon_3} \sigma d\epsilon$$

where $\epsilon_3 = \epsilon_2 + \epsilon_1$

Assuming q_o to be the mean normal die pressure for frictionless extrusion,

$$q_o = \frac{R}{R-1} \cdot p_H$$

$$= \frac{R}{R-1} \int_{\epsilon_1}^{\epsilon_2} \sigma d\epsilon$$

from pseudo-equilibrium considerations. The rate of dissipation of work in overcoming friction is given by $\pi\frac{D_1^2}{4} \cdot p_{FD} \cdot U_1 = \int_{D_2/2}^{D/2} 2\pi r \cdot \mu q v \, dr/\sin\alpha$

where q is the mean normal die pressure and assuming

$$\frac{v}{U_1} = \frac{D^2}{4 \cdot r^2}$$

$$p_{FD} = \frac{2\mu q}{\sin\alpha}\int_{\frac{D}{2}}^{\frac{D}{2}} \frac{dr}{r}$$

$$= \frac{\mu q}{\sin\alpha} \cdot \ln R$$

Assuming $q \simeq q_o$ for $\mu \leq 0.10$,

$$p_{FD} = \frac{\mu R \ln R}{\sin\alpha(R-1)} \cdot \int_{\epsilon_1}^{\epsilon_2} \sigma d\epsilon$$

Thus gathering the components we get

$$p = p_R + p_H + p_{FD} = p_{R1} + p_{R2} + p_H + p_{FD}$$

$$= \int_0^{\epsilon_1} \sigma d\epsilon + \int_{\epsilon_2}^{\epsilon_3} \sigma d\epsilon + \int_{\epsilon_1}^{\epsilon_2} \sigma d\epsilon + \frac{\mu R \ln R}{\sin\alpha(R-1)} \int_{\epsilon_1}^{\epsilon_2} \sigma d\epsilon$$

$$= \int_0^{\epsilon_3} \sigma d\epsilon + \frac{R \cdot \mu \cdot \ln R}{\sin\alpha\ (R-1)} \cdot \int_{\epsilon_1}^{\epsilon_2} \sigma d\epsilon$$

where $\epsilon_1 = \frac{1}{2}\left(\frac{\alpha}{\sin^2\alpha} - \cot\alpha\right)$; $\epsilon_2 = \epsilon_1 + \ln R$

$$\epsilon_3 = 2\epsilon_1 + \ln R$$

By comparison with experimental results of mean strain ϵ_m given by $p_o = \int_0^{\epsilon_3} \sigma d\epsilon$, and assuming friction to be small Pugh arrives at the result $\epsilon_1 = 0.462\left(\frac{\alpha_a}{\sin^2\alpha} - \cot\alpha\right)$. The expression for extrusion pressure has an inplicit optimum die angle for an extrusion ratio R and a coefficient of friction μ.

4.3 An upper-bound for axi-symmetric extrusion

This method is due to Avitzur [24]. This method, unlike the numerical methods, gives an algebraic expression for extrusion pressure. The velocity field and the notation used are given in Fig. (10). The

material is divided into three regions I, II and III representing the billet, the deforming zone and the product respectively. The (axial) inlet velocity and the outlet (axial) velocity are related by constancy of volume thus;

$$v_i = v_f \frac{R_f^2}{R_i^2} = v_f \frac{r_f^2}{r_i^2} \qquad 1.$$

In zone II the velocity components in the spherical co-ordinate system (r, θ, φ) are given by

$$\left.\begin{aligned} U_r = v &= - v_f^2 \cdot r_f^2 \cdot \frac{\cos\theta}{r^2} \\ U_\theta &= U_\varphi = 0 \end{aligned}\right\} \qquad 2.$$

The strain rates are given by

$$\left.\begin{aligned} \dot{\epsilon}_{rr} &= \frac{\partial U_r}{\partial r} = 2 v_f r_f^2 \cdot \frac{\cos\theta}{r^3} \\ \dot{\epsilon}_{\theta\theta} &= \frac{1}{r}\frac{\partial U_\theta}{\partial \theta} + \frac{U_r}{r} = - v_f r_f^2 \frac{\cos\theta}{r^3} = - \frac{\dot{\epsilon}_{rr}}{2} \\ \dot{\epsilon}_{\varphi\varphi} &= \frac{U_r}{r} + \frac{1}{r\sin\theta}\frac{\partial U_\varphi}{\partial \varphi} + \cot\theta \frac{U_\theta}{r} = - v_f \cdot r_f^2 \cdot \frac{\cos\theta}{r^3} = - \frac{\dot{\epsilon}_{rr}}{2} \\ \dot{\epsilon}_{r\theta} &= \frac{1}{2}\left(\frac{\partial U_\theta}{\partial r} - \frac{U_\theta}{r} + \frac{1}{r}\frac{\partial U_r}{\partial \theta}\right) = \frac{1}{2} v_f r_f^2 \frac{\sin\theta}{r^3} \end{aligned}\right\} \qquad 3.$$

$$\dot{\epsilon}_{\theta\varphi} = \dot{\epsilon}_{\varphi r} = 0$$

The equivalent strain rate

$$\bar{\dot{\epsilon}} = \sqrt{\frac{2}{3}\left[\dot{\epsilon}_{rr}^2 + \dot{\epsilon}_{\theta\theta}^2 + \dot{\epsilon}_{\varphi\varphi}^2 + 2\left(\dot{\epsilon}_{r\theta}^2 + \dot{\epsilon}_{\theta\varphi}^2 + \dot{\epsilon}_{\varphi r}^2\right)\right]}$$

$$= \sqrt{\dot{\epsilon}_{rr}^2 + \frac{4}{3}\dot{\epsilon}_{r\theta}^2} \quad \text{from 3}$$

Power dissipated in zone II,

$$W_i = \int_0^V \bar{\sigma}\bar{\dot{\epsilon}}\, dV = \bar{\sigma} \int_0^V \bar{\dot{\epsilon}} dV, \quad \sigma = \bar{\sigma} = \text{constant yield stress}$$

and V is the volume between the spherical boundaries.

$$= \bar{\sigma} \int_o^V 4v_f^2 v_f^4 \frac{\cos^2\theta}{r^6} + \frac{1}{3} v_f^2 r_f^4 \frac{4\sin^2\theta}{r^6} \cdot dV$$

$$= \bar{\sigma}\, v_f \cdot r_f^2 \int_o^V \frac{1}{r^3} \sqrt{4\cos^2\theta + \frac{1}{3}\sin^2\theta} \cdot dV$$

$$= 2\bar{\sigma}\, v_f r_f^2 \cdot \int_o^V \frac{1}{r^3} \sqrt{1 - \frac{11}{12} \cdot \sin^2\theta}\, dV$$

On spherical polar co-ordinates with axial symmetry

$$dV = 2\pi \cdot r^3 \cdot \sin\theta d\theta$$

$$\therefore W_i = 4\pi\bar{\sigma} v_f r_f^2 \cdot \int_o^{\alpha} \sqrt{1 - \frac{11}{12} \cdot \sin^2\theta} \cdot \sin\theta \cdot \int_{r_f}^{r_i} dr \cdot d\theta$$

$$= 4\pi\bar{\sigma} v_f r_f^2 \cdot \ln\frac{r_i}{r_f} \cdot \int_o^{\alpha} \sqrt{1 - \frac{11}{12}\sin^2\theta} \cdot \sin\theta d\theta$$

which can be integrated by parts to give

$$W_i = 2\pi\bar{\sigma} \cdot v_f \cdot r_f^2 \cdot \ln\frac{r_i}{r_f} \left[1 - \cos\alpha \sqrt{1 - \frac{11}{12}\sin^2\alpha} + \frac{1}{\sqrt{11*12}} \ln \frac{1 + \sqrt{11/12}}{\sqrt{\frac{11}{12}} \cdot \cos\alpha + \sqrt{1 - \frac{11}{12}\sin^2\alpha}} \right]$$

Also by way of geometry

$$\frac{r_i}{r_f} = \frac{R_i}{R_f} \text{ and } R_f = r_f \cdot \sin\alpha$$

$$\text{hence } W_i = \frac{2\pi\bar{\sigma} v_f R_f^2}{\sin^2\alpha} \cdot \ln\frac{R_i}{R_f} \left[1 - \cos\alpha \sqrt{1 - \frac{11}{12}\sin^2\alpha} + \frac{1}{\sqrt{11*12}} \cdot \ln \left\{ \frac{1 + \sqrt{\frac{11}{12}}}{\sqrt{\frac{11}{12}} \cdot \cos\alpha + \sqrt{1 - \frac{11}{12}\sin^2\alpha}} \right\} \right]$$

Power dissipated in shear across the velocity discontinuities along surfaces Γ_1 and Γ_2,

$$\dot{W}s12 = \int_{s\Gamma_1} k \cdot \Delta v \cdot ds = \int_{s\Gamma_1} k \cdot \Delta v_1 \cdot ds_1 + \int_{s\Gamma_1} k \cdot \Delta v_2 \cdot ds_2$$

where the yield shear stress, $k = \bar{\sigma}/\sqrt{3}$ by the von Mises criterion

Δv_1, Δv_2 are velocity discontinuities across Γ_1 and Γ_2 and are equal to $v_i \sin\theta$ and $v_f \cdot \sin\theta$ respectively.

$ds_1 = 2\pi r_i^2 \sin\theta d\theta$, $ds_2 = 2\pi r_f^2 \sin\theta d\theta$ are the elemental areas of Γ_1 and Γ_2 respectively.

$$\therefore \dot{W}s12 = \int_0^{\alpha} (kv_i \sin\theta \cdot 2\pi r_i^2 \sin\theta + kv_f^2 \sin\theta \cdot 2\pi r_f^2 \sin\theta) d\theta$$

$$= 4\pi \cdot v_f r_f^2 \cdot k \int_0^{\alpha} \sin^2\theta d\theta \text{ since } v_i r_i^2 = v_f r_f^2$$

$$= 2\pi v_f r_f^2 k \, (\alpha - \sin\alpha\cos\alpha)$$

But $r_f = R_f/\sin\alpha$

$$\therefore \dot{W}s12 = 2\pi R_f^2 v_f k \left(\frac{\alpha}{\sin^2\alpha} - \cot\alpha\right)$$

Along the die-metal interface, Γ_3 Sachs' expression for die pressure in wire-drawing process is used thus

$$\sigma_\theta = \sigma_{xf} + \bar{\sigma} \ln R_f^2 - \bar{\sigma} (1 + \ln R^2)$$

where R is the radius measured from the axis to any point on the cone. Power dissipation along this surface is given by

$$\dot{W}s3 = \int_{s\Gamma_3} \tau \cdot \Delta v \cdot ds$$

where frictional shear stress, $\tau = \mu\sigma_\theta$ assuming Coulomb friction.

$$\Delta v = -v_f r_f^2 \cdot \frac{\cos\alpha}{r^2}$$ (relative velocity between the die and deforming metal) and $ds = 2\pi R \cdot dr = 2\pi R dR/\sin\alpha$.

$$\therefore \dot{W}s3 = \int_{R_f}^{R_i} \tau \cdot v_i \cdot \left(\frac{R_i}{R_f}\right)^2 \cdot \left(\frac{R_f}{R}\right)^2 \cdot \cos\alpha \cdot \frac{2\pi R dR}{\sin\alpha}$$

$$= 2\pi\cot\alpha \cdot v_i \cdot R_i^2 \mu \int_{R_f}^{R_i} \left[\frac{\sigma_{xf} + \bar{\sigma}\ln R^2}{R} - \bar{\sigma}\left(\frac{1}{R} + \frac{\ln R^2}{R}\right)\right] dR$$

After integration it becomes

$$\dot{W}s3 = -2\pi \cdot \cot\alpha \cdot v_i R_i^2 \cdot \mu\left[(\sigma_{xf} + \bar{\sigma}\ln R_f^2)\ln R - \bar{\sigma}\ln R - \bar{\sigma}(\ln R)^2\right]_{R_f}^{R_i}$$

After simplification it becomes

$$= 2\pi\cot\alpha \cdot v_f \cdot R_f^2 \cdot \mu \cdot \bar{\sigma} \cdot \ln\frac{R_i}{R_f}\left(1 + \ln\frac{R_i}{R_f} + \frac{\sigma_{xf}}{\bar{\sigma}}\right)$$

Along the die land the von Mises yield criterion gives

$$\bar{\sigma} = \sigma_\theta - \sigma_{xf}$$

$$\therefore \dot{W}s4 = \int_{s_4} \tau\Delta v \cdot ds$$

where $\dot{W}s4$ is the power dissipated in the die land.

$$\tau = \mu\sigma_\theta = \mu(\bar{\sigma} + \sigma_{xf})$$

$$\Delta v = v_f$$

$ds = 2\pi R_f \cdot dx$ where x is measured along the die land

$$\therefore \dot{W}s4 = \int_0^L \mu(\bar{\sigma} + \sigma_{xf})\ v_f \cdot 2\pi R_f \cdot dx = 2\pi\mu v_i R_f^2 \frac{L}{R_f}(\bar{\sigma} + \sigma_{xf})$$

where L is the length of the die land.

Power extracted by frontal compressive stress, $\dot{W}_f = \pi R_f^2 V_f \sigma_{xf}$

Power supplied by pressure at the back end of the billet, $\dot{W} = \pi R_i^2 v_i \sigma_{xb}$

$$\therefore \dot{W} - \dot{W}_f = \dot{W}_i + \dot{W}s12 + \dot{W}s3 + \dot{W}s4$$

hence

$$\pi v_i R_i^2 \cdot \frac{\sigma_{xb}}{\bar{\sigma}} = \pi v_f R_f^2 \left[\frac{\sigma_{xf}}{\bar{\sigma}} + 2f(\alpha)\ln\frac{R_i}{R_f} + \frac{2}{\sqrt{3}}\left(\frac{\alpha}{\sin^2\alpha} - \cot\alpha\right)\right.$$

$$+ 2\mu\cot\alpha \ln\frac{R_i}{R_f}\left(\frac{\sigma_{xf}}{\bar{\sigma}} + 1 + \ln\frac{R_i}{R_f}\right) + \frac{2\mu L}{R_f}\left(1 + \frac{\sigma_{xf}}{\bar{\sigma}}\right)]$$

It can be simplified to give

$$\frac{\sigma_{xb}}{\bar{\sigma}} = \frac{\sigma_{xf}}{\bar{\sigma}} + 2f(\alpha) \cdot \ln\frac{R_i}{R_f} + \frac{2}{\sqrt{3}}\left(\frac{\alpha}{\sin^2\alpha} - \cot\alpha\right) + 2\mu[\cot\alpha \left(\frac{\sigma_{xf}}{\bar{\sigma}} + 1 + \ln\frac{R_i}{R_f}\right)$$

$$\cdot \ln\frac{R_i}{R_f} + \frac{L}{R_f}\left(1 + \frac{\sigma_{xf}}{\bar{\sigma}}\right)]$$

where $f(\alpha) = \frac{1}{\sin^2\alpha}\left[1 - \cos\alpha\sqrt{1 - \frac{11}{12}\sin^2\alpha} + \frac{1}{\sqrt{11*12}} \ln \frac{1 + \sqrt{\frac{11}{12}}}{\sqrt{\frac{11}{12}}\cos\alpha + \sqrt{1 - \frac{11}{12}\sin^2\alpha}}\right]$

4.4 Estimation of friction in hydrostatic extrusion

The method that will be used is due to Evans and Avitzur [62]. For a given reduction of any particular material there exists an optimum die angle for minimum extrusion pressure. For the same material this optimum die angle increases as reduction increases. It is also found to increase with harder materials (i.e. as the yield strength of the material increases). In the ideal case when friction is zero the optimum die angle would be zero, whatever the material or the reduction, since the extrusion pressure for any reduction would be expected to increase with die angle due to increased redundant work. In view of this the optimum die angle can be taken as a measure of friction (direct determination of friction in hydrostatic extrusion requires elaborate and careful measurement of the pressure distribution between the die and the deforming metal and precise measurement of the extrusion pressure). Using the analysis put forward by Evans and Avitzur one can estimate the value of coefficient of friction if the optimum die angle

can be found. Though this analysis is based on an upper-bound solution by Avitzur [24] it allows determination of the coefficient of friction without recourse to the mechanics of friction. In hydrostatic extrusion the optimum die angles recorded lie in the range 0° to 70°. Hardly any cases of dead metal zone formation have been recorded. In conventional extrusion, however, this angle lies between 90° and 180° approximately and cases of dead metal formation are not infrequent. Thus it is possible to compare the coefficients of friction in hydrostatic extrusion with those obtainable in conventional extrusion. This simple analysis can be applied to any material as the yield strength of the material does not appear explicitly in the expression for the coefficient of friction.

The coefficient of friction μ_o is obtained as follows:-

Now

$$\frac{p_o}{\sigma} = f(\alpha) \cdot \ln R + \frac{2}{\sqrt{3}}\left(\frac{\alpha}{\sin^2\alpha} - \cot\alpha\right) + 2\mu_o\left[\cot\alpha\left(1 + \frac{1}{2}\ln R\right)\frac{\ln R}{2} + \frac{L}{R_f}\right]$$

is the expression for extrusion pressure, from Avitzur's theory given in the previous section with the notation given in chapter 2. Differentiating this with respect to α and equating to zero gives

$$\mu_o = \frac{\sin\alpha_o\left[\sqrt{1 - \frac{11}{12}\sin^2\alpha_o} - f(\alpha_o)\cos\alpha_o\right]\ln R + \frac{2}{\sqrt{3}}\left(1 - \frac{\alpha_o\cos\alpha_o}{\sin\alpha_o}\right)}{\frac{1}{2}\ln R\left(1 + \frac{1}{2}\ln R\right)}$$

Using the above equation the coefficient of friction may be calculated as a function of optimum die angle and extrusion ratio. Fig. (11) shows curves illustrating this function for several extrusion ratios.

4.41 Friction in billet augmented hydrostatic extrusion

Avitzur's analysis given in section 4.33 does not predict

any change in the total extrusion pressure with billet augmentation. This could only be incorporated by a change in the coefficient of friction with augmentation. The observations made in the present experiments with billet augmentation indicate that the coefficient of friction increases with augmentation. A method of estimating the coefficient of friction in such cases is given below.

For a given material and reduction in simple hydrostatic extrusion, the average coefficient of friction μ_o can be calculated from the optimum die angle using the method already described.

To determine the coefficient of friction μ in billet augmented extrusion, the coefficient of friction μ_o and extrusion pressure p_o in simple hydrostatic extrusion could be used as the starting point. With reference to the Fig. (12) there are two components to be isolated from the total extrusion pressure to obtain the component due to increased friction at any augmenting stress, namely:-

1. The component due to increased extrusion ratio caused by the bulging of the billet.
2. The component due to increased mean yield stress caused by the work hardening of the bulged billet.

For the same coefficient of friction as in simple hydrostatic extrusion the component due to increased extrusion ratio R, caused by bulging can be given by the line $p = a + b\ln R$ for simple hydrostatic extrusion, if increase in R is small compared to R. However this is for a material with the same initial conditions (non-work hardened). To allow approximately for work hardening of the billet by bulging, this pressure p is multiplied by $\frac{(\sigma_m)_A}{(\sigma_m)_{\ln R}}$ neglecting the effect of friction.

$(\sigma_m)_{\ln R}$ is the mean yield stress for extrusion at a ratio R

starting with annealed material.

$(\sigma_m)_A$ is the mean yield stress for extrusion at a ratio R of the deformed billet, determined as follows:-

Referring to Fig. (12) again and considering the homogeneous work done,

$$(\sigma_m)_A \cdot \ln R = (\sigma_m)_{\ln R+2\epsilon} \cdot [\ln R_o + 2\epsilon] - (\sigma_m)_\epsilon \cdot \epsilon$$

where $\ln R = \ln R_o + \epsilon$ = strain imposed on the bulged billet by extrusion

ϵ = true strain due to bulging

$\ln R + \epsilon = \ln R_o + 2\epsilon$ = total strain suffered by the original billet due to both bulging and extrusion.

For small ϵ, $(\sigma_m)_A \quad (\sigma_m)_{\ln R}$

With the above modifications to the measured pressures and augmenting stresses, μ can be calculated on the assumption that the die pressure does not change appreciably with change in μ. This is a good approximation if μ is less than 0.1.

Referring to the models in Fig. (13) with

p_o^* = fluid pressure for simple hydrostatic extrusion of work hardened material through extrusion ratio R.

q = mean die pressure

Equating the die loads in the axial direction in each case

$$Ap_o^* = \frac{R-1}{R} A\,(q \sin\alpha + \mu_o q \cos\alpha)$$

and

$$A(p_A + \sigma_A) = \frac{R-1}{R} A\,(q \sin\alpha + \mu q \cos\alpha)$$

$$\therefore q = \frac{R}{R-1} \cdot \frac{p_o^*}{(\sin\alpha + \mu_o \cos\alpha)}$$

and $\mu = \dfrac{p_A + \sigma_A}{p_o^*}\ (\tan\alpha + \mu_o) - \tan\alpha$

$$= \tan\alpha \left(\frac{p_A + \sigma_A}{p_o} - 1\right) + \frac{p_A + \sigma_A}{p_o^*} \cdot \mu_o$$

where $p_o^* = \frac{(\sigma_m)_A}{(\sigma_m)_{lnR}} \cdot p$; $p_o = a + b\ln R$

When bulging is negligible, p_o, p and μ is given simply by

$$\mu = \tan\alpha \left(\frac{p_A + \sigma_A}{p_o} - 1\right) + \frac{p_A + \sigma_A}{p_o} \cdot \mu_o$$

4.42 Friction in product augmented hydrostatic extrusion

Avitzur's analysis applied to product augmentation gives

$$\frac{\sigma_p + p_A}{\sigma_o} = f(\alpha)\ln R + \frac{2}{\sqrt{3}}\left(\frac{\alpha}{\sin^2\alpha} - \cot\alpha\right) + \mu\cot\alpha \left(1 - \frac{\sigma_p}{\sigma_o} + \frac{1}{2}\ln R\right) \ln R$$

neglecting the effect of the die land.

Assuming a constant coefficient of friction μ, according to this equation the total extrusion pressure $(\sigma_p + p_A)$ should decrease with increase of σ_p. In the experiments carried out by Parsons, Bretherton and Cole [46] this total pressure decreased with increasing σ_p giving a minimum, and increased with further increase in σ_p. Thus this equation does not satisfy their experimental results. This can perhaps be attributed to the deterioration of lubrication at the die-billet interface as the fluid pressure p_A is decreased while σ_p is increased. Thus as the fluid pressure is reduced with increased product augmentation, the die pressure decreases while the coefficient of friction increases. Beyond the optimum augmentation the advantage of reduced die pressure with product augmentation is offset by the break-down of lubrication.

In simple theories of extrusion, the extrusion pressure is made up of separate terms for homogeneous, redundant and frictional work. On this basis the validity of the frictional term such as in the equation given above can be tested using the coefficients of friction measured

in product augmentation experiments where the homogeneous work or the redundant work due to the geometry of the die can be assumed not to change with augmentation. The redundant deformation, if any, caused by friction may be neglected if the coefficient of friction is less than 0.1. Therefore, subtracting the expression for product augmented extrusion from that for simple hydrostatic extrusion we get

$$\frac{p - p_A - \sigma_p}{\sigma_o} = [\mu_o(1 + \frac{1}{2}\ln R) - \mu(1 - \frac{\sigma_p}{\sigma_o} + \frac{1}{2}\ln R)]\cot\alpha \cdot \ln R$$

$$= [(\mu_o - \mu)(1 + \frac{1}{2} \cdot \ln R) + \frac{\mu\sigma_p}{\sigma_o}] \cot\alpha \cdot \ln R$$

4.5 Limits of augmentation

Since augmented extrusion processes rely on the strength of the billet or the product or both there are limits to the magnitudes of augmenting stresses. In product augmented hydrostatic extrusion the limit is imposed by the tensile strength of the billet. Even within this limit the deformation of the product at high augmenting stresses may be appreciable and to obtain a product to specified tolerances the augmenting stress has to be further limited.

In billet augmented extrusion, in addition to the limit imposed by the compressive strength of the billet there is another restriction on the length of the billet due to its possible buckling. The larger the initial work hardening rate and the yield stress the more useful the billet augmented processes are since large augmenting stresses can be applied. Even for soft materials the product augmented extrusion process is useful and does not need straight billets; coiled billets could in fact be used. Considerable reduction in die pressures

could also be expected. On the other hand there is an additional limitation in the billet augmented process due to the reduced lateral support given by the fluid pressure on the die. These limits are derived and discussed below.

4.51 Bulging limit in billet augmentation

The application of augmenting stress to the billet will deform it to a certain extent before extrusion starts. The amount of bulge or deformation of the billet entering the die depends on the magnitude of the augmenting stress and the stress-strain characteristic of the material. Materials with rapid work-hardening from the elastic limit could sustain considerable augmenting stress before any appreciable plastic deformation of the billet occurs. The limit to the augmenting stress could be visualised as the stress beyond which the increase in augmenting stress associated with the deformation of the billet will no longer be able to provide the 'total extrusion pressure', $(p_A + \sigma_A)$ necessary for extrusion of the deformed billet. This argument is true, in general, for any hydrostatic extrusion process with billet augmentation.

To determine accurately the limits of augmenting stress, the stress-strain curve of the material and the mechanics of the process must be known. Also this limit varies with the mode of augmenting. Examples are (i) constant pressure augmentation, (ii) proportional augmentation, where augmenting load is proportional to the fluid pressure. The stress-strain curve can be determined readily by the Cook and Larke test or by any other standard test. The mechanics of the process are complicated however and available solutions are only approximate upper-

bounds or empirical ones. The coefficient of friction also varies with different augmenting conditions and is difficult to predict beforehand. This makes it necessary to base any reliable prediction on empirical results. These limits could also be determined experimentally by noting the stress at which extrusion becomes unstable.

4.51.1 Constant fluid pressure augmentation

With reference to Fig. (14), the fluid pressure p_A is insufficient to extrude the material through extrusion ratio R_o, in simple hydrostatic extrusion. If p_A is only slightly less than p, the simple hydrostatic extrusion pressure for ratio R_o and the increase in coefficient of friction due to augmenting is small, then the extrusion proceeds with elastic deformation of the billet. Since elastic strain is small this will not contribute significantly to increase the extrusion ratio by bulging. Thus augmented extrusion takes place with the original extrusion ratio R_o. If p_A is further reduced (say $p - p_A >$ elastic limit), the billet will deform beyond the elastic limit, increasing the instantaneous extrusion ratio and work-hardening the material until an equilibrium is reached when $(p_A + \sigma_A)$ is sufficient to extrude the billet having been bulged by a fixed amount with extrusion ratio R. However if $p - p_A$ is large, the billet bulges with increased extrusion ratio and $p_A + \sigma_A$ will not be sufficient to extrude the bulged billet. Thus the maximum augmenting stress at which a steady extrusion is possible is the limit of the augmenting stress in bulging.

A construction for determining this limit in experiments with augmented extrusion is as follows;

With reference to Fig. (14) consider a billet with an initial

extrusion ratio R_o. Suppose from experiments p_A, σ_A and R are obtained for several p_A. If enough experimental points are obtained at large steady augmenting stresses, the total extrusion pressure $\sigma_A + p_A$ at the limit can be obtained by extrapolation. As shown in the figure the stress-strain curve of the material is superimposed on the total extrusion pressure vs lnR diagram. At steady (p_A, σ_A) the ($\sigma_A + p_A$) vs lnR curve cuts the stress-strain curve determining the bulge strain for (p_A, σ_A). If we consider a very low p_A then ($\sigma_A + p_A$) vs lnR curve is well above the stress-strain curve superimposed on p_A showing that there is no possible steady augmenting stress σ_A for this p_A. Somewhere between these two cases there exists a σ_A when the extrapolated ($\sigma_A + p_A$) vs lnR curve will touch the stress-strain curve superimposed. This will give the limit of augmenting stress. Instead of superimposing the stress-strain curve if we draw a tangent ,with slope equal to that of the ($\sigma_A + p_A$) vs lnR curve at large σ_A, to touch the stress-strain curve the corresponding stress will give the limiting augmenting stress. If, however, we make a few simplifications the limiting augmenting stress may be obtained mathematically. The simplifications are (i) that the hardening of the bulged billet may be neglected, (ii) that the bulged billet follows 'p = a + blnR' of the simple hydrostatic extrusion but modified as $p_A + \sigma_A = a + b\ln R$.

With these simplifications the method of Thompson [45] applies as follows;

If the extrusion ratio were increased from R_o to R keeping p_A constant, the rate of change of augmenting stress required to maintain extrusion would be $\frac{d\sigma_A}{d(\ln R)} = b$ as illustrated in Fig. (15). This change of augmenting stress would lead to an incremental equivalent strain due to bulging of $d\bar{\epsilon}$ associated with a change of stress $d\sigma$ on

the stress-strain curve, where $d\sigma = d\sigma_A$. Hence if $\frac{d\sigma_A}{d(\ln R)} > \frac{d\sigma}{d\epsilon}$ (of stress-strain curve) bulging will proceed rather than extrusion.

If $\frac{d\sigma_A}{d(\ln R)} < \frac{d\sigma}{d\epsilon}$ extrusion will proceed steadily with the billet having been bulged by a fixed amount ($d\epsilon$). A construction for determining this amount is shown in Fig. (15).

4.51.2 Proportional augmentation

In this case the augmenting load = $\omega \cdot p_A \cdot A_o$

where ω is the constant of proportionality and

A_o is the initial area of cross-section of the billet.

Due to bulging the area of cross-section of the billet will increase and σ_A is given by,

$$\sigma_A + \frac{R_o}{R} \omega p_A$$

Thus σ_A will depend on ω, p_A and the new area of cross-section.

The total extrusion pressure, $p_A + \sigma_A = \sigma_A + \sigma_A \cdot (\frac{R}{R_o \omega})$

$$= \sigma_A(1 + e^{\epsilon}/\omega)$$

where ϵ is the bulge strain = $\ln R/R_o$

Thus the rate of increase of total extrusion pressure associated with bulge strain ϵ, $= \frac{d}{d\epsilon}(p_A + \sigma_A) = \frac{d}{d\epsilon}(\sigma_A(1 + \frac{e^{\epsilon}}{\omega}))$

$$= \frac{d\sigma_A}{d\epsilon}(1 + \frac{e^{\epsilon}}{\omega}) + \sigma_A \cdot \frac{e^{\epsilon}}{\omega}$$

The rate of increase of total extrusion pressure needed for the increased extrusion ratio caused by bulging is

$$= \frac{d}{d(\ln R)} (a + b \ln R) = b$$

Thus instability will occur when $\frac{d\sigma_A}{d\epsilon}(1 + \frac{e^{\epsilon}}{\omega}) + \frac{\sigma_A e^{\epsilon}}{\omega} \leq b$

i.e. when the slope of the stress-strain curve

$$\frac{d\sigma}{d\epsilon} \leq \left(\frac{b - \frac{\sigma_A e^{\epsilon}}{\omega}}{1 + e^{\epsilon/\omega}}\right) \text{, where } d\sigma = d\sigma_A$$

If ω is large when it becomes open die extrusion

$$\frac{d\sigma}{d\epsilon} \leq b \text{ for instability}$$

If ω is small as in most proportional augmentation the limiting σ_A is larger than that given by $\frac{d\sigma}{d\epsilon} = b$

4.52 Buckling limit in billet augmentation

Both ends of the billet may be considered as fixed. At the die end this may not be entirely true because the die angle and the reduction (due to unsupported area) would have some effect on this condition. At the back end this depends on the type of support. If the billet were held rigidly in a clamp this would be justified. For a fixed end strut, the Euler buckling load is given by

$$P_{CR} = \frac{4\pi^2 EI}{l^2}$$

where E = Young's Modulus

I = Second moment of area of section

$= \pi D_1^4/64$ for a circular billet of diameter D_1

l = length of the strut (billet)

Since the augmenting stresses can be high, the possibility of plastic buckling exists in billet augmenting. For calculating the plastic buckling load the reduced formula and the tangent modulus formula are available. These are obtained by substituting for E, in the Euler formula, the reduced modulus Er, or the tangent modulus Et respectively. In the reduced

modulus formula, Er depends on the shape of the section and gives a higher value for buckling load, than the tangent modulus formula. This formula also implies a stress reversal at constant buckling stress. The tangent modulus formula is easier to manipulate and gives a conservative estimate of the buckling load. Also in its derivation [64] it is assumed that the bending moment and the axial load are increased simultaneously. This condition is most probably realised in billet augmented extrusion where there may be slight eccentricity in loading and the billet may not be expected to be perfectly straight. It has also been shown that for very short struts the experimental buckling loads tend to approach the reduced modulus value. Therefore it remains to be shown in augmented extrusion experiments as to which formula gives the appropriate buckling loads in these cases.

Using the tangent modulus formula

$$P_{CR} = 4\pi^2 EtI/l^2$$

where Et = tangent modulus = slope of the stress-strain curve at the corresponding stress. This buckling load can also be given in terms of a critical buckling stress, S_{CR} where $S_{CR} = P_{CR}/(\pi D_1^2/4)$. For a material with a stress-strain curve if we assume that any stress on the curve is a critical stress for buckling, we can calculate the corresponding critical slenderness ratio l/r. Up to the elastic limit the Euler buckling load and above this limit the tangent modulus formula will be used to calculate the critical slenderness ratios. These values for copper and mild steel are given in Tables (2, 3) and plotted in Figs. (16a and b).

4.53 Limits to product augmentation

The limiting product augmenting stress that can be applied to the product is its yield strength. This strength depends on how the

'tag' has been produced. If the billet were machined with a tag then it is the yield strength of the original material. However if it was formed by extrusion, with the maximum fluid pressure available at a smaller extrusion ratio than that is to be achieved, the strength of the tag will be higher, equal to the yield strength of the extruded product. For this purpose it can be assumed that the strength of the extruded product is the flow stress at the strain corresponding to the extrusion ratio. A construction to determine the maximum extrusion ratio achievable with a given maximum fluid pressure is given in Fig. (17), for product and billet augmentation .

Since the augmenting stress is applied to the product this stress cannot be high even if it may be stable extrusion because the deformation of the product by the applied stress has to lie within the tolerance allowed. This restriction is not present in billet augmentation.

4.6 Hydrodynamic lubrication in the general hydrostatic extrusion process

Basic equations:- With reference to fig. (18) the basic equilibrium equation for an element of the fluid, assuming η to be constant with respect to the y-direction is:-

$$\frac{dp}{dx} = \eta \frac{d^2v}{dy^2}$$

where v is the velocity of lubricant at (x, y)

After integration

$$\frac{dv}{dy} = \frac{1}{\eta} \cdot \frac{dp}{dx} \cdot y + c_1 \qquad 1.$$

$$v = \frac{1}{2\eta} \cdot \frac{dp}{dx} \cdot y^2 + c_1 y + c_2$$

Hence

$$\frac{Q}{x} = \frac{Q'}{\pi D} = \int_o^h v \cdot dy = \left[\frac{h^3}{12\eta} \cdot \frac{dp}{dx} + \frac{c_1}{2} \cdot h^2 + c_2 h\right] \qquad 2.$$

and

$$\frac{dp}{dx} = \frac{6\eta}{h^3} \cdot \left(\frac{Q}{x} - \frac{c_1 \cdot h^2}{2} - c_2 \cdot h\right) \qquad 3.$$

where $$\eta = \eta_o \cdot e^{\gamma p} \qquad 4.$$

Q, Q' are assumed constant in the inlet, deforming and the outlet regions and p, $\frac{dp}{dx}$ are piece-wise continuous in all the regions and where they meet.

$v = 0$ at $y = 0$ in all the regions,

$v = -U_1$ in the inlet zone (if there is no 'curving in'),

$v = -U_1\left(\frac{x_1}{x}\right)^2$ in the deforming zone,

and $v = -U_2 = -U_1\left(\frac{x_1}{x_2}\right)^2$ in the outlet region, when

$y = h$.

With the first one of these velocity boundary conditions $c_2 = 0$.

The pressure boundary conditions are

$$\text{At } h = h_1,\ p_1 = \sigma + p_A + \sigma_A$$

$$h = h_2,\ p_2 = \sigma + p_3 - \sigma_p$$

where p_A is the pressure at the entrance to the die and p_3 is the pressure at the exit of the die land (back pressure). From the geometry, the film thickness, in the deformation zone

$$h = x \cdot \tan \alpha - \frac{D}{2 \cos \alpha} \cdot$$

In the outlet zone with a parallel die land assuming the deformation of the product to be elastic and the die land to be rigid, the film thickness his given by;

$$h = h_2 + \frac{D_2}{2E} \cdot (1 - \nu)\ (p - p_2)$$

Analysis of the deformation zone

Substitution of the velocity boundary conditions give

$$v = \frac{1}{2\eta} \cdot \frac{dp}{dx} \cdot (y^2 - yh) - \frac{U_1}{h} \cdot \left(\frac{x_1}{x}\right)^2 \cdot y\ ,$$

$$Q = -x\left[\frac{h^3}{12\eta} \frac{dp}{dx} + \frac{U_1}{2} \left(\frac{x_1}{x}\right)^2 \cdot h\right] \qquad 5.$$

$$\frac{dp}{dx} = -\frac{12\eta}{h^3} \cdot \left[\frac{Q}{x} + \frac{U_1}{2} \cdot \left(\frac{x_1}{x}\right)^2 h\right] \qquad 6.$$

and

$$\tau = -\eta \left(\frac{dv}{dy}\right)_h = \frac{\eta U_1}{h} \left(\frac{x_1}{x}\right)^2 - \frac{h}{2} \cdot \frac{dp}{dx} \qquad 7.$$

Considering the equilibrium of an element in the deforming zone

$$x \left(\frac{dp}{dx} - \frac{d\sigma}{dx}\right) - 2\sigma - 2\tau/\tan \alpha = 0 \qquad 8.$$

and $\sigma z + p = \sigma$ Tresca yield condition (approximately).

Substituting for τ, equation 8. becomes

$$\left(\frac{x}{2} + \frac{h}{2 \tan \alpha}\right) \frac{dp}{dx} - \frac{x}{2} \frac{d\sigma}{dx} - \sigma - \frac{\eta U_1}{h \tan \alpha} \cdot \left(\frac{x_1}{x}\right)^2 = 0 \qquad 8^*.$$

Inlet zone

$$v = \frac{1}{2\eta} \cdot \frac{dp}{dx} (y^2 - yh) - \frac{U_1 y}{h} ,$$

$$Q = -x_1 \left[\frac{h^3}{12\eta} \cdot \frac{dp}{dx} + \frac{U_1 h}{2}\right] \qquad 9.$$

and

$$\frac{dp}{dx} = - \frac{12\eta}{h^3} \left[\frac{Q}{x_1} + \frac{U_1 h}{2}\right] \qquad 10.$$

Outlet zone

$$v = \frac{1}{2\eta} \frac{dp}{dx} (y^2 - yh) - \frac{U_1}{h} \left(\frac{x_1}{x_2}\right)^2 y ,$$

$$Q = -x_2 \left[\frac{h^3}{12\eta} \cdot \frac{dp}{dx} + \frac{U_1 h}{2} \left(\frac{x_1}{x}\right)^2\right] \qquad 11.$$

and

$$\frac{dp}{dx} = - \frac{12\eta}{h^3} \cdot \left[\frac{Q}{x_2} + \frac{U_1 h}{2} \cdot \left(\frac{x_1}{x}\right)^2\right] \qquad 12.$$

4.61 Rigid-plastic material analysis

σ = constant, therefore $\frac{d\sigma}{dx} = 0$

In equation 8* h/tan α may be neglected compared to x since h is small.

Hence from 8*

$$\left(\frac{dp}{dx}\right)_{x_1} = \frac{2}{x_1} \left(\sigma + \frac{\eta_o \cdot e^{\cdot \gamma_p} \cdot U_1}{h_1 \tan \alpha}\right)$$

Also from equation 5 or 9

$$\frac{Q}{x_1} = -\left[\frac{h_1^3}{12\eta_o e^{\gamma p_1}} \cdot \left(\frac{dp}{dx}\right)_{x_1} + \frac{U_1 \cdot h_1}{2}\right] = -C_3 \text{ (say)}$$

Substituting for $\left(\frac{dp}{dx}\right)_{x_1}$

$$\frac{Q}{x_1} = -\left[\frac{h_1^3}{12\eta_o e^{\gamma p_1}} \cdot \frac{2}{x_1} \cdot \left(\sigma + \frac{\eta_o e^{\gamma p_1} U_1}{h_1 \tan\alpha}\right) + \frac{U_1 h_1}{2}\right]$$

Substituting for $\frac{Q}{x_1}$ in equation 10 we get in the inlet zone,

$$\frac{dp}{dx} = \frac{12\eta_o e^{\gamma p}}{h^3} \cdot \left[\frac{h_1^3}{12\eta_o e^{\gamma p_1}} \cdot \frac{2}{x_1} \cdot \left(\sigma + \frac{\eta_o e^{\gamma p_1} U_1}{h_1 \tan\alpha}\right) + \frac{U_1}{2}(h_1 - h)\right] \quad 10^*.$$

And in the deforming zone, from equation 6,

$$\frac{dp}{dx} = \frac{12\eta_o e^{\gamma p}}{h^3} \left[\frac{h_1^3}{12\eta_o e^{\gamma p_1}} \cdot \frac{2}{x} \cdot \left(\sigma + \frac{\eta_o e^{\gamma p_1} U_1}{h_1 \tan\alpha}\right) + \frac{U_1 x_1}{2x}\left(h_1 - \frac{h x_1}{x}\right)\right] \quad 13.$$

Also in the deforming zone, from equation 8*

$$\frac{dp}{dx} = \frac{2}{x}\left[\sigma + \frac{\eta_o e^{\gamma p_1} U_1}{h \tan\alpha} \cdot \left(\frac{x_1}{x}\right)^2\right] \quad 14.$$

The values of $\frac{dp}{dx}$ in equations 13 and 14 are obviously the same quantity and therefore h should vary accordingly. Thus equating and re-arranging equations 13 and 14 we get

$$\frac{h^3}{12\eta_o e^{\gamma p}} \cdot \frac{2}{x} \cdot \left(\sigma + \frac{\eta_o e^{\gamma p} U_1}{h \tan\alpha} \cdot \left(\frac{x_1}{x}\right)^2\right) = \frac{h_1^3}{12\eta_o e^{\gamma p_1}} \cdot \frac{2}{x} \cdot \left(\sigma + \frac{\eta_o e^{\gamma p_1} U_1}{h_1 \tan\alpha}\right) + \frac{U_1 x_1}{2x} \cdot \left(h_1 - \frac{h x_1}{x}\right) \quad 15.$$

If we neglect terms containing h^3, h_1^3, h^2, h_1^2 compared to those containing h or h_1, (for small h, h_1) we get

$$\frac{h}{h_1} \approx \frac{x}{x_1}$$

Thus equation 8* becomes

$$\frac{x}{2}\frac{dp}{dx} - \sigma - \frac{\eta_o U_1}{h_1}\left(\frac{x_1}{x}\right)^3 \cdot e^{\gamma p} = 0 .$$

Changing to dimensionless parameters defined in the notation

$$\frac{dB}{dX} + \frac{2GB}{X} = -\frac{2\eta_o U_1}{h_1} \cdot \frac{\gamma}{\tan\alpha} \cdot \frac{1}{X^4}$$

where $X = x/x_1$

Hence the solution

$$B = e^{-\gamma p} = -\frac{A}{X^3} + \frac{C}{X^{2G}} \qquad 16.$$

where $A = \frac{2\eta_o U_1}{h_1 \tan\alpha} \cdot \frac{\gamma}{(2G-3)}$ and C is a constant to be determined.

At the inlet edge of the deforming region $X = 1$ and $p_1 = p_A + \sigma_A + \sigma$

$$\therefore B_1 = e^{-\gamma(p_A + \sigma_A + \sigma)} = C - A \text{ from 16.}$$

Substituting for C in equation 16 we get

$$B = -A\left(\frac{1}{X^3} - \frac{1}{X^{2G}}\right) + \frac{e^{-\gamma(p_A + \sigma_A + \sigma)}}{X^{2G}} \qquad 17.$$

At $X = X_2 = \sqrt{\frac{1}{R}}$, $B_2 = e^{-\gamma(\sigma + p_3 - \sigma_p)}$

Hence from equation 17

$$e^{-\gamma(p_3 + \sigma - \sigma_p)} = -A\,(R^{3/2} - R^G) + R^G e^{-\gamma(\sigma + p_A + \sigma_A)} \qquad 18.$$

Equation 18 relates p_A, p_3, σ_A, σ_p for a particular h_1 contained in the constant A.

The values of h_1 and A could be determined from the inlet conditions as follows;

From equation 10*, in the inlet zone $\frac{dp}{dx}$ is given by

$$\frac{dp}{dx} = \frac{12\eta_o e^{\gamma p}}{h^3}\left[\frac{h_1^3}{12\eta_o e^{\gamma p_1}} \cdot \frac{2}{x_1}\left(\sigma + \frac{\eta_o e^{\gamma p_1} U_1}{h_1 \tan\alpha}\right) + \frac{U_1}{2}(h_1 - h)\right]$$

$$= \frac{12\eta_o e^{\gamma p}}{h^3}\left(C_3 - \frac{U_1 h}{2}\right) \qquad 19.$$

but $h = x \tan\alpha - D/2 \cos\alpha$

$\therefore$ $dh = dx \tan\alpha$ since dD is zero

$\therefore$ $\tan\alpha \frac{dp}{dh} = \frac{12\eta_o e^{\gamma p}}{h^3}\left(C_3 - \frac{U_1 h}{2}\right)$ from equation 19.

Integrating this equation we get

$$-\frac{e^{-\gamma p}}{\gamma} = \frac{12\eta_o}{\tan\alpha}\left[-\frac{C_3}{2h^2} + \frac{U_1}{2h}\right] + C_4$$

but $h \to \infty$ as $p \to p_A$ at the billet

$$\therefore \frac{1}{\gamma}\left(e^{-\gamma p_A} - e^{-\gamma p}\right) = \frac{12\eta_o}{\tan\alpha}\left(-\frac{C_3}{2h^2} + \frac{U_1}{2h}\right) \qquad 20.$$

At $x = x_1$, $p = p_1 = p_A + \sigma_A + \sigma$ and $h = h_1$

$\therefore$ from equation 20

$$\left(e^{-\gamma p_A} - e^{-\gamma p_1}\right) = \frac{12\eta_o \gamma}{\tan\alpha}\left(-\frac{C_3}{2h_1^2} + \frac{U_1}{2h_1}\right)$$

$$= \frac{12\eta_o \gamma}{\tan\alpha}\left[\frac{U_1}{2h_1} - \frac{1}{2h_1^2}\left\{\left(\frac{2h_1^3}{12\eta_o e^{\gamma p_1 x_1}}\right) \cdot \left(\sigma + \frac{\eta_o e^{\gamma p_1} U_1}{h_1 \tan\alpha}\right) + \frac{U_1 h_1}{2}\right\}\right]$$

$$= \frac{12\eta_o \gamma}{\tan\alpha}\left[\frac{U_1}{4h_1} - \frac{\sigma}{12\eta_o e^{\gamma p_1 x_1}} \cdot h_1 - \frac{U_1}{12 x_1 \tan\alpha}\right] \qquad 20^*.$$

If the term containing h_1 can be neglected compared to the term containing $1/h_1$ in the right hand side of equation 20*,

$$e^{-\gamma p_A} - e^{-\gamma p_1} = \frac{3\eta_o U_1 \gamma}{\tan\alpha} \cdot \frac{1}{h_1} - \frac{\eta_o U_1 \gamma}{x_1 \tan^2\alpha}$$

$$\text{hence } h_1 = \frac{3\eta_o U_1 \gamma}{\tan\alpha} \cdot \frac{1}{\left(\frac{U_1 \eta_o \gamma}{x \tan^2\alpha} + e^{-\gamma p_A} - e^{-\gamma p_1}\right)} \qquad 21.$$

Hence

$$A = \frac{2\eta_o U_1 \gamma}{h_1 \tan\alpha} \cdot \frac{1}{(2G - 3)} = \frac{2}{3(2G - 3)} \left[\frac{U_1 \eta_o \gamma}{x_1 \tan^2\alpha} + e^{-\gamma p_A} - e^{-\gamma(p_A + \sigma_A + \sigma)}\right]$$

.... 22.

Substituting for A in equation 18 we get

$$e^{-\gamma(p_3 + \sigma - \sigma_p)} = R^G e^{-\gamma(p_A + \sigma_A + \sigma)} - \frac{2(R^{3/2} - R^G)}{3(2G - 3)} \cdot \left[\frac{U_1 \eta_o \gamma}{x_1 \tan^2\alpha} + e^{-\gamma p_A} - e^{-\gamma(p_A + \sigma_A + \sigma)}\right]$$

After re-arranging it becomes

$$e^{\gamma(p_A + \sigma_A + \sigma_p - p_3)} = R^G\left[1 + \frac{2(R^{\frac{3-2G}{2}} - 1)}{3(3 - 2G)} \cdot \left(\frac{U_1 \eta_o \gamma}{x_1 \tan^2\alpha} e^{\gamma(p_A + \sigma_A + \sigma)} + e^{\gamma(\sigma_A + \sigma)} - 1\right)\right] \quad 23.$$

It can be shown that the term within the square bracket is positive for all values of G.

Hence taking the logarithm of equation 23.

$$(p_A + \sigma_A + \sigma_p - p_3) = \sigma \ln R + \frac{1}{\gamma} Ln\left[1 + \frac{2(R^{\frac{3-2G}{2}} - 1)}{3(3-2G)}\left(\frac{U_1 \eta_o \gamma}{x_1 \tan^2\alpha} e^{\gamma(p_A + \sigma_A + \sigma)} + e^{\gamma(\sigma_A + \sigma)} - 1\right)\right] \quad 24.$$

Driving stress or (External work) = Homogenous Work = p_H + Frictional work, p_{FD}

Therefore the frictional contribution to 'extrusion pressure' or 'driving stress' in hydrodynamic lubrication,

$$p_{FD} = \frac{1}{\gamma} Ln\left[1 + \frac{2(R^{\frac{3-2G}{2}} - 1)}{3(3 - 2G)}\left(\frac{U_1 \eta_o \gamma}{x_1 \tan^2\alpha} \cdot e^{\gamma(p_A + \sigma_A + \sigma)} + e^{\gamma(\sigma_A + \sigma)} - 1\right)\right] \quad 25.$$

It is obvious from equation 25 that the frictional contribution depends on R, p_A, σ_A, σ, U_1 and tan α apart from the material properties of the

lubricant. The term containing U_1 may be neglected if U_1 is small and α is large.

4.61.1 Theory of a double reduction die

Equation 21 of section 4.61 for film thickness at the die entrance gives;

$$h_1 = \frac{3\eta_o U_1 \gamma}{\tan \alpha} \cdot \frac{e^{\gamma p_A}}{(1 - e^{-\gamma(\sigma_A + \sigma)})} \quad \text{if the velocity term}$$

in the denomenator is neglected.

Thus if σ_A is negative augmentation, h_1 may be increased considerably, other factors being the same, due to increased p_A associated with negative σ_A and decreased denomenator in the above equation. If we look at the equation in another way, the velocity U_1 required to form a certain film thickness is reduced by increased negative σ_A.

Under these conditions, the equation 25 of section 4.61 gives;

$$p_{FD} = \frac{1}{\gamma} \mathrm{Ln}\left[1 + \frac{2}{3} \frac{(R^{\frac{3-2G}{2}} - 1)}{(3 - 2G)} (e^{\gamma(\sigma_A + \sigma)} - 1)\right]$$

neglecting the velocity term within the square brackets. It is again obvious that if σ_A is made increasingly negative the frictional component decreases correspondingly. The above analysis applies to the second reduction (major) R_2 in the double reduction die (fig (52)).

In the first reduction it can be shown that the frictional component is not altered. But the fluid film is increased and more stable because of the presence of high pressure fluid on the billet and the product sides.

4.62 Work hardening material analysis

With the assumptions and approximations as in section 4.61 except that

σ is variable and is given, for simplicity by;

$$\sigma = \sigma_o + (H - \sigma_o)\ (1 - e^{-n\varepsilon}) \qquad 26.$$

where $\varepsilon = 2\ (D_1/D)$ 27.

From equation 8., neglecting h/2 tan α as before, we get

$$x\left(\frac{dp}{dx} - \frac{d\sigma}{dx}\right) - 2\sigma - \frac{2\eta_o U_1}{h_1 \tan\alpha} \cdot \left(\frac{x_1}{x}\right)^3 \cdot e^{\gamma p} = 0$$

With the use of equations 26, 27 and the assumption that $\frac{h}{h_1} = \frac{x}{x_1}$

as before, we get

$$x\frac{dp}{dx} + 2n\left(\frac{H - \sigma_o}{x_1^{2n}}\right) \cdot x^{2n} - 2H - 2(H - \sigma_o)\left(\frac{x}{x_1}\right)^{2n} - \frac{2\eta_o U_1}{h_1}\left(\frac{x_1}{x}\right)^3 \frac{e^{\gamma p}}{\tan\alpha} = 0$$

i.e.

$$e^{\gamma p}\frac{dp}{dx} + e^{-\gamma p} \cdot \left(\frac{2(H-\sigma_o)(n+1)}{x_1^{2n}} \cdot x^{2n-1} - \frac{2H}{x} - \frac{2\eta_o U_1 x_1^3}{h_1 \tan\alpha} \cdot \frac{1}{x^4}\right) = 0 \qquad 28.$$

Since $e^{-\gamma p} = B$ and $x/x_1 = X$, equation 30 becomes

$$\frac{dB}{dX} - \gamma B\left(2(H - \sigma_o)(n + 1)\ X^{2n-1} - \frac{2H}{X}\right) = -\frac{2\eta_o U_1 \gamma}{h_1 \tan\alpha} \cdot \frac{1}{X^4} \qquad 29.$$

$$\left.\begin{aligned} \text{Let } 2\gamma(H - \sigma_o)(n + 1) &= I_1 \\ 2\gamma H &= I_2 \\ \text{and } \frac{2\gamma\eta_o}{h_1 \tan\alpha} &= I_3 \end{aligned}\right\} \qquad 30.$$

$$\text{Then } \frac{dB}{dX} - B\left(I_1 X^{2n-1} - \frac{I_2}{X}\right) = \frac{-I_3}{X^4} \qquad 31.$$

Hence the solution

$$BX^{I_2} \cdot e^{\frac{-I_1}{2n} X^{2n}} = -I_3 \int X^{I_2 - 4} \cdot e^{\frac{-I_1}{2n} \cdot X^{2n}} \cdot dX + C_5 \qquad 32.$$

Integration of the right hand side integral is given in Appendix II.

Thus

$$X^{I_2} \cdot e^{-(\gamma p + \frac{I_1}{2n} X^{2n})} = \frac{-I_3 X^{I_{2-3}}}{2n} \cdot \sum_{j=0}^{\infty} \frac{(-1)^j (\frac{I_1}{2n})^j \cdot X^{2nj}}{(\frac{I_{2-3}}{2n} + j) \lfloor j} + C_5$$

.... 33.

at $X = 1, p = p_1 = p_A + \sigma_A + \sigma_o$

$$\therefore C_5 = e^{-\gamma(p_A + \sigma_A + \sigma_o)} - \frac{I_1}{2n} + \frac{I_3}{2n} \sum_{j=o}^{\infty} \frac{(-1)^j (\frac{I_1}{2n})^j}{(\frac{I_{2-3}}{2n} + j) \lfloor j}$$

and

$$X^{I_2} \cdot e^{-(\gamma p + \frac{I_1}{2n} X^{2n})} = \frac{I_3}{2n} [\sum_{j=o}^{\infty} \frac{(-1)^j (\frac{I_1}{2n})^j}{(\frac{I_{2-3}}{2n} + j) \lfloor j} \cdot (1 - X^{2nj + I_{2-3}})]$$

$$+ e^{-\gamma(p_A + \sigma_A + \sigma_o)} - I_1/2n \qquad 34.$$

As in the previous section h_1 is found to be,

$$h_1 = \frac{3\eta_o U_1 \gamma}{\tan \alpha} \cdot \frac{1}{(\frac{U_1 \eta_o \gamma}{x_1 \tan^2 \alpha} + e^{-\gamma p_A} - e^{-\gamma(p_A + \sigma_A + \sigma_o)})} \qquad 35.$$

and from equation 30

$$I_3 = \frac{2}{3} (\frac{U_1 \eta_o \gamma}{x_1 \tan^2 \alpha} + e^{-\gamma p_A} - e^{-\gamma(p_A + \sigma_A + \sigma_o)}) \qquad 36.$$

Substituting for I_3 in equation 34.

$$e^{-\gamma(p + (\frac{H - \sigma_o}{n})(n + 1) X^{2n})} \cdot X^{2\gamma H} = \frac{1}{3n} (\frac{U_1 \eta_o \gamma}{x_1 \tan^2 \alpha} + e^{-\gamma p_A} - e^{-\gamma(p_A + \sigma_A + \sigma_o)})$$

$$\cdot [\sum_{j=0}^{\infty} \{\frac{(-1)^j (\gamma(H-\sigma_o)(\frac{n+1}{n}))^j}{(\frac{2\gamma H - 3}{2n} + j) \lfloor j} (1 - X^{2nj + 2\gamma H - 3})\}] + e^{-\gamma(p_A + \sigma_A + \sigma_o + (\frac{H-\sigma_o}{n})(n+1))}$$

.... 37.

Equation 37 gives the pressure distribution along the die

When $X = X_2 = \frac{1}{\sqrt{R}}$, $p_2 = \sigma_o + (H - \sigma_o)(1 - R^{-n}) + p_3 - \sigma_p$

by Tresca's yield criterion approximately.

Hence from equation 37,

$$R^{-\gamma H} \cdot e^{-\gamma(\sigma_o - p_3 + \sigma_p + (H - \sigma_o)(1 - R^{-n}) + \frac{(H - \sigma_o)}{n}(n + 1)R^{-n})}$$

$$= \frac{1}{3n}\left(\frac{U_1 \eta_o \gamma}{x_1 \tan^2\alpha} + e^{-\gamma p_A} - e^{-\gamma(p_A + \sigma_A + \sigma_o)}\right) \cdot$$

$$\cdot\left[\sum_{j=o}^{\infty} \left\{\left(\frac{(-1)^j(\gamma \frac{(H - \sigma_o)}{n}(n + 1)^j}{(\frac{2\gamma H - 3}{2n} + j)\,\underline{|j}}\right)(1 - R^{3/2 - \gamma H - nj})\right\}\right]$$

$$+ e^{-\gamma(p_A + \sigma_A + \sigma_o + \frac{n + 1}{n}(H - \sigma_o))} \qquad \text{38.}$$

Equation 38 may be simplified to give the work of homogeneous deformation and frictional work, thus

$$(p_A + \sigma_A - p_3 + \sigma_p) = \sigma_o \ln R + (H - \sigma_o)(\ln R + \frac{R^{-n} - 1}{n}) + p_{FD}$$

.... 39.

'Total Extrusion pressure' or 'driving stress' — Work of homogeneous deformation — Frictional Component

where

$$p_{FD} = \frac{1}{\gamma} \ln \left[1 + e^{\gamma(p_A + \sigma_A + \sigma_o + \frac{(n + 1)}{n}(H - \sigma_o))} \cdot \left\{\frac{U_1 \eta_o \gamma}{x_1 \tan^2\alpha} + e^{-\gamma p_A} - e^{-\gamma(p_A + \sigma_A + \sigma_o)}\right\} \cdot \left\{\sum_{j=o}^{\infty} \frac{(-1)^j(\gamma \frac{(H - \sigma_o)}{n}(n + 1))^j}{(\frac{2\gamma H - 3}{2n} + j)\,\underline{|j}} \cdot (1 - R^{3/2 - \gamma H - nj})\right\}\right]$$

.... 40.

For small U_1 and large x_1 the term containing U_1 may be neglected and p_{FD} will be independent of p_A.

4.63 Modification to include redundant work approximately

In both sections 4.61 and 4.62 the equation for 'driving stress' is given by;

$$(p_A + \sigma_A + \sigma_p - p_3) = p_H + p_{FD}$$

The redundant shearing at the entrance and exit in the simplified model using optimum conical boundaries can be given by

$$\epsilon_1 = \frac{2}{3} \tan \alpha/2$$

Then by power balance,

$$(p_A + \sigma_A + \sigma_p - p_3) = \int_0^{\epsilon_1} \sigma d\epsilon + \int_{\epsilon_1}^{\epsilon_2} \sigma d\epsilon + \int_{\epsilon_2}^{\epsilon_3} \sigma d\epsilon + p_{FD}$$

$$= \int_0^{\epsilon_3} \sigma d\epsilon + p_{FD}$$

where $\epsilon_3 = \ln R + 2\epsilon_1 = \ln R + \frac{4}{3} \tan \alpha/2$

Hence equations 24 and 39 may become

$$(p_A + \sigma_A + \sigma_p - p_3) = \int_0^{\epsilon_3} \sigma d\epsilon + p_{FD} \qquad 41.$$

4.64 A numerical method for hydrodynamic lubrication with a work hardening material to include the deformation of the billet in the inlet zone

In sections 4.61 and 4.62 it was assumed that the billet remains rigid and does not deform in the inlet zone. This may be true for a rigid-plastic material with low billet velocities. But for a work-hardening materials with initial yield at very low values at large velocities the pressure rise due to the hydrodynamic wedge at the inlet zone may be sufficient to deform it. This deformation though small will

considerably change the film thickness at the inlet zone and thus the quantity of lubricant draged in. In sections 4.61 and 4.62 this quantity is determined using the inlet conditions. Unfortunately this cannot be done in this case.

Therefore the value of Q has to be determined by an entirely different method. This is done by assuming that the extruded product expands elastically in the die land. With certain assumptions Q is determined as follows;

With reference to Fig. (19), in the die land region

$$h = h_2 + \frac{D_2}{2E}(1 - \nu)(p - p_2) \qquad 1.$$

assuming that the die land is rigid and $\parallel^{L}$ to the axis.

Let $K = \frac{D_2}{2E}(1 - \nu)$

The pressure gradient in the die land is given by;

$$\frac{dp}{dx} = - \frac{12\eta_o e^{\gamma p}}{h^3} \left(\frac{Q}{\pi D_2} + \frac{U_2 h}{2}\right) \qquad 2.$$

where x is measured $\parallel^{L}$ to the die land.

Thus, substituting for h and integrating equation 2, we get

$$\int_{p_3}^{p_2} \frac{e^{-\gamma p} \cdot (h_2 + k(p - p_2))^3 dp}{\left(\frac{KU_2}{2}(p - p_2) + \frac{U_2 h_2}{2} + \frac{Q}{\pi D_2}\right)} = -12\eta_o L \qquad 3.$$

where L is the length of the die land.

Let $a = \frac{h_2}{K} + \frac{2Q}{\pi D_2 U_2 K} - p_2$,

$$b = - \frac{2Q}{\pi D_2 U_2 K}$$

and

$$p = p + a$$

Then equation 3 becomes

$$\int_{p_3+a}^{p_2+a} e^{-\gamma p}\left(\frac{P+b}{P}\right)^3 dP = -\frac{6\eta_o U_2}{K^2}\, e^{-\gamma a} \cdot L$$

which when integrated becomes

$$\left[-e^{-\gamma p} \cdot \left\{\frac{P^2}{\gamma} + \frac{3bP}{\gamma} + \frac{2P}{\gamma^2} + \frac{2}{\gamma^3} + \frac{3b}{\gamma^2} + \frac{3b^2}{\gamma}\right\} + b^3\left\{\ln|P| + \sum_{l=1}^{\infty} \frac{(-1)^l (P\gamma)^l}{l\,l!}\right\}\right]_{p_3+a}^{p_2+a} = \frac{-6\eta_o U_2 L}{K^2 \cdot e^{\gamma a}} \qquad 4.$$

Now in the deforming zone (including inlet zone),

$$\frac{dp}{dx} = -\left[\frac{Q}{\pi D} + \frac{U_2}{2}\left(\frac{D_2}{D}\right)^2 \cdot h\right] \cdot \frac{12\eta_o e^{\gamma p}}{h^3} \qquad 5.$$

$$\sigma = \sigma_o + (H = \sigma_o)(1 - e^{-n\epsilon}) \qquad 6.$$

$$\epsilon = 2\ln D_1/D \qquad 7.$$

Equilibrium equation becomes

$$D\left(\frac{d\sigma}{dD} - \frac{dp}{dD}\right) + 2\sigma + \frac{2\tau}{\frac{dD}{dz}} = 0 \qquad 8.$$

$$\tau = \frac{\mu_o e^{\gamma p} U_2}{h} \cdot \left(\frac{D_2}{D}\right)^2 - \frac{h}{2}\frac{dp}{dx} \qquad 9.$$

$$\text{and } h = x\tan\theta - D/2\cos\theta \qquad 10.$$

Differentiating equation 10

$$\frac{dD}{dx} = 2\sin\theta - 2\cos\theta\frac{dh}{dx} \qquad 11.$$

$\frac{dh}{dx}$ which was small and neglected in sections 4.61 and 4.62 will become significant in the 'inlet zone' and thus included here.

From equations 5 and 2 $\left(\frac{dp}{dx}\right)_2$ could be equated to give

$$\frac{2}{x_2}\left(\sigma_2 + \frac{\eta_o U_2 e^{\gamma p_2}}{h_2 \tan\alpha}\right) = -\frac{12\eta_o e^{\gamma p_2}}{h_2^3}\left(\frac{Q}{\pi D_2} + \frac{U_2 h_2}{2}\right) \qquad 12.$$

where $\sigma_2 = \sigma_o + (H - \sigma_o)(1 - R^{-n})$

Equations 4 and 12 contain Q and h_2 as unknowns, the other quantities being known. A computer programme for solving these two equations has been written using Newton's iteration formula.

Having determined h_2 and Q the differential equation in the deforming and the inlet zone is solved numerically using increments of x by an iteration procedure using equations 5 through 11. The complete computer programme is given in Appendix (III).

5. EXPERIMENTAL WORK

The experimental work performed in billet augmented hydrostatic extrusion is described in this chapter. The double reduction die, shown in Fig. 20, designed to achieve back tension or negative augmentation was also used in a series of tests to assess the feasibility of using this die in hydrostatic extrusion.

5.1 Extrusion equipment

The experimental tools comprise essentially a horizontal hydraulic press, a sub-press for billet augmented and simple hydrostatic extrusion and a recorder console for recording various quantities measured in the tests.

5.11 Extrusion press

This consists of a horizontal hydraulic press with two rams in opposition and a third ram moving perpendicular to the other two, all three rams being in a horizontal plane. These detachable rams are mounted on a fabricated steel yoke, as shown in Fig. 21. The yoke has provision for closing the open side with a large "keep" bar and two heavy pins. In all experiments in hydrostatic extrusion the yoke was closed with the keep bar. The third ram was removed. This press is free to slide on rails fixed to the floor. Details of the press are as follows:-

Diameter of the pistons = $11\frac{1}{2}$ ins.

Diameter of the piston rods = 8 ins.

Stroke of each ram = 6 ins.

Distance between the opposed rams

when fully withdrawn = 54 ins.

Maximum pressing load of each ram = 200 tons.

Maximum draw-back load of each ram = 100 tons.

Maximum pressing speeds of the two opposed rams = 60 ins./min.

The hydraulic drive operating these rams is known as the 'Fraser' system. This embodies three hydraulic pumping units, connected to the rams throught the manually operated control valves. Valves V20, V22, V23, V27, V24 and V26 as shown in Fig. 22 connect pump units 2 and 3 to the horizontal rams used in the experiments. Pump unit No. 1 is used only to drive the main ram of a Fielding vertical press. Pump units No. 2 and 3 are identical and are used either in combination with unit No. 1 to drive the main ram or alone to drive the opposed rams. Pump unit No. 1 consists of a single positive displacement pump which has a fixed capacity of 25 gal/min at 4480 lb/in^2 and is driven by an 85 H.P. electric motor. Pump units 2 and 3 each comprise two positive displacement pumps driven by a 75 H.P. electric motor having a double shaft extension; one pump has a fixed capacity of 7.7 g.p.m. at 4480 lb/in^2 and the other has a variable capacity of 0 - 15 g.p.m. at 4480 lb/in^2. Within each of these two units, control over the output of the variable delivery pump is effected by a $\frac{1}{2}$ H.P. geared electric motor arranged to drive the delivery adjustment shaft an indication of the output at any instant being read off a Weir indicator unit at the control console.

The manually-operated two-position control valves V23, V27, V24 and V26 connect the pump units 1 and 2 to the rams as required. Valves V23 and V27 connect pump units Nos. 2 and 3 either to the main ram circuit or to the horizontal rams by way of the valves V20 and V22.

The valves V24 and V26 are used to by-pass the flows from the fixed-delivery pumps within the pump units Nos. 2 and 3 to the supply tank when they are not required. The valves V20 and V22 are three position valves to enable the horizontal rams to be driven forward, held in any desired position or retracted. The rams are protected by relief valves R20 and R22 which can be pre-set to cause the rams to stop when the load it sustains reaches any predetermined value within their capacities.

5.12 Tooling for hydrostatic extrusion

The experimental sub-press has been designed to fit into the yoke. Fig. 23 shows the general arrangement of the sub-press and Fig. 24 shows the sub-press in position within the yoke. The design of this sub-press is such that both billet augmented and simple hydrostatic extrusion can be performed. Moreover, this sub-press can also be used for fluid-to-fluid extrusion with modifications as shown in the schematic diagram, Fig. 25. The stroke of each ram is only six inches and this imposed a serious restriction on the design of the sub-press. Thus the length of the billet that can be extruded in this sub-press is less than four inches. The large end of the bore of the pressure vessel is $1\frac{1}{2}$ inches in diameter so that pressures up to 110 T/in^2 can be obtained within the load capacity of the press.

The sub-press comprises the container (pressure vessel) with the two plungers and their supports. The container rests on a support placed on a fabricated platform with four screws for levelling the container. Since there is no resultant vertical force on the container except for its weight this simple support is sufficient. The mild steel tube, firmly attached to the yoke at one end, supports the resultant horizontal force on the container during extrusion. The

end of the tube which is in contact with the container is lined with lead sheet so that the container will not be tilted by any small lack of parallelism between the container and the tube. At this end a $1\frac{1}{2}$ inches thick circular ring is attached to the tube by six bolts around its circumference. This ring is in turn screwed to the container by six bolts and once the container is aligned these bolts are tightened to keep the container in place. This tube also has two rectangular cuts 6" x 4" to take the lead wires from the container and to remove the small plunger if necessary. This plunger has a spherical base which rests on a pad with spherical face to match the plunger. This pad is placed against the face of the ram and the plunger is held in place by a cap screwed on to the attachment to the ram. The large plunger is attached to the thick cylinder, with provision for holding the extrusion product which in turn is firmly attached to the ram. This cylinder is also supported by a pedestal fixed to the fabricated platform to prevent it creeping down due to its weight.

Alignment of the container and the punches is achieved as follows; the two plungers are fixed to the rams, and a tube of outer diameter equal to that of the large plunger is fitted closely to the small plunger. The plungers are then adjusted to be in line using a dial gauge. Once this is done the tube on the small plunger is removed, the container is placed in position and the screws of the fabricated platform are adjusted till the large plunger moves freely in the container. The container is then locked in position and the small plunger is removed and placed as far as possible in the bore of the container. The ram is brought forward to take this plunger and the cap screwed on. A rubber 'O' ring between this plunger and the cap allows the plunger to adjust itself on the spherical seat.

For augmented extrusion tests the small and the large plungers have to move with speeds of ratio (A2 - A)/A1 to keep the pressure constant, where A1, A2, A are the areas of cross section of the small bore, large bore and the billet respectively. In the case of fluid-to-fluid extrusion where the die is placed on the shoulder of the liner and the product emerges in the small bore, the speed ratio has to be A2/A1 provided the extrusion is steady under constant pressures.

In the case of simple hydrostatic extrusion however the die is carried on the large hollow plunger and both the plungers can then be moved independently to attain the necessary pressure.

The speed ratio in the first two cases is achieved thus; the speed of the large plunger is set at a desired value and that of the other is controlled by a screw device attached to the manual valve V20 at the control panel, to vary the opening of this valve until the constant pressure required is achieved and indicated on the U-V recorder. If this adjustment is made prior to commencement of augmented extrusion, it will be slightly upset due to the bulging of the billet caused by augmenting. This could be corrected by adjusting the device once the extrusion starts.

The container consists of a tapered liner with stepped bore placed inside a cylinder with tapered inside as shown in Fig. 26. Both the liner and the cylinder were made of En30B steel. The liner was heat treated to a strength of 100 T/in^2 while the cylinder was heat treated to 90 T/in^2. The axial force produced by the fluid pressure in the vessel is transferred to the outer cylinder by the liner moving in and thus receiving the radial pressure support from the outer cylinder. Thus the higher the fluid pressure in the vessel the more the interface pressure on the liner. However, the liner does not receive the full radial support from the cylinder because of the friction at the inter-

face which partly supports the axial force on the liner.

Due to repeated scoring of the large bore of the liner caused by the tilting of the pads placed in it to support the billet, this simple liner was replaced by a new one with a thin sleeve for the large bore. Due to the axial load on the sleeve caused by fluid pressure it has to be supported by a screwed plug as shown in Fig. (26). It also incorporates a seal as seen from the figure. With this liner the filling of the fluid is also made easier by having two holes drilled and pumping the fluid through the lower one and expelling the air through the upper one. The screwed plug supports the axial load, of about 46 tonsf., at 100 T/in^2 fluid pressure, from the sleeve. This thin sleeve of thickness 0.094 ins, made of EN30B steel to a strength of 100 T/in^2, could be easily replaced if damaged by scoring.

5.2 Instrumentation

The fluid pressure, augmenting load, displacement of the extrusion product and the displacement of the large ram for each extrusion test are recorded on a U-V recorder. The fluid pressure is measured by a manganin coil of 100 ohms resistance and the augmenting load by a strain gauge load cell placed inside the pressure vessel. The augmenting ram displacement and the extrusion product displacement are measured by two displacement transducers. The signals thus transduced from the instruments for measuring pressure, augmenting load and the displacements are supplied to the respective Wheatstone bridge circuits located in the recorder console and the resulting signals are fed into the separate channels of the recorder where they are recorded simultaneously on a photosensitive paper driven at constant speed.

5.21 Recorder console

The recorder console shown in Fig. (27) has been designed and built to the specification by Lengyel (58) for general use with the Fielding and Platt press and its yoke. It essentially comprises a 12-channel U-V recorder, electrical bridges, for measuring pressure, load, displacement and temperature, and a stabilized 4 Volts D.C. supply.

The U-V recorder incorporates an ultra-violet lamp which sends out beams of light to pencil type moving mirror galvanometers. The deflected beams from these galvanometers are in turn directed on to the photosensitive paper chart. This paper is driven by a synchronous motor via a gear-box and clutch, with provision for several constant chart speeds from 0.2 to 10 cms/sec. Four galvanometers of a sensitivity of 0.130 mV/cm deflection and one of 0.035 mV/cm are used for the extrusion tests.

The width of the trace may be changed, within limits, by adjusting the intensity of the ultra-violet lamp and also by adjusting the galvanometer in the vertical plane.

An electronic timing device is incorporated in the U-V recorder, based on the frequency of the mains supply. Lines are printed across the full width of the chart at intervals of several preselected periods from 1-25 secs for which provision is made in the recorder. Reference lines, at 2 mm intervals, along the length of the paper are also printed simultaneously with recordings and timing lines. This facilitates the evaluation of recordings and allows for any shrinkage or misalignment of the paper. Once the record is obtained it may be stabilized by spraying it with Kodak lingograph stabilizing lacquer.

5.22 Measurement of fluid pressure

Measurement of fluid pressure is effected by manganin coils of 100 ohms resistance placed in the pressure vessel. In the augmented extrusion tests one such coil was situated on the small plunger and leads taken through the terminals on the plunger. The coil consists of double silk covered 40 gauge manganin wire wound non-inductively (doubled wire) on a nylon reel. The leads of this coil are connected to the third arm of a Wheatstone bridge, each arm of 100 ohms resistance, situated in the recorder console. The electrical circuit diagram is shown in Fig. (28). When there is no pressure in the vessel, the bridge is balanced by a potentiometer in the front of the recorder console, where a switch for check balance, balance and with the recording galvanometer is also available. In the case of fluid-to-fluid extrusion and in the calibration of the load cell under pressure two manganin coils are used situated one at each plunger, to measure the pressures in the two bores.

The manganin coils are calibrated with a Harwood dead-weight tester whose accuracy is better than 0.02% at 200,000 lb/in^2. The basis on which this sophisticated equipment works is as follows:- a tungsten carbide piston of diametral tolerance better than one micron lies in a cylinder containing the fluid under pressure. This cylinder is surrounded by a jacket containing the same fluid under pressure which is less than the pressure under calibration by a fixed amount. The object of the jacket containing fluid under pressure is to control the clearance between the piston and the cylinder. The top of the piston supports weights corresponding to the maximum pressure to be calibrated. The manganin coil is placed in a vessel connected with the cylinder such that the same pressure is present at any time, at the piston and at the

coil. The pressures in the cylinder and the jacket are increased keeping the pressure in the jacket always at about 15 T/in^2 less than that in the cylinder thus ensuring the piston from becoming seized in the cylinder. These pressures are obtained by intensifiers incorporated in the tester and are indicated on two circular charts transduced by manganin coils calibrated by the manufacturers. Once the pressure in the cylinder, indicated by the gauge, is close to the value desired the pressure is increased slowly to the correct value. When the pressure is enough to balance the weights on the piston and a little more, the arms on which the weights are suspended move up slowly, indicated by a dial gauge graduated to 0.0001 inch. The pressure is finely adjusted until the desired time of rise of the piston for a fixed height is achieved. Simultaneously, recording is made of the pressure, by the manganin coil to be calibrated. This procedure is repeated for when the piston is falling, to eliminate the effect of friction due to leakage of oil between the piston and the cylinder. The accurate pressure is calculated from the dead weights on the piston and the area of the piston, with corrections for temperature, elastic deformation and for leakage. However this accuracy is not required as such effects can hardly be detected on the U-V recorder.

5.23 Measurement of the augmenting load

The load cell consists of a cylindrical tube with electrical strain gauges cemented on to it. Two load cells were designed with different types of compensation for pressure effects. Both consist of a strain gauge half bridge with three gauges in series forming each of the two arms. Thus three connections have to be taken out of the container. This half bridge also allows for temperature compensation. The connections from the load cell to the terminals on the small plunger was achieved by

thin flexible wires with P.V.C. insulation coiled in a helical form. Since the small plunger moves about four inches during extrusion the connections to the terminals are liable to break after a few tests due to fatigue of the connection. This difficulty which was experienced during the early tests was overcome by anchoring the wires firmly to the load cell at that end and soldering the other ends to terminals, on an insulating disc, which have some freedom of movement. These terminals are connected to the terminals on the plunger.

The electrical circuit of the bridge for measuring the augmenting load is shown in Fig. (29). The strain gauges form two of the arms of 360 ohms each. The other two arms consist of two 350 ohms foil type precision resistors with a tolerance of 0.02%. A potentiometer of 10 ohms is included to effect the initial balance. The voltage is supplied by a power pack with variable voltage. Load ranges of 0 to 1.5, 0 to 7 and 0 to 30 tons could be obtained with these two load cells and the two galvanometers of 0.13 mV/cm and 0.032 mV/cm sensitivities with 6 and 12 Volts supply from the power pack.

Both the load cells were calibrated in a testing machine whose loading scale was tested at a few loads and found to be better than 0.5 per cent. The calibration curves for the load cells with different galvanometers and voltages are shown in Fig. (30). The effect of temperature on the strain gauges would be a minimum as the two arms of the bridge are made up of strain gauges.

5.23.1 Design of the load cell

The augmenting load on the billet must be measured inside the pressure vessel as any measurement of this load outside would give rise to considerable errors and uncertainty owing to the following factors:-

1. The frictional force at the high pressure seal on the plunger (or the die), which is a function of the pressure inside is difficult to determine. This may also vary with different tests and is comparable in magnitude to that of the augmenting load.

2. Any external load measuring device has to measure the full load on the plunger, due to fluid pressure alone and yet be sensitive enough to measure a much smaller augmenting load with accuracy. This poses a demand for very high accuracy on the load cell which is difficult to achieve. It must be remembered that a load cell inside the pressure vessel needs calibration under pressure because of the effect of pressure on the strain measuring device.

Several types of load cell have been used by research workers in high pressure (65, 66) to measure load inside a pressure vessel. The most attractive type is that in which electrical resistance strain gauges are used. There are a few difficulties to be overcome in using a strain gauge load cell under high pressure environment, namely:-

1. Strain gauges cemented to the load cell tend to peel off after a few cycles of pressure.
2. The effect of pressure on the performance of electrical strain gauges must be allowed for.
3. Calibration of the load cell must be carried out under different pressures.
4. The correct pressure transmitting fluid must be selected to minimise its effect on the strain gauge backing and on the adhesive when used for any considerable time.

The first difficulty was overcome by using foil gauges with

epoxy backing cemented on to the load cell by the suppliers of the strain gauges (taking necessary precautions to obtain a good bond and to eliminate any air bubbles). The difference in compressibility between the load cell material and the strain gauge backing has to be kept small to prevent breakdown of the bond due to shear stresses in the bond imposed by hydrostatic pressure. A transparent coating (Gage Kote II *) was applied to the strain gauges to prevent seepage of oil into the bonding.

The effect of hydrostatic pressure on the performance of strain gauges has been investigated by several research workers (67, 68) and differing results have been obtained. The 'pressure effect' as defined by them is the difference between the measured strain and that calculated from the Bulk Modulus of the material on which the strain gauges are cemented. The value of this pressure effect, recorded by Pugh and Gunn (65), varies from -0.2×10^{-8} to $+0.56 \times 10^{-8}$ $lbin^{-2}$. Milligan (69) in his experiments with strain gauges under hydrostatic pressure has shown that this pressure effect could be accounted for if one uses the general approach to the problem of relating strain and electrical resistivity as outlined by Brace (70). Milligan has also shown experimentally that this pressure effect is only slightly affected by the type of backing or the adhesive used.

However, these pressure effects are of secondary importance in the design of the load cell since they can be eliminated or minimised by the use of compensating gauges. Two forms of compensation were used as shown in Figs. (32). Taking the above mentioned factors into account two load cells were designed both made of tool steel heat treated to a yield strength of about 100 T/in^2. The areas of cross section of them were so chosen that at their respective maximum design loads they would

---

* Supplied by Welwyn Electric Ltd.

be stressed to about 60 T/in^2 in compression. Tool steel was chosen because of its high limit of proportionality so that better sensitivity could be obtained than any other steel with a lower limit of proportionality (the variation of Young's Modulus with most steels is small).

The first load cell, shown in Fig. (32a), was designed to accept a maximum load of 30 tons. This comprises, essentially, a hollow cylinder and a loosely fitting ring which is not loaded, also of the same material. The outer diameter of the ring and the cylinder are equal. Three active gauges were mounted axially on the cylinder, while three compensating gauges were mounted axially on the ring.

The second load cell, shown in Fig. (32b), was designed to accept a maximum load of 7 tons. It consists of a hollow cylinder with three active gauges mounted axially on the outer diameter of the cylinder while three compensating gauges were mounted circumferentially on the same cylinder.

The circuit diagram of the Wheatstone bridge used in either case is given in Fig. (29).

For the first cell, with the usual notation

$$\Delta V_{AB} \simeq \frac{V}{720} \times \frac{KP/A}{A} \times 360 = \frac{KV}{2AE} \cdot P$$

for the second cell

$$\Delta V_{AB} \simeq \frac{V}{720} \cdot \frac{KP}{AE} \cdot (1 + \nu) \cdot 360 = \frac{KV}{2AE} \cdot (1 + \nu) \cdot P$$

When the load cell was first tested under high pressure the fluid used was Shell Tellus 27 oil which was very satisfactory. But this oil is known to freeze at about 60 T/in^2. The cell was therefore tested in a mixture of 75% castor oil and 25% methyl alcohol, so that pressures up to 100 T/in^2 could be achieved without the fluid freezing. In this case the coating of the gauges dissolved in the fluid and peeled off. A few gauges also peeled off. Unless a coating that

does not dissolve in alcohol is applied to the load cell, this mixture of castor oil and alcohol could not be used as the pressure transmitting fluid. Pure castor oil gave satisfactory results although it is said to freeze at 70 T/in^2.

5.23.2 Calibration of the load cell under pressure

The load cells were calibrated at atmospheric pressure in a testing machine. The calibration curves are linear with a little hysterises for loading and unloading as shown in Figs. (30). Pugh and Gunn [65] have found by calibrating a strain gauge load cell at atmospheric pressure and, at several pressures up to about 60 T/in^2 that all calibration curves lie within $\pm$ 1.5% of the atmospheric calibration curve. Voronov and Vereshtchagin [71] have found that the modulus of elasticity of steel increases by about 2.6% for an increase in pressure of about 60 T/in^2. Therefore an error of about 2.6 % may be expected in principle if the atmospheric calibration curve is used up to 60 T/in^2.

The loading device as shown in Fig. (33) consists of a $\frac{3}{8}$ in diameter piston and a closely fitting cylinder. Both were made of EN30B steel heat treated to a yield strength of about 90 T/in^2. The piston was ground and honed and the best fit with the piston found by trial and error. The piston has a collar $\frac{1}{8}$ in thick and a threaded end. A disc of $\frac{1}{4}$ in thickness is attached to this end of the piston and held in place by a weak nut. Load is applied to the load cell via the disc as the pressure differential is brought across the ends of the piston. To prevent overloading of the load cell due to accidental loss of pressure in the small bore, the fastening nut is made weak so that it fails above a load of 7 tons, releasing the load on the load cell. Also, as an added safety precaution

the maximum strain on the load cell is limited to about 0.5%, and above this value the collar on the piston comes into contact with the cylinder thus protecting the load cell.

The method of calibration used by Pugh and Gunn was used in the present equipment with the second load cell, which is the most convenient one for calibration under pressure. This arrangement as shown in Fig. (34) is the same as that used in the augmented extrusion experiments except that it has a 'solid' plunger with terminals, at the big end of the bore and the loading device for the load cell. The vessel was filled with the fluid. The load cell and the loading device were kept in the vessel in such a way that fluid filled both the bigger and the smaller bore. The large plunger was then advanced so that fluid in both the bores was pressurised to the same pressure. Once the plunger came into contact with the light spring it pushed the spring which in turn pushed the load cell and the loading device against the shoulder of the liner. This caused the 'o' ring (at the loading device) to seal the bigger bore from the smaller one. Any leakage could only pass through the close fitting piston and the cylinder of the loading device. Any further movement forward of the plunger would increase the pressure in the bigger bore and apply a load on the load cell unless the smaller plunger was also advanced to equalise the pressures. Thus the pressures in both the bores were brought to a value slightly below the value at which calibration is desired. Then the larger plunger was held and the smaller one moved forward to increase both the pressures exactly to the desired value. This ensured that there was no load on the load cell. Now the load cell was balanced and the smaller plunger was withdrawn to apply the load on the load cell. Calibration was limited to one load at three pressures. The best pressure difference was found to be about 15 T/in^2. The thin cylinder of the loading device was deliberately made

thin so that under pressure difference the elastic deformation of it would decrease the clearance between the piston and the cylinder and minimise leakage. These calibration points are shown in Fig. (30) together with the calibration curve at atmospheric pressure.

5.24 Measurement of displacements and speeds of the product and the augmenting ram

Two identical displacement transducers were used, one for the movement of the augmenting plunger and the other for measuring the displacement of the product. Each transducer comprises a multi-turn slide-wire and a wiper controlled by rack and pinion movement. The slide-wire forms the two arms of the bridge with the wiper separating each position. The other two arms are situated in the recorder console. A coarse potentiometer located within the recorder console may be adjusted to obtain the maximum desirable travel of the transducer within the paper width. A 25 ohms fine potentiometer at the front panel of the recorder console is used to balance the bridge before transducing any movement during the tests.

To measure the displacement of the augmenting plunger, the main body of the transducer was fixed to the yoke and the rack to the cylinder connected to this plunger.

Since the augmenting ram carrying the die is in motion during extrusion, the transducer for measuring the displacement of the extrusion product has to be fixed to the cylinder carrying this plunger. A light Dexion frame was attached to the cylinder and was perpendicular to it lying in the horizontal plane. The transducer was fixed to this frame. One end of the rack was connected to the nose of the billet by a Bowden cable passing over a small pulley at the ram end of the cylinder

and running along the axis of the cylinder: the cable being attached to the nose by a 6BA screw screwed on to it. The other end of the rack was attached to the end of the Dexion frame by springs to keep the cable taut for at least 10 ins of the travel of the product.

This transducer was found to be extremely useful to determine the start of extrusion and thus control it. The trace of the displacement was linear for all practical purposes and the velocity of extrusion may be estimated using the displacement trace and the timing lines on the chart.

5.3 Materials used

It was decided to test two metals with different values of yield strength in billet augmentation. Copper and mild steel in the annealed condition were used in these tests.

For extrusion with the double reduction die aluminium and copper were chosen as ductile metals and an aluminium alloy as a brittle metal.

The copper and aluminium used in all the tests were of the commercially pure quality. The mild steel used is to the specification EN1A. Aluminium, copper and steel were all fully annealed at 210^{o}C, 610^{o}C and 900^{o}C respectively, being soaked for one hour. The aluminium alloy (composition: Si 9.25%, Fe 0.25%, Mn 0.010%, Cu 0.013% and balance Al.) was used as machined from the cast billets. The annealed materials were cleaned of any scale and emery-papered to a constant finish as far as possible. The billets in billet augmented and simple hydrostatic extrusion tests were about 2 ins long with machined noses to fit the corresponding die. For the double reduction die the billets were machined with double noses. The diameters of the billet used

varied from $\frac{1}{2}$ in to $\frac{7}{8}$ in.

The pressure transmitting fluids used were Shell Tellus 27 oil with aluminium and copper and castor oil with mild steel. In the double reduction tests both the fluids were used to assess the effect of each.

5.31 Stress-strain curves for the materials tested

From each material four specimens were obtained of 0.750 ins diameter and lengths of 0.250, 0.375, 0.750 and 1.500 ins. These specimens were annealed as for the extrusion billets and cleaned. Cook and Larke tests were then carried out on these specimens using a 50 tons testing machine. The end faces of the specimens were lubricated with Molyslip (grease) before each loading to reduce friction. Tables 4 and 5 give the heights of the specimens against load for several loads. The true reduction in height for an imaginary infinite specimen with no end effects from friction is obtained by extrapolation as shown in Fig. (35a and b) for copper and mild steel respectively. The true stress-strain curve was then calculated assuming constant volume during deformation and the average diameter thus obtained. The true stress-strain curves for copper and mild steel are given in Fig. (36 a and b) respectively.

5.4 Extrusion Tests

5.41 Billet augmented extrusion

The sub-press, once aligned in position within the yoke was ready for extrusion tests.

The large plunger was detached from the sub-press and the Bourden cable for the displacement transducer threaded through it and through the die and attached to the billet. The billet and the die were placed in the vessel entrance and the plunger attached in position. The cable was kept tight by the springs attached to the rack of the transducer. This kept the die and the billet against the plunger. Then all the instruments were connected to the recorder and the transducers balanced. The large plunger was brought forward in position within the plug at the big end of the bore. The fluid was pumped through the bottom hole in the liner while expelling air through the upper hole. In a few minutes the vessel was completely filled with the fluid. The small plunger was next kept in the correct position so that when the fluid was pressurized to the desired value and the billet was about to be augmented, this plunger was almost at its innermost position within the container. This ensures that the maximum possible length of the billet was extruded. The large plunger was then moved forward and pressurization took place. The small plunger was moved to its innermost position to achieve the desired pressure. Then the large plunger was moved forward whilst the small one was withdrawn keeping the pressure at the desired value using the screw device at the control valve. As the augmenting load was applied by the shoulder of the liner via the load cell and the pads extrusion took place. When the small plunger was about $\frac{1}{2}$ inch from the end of the container the extrusion was stopped and the fluid de-pressurized by withdrawing the large plunger. Then the product was cut off and removed.

During extrusion the movement of the small plunger was indicated by a pointer attached to the corresponding ram. The fluid pressure, augmenting ram movement and the product movement were monitored from the recorder.

In the case of simple hydrostatic extrusion the above experimental procedure applies except that both the plungers may be used to pressurize the fluid during extrusion. The load cell can be removed in this case so as to contain as long a billet as possible.

5.42 Fluid-to-Fluid extrusion

Fluid-to-fluid extrusion is possible with this sub-press and the operating sequence is given below. As shown in Fig.(25) the die with the seals is placed on the shoulder of the liner. A 'solid' plunger with terminals and a manganin coil is substituted for the large plunger. The billet is placed on a support ring with slots to allow the flow of fluid past it, and kept about $\frac{1}{4}$ inch in front of the die. A light spring touches the support ring and extends up a certain distance from the end of the large bore.

First of all, the large plunger is brought in position to fill the vessel with the fluid. The fluid is pumped in and since there is a free passage from the large to the small bore, the fluid fills both bores. The small plunger is kept in the desired position, depending on the extrusion ratio, to ensure the maximum product length of about $4\frac{1}{2}$ inches. Next, the large plunger is moved forward to pressurize the fluid. When this plunger touches the spring any further movement pushes the billet against the die. Once the billet is forced on to the die any further movement of the large plunger seals the large bore from the small bore and the pressure in the large bore will increase, whilst the pressure in the small bore remains at the pressure just before the die was sealed by the billet.

As movement continues the pressure in the large bore is increased and also that in the small bore which has to be less than the

former for the seal at the die-billet interface to remain intact. The pressure in the small bore is kept at the desired value and that in the large one increased until extrusion starts. This start of extrusion is indicated by a rise in pressure in the small bore.

The small plunger is then withdrawn to keep the pressure constant whilst the large plunger is moving forward to extrude the billet. Once the maximum length of product possible is achieved without damaging the manganin coil on the small plunger, both plungers are held stationary. The large plunger is then withdrawn to release the pressures. The die and product can then be removed.

5.43 Tests with the double reduction die

Billets made with double noses, so as to effect an initial seal at the die, were used with the double reduction die. The experimental procedure is the same as for simple hydrostatic extrusion.

5.5 Surface finish measurements

The surface finish of the billet, product and the deforming zone were measured using a Talysurf machine, its stylus being moved along the axis. Fig. (37) shows a record of such surface profiles for extrusion of copper. It is clear from this figure that the surface finish of the product improves with increase in extrusion ratio.

In billet augmented extrusion the surface finish improved with increased augmentation and the surface profile also showed that most of the asperities were smoothened out.

6. RESULTS AND DISCUSSION

6.1 Billet augmented hydrostatic extrusion

Annealed commercially pure copper billets of 0.5 and 0.625 inch diameter were extruded through dies with cone angles of 40°, 60° and 90° to give products of 0.313 inch diameter, i.e. with extrusion ratios of 2.5 and 4 respectively. With mild steel the single extrusion ratio of 2.5 was used through the same three dies. The simple hydrostatic extrusion pressure was determined for each die angle and extrusion ratio, prior to tests with billet augmentation. The fluid pressure was reduced to a fixed value and augmented extrusion carried out. Five tests were performed with each die angle and extrusion ratio and the fluid pressure was reduced in steps so that at the lowest pressure, the extrusion became almost unstable. All the augmented extrusion tests were carried out at approximate product speeds of 1 to 3 ins/min.

The cases of steady extrusion were recognized by the existence of a constant value of augmenting load for a certain fluid pressure. Fig. (38) shows the record of such an augmented extrusion. In the case of unsteady extrusion the augmenting load steadily increased throughout the extrusion. Extrusion was smooth and steady with no peak in the augmenting load or the fluid pressure in the case of augmented extrusion. In simple hydrostatic extrusion the products often tended to come out with large velocities or accompanied with "stick-slip" as shown in Fig. (39).

The fluid pressure, augmenting load, diameter of the bulged billet etc. observed in billet augmented extrusion are given

in Tables 6a,b,c, 7a,b,c and 8a,b,c. Simple hydrostatic extrusion pressures for copper billets with an extrusion ratio of 5.75 are given in Table 9. Table 10 gives these values for mild steel with an extrusion ratio of 4. Variation of augmenting stress with fluid pressure for copper and mild steel billets are given in Figs. (40) and (41) respectively.

It is clear from these results that the reduction in fluid pressure achievable is not equal to the augmenting stress but is in fact much less.

6.11 Estimation of the coefficient of friction in billet augmented hydrostatic extrusion

The total extrusion pressure versus ln R curves are given in Figs. (42, 43 and 44). The simple hydrostatic extrusion pressures in that range of ln R and the modifications for bulged billets are also shown in those figures. Fig. (45) shows the simple hydrostatic extrusion pressure versus die angle for extrusion ratios of 2.5 and 4 for copper billets. Fig. (45) also shows these values for mild steel with an extrusion ratio of 2.5. The coefficients of friction calculated using these tests are given in Tables 11, 12 and 13.

The coefficients of friction calculated in billet augmented extrusion are higher than for simple hydrostatic extrusion - calculated using Evans and Avitzur's formula. There are three possible reasons for these higher values of coefficient of friction, namely:-

1. Due to the initial peak in pressure and the subsequent acceleration of the product to large velocities, lubrication in

simple hydrostatic extrusion may approach hydrodynamic conditions, whereas in billet augmentation the velocity of the product may be too low for hydrodynamic lubrication.

2. Since in billet augmentation the die pressure-fluid pressure difference is larger than in simple hydrostatic extrusion the hydrodynamic forces may not be able to produce an adequate film thickness to overcome this pressure difference.

3. The imposition of the bulge strain and the work-hardening that results will cause this pressure difference to be even higher. This would probably result in break down of the fluid film, if any, causing boundary lubrication with a consequent high coefficient of friction.

6.12 Bulging limit

The variation of augmenting stress with bulge strain in these tests and the stress-strain curves for comparison with these experimental points are shown in Figs. (46, 47) for copper billets and Fig. (48) for steel billets respectively. Also indicated in these figures are the extrusions which were unstable. The limits of bulging obtained by the methods given in the theory are tabulated in Tables 14 and 15 for copper and steel billets respectively. The experimental values of augmenting stress representing unstable extrusion are found to be higher than the values predicted by the theory. This is because the billet bulges rapidly when the augmenting stress is past the limit of bulging. Actual extrapolation of the total extrusion pressure versus ln R curves to obtain the bulging limits in the case of copper shown in Figs. (49)

From the theories of the limit of bulging (sections 4.51.1 and 4.51.2) it is shown that this limit for proportional billet augmentation is always higher than the corresponding limit for constant fluid pressure billet augmentation. But the usefulness of this increased limit is restricted because the stress-strain curve becomes flatter as the stress is increased thus resulting in a large bulge strain which may not be practicable.

6.13 Buckling limit

The initial length of the billets in these experiments in billet augmented extrusion was 2 inches. The billets with $\frac{1}{2}$ in. diameter thus correspond to the highest slenderness ratio, i.e.

$l/r = 8$. Though the length and the diameter of the billets vary as extrusion proceeds, it may be assumed that buckling, if it occurs, starts as the billet is augmented. Thus it may be assumed that $l/r = 8$ for the purpose of calculating the critical buckling stress, S_{CR} Corresponding to $l/r = 8$, the critical buckling stresses S_{CR} for copper and mild steel are 11.3 and 25.0 T/in^2 respectively. In some of the tests with large augmenting stress, the billets buckled with the form shown in Fig. (50). However, most of the extrusions were free from buckling even at large augmenting stresses near the bulging limit. If long billets are to be extruded in billet augmented extrusion then the augmenting stress will be limited to low values as can be seen from Figs. (16a and b). Eccentricity of loading will considerably lower the critical buckling stress that can be sustained by the billet.

6.14 Die stresses due to billet augmentation

In simple hydrostatic extrusion, the die is usually designed so that it receives support from the fluid pressure on the outside. These dies are normally thin walled and serve well for extrusion of most materials and reductions. This is mainly due to the increased pressure support as the extrusion pressure and thus the die stresses are increased.

In billet augmented hydrostatic extrusion, however, the fluid support is diminished and there will be a tendency for the die to fail due to the circumferential tensile stresses. These stresses will be higher with smaller die angles and large augmenting stress/ fluid pressure ratios. In the present series of experiments no die failure occurred due to billet augmenting. This may be partly due to

increased coefficients of friction obtained which reduces the bursting load on the die. However, if large augmenting stress/fluid pressure ratios are used, excessive die stresses may become a serious problem.

6.2 Hydrostatic extrusion with the double reduction die

With reference to Fig. (51), R_1 and R_2 are the extrusion ratios in the first and second reductions respectively. R_2 is fixed by the geometry of the die ($R_2 = 3.23$ in the die used). R_1 may be varied by using billets of different diameters. The first reduction is, if effect, drawing with all round hydrostatic pressure p. The second reduction is hydrostatic extrusion with 'back tension' or negative augmentation (magnitude σ_A). The overall extrusion ratio, $R = R_1 R_2$. Since the intermediate product is in a state of tension depending on R_1, there exists a limit to R_1. For a particular R_2, there is another limit to R_1 due to possible leakage of fluid through the die-metal interface. It can be shown that, approximately, the mean die pressure in the second reduction will be less than the fluid pressure, p if $\sigma_A > p(1 - \frac{R_2-1}{R_2}(1 + \mu\cot\alpha))$.

If we assume the empirical formula $p = a + b \ln R$ to apply to both reductions, then

$$\sigma_A = a + b \ln R_1 \text{ for the first reduction}$$

and $$p - \sigma_A = a + b \ln R_2 \text{ for the second reduction}$$

hence $$p = 2a + b \ln R_1 R_2 = 2a + b \ln R.$$

It appears from the above equation that the extrusion pressure would be higher than that with a simple die for the same extrusion ratio R. But 'a' and 'b' are in general dependent on the redundant work and friction. Though the redundant work is increased by the use of two

reductions, the friction may be reduced. Thus the extrusion pressure under certain conditions may be lower than that with a simple die.

Lubrication at the first reduction is excellent because of the presence of high pressure fluid at both ends of the die. In all the tests with this die the surface of the intermediate product had no signs of touching the die during deformation. The machining marks on the billet were preserved and it appeared as if it was stretched in tension. This is positive evidence of the existence of a fluid film (hydrodynamic lubrication).

Lubrication at the second reduction is better than that possible with a simple die, because of:

a. possible deformation of the billet before touching the die caused by back tension.

b. the interface pressure being reduced by the application of back tension.

Commercially pure aluminium and copper billets of diameters 0.625, 0.688, 0.715, 0.750 and 0.813 inches were extruded using (i) Tellus 27 oil (ii) castor oil as the pressurizing fluid. Hydrostatic extrusion tests with a simple die (included angle 40°) for all the diameters and the fluids were also conducted. The results of these tests are given in Tables 16 and 17 and plotted in Figs. (52) and (53) for aluminium and copper respectively. With a cast aluminium alloy (composition: Si 9.25%, Fe 0.25%, Mn 0.01%, Cu 0.013% and balance Al), billets of diameters 0.625 and 0.688 were used with the simple and double reduction dies with both the fluids. The results of these tests are given in Table 18. The double reduction die gave no significant change in the brittle nature of the products obtained from hydrostatic extrusion of this material.

For aluminium and copper billets, with reference to Figs. (52 and 53), the following observations were made:

1. The extrusion pressure was higher than that using a simple die, at small R_1.

2. At larger R_1, the extrusion pressure was lower than that using a simple die.

3. At still higher R_1, the fluid started leaking at a certain pressure.

As R_1 is gradually increased, contact with the die in the second reduction was reduced with more free deformation of the intermediate product, and at large R_1 the billet in the second reduction curved in to touch the die near the die throat Fig. (59). This effect was observed to be more pronounced with castor oil than with Tellus 27 as the pressuring medium. More and more surface marks were retained in the final product as R_1 was increased.

Thus, as expected, reduction in friction and increase in redundant work were obtained in the experiments with the double reduction die. For harder materials like steel etc., this die may be useful in reducing friction and possible "stiction" to the die. Since the reductions are separate and the fluid pressure support is higher than obtainable in simple hydrostatic extrusion of the two reductions separately, the fluid pressure support to this die is better than with a simple die. Hence this die may be used in billet augmented extrusion to offset the reduction in fluid pressure support caused by augmenting. Also this die may help reduce the high coefficients of friction encountered in billet augmented extrusion with a simple die.

Since there is enhanced fluid film lubrication the double

reduction die should give increased die life. In practice, instead of a single double reduction die two separate dies may be used with provision for high pressure fluid to enter the second reduction.

6.3 Theories of hydrodynamic lubrication in hydrostatic extrusion

6.31 Rigid plastic material analysis

From equation 25 of section 4.61, the term containing U_1 may be neglected for small U_1, η_o, γ and large α and billet diameter. Then the driving stress is given by

$$(p_A + \sigma_A + \sigma_p - p_3) = \sigma \ln R + \frac{1}{\gamma} \ln\left[1 + \frac{2(R^{\frac{3 - 2G}{2}} - 1)}{3(3 - 2G)}(e^{\gamma(\sigma_A + \sigma)} - 1)\right]$$

In the case of simple hydrostatic extrusion when $\sigma_A = \sigma_p = p_3 = 0$ and $p_A = p$,

$$p = \sigma \ln R + \frac{1}{\gamma} \ln\left[1 + \frac{2(R^{\frac{3 - 2G}{2}} - 1)}{3(3 - 2G)}(e^{\gamma\sigma} - 1)\right]$$

Therefore the frictional component of extrusion pressure is a function of γ, R and σ.

This rigid-plastic analysis is not adequate for an annealed material which rapidly work hardens from a low value of yield stress in the initial stages of deformation. The film thickness calculated would be too small because a mean yield stress has to be assumed in this theory instead of the initial value. However this will serve for materials which are work-hardened, with a flat stress-strain curve.

6.32 Work-hardening material analysis

Equation 40 of section 4.62 gives the frictional component of the driving stress for a work-hardening material. If the term containing U_1 is neglected for small U_1 and large billet diameter, then

$$p_{FD} = \frac{1}{\gamma} \ln \left[1 + e^{\gamma \frac{n+1}{n}(H - \sigma_o)} \cdot (e^{\gamma(\sigma_A + \sigma_o)} - 1) \cdot \left\{ \sum_{j=0}^{\infty} \frac{(-1)^j \left(\gamma(H - \sigma_o)\frac{(n+1)}{n}\right)^j}{\left(\frac{2\gamma H - 3}{2n} + j\right) \underline{/j}} \cdot (1 - R^{3/2} - \gamma H - nj) \right\} \right]$$

Equation 41 of secion 4.63, modified for redundant shear at entrance and exit gives

$$(p_A + \sigma_A + \sigma_p - p_3) = \int_o^{\epsilon_3} \sigma d\epsilon + p_{FD}$$

where $\epsilon_3 = \ln R + 4/3 \tan\alpha/2$

p_{FD} can be calculated for a material by fitting an approximation $\sigma = \sigma_o + (H - \sigma_o)(1 - e^{-n\epsilon})$ to the stress strain curve.

$\int_o^{\epsilon_3} \sigma d\epsilon$ is obtained by the integral of the stress strain curve up to ϵ_3:

For annealed copper, $\sigma = 3.0 + (25.4 - 3)(1 - e^{-3.8\epsilon})$ T/in^2

The simple hydrostatic extrusion pressure for copper for various α and R were calculated using a computer and plotted in Fig. (54). This theory of hydrodynamic lubrication does not give an optimum die angle for extrusion with an extrusion ratio R. This is perhaps due to the effect of velocity not being taken fully into account while extrusions with different die angles may be accompanied

by different velocities. Also there is a possibility that there exists mixed lubrication at certain die angles. However, in the following section an attempt is made to determine the velocity associated with simple hydrostatic extrusion, using a different approach.

The theoretical pressure distribution along the die derived from work hardening material analysis for extrusion of copper at an extrusion ratio of 3 and die angle of 45^{o} is given in Fig. (55).

Fig. (56) shows the theoretically predicted variation of total extrusion pressure with billet augmenting stress for extrusion with an extrusion ratio of 2.5, for copper billets. The effect of bulging is included fully (cf Appendix V).

In all these calculations of hydrodynamic lubrication the fluid properties were taken as those of castor oil whose coefficient of viscosity and the pressure coefficient of viscosity are known;

$$\eta_o = 1.13 \times 10^{-7} T/in^2 sec$$

$$\gamma = 0.112\ in^2/ton$$

The effect of size is predicted by equation 40 of section 4.62. Assuming a billet velocity of 100 ins/sec the size effect calculated for copper billets for an extrusion ratio of 4 is shown in Fig. (57).

6.33 Numerical analysis including the possible deformation of the billet in the inlet zone

In this method the lubricant flow rate and the film thickness at the die throat may be determined by using the elastic

deformation of theproduct in the die land region. Thus, assuming a certain billet velocity, these two quantities were determined and integration of the equations given in section 4.63 was made taking increments along the die surface. Thus the film thickness, the pressure and the shear stress at any point are determined by iterations using the values at the previous point. The shear stress and the pressure components resolved along the axis were also integrated simultaneously to give the driving load and thus the driving stress. Thus the driving stress and the fluid pressure at the entrance to the die were obtained. The film thickness increases almost linearly from the die throat to the die entrance, but near the die entrance the film thickness starts increasing rapidly to large values. In simple hydrostatic extrusion the driving stress is equal to the extrusion pressure. Therefore the velocity of the billet is changed and the procedure repeated until both are equal. The fluid pressure, shear stress and film thickness along the die for a die angle of 20° and extrusion ratio of 4 is shown in Fig. (58) for copper billets in simple hydrostatic extrusion. The velocity of simple hydrostatic extrusion thus calculated is 52.5 ins/sec for the extrusion of copper with extrusion ratio 4 and die angle 20°.

This method of analysis associates a certain velocity with the external stress system, (σ_A, σ_p, p_A, p_3), whereas the previous methods in sections 4.61 and 4.62 do not. This method also gives larger film thickness compared to the previous ones because a different method of obtaining the die throat film thickness is used.

The computer programme for these calculations is given in Appendix III.

7. SUGGESTIONS FOR FURTHER WORK

If the usefulness of the billet augmented hydrostatic extrusion process is to be fully exploited harder metals must be tested. Materials with flow stresses as high as 90 T/in^2 could be extruded with increased extrusion ratios which would be attractive if achievable with the fluid pressure of 100 T/in^2 available. These materials will also bring the problem of excessive die stresses which were not encountered in the present series of tests. To decrease the high values of coefficient of friction found in billet augmentation and to reduce the excessive die stresses the double reduction die designed and used in these experiments may be used.

The principle of imposing fluid pressure between two reductions may be tested by designing double reduction dies with different angles for the two reductions and with different second reductions R_2. This die may also be used with hard materials to test for any reduction in extrusion pressure possible.

This die may be used with product augmentation to inhibit heavy leakage of fluid at large extrusion ratio R_1 and, perhaps, obtain lower coefficients of friction in product augmentation at low speeds. Since this die needs double nosed billets this operation may not be wasteful if the tag, formed from this part with the maximum fluid pressure available, is utilized for product augmentation.

It is improbable that hydrodynamic lubrication exists in hydrostatic extrusion at low speeds. Thus it is desirable to know the effect of fluid pressure on the coefficient of friction in these cases. To simulate these conditions the ring test devised by Male and Cockcroft [72] could be used.

For this purpose the loading device used in the calibration of the load cell under pressure may be used. In this case the load cell is replaced by the ring specimen to be deformed. The procedure would be almost the same as for the calibration of the load cell except that the measurement of the load is not essential, it being necessary simply to measure the amount of deformation imposed. Only the fluid pressure need be determined accurately. In the present loading device a difference of about 9 T/in^2 is needed to impose a load of 1 Ton. To test stronger materials a larger piston and cylinder loading device would be required.

8. CONCLUSIONS

The billet augmented hydrostatic extrusion process is found to be stable with no stick-slip and velocity instability. The coefficient of friction is, however, found to increase with augmenting stress. The limit of bulging is predicted satisfactorily from the theory. Due to bulging and the increase in coefficient of friction the billet augmenting stress is not fully available for reducing the fluid pressure required in augmented extrusion. Particularly for soft metals the reduction in fluid pressure is not appreciable. However for hard metals with rapid work-hardening characteristics there is a quite significant reduction in the fluid pressure needed. The limitation due to buckling cannot be ignored at high levels of augmentation if substantial lengths of billet are to be extruded. Here again a rapidly work-hardening stress-strain curve would give a higher limit of buckling.

The double reduction die experiments indicate that hydrodynamic lubrication can be enhanced by this die and at certain 'first reductions', depending on the material, significant reduction in pressure could be achieved with hard materials which exhibit high friction with a simple die. This die would also decrease die wear and thus increase die life. Also because of the increased die support by fluid pressure it may be useful for billet augmented extrusion thereby minimising the possibility of breakage of the die due to increased die stresses caused by augmenting. Also it can help reduce friction in billet augmented extrusion.

Section 4.61, 4.62 and 4.63 of the hydrodynamic lubrication theory proposed predict the extrusion pressure in hydrostatic extrusion processes quite satisfactorily. Section 4.64, as opposed to sections

4.61, 4.62 and 4.63 predicts that there is a certain velocity associated with the parameters of extrusion (p_A, σ_A etc.). The high velocities encountered in simple hydrostatic extrusion are, perhaps, explained by this theory.

REFERENCES

1. PUGH, H.Ll.D., Recent developments in cold forming, The Bulleid Memorial Lectures, Vol. IIIB, 1965, Univ. of Nottingham.
2. LOW, A.H. and DONALDSON, C.J.H., An investigation of speed instability in hydrostatic extrusion, NEL Report, May 1967.
3. DUFFILL, A.W., HOOKE, C.J. and MELLOR, P.B., Design of straight conical dies for hydrostatic extrusion, 9th Int. M.T.D.R. Conf., Univ. of Manchester, Sept. 1968.
4. DUFFILL, A.W. and MELLOR, P.B., A comparison between the conventional and hydrostatic methods of cold extrusion through conical dies, C.I.R.P., Sept. 1968.
5. KAMYAB, S., Private communication, Imperial College.
6. FIORENTINO, R.J., RICHARDSON, B.D. and SABROFF, A.M., The role of die design and residual stress formation in the hydrostatic extrusion of brittle materials, ASTME, MF69-169, 1969.
7. HORNMARK, Nils, Lecture 21, Post-Experience Course - Hydrostatic Extrusion, Dept. of Mechanical Engineering, Imperial College, London, July 1969.
8. LENGYEL, B., BURNS, D.J. and PRASAD, L.V., Design of containers for a semi-continuous hydrostatic extrusion production machine, Proc. 7th Int. M.T.D.R. Conf., p. 319-314, 1967.
9. WILSON, W.R.D. and SKELTON, W.J., Design of high pressure cylinders, High Pressure Engineering Conference, Proc.I.Mech.E., Vol. 182, Part 3C, p. 1, 1967-68.
10. HARVEY, D.C. and LENGYEL, B., Pressure vessels under cyclic loading: test rig and initial results, 9th Int. M.T.D.R. Conf., Sept. 1968.
11. GERDEEN , J.C. and FIORENTINO, R.J., Analysis of several high pressure container concepts, Proc.I.Mech.E., Vol. 182, Part 3C,

p.11, 1967-68.

12. GREEN, D., Automatic 1600 Tons hydrostatic extrusion press, Lectures 17 and 18, Post-Experience Course - Hydrostatic Extrusion, Dept. of Mechanical Engineering, Imperial College, July 1969.

13. ALEXANDER, J.M. and LENGYEL, B., Semi-continuous hydrostatic extrusion of wire, Proc.I.Mech.E., Vol. 180, Part 3I, 1965-66.

14. LENGYEL, B. and ALEXANDER, J.M., Design of a production machine for semi-continuous hydrostatic extrusion, Proc.I.Mech.E., Vol. 182, Part 3C, p. 207, 1967-68.

15. LENGYEL, B. and ASHFORD, P.G., An experimental pre-production unit for semi-continuous hydrostatic extrusion, 8tn Int. M.T.D.R. Conf. Sept. 1967, p. 993, Univ. of Manchester, Pergamon Press.

16. PUGH, H.Ll.D., On intermittent (semi-continuous) hydrostatic extrusion machine, NEL Report No. 344, Feb. 1968.

17. LENGYEL, B. and CULVER, L.E., Properties of materials extruded by orthodox hydrostatic extrusion, J. Inst. of Metals, Vol. 97, p. 97, 1969.

18. BERESNEV, B.I., VERESHCHAGIN, L.F., RIABININ, YU. N. and VIVSHITS, L.D., Some problems of large deformation of metals at high pressures, 1963, Pergamon Press.

19. HERØ, H. and MIKKELSEN, J.A., Some mechanical and structural properties of hydrostatically extruded aluminium alloys, J. Inst. Metals, Vol. 97, p. 18, 1969.

20. PUGH, H.L.D., The mechanical properties and deformation characteristics of metals and alloys under pressure, Int. Conf. on Materials, A.S. Test. Mater, Feb. 1964.

21. KUDO, H., Some analytical and experimental studies of axi-symmetric cold forging and extrusion I, Int. J. Mech. Sci. Vol. 2, p. 102, 1960.

22. KOBAYASHI, S., Upper-bound solutions of axi-symmetric forming problems - II, Trans. A.S.M.E. J. Engineering for Industry, 1964, Vol. 86, p. 326.

23. AVITZUR, B., Analysis of wire-drawing and extrusion through conical dies of small cone angles, J. Engineering for Industry, Trans. A.S.M.E., Vol. 89, Feb. 1963.

24. AVITZUR, B., Analysis of wire-drawing and extrusion through conical dies of large cone angles, Trans. A.S.M.E., J. Engineering for Industry, Vol. 86, p. 305-316, 1964.

25. AVITZUR, B., Strain hardening and strain rate effects in plastic flow through conical dies.

26. HALLING, J. and MITCHELL, L.A., Upper-bound solution for axi-symmetric extrusion, Int. J. Mech. Sci. Vol. 7, p. 277, 1965.

27. LAMBERT, E.R. and KOBAYASHI, S., A theory on the mechanics of axisymmetric extrusion through conical dies, J. Mech. Engineering Sci. Vol. 10, No. 5, p. 367, 1968.

28. LAMBERT, E.R. and KOBAYASHI, S., An approximate solution for the mechanics of axisymmetric extrusion, 9th Int. M.T.D.R. Conf. Sept. 1968, Univ. of Manchester.

29. LAMBERT, E.R., MEHTA, H.S. and KOBAYASHI, S., A new upper-bound method for analysis of some steady-state plastic deformation processes, Trans. A.S.M.E. J. of Engineering for Industry Vol. August 1969, p. 731.

30. HOFFMAN, O. and SACHS, G., Introduction to the theory of plasticity for engineers, Mc.Graw-Hill, 1953, p. 163, 177.

31. PUGH, H.Ll.D, Redundant work and friction in the hydrostatic extrusion of pure aluminium and an aluminium alloy, J. Mech. Eng. Sci., Vol. 6, No. 4, 1964. p. 362.

32. SHABAIK, A. and KOBAYASHI, S., Computer application to the visioplasticity method, Trans. A.S.M.E., J. Engineering for Industry, May 1967, p. 339.

33. SHABAIK, A., LEE, C.H. and KOBAYASHI, S., Application of the visioplasticity method to extrusion through a conical die, 7th Int. M.T.D.R. Conf., Sept. 1966, Birmingham.

34. SHABAIK, A. and THOMSEN, E.G., A theoretical method for the analysis of metal working problems, Trans. A.S.M.E., J. Engineering for Industry, May 1968, p. 343.

35. SHABAIK, A.H. and THOMSEN, E.G., Friction studies by the visioplasticity method, 9th Int. M.T.D.R. Conf., Sept. 1968, Birmingham.

36. ATKINS, A.G., Consequences of high strain rates in cold working, J. Inst. Metals, Vol. 97, p. 2538, 1969.

37. BERESNEV, B.I., BULYCHEV, D.K. and RODIONOV, K.P., Features of the process of extruding metals with high pressure liquid at elevated temperatures, Fiz. Metal. Metalloved, 11, No. 1, p. 115-121, 1961.

38. ALTAN, T. and KOBAYASHI, S., A numerical method for estimating the temperature distributions in extrusion through conical dies, Trans. A.S.M.E., J. Eng. for Industry, Feb. 1968, p. 107.

39. LOW, A.H., DONALDSON, C.J. and WILKINSON, P.T., Developments in hydrostatic extrusion at the National Engineering Laboratory, Proc.I.Mech.E., 1967-68, Vol. 182, Part 3C, p. 188 and p. 340 (discussion).

40. LOWE, B.W.H. and GOOLD, D., An account of some recent experimental work on the hydrostatic extrusion of non-ferrous metals, Conf. on High Pressure Eng., Sept. 1967, Proc.I.Mech.E., 1967-68, Vol. 182, Part 3C, p. 197 and (discussion p.341).

41. AVITZUR, B., High Pressure Eng. Conf. 1967, Proc.I.Mech.E.,

Vol. 182, Part 3C, - Discussion, p. 295.

42. LOWE, B.W.H. and GOOLD, D., Ibid, 1967, Discussion - p. 342.

43. THOMPSON, P.J., The hydrostatic extrusion of steel, M.Sc. Thesis, The Univ. of Aston in Birmingham, 1968.

44. SLATER, H.K. and GREEN, D., Augmented hydrostatic extrusion of continuous bar, Proc.I.Mech.E., Vol. 182, Part 3C, 1967-68, p. 217.

45. THOMPSON, P.J., Hydrostatic extrusion of steel, 9th Int. M.T.D.R. Conf. Sept. 1968, Univ. of Manchester, Pergamon Press.

46. PARSONS, B., BRETHERTON, D. and COLE, B.N., A preliminary investigation of the combined hydrostatic extrusion and drawing process, 9th Int. M.T.D.R. Conf., 1968, Univ. of Manchester, Pergamon Press.

47. RICHARDSON, B.D., FIORENTINO, R.J. and SABROFF, A.M., Comparison of hydrostatic and conventional methods of extrusion and drawing, A.S.T.M.E., MF 68-217, 1968.

48. SABROFF, A.M. and FIORENTINO, R.J., Discussion on High Pressure Eng. Conf., Sept. 1967, Proc.I.Mech.E., 1967-68, Part 3C, p. 328.

49. CHRISTOPHERSON, D.G. and NAYLOR, H., Promotion of fluid lubrication in wire drawing, Proc.I.Mech.E., Vol. 169, p. 643-653, 1955.

50. TATTERSALL, G.H., Hydrodynamic lubrication in wire drawing, J.Mech.Engineering Sci., Vol. 3, No. 4, 1961, p. 378.

51. OSTERLE, J.F. and DIXON, J.R., Viscous lubrication in wire drawing, Trans. A.S.L.E. 5, 1962, p. 233-241.

52. BEDI, D.S., A hydrodynamic model for wire drawing, Int. J. Prod. Res., Vol. 6, No. 4, 1968, p. 329.

53. WISTREICH, J.G., Investigation of the mechanics of wire drawing, Proc.I.Mech.E., Vol. 169, 1955, p. 654-670.

54. ROZNER, A. and FAUPEL, J.H., Some considerations of the mechanics of hydrostatic extrusion, J. of the Franklin Institute, No. 277,

p. 217, 1964.

55. HILLIER, M.J., Hydrodyanmic model of hydrostatic extrusion, Int. J. Prod. Res., Vol. 5, No. 2, p. 171, 1966.

56. IYENGAR, H.S.R. and RICE, W.B., Lubrication in hydrostatic extrusion, C.I.R.P., Sept. 1968.

57. WILSON, W.R.D., and WALOWIT, J.A., An isothermal hydrodynamic lubrication theory for hydrostatic extrusion and drawing process with conical dies, Battelle Memorial Institute, 1969.

58. LENGYEL, B., Ph.D. Thesis, University of London, 1965.

59. WHITLOCK, B.C., Ph.D. Thesis, University of London, 1968.

60. ADIE, J.F. and ALEXANDER, J.M., A graphical method of obtaining hodographs for upper-bound solutions to axi-symmetric problems, Int. J. Mech. Sci., Vol. 9, p. 349-357, 1967.

61. SHIELD, R.T., Plastic flow in a converging conical channel, J. Mechanics and Physics of Solids, Vol. 3, p. 246-258, 1955.

62. EVANS, W. and AVITZUR, B., Measurement of friction in drawing, extrusion, and rolling, Trans. A.S.M.E., Vol. 90, Series F(1), 72-80, 1968.

63. HILL, R., Mathematical theory of plasticity, The Oxford University Press, 1967.

64. JOHNSON, W. and MELLOR, P.B., Plasticity for mechanical engineers, D. Van Nostrand Co., 1966.

65. PUGH, H.Ll.D. and GUNN, D.A., A strain gauge load cell for use under high hydrostatic pressure, Proc.I.Mech.E., Vol. 182, Part 3C, 1967-68.

66. BRANDES, M., A method of recording the full load extension curve while studying mechanical properties of materials under hydrostatic pressures up to 30,000 kg/cm^2, Ibid, Vol. 182, Part 3C, 1967-68.

67. CLOUGH, W.R., SHANK, M.E. and ZAID, M., The behaviour of SR-4 wire resistance strain gauges on certain materials in the presence of hydrostatic pressure, Proc. Soc. Exper. Stress Analysis, Vol. 10(2), p. 167, 1953.

68. MILLIGAN, R.V., The effects of high pressure on foil strain gauges, Exper. Mech. Vol. 4(2), p. 25, 1964.

69. MILLIGAN, R.V., The gross hydrostatic pressure effect as related to foil and wire strain gauges, Ibid, Vol. 7, Feb. 1967.

70. BRACE, W.F., On the effect of pressure on electric-resistance strain gauges, Ibid, Vol. 4(7), p. 212, 1964.

71. VORONOV, F.F. and VERESHTCHAGIN, L.F., The influence of hydrostatic pressure on the elastic properties of metals, 1. Experimental Data (Translation), Fiz. Metal. Metalloved, Vol. 11, No. 3, p. 443-450, 1961.

72. MALE, A.T. and COCKCROFT, M.G., A method for the determination of the coefficient of friction of metals under conditions of bulk plastic deformation, J. Inst. Metals, Vol. 93, p. 38, 1964-65.

73. ZIMMERMAN, Z. and AVITZUR, B., Metal flow through conical converging dies - a lower upper-bound approach using generalised boundaries of the plastic zone, Trans. A.S.M.E., J. of Engineering for Industry, Feb. 1970, p. 119.

74. FUCHS, Contribution to the Conference on High Pressure, Aviemore, May 1970.

75. GREEN, D., Private communication.

ACKNOWLEDGMENT

The author wishes to express his sincere thanks to Professor J.M. Alexander for much helpful advice and encouragement throughout the investigation.

He acknowledges helpful discussions with Dr. B. Lengyel, Mr. S. Kamyab and Mr. P.G. Ashford; the technical assistance given by the staff of the metal working laboratory and the valuable assistance given by Mr. J.H. Pooley in the experimental work.

The author is grateful to the Ceylon Government for awarding the Government University Scholarship which enabled him to carry out this work.

LIST OF FIGURES

TABLES

Appendix I

An expression for redundant work in axi-symmetric extrusion using parabolic boundaries

Referring to Fig. (8), the velocity discontinuity,

$$V^* = \frac{U_1 \sin\theta}{\sin(\theta+\varphi)} \quad \text{at the entrance to the die.} \qquad 1.$$

Assuming the equation to the parabolic boundary to be;

$$r^2 = -A\,(z - z_1)$$

$$r_1^2 = -A\,(r_1/\tan\alpha - z_1) \quad \text{from geometry} \qquad 2.$$

$$\therefore \quad (r^2 - r_1^2) = -A\,(z - r_1/\tan\alpha) \quad \text{Equation to the parabola.} \qquad 3.$$

$$\text{and } 2r\frac{dr}{dz} = -A \qquad 4.$$

$$\tan\varphi = -\frac{dr}{dz} = A/2r \quad \text{from Equation 4.}$$

also $\tan\theta = r/z$ from geometry.

Hence the redundant shear work expended at the entrance to the die,

$$\frac{dW}{dt} = \int_0^{r_1} 2\pi r k V^* ds.$$

$$= 2\pi k \int_0^{r_1} \frac{r U_1 \sin\theta}{\sin(\theta+\varphi)} \cdot \frac{dr}{\sin\varphi}$$

$$= 2\pi k U_1 \int_0^{r_1} \frac{r^2(A^2 + 4r^2)\,dr}{A(r^2 + Az_1)}$$

$$= \frac{8\pi k U_1}{A}\left[\int_0^{r_1} r^2 dr + \left(\frac{A^2}{4} - Az_1\right)\left\{\int_0^{r_1} dr - Az_1 \int_0^{r_1} \frac{dr}{(r^2+Az_1)}\right\}\right]$$

$$= \frac{8\pi k U_1}{A}\left[\frac{r_1^3}{3} + \left(\frac{A^2}{4} - Az_1\right)\left(r_1 - \sqrt{Az_1} \cdot \tan^{-1}\frac{r_1}{\sqrt{Az_1}}\right)\right]$$

Substituting for z_1, we get

$$\frac{dw}{dt} = 8\pi kU_1\left[\frac{-2r_1^3}{3A} - \frac{r_1^2}{\tan\alpha} + \frac{Ar_1}{4} + \left(\frac{r_1^2}{4} + \frac{r_1}{\tan\alpha} - \frac{A}{4}\right)\sqrt{\frac{r_1 A}{\tan\alpha} + r_1^2} \cdot \tan^{-1}\right.$$

$$\left.\frac{r_1}{\sqrt{\frac{r_1 A}{\tan\alpha} + r_1^2}}\right]$$

$$= 8\pi kU_1 r_1^2\left[\frac{-2r_1}{3A} - \frac{1}{\tan\alpha} + \frac{A}{4r_1} + \left(\frac{r_1}{A} + \frac{1}{\tan\alpha} - \frac{A}{4r_1}\right)\sqrt{1 + \frac{A}{r_1\tan\alpha}} \cdot \tan^{-1}\right.$$

$$\left.\frac{1}{\sqrt{1 + \frac{A}{r_1\tan\alpha}}}\right]$$

Let $r_1/A = x$

Then

$$\frac{dw}{dt} = 8\pi kU_1 r_1^2\left[\frac{-2x}{3} - \frac{1}{\tan\alpha} + \frac{1}{4x} + \left(x + \frac{1}{\tan\alpha} - \frac{1}{4x}\right)\sqrt{1 + \frac{1}{x\tan\alpha}} \cdot \tan^{-1}\right.$$

$$\left.\sqrt{\frac{1}{1 + \frac{1}{x\tan\alpha}}}\right]$$

Hence $\frac{p_{RI}}{2k} = \frac{dw/dt}{(\pi r_1^2 U_1)2k}$

$$= 4\left[\frac{-2x}{3} - \frac{1}{\tan\alpha} + \frac{1}{4x} + \left(x + \frac{1}{\tan\alpha} - \frac{1}{4x}\right)\sqrt{1 + \frac{1}{x\tan\alpha}} \cdot \tan^{-1}\sqrt{\frac{1}{1 + \frac{1}{x\tan\alpha}}}\right]$$

The minimum value of this expression may be obtained using a computer. It can be shown, as follows, that the same expression would result for exit boundary, for the kinematically admissible field chosen. For kinematic admissibility of the entrance and exit parabolae; $\frac{r_1}{r_2} = \frac{r}{r'} = \frac{z}{z'}$

Substituting for r and z in equation 3, we get the equation to the exit boundary as;

$$\left(\frac{r_1^2 \cdot r'^2}{r_2^2} - r_1^2\right) = -A\left(\frac{r_1}{r_2} z' - r_1/\tan\alpha\right)$$

i.e.

$$(r'^2 - r_2^2) = -A \frac{r_2}{r_1}(z' - r_2/\tan\alpha)$$

i.e.

$$(r'^2 - r_2^2) = -A'(z' - r_2/\tan\alpha)$$

This equation is of the same form as the previous one except for A'. Therefore it will give the same minimum value for $\frac{p_{R2}}{2k}$ as $\frac{p_{R1}}{2k}$

Appendix II

$$I = \int X^{I_2-4} \cdot e^{-\frac{I_1}{2n} X^{2n}} \cdot dX$$

Let $\frac{I_1}{2n} = b$; $X^{2n} = t$; $(\frac{I_2-3}{2n} - 1) = a$

Then $I = \frac{1}{2n} \cdot \int t^a \cdot e^{-bt} \cdot dt$

Since the sign of a is not known beforehand and need not be an integer, the integration is performed in series.

$$I = \frac{1}{2n} \int (t^a - \frac{bt^{a+1}}{1!} + \frac{b^2t^{a+2}}{2!} - \cdots + \frac{(-1)^r b^r t^{a+r}}{r!} + \cdots)dt$$

$$= \frac{1}{2n} [\frac{t^{a+1}}{a+1} - \frac{bt^{a+2}}{(a+2)\ 1!} + \frac{b^2t^{a+3}}{(a+3)\ 2!} - \cdots + \frac{(-1)^r b^r t^{a+1+r}}{(a+1+r)\ r!} + \cdots]$$

$$= \frac{t^{a+1}}{2n} [\frac{1}{a+1} + \sum_{r=1}^{\infty} \frac{(-1)^r (bt)^r}{(a+1+r)\ r!}]$$

$$= \frac{X^{I_2-3}}{2n} [\frac{2n}{I_2-3} + \sum_{r=1}^{\infty} \frac{(-1)^r b^r X^{2nr}}{(\frac{I_2-3}{2n} + r)\ r!}]$$

$$= X^{I_2-3} [\sum_{r=0}^{\infty} \frac{(-1)^r (\frac{I_1}{2n})^r X^{2nr}}{(\frac{I_2-3}{2n} + r)\ r!}] \quad , \ r + \frac{I_2-3}{2n} \neq 0$$

If $r + \frac{I_2-3}{2n} = 0$ then the r^{th} term in the bracket tends to ∞, but this could be avoided by taking the limit in equation 38 of section 4.62, thus

$$\text{Lt}_{\frac{2\gamma H-3}{2n} + r \to 0} \frac{1 - R^{(3/2 - \gamma H - nr)}}{(\frac{2\gamma H - 3}{2n} + r)} = -n \ln R.$$

APPENDIX III COMPUTER PROGRAMME FOR THE NUMERICAL ANALYSIS OF HYRRODYNAMIC LUBRICATION(SECTION 4.64).

```
$IBFTCMAIN
C              HYDRODYNAMIC  LUBRICATION  IN  HYDROSTATIC  EXTRUSION
C              FOR A WORK-HARDENING MATERIAL ALLOWING FOR
C              DEFORMATION OF THE BILLET IN THE INLET ZONE
C-------------------------------------------------------------------
C                LISTING
C-------------------------------------------------------------------
C          MOST CONSTANTS AND VARIABLES RETAIN THEIR ORIGINAL NAMES
C            AS GIVEN IN THE THESIS
C       THE NAMES WHICH ARE DIFFERENT ARE IDENTIFIED AS FOLLOWS
C       HH=H. FN=N. V=POISSON.S RATIO. XL =L. RDASH=P3. T=SIGMA.XMUO=ETAO.
C       XK=K. EXTRUSION PRESSURE=PA. DRIVING STRESS=(PA+SIGMAA+SIGMAP-P3)
C-------------------------------------------------------------------
        COMMON SIGMA.GAMMA.D2.V.E.U2.XL.R.XMUO.XK.P2.X2.THETA
        COMMON H2.NN.RDASH.T
C-------------------------------------------------------------------
        FTAU(P.H.D) = (U2*(XMUO/H))*EXP(GAMMA*P)*((D2/D)**2)-(H/2.)*DPDX2
        DPDX(X.TAU)=(2./X)*(SIGMA + TAU/TAN(THETA))
C       MATERIAL CONSTANTS    AND OTHER DATA
        SIGMAO = 3.
        HH = 25.4
        FN = 3.8
        GAMMA = .112
        D1 = 1.00
        V = 0.285
        E = 8500.0
        XL = 0.125
        R = 4.0
        RDASH = 0.0
        T = 0.0
        XMUO = 1.130*10.**(-7)
        ALPHA = 10.
C-------------------------------------------------------------------
C     DETERMINATION  OF  THE  FILM  THICKNESS  AT  THE  DIE  THROAT  AND
C     THE  LUBRICANT  FLOW  RATE
C------ --------------------------------------------------------------
        WRITE(6.03001)ALPHA
03001 FORMAT(1X.6HALPHA=.F9.4)
        THETA = ALPHA*0.01745
        D2 = D1/SQRT(R)
        X2 = D2/(2.*SIN(THETA))
        X1 = X2*SQRT(R)
        XK = D2*(1.-V)/(2.*E)
        SIGMA = SIGMAO + (HH-SIGMAO)*(1.-(D2/D1)**(2.*FN))
        P2 = SIGMA + RDASH - T
        U1 = 52.5
        WRITE(6.3000)U1
03000 FORMAT(1X.3HU1=.F12.4)
        U2 = U1*R
        NN = 0
        H2 = 5.*10.**(-4)
00003 CONTINUE
        CALL PRO(FQH1.Q)
        Q2 = Q
        H2 = H2 + (10.**(-4))/2.
```

```
      CALL PRO(FQH2,Q)
      Q3 = Q
      IF(((FQH1.LE.0.).AND.(FQH2.GE.0.)).OR.((FQH1.GE.0.).AND.(FQH2.LE.0
     1.))) GO TO 4
      GO TO 3
00004 H2 = H2 - (10.**(-4))/2.
00013 CONTINUE
      CALL PRO(FQH1,Q)
      Q2 = Q
      H6 = H2
      H2 = H2 + (10.**(-5))/4.
      H5 = H2
      CALL PRO(FQH2,Q)
      Q3 = Q
      IF(((FQH1.LE.0.).AND.(FQH2.GE.0.)).OR.((FQH1.GE.0.).AND.(FQH2.LE.0
     1.))) GO TO 5
      GO TO 13
C****** NEWTON.S ITERATION FOR THE SIMULTANEOUS EQUATIONS *********
C****** G(Q,H) = 0 , F(Q,H) = 0 ***********************************
00005 H2 = H2 - (10.**(-5))/8.
      CALL PRO(FQH,Q)
00008 G = Q+D2*(U2*H2/2.+(EXP(-GAMMA*P2)/(6.*X2*XMUO))*(((SIGMA*H2)*H2)*
     1H2+(XMUO*U2*EXP(GAMMA*P2)*H2)*H2/TAN(THETA)))
      GDASHH= D2*(U2/2.+(EXP(-GAMMA*P2)/(6.*X2*XMUO))*((3.*SIGMA*H2)*H2+
     1(2.*XMUO*U2*EXP(GAMMA*P2)*H2/TAN(THETA))))
      GDASHQ = G -Q + 1.
      H4 = H2
      NN = 1
      CALL PRO(FQH,Q)
      F = FQH
      QO = Q
      DELQ = 0.00002
      Q1 = Q + DELQ
      CALL PRO(FQ1H,Q1)
      DELFQ = FQ1H - F
      FDASHQ = DELFQ/DELQ
      DELH = 10.**(-6)
      H2 = H2 + DELH
      CALL PRO(FQ2H,QO)
      DELFH = FQ2H - F
      FDASHH = DELFH/DELH
      XJACOBI = GDASHH*FDASHQ - FDASHH*GDASHQ
      H2 = H4
      H2 = H2 -(G*FDASHQ-F*GDASHQ)/XJACOBI
      Q = QO - (F*GDASHH - G*FDASHH)/XJACOBI
      IF((ABS(H2-H4).LE.10.**(-15)).AND.(ABS(Q-QO).LE.10.**(-15))) GO TO
     16
      GO TO 00008
00006 WRITE(6,7)H2,Q
00007 FORMAT(1X,4HH2= ,1PE14.5,2X,3HQ= ,1PE14.5//)
C****** NEWTON.S ITERATION ENDS HERE H2,Q ARE DETERMINED ********
C-----------------------------------------------------------------------
C  DEFORMING ZONE ANALYSIS
C  NUMERICAL INTEGRATION OF TWO SIMULTANEOUS DIFFERENTIAL EQUATIONS
C  USING NEWTON.S ITERATION PROCEDURE
C   ITRATIVE SOLUTION FOR FILM THICKNESS, PRESSURE ALONG THE DIE
C-----------------------------------------------------------------------
C
      HO = H2
```

```
C   DPDX  IS THE PRESSURE GRADIENT AT ANY X
      DPDX2 = (2./X2)*( SIGMA+(XMUO/HO)*U2*EXP(GAMMA*P2)/TAN(THETA))
      TAU = FTAU(P2,HO,D2)
00999 DPDXO = DPDX(X2,TAU)
      DPDX2 = DPDXO
      TAU1 = FTAU(P2,HO,D2)
      IF(ABS(TAU-TAU1).LE.10.**-6)GO TO 01000
      TAU = TAU1
      GO TO 00999
01000 PO = P2
      WRITE(6,02499)
02499 FORMAT(1X,14HDIST ALONG DIE,2X,14HFILM THICKNESS,2X,8HPRESSURE,2X,
     112HSHEAR STRESS,2X,8HDIAMETER,3X,5HDELTA//)
      WRITE(6,2121)X2,HO,PO,TAU,D2,THETA
02121 FORMAT(5X,F7.5,8X,F7.6,6X,F8.4,4X,F7.4,6X,F7.5,2X,F7.5)
      PSUM = 0.
      TSUM = 0.
C   DELX IS THE INCREMENT OF X
      DX = 0.002
      H3 = HO
      P3 = PO
      D3 = D2
      DPDX1 = DPDXO
      DPDX2 = DPDXO
      DPDD1 = DPDX1/(2.*SIN(THETA))
      H = HO
      X = X2
      DH = H2*DX/X2
      DELTA = THETA
02500 CONTINUE
      DX = 0.002
      IF((THETA-DELTA).LE.0.01)DX = 0.01
      X = X + DX
      H = H3 + DH
      P = P3 + DX*DPDX1
02410 D = (X*TAN(THETA)-H)*(2.*COS(THETA))
      DH = H -H3
      DD = D - D3
      BETA = ATAN(DH/DX)
      DELTA = THETA - ATAN(DH/DX)
      EX = EXP(GAMMA*P)
      XH = XMUO/(H**2)
      DPDX2 = -(Q/D + U2*((D2/D)**2)*H/2.)*12.*(XH/H)*EX
      SIGMA = SIGMAO + (HH-SIGMAO)*(1. - (D1/D)**(-2.*FN))
      TAU = FTAU(P,H,D)
      DPDD2 = (2./D)*(SIGMA+TAU/TAN(DELTA)-(HH-SIGMAO)*FN*((D/D1)**(2.*
     1FN)))
      F = P3 - P + (DX/2.)*(DPDX1+DPDX2)
      FP = -1 + (DX/2.)*DPDX2*GAMMA
      DPDX2H = 12.*EX*XH*(3.*(Q/H**2)/D + U2*((D2/D)**2)/H)
      FH = (DX/2.)*DPDX2H
      DDDX2 = 2.*SIN(THETA) - 2.*COS(THETA)*(DH/DX)
      G = DPDX2 - DPDD2*DDDX2
      GP = GAMMA*DPDX2 - (2./D)*(GAMMA*FTAU(P,H,D)/TAN(DELTA))*DDDX2
      GH = DPDX2H + DPDD2*(2.*COS(THETA)/DX) + DDDX2*(2./D)*(FTAU(P,H,D)
     1/H + DPDX2     + (H/2.)*DPDX2H)/TAN(DELTA)
      ZJAC = GH*FP - FH*GP
      IF(ZJAC.EQ.0.0) STOP
      H1 = H - (G*FP-F*GP)/ZJAC
```

```
      P1 = P - (F*GH - G*FH)/ZJAC
      IF((ABS(P-P1).LE.10.**(-9)).AND.(ABS(H-H1).LE.10.**(-14)))GO TO
     1 02460
      H = H1
      P = P1
      GO TO 02410
02460 P3 = P1
      DH = H1 - H3
      H3 = H1
      D3 = (X*TAN(THETA)-H3)*(2.*COS(THETA))
      DPDD1 = DPDD2
      DPDX1 = DPDX2
      TAU = FTAU(P1,H1,D3)
      WRITE(6,02470)X,H1,P1,TAU,D3,DELTA
02470 FORMAT(5X,F7.5,8X,F7.6,6X,F8.4,4X,F7.4,6X,F7.5,2X,F7.5)
      PSUM=PSUM+ D3*P3*DX*SIN(DELTA)/COS(BETA)
      TSUM =TSUM+D3*TAU*DX*COS(DELTA)/COS(BETA)
      IF(DELTA.LT.0.0010) GO TO 02602
      IF(D.GE.0.99999*D1) GO TO 02602
      GO TO 02500
02602 P = P3
      H = H3
      D = D3
      DRISTR=-(1./GAMMA)*ALOG(EXP(-GAMMA*P )+6.*GAMMA*XMUO*(Q/H**2/D1+U1
     1/H)/TAN(THETA))
      WRITE(6,02601)DRISTR
02601 FORMAT(1X,21HEXTRUSION PRESSURE = ,F7.3)
      PTSUM = (PSUM + TSUM)/((D**2)/4.)
      WRITE(6,00061)PTSUM
00061 FORMAT(1X,17HDRIVING STRESS = ,F7.3)
00060 CONTINUE
00070 CONTINUE
      STOP
      END
$IBFTCDEST
      SUBROUTINE EST(AA,B,Q)
      COMMON SIGMA,GAMMA,D2,V,E,U2,XL,R,XMUO,XK,P2,X2,THETA
      COMMON H2,NN,RDASH,T
      IF(NN.EQ.1) GO TO 00005
      HXMUO = (H2**2)/XMUO
      UUUU = (U2*EXP(GAMMA*P2)*H2)*H2/TAN(THETA)
      YYYY = (EXP(-GAMMA*P2)/(6.*X2))
      Q = -D2*(U2*H2/2. +YYYY*(HXMUO*(SIGMA*H2)+UUUU ))
00005 B = -2.*(Q/XK)/(D2*U2)
      AA = H2/XK-B-P2
      RETURN
      END
$IBFTCDSSUM
      SUBROUTINE SSUM(P,SUM)
      COMMON SIGMA,GAMMA,D2,V,E,U2,XL,R,XMUO,XK,P2,X2,THETA
      COMMON H2,NN,RDASH,T
      Y = 1.
      SUM =0.0
      DO 20 I = 1,100,1
      FI = FLOAT(I)
      Y = -(Y/FI)*GAMMA*P
      XSUM = Y/FI
      SUM = SUM + XSUM
      IF(ABS(XSUM).LE.10.**(-15)) GO TO 00040
```

```
00020 CONTINUE
00040 CONTINUE
      RETURN
      END
$IBFTCDPRO
      SUBROUTINE PRO(FQH,Q)
      COMMON SIGMA,GAMMA,D2,V,E,U2,XL,R,XMUO,XK,P2,X2,THETA
      COMMON H2,NN,RDASH,T
      FUN(P) = (B**3)*(ALOG(W)+SUM)-EXP(-GAMMA*P)*(P**2/GAMMA+P*(2./GAMM
     1A**2+3.*B/GAMMA)+3.*(B**2)/GAMMA+3.*B/(GAMMA**2)+2./(GAMMA**3))
      CALL EST(AA,B,Q)
      CALL SSUM(P2+AA,SUM)
      W = ABS(P2 + AA)
      FP2AA = FUN(P2+AA)
      CALL SSUM(RDASH+AA,SUM)
      W = ABS(RDASH +AA)
      FRDAA= FUN(RDASH+AA)
      FQH =FP2AA -FRDAA                    +(XMUO/XK)*(6.*U2*XL)/(EXP(GAMMA*AA)
     1*XK)
      RETURN
      END
```

APPENDIX IV

Analysis of hydrodynamic lubrication for a work-hardening material using a more accurate formula for the stress-strain curve

This analysis is similar to that in section 4.62 except that σ is given by a more accurate expression given below. The equation numbers with asterisks given here are corresponding to the equation numbers without asterisks in section 4.62.

$$\sigma = \sigma_o + (H + \beta\varepsilon - \sigma_o)(1 - e^{-n\varepsilon}) \qquad 26^*.$$

where $\quad = 2\ln (D_1/D) = 2\ln (X_1/x) \qquad 27^*.$

Therefore $\frac{d\sigma}{dx} = -\frac{2ne^{-n\varepsilon}}{x} \cdot (H + \beta\varepsilon - \sigma_o) - \frac{2\beta}{x}(1 - e^{-n\varepsilon})$

$$= \frac{-2nX^{2n}}{x}(H - 2\beta\ln X - \sigma_o) - \frac{2\beta}{x}(1 - X^{2n})$$

where $X = x/x_1$

As in section 4.62, the equilibrium equation is;

$$x\left(\frac{dp}{dx} - \frac{d\sigma}{dx}\right) - 2\sigma - \frac{2\eta_o U_1}{h_1 \tan\alpha}(x_1/x)^3 \cdot e^{\gamma p} = 0$$

Substituting for σ and $\frac{d\sigma}{dx}$ it becomes:

$$x\frac{dp}{dx} + 2X^{2n} \cdot ((H - \sigma_o)(n + 1) - \beta - 2\beta(n + 1)\ln X) + 4\beta\ln X + 2(\beta - H) = \frac{2\eta_o U_1 \gamma}{h_1 \tan\alpha} \cdot \frac{e^{\gamma p}}{X^3}$$

Since $B = e^{-\gamma p}$ and $X = x/x_1$, the above equation becomes,

$$\frac{dB}{dX} - 2\gamma B\left[X^{2n-1} \cdot ((n+1)(H - 2\beta\ln X - \sigma_o) - \beta) + \frac{2\beta\ln X}{X} + \frac{\beta - H}{X}\right] = \frac{2\eta_o U_1 \gamma}{h_1 \tan\alpha} \cdot \frac{1}{X^4}$$

.... 29^*.

$$\text{Let } 2\gamma\,[(H - \sigma_o)(n+1) - \beta] = A$$

$$2\gamma\,(H - \beta) = C$$

$$\frac{2\eta_o U_1 \gamma}{h_1 \tan\alpha} = D \qquad \text{30*.}$$

$$4\gamma\beta(n+1) = E$$

$$\text{and } 4\gamma\beta = F$$

$$\text{Then } \frac{dB}{dX} - B\left[X^{2n-1} \cdot (A - E\ln X) + F\frac{\ln X}{X} - \frac{C}{X}\right] = -\frac{D}{X^4} \qquad \text{31*.}$$

The integration factor,

$$I = e^{-\int\left[X^{2n-1} \cdot (A - E\ln X) + F\frac{\ln X}{X} - c/\chi\right) dX}$$

$$= e^{-\frac{A}{2n}X^{2n} + \frac{E}{2n}\ln X \cdot X^{2n} - \frac{EX^{2n}}{4n^2} + C\ln X - \frac{F}{2}(\ln X)^2}$$

$$\text{Let } \frac{A}{2n} + \frac{E}{4n^2} = L \text{ and } \frac{E}{2n} = M$$

Then,

$$I = e^{-LX^{2n} + M\ln X \cdot X^{2n} + C\ln X - \frac{F}{2}(\ln X)^2}$$

$$= X^{MX^{2n}+C} \cdot e^{-LX^{2n} - \frac{F}{2}(\ln X)^2}$$

Hence the solution

$$BX^{MX^{2n}+C} \cdot e^{-LX^{2n} - \frac{F}{2}(\ln X)^2} = -D\int e^{-LX^{2n} - \frac{F}{2}(\ln X)^2} \cdot X^{MX^{2n}+C-4} \cdot dX + C5$$

.... 32*.

Substituting the boundary conditions;

$$\text{at } X = 1,\ p = p_A + \sigma_A + \sigma_o$$

$$\text{and } X = \frac{1}{\sqrt{R}}\ p = p_2 = p_3 + [\sigma_o + (H + \beta\ln R - \sigma_o)(1 - R^{-n})] - \sigma_p$$

$$e^{-\gamma(p_A + \sigma_A + \sigma_o)} - e^{-\gamma(p_3 + \sigma_o + (H + \beta\ln R - \sigma_o)(1 - R^{-n}) - \sigma_p) - LR^{-n}} \cdot$$

$$e^{-\frac{F}{8}(\ln R)^2} \cdot R^{-\frac{1}{2}(MR^{-n} + C)} = -D\int_{\frac{1}{R}}^{1} e^{-LX^{2n} - \frac{F}{2}(\ln X)^2} \cdot X^{MX^{2n} + C - 4} \cdot dX$$

$$= - D \cdot S \quad \text{(say)} \qquad 38^*.$$

As before, re-arranging the equation and taking the logarithm, we get

$$(p_A + \sigma_A - p_3 + \sigma_p) = [\sigma_o \ln R + (H - \sigma_o)(\ln R + \frac{R^{-n} - 1}{n}) + \frac{\beta}{n^2 R^n} + \frac{\beta \ln R}{R^n}$$

$$+ \frac{\beta}{2} (\ln R)^2 - \frac{\beta}{n^2} + p_{FD} \qquad 39^*.$$

$$\text{where } p_{FD} = \frac{1}{\gamma} \ln [1 + D \cdot S \cdot e^{\gamma(p_A + \sigma_A + \sigma_o) + L}] \qquad 40^*.$$

The integration of $S = \int_{\frac{1}{\sqrt{R}}}^{1} e^{- LX^{2n} - \frac{F}{2} (\ln X)^2} \cdot X^{MX^{2n} + C - 4} \cdot dX$ is difficult and has to be performed by a standard numerical method.

h_1 is given by the same expression as in equation 35 of section 4.62.

APPENDIX V

Modification to the formula for driving stress in section 4.62 (work-hardening analysis) to allow for bulging in billet augmentation

Let D_o, D_1 be the initial and final (bulged) diameters of the billet respectively. Then the equations 26 and 27 (of section 4.62) become

$$\sigma = \sigma_o + (H - \sigma_o)(1 - e^{-n\epsilon}) \qquad 26.$$

where $$\epsilon = 2\ln (D_1/D) + 2\ln (\frac{D_1}{D_o}) \qquad 27^{**}.$$

$$= 2\ln (X_1/X) + 2\ln (D_1/D_0)$$

Thus $$\sigma = \sigma_o + (H - \sigma_o)(1 - (\frac{x}{x_1})^{2n} \cdot (\frac{D_o}{D_1})^{2n})$$

and $$\frac{d\sigma}{dx} = - 2n(H - \sigma_o)(\frac{D_0}{D_1})^{2n} \cdot \frac{x^{2n-1}}{x_1^{2n}}$$

Hence equation 28 (section 4.62) becomes

$$e^{-\gamma p} \cdot \frac{dp}{dx} + e^{-\gamma p}(\frac{2(H - \sigma_o)(n + 1)}{x_1^{2n}} \cdot (\frac{D_o}{D_1})^{2n} \cdot x^{2n-1} - \frac{2H}{x}) - \frac{2\eta_o U_1 x_1^3}{h_1 \tan\alpha} \cdot \frac{1}{x^4} = 0$$

.... 28^{**}.

and equation 29 (section 4.62) becomes

$$\frac{dB}{dX} - \gamma B \left[2(n + 1)(H - \sigma_o)(\frac{D_o}{D_1})^{2n} \cdot X^{2n-1} - \frac{2H}{X}\right] = - \frac{2\eta_o U_1 \gamma}{h_1 \tan\alpha} \cdot \frac{1}{X^4} \qquad 29^{**}.$$

Let

$$2\gamma(n + 1)(H - \sigma_o)(\frac{D_o}{D_1})^{2n} = I_1^*$$

$$2\gamma H = I_2 \qquad 30^*.$$

and $$2\gamma\eta_o/h_1\tan\alpha = I_3$$

Then $$\frac{dB}{dX} - B\left(I_1^* \cdot X^{2n-1} - \frac{I_2}{X}\right) = -\frac{I_3}{X^4} \qquad 31^{**}.$$

Hence the solution, as before, except that I_1 is replaced by I_1^*

$$B \cdot X^{I_2} \cdot e^{-\frac{I_1^*}{2n} \cdot X^{2n}} = -I_3 \int X^{I_2-4} \cdot e^{-\frac{I_1^*}{2n} \cdot X^{2n}} dX + C5 \qquad 32^{**}.$$

After substituting the boundary conditions that,

at $X = 1$ $p = p_A + \sigma_A + \sigma_1$

where $\sigma_1 = \sigma_o + (H - \sigma_o)\left(1 - \left(\frac{D_o}{D_1}\right)^{2n}\right) = \sigma_A$

and at

$$X = \frac{1}{\sqrt{R}} \quad p = p_3 - \sigma_p + \sigma_2$$

where $\sigma_2 = \sigma_o + (H - \sigma_o)\left(1 - R^{-n} \cdot \left(\frac{D_1}{D_o}\right)^{-2n}\right)$

and the equation 35 for h_1 which now becomes,

$$h_1 = \frac{3\eta_o U_1 \gamma}{\tan\alpha} \cdot \frac{1}{\left(\frac{U_1 \eta_o \gamma}{x_1 \tan^2\alpha} + e^{-\gamma p_A} - e^{-\gamma(p_A + \sigma_1 + \sigma_A)}\right)} \qquad 35^{**}.$$

The formula for driving stress becomes

$$(p_A + \sigma_A + \sigma_p - p_3) = H \ln R + \frac{(H - \sigma_o)}{n}\left(\frac{D_o}{D_1}\right)^{2n}\left[R^{-n} - 1\right] + p_{FD} \qquad 39^{**}.$$

Driving stress Work of homogeneous deformation

where p_{FD} (frictional component) is given by

$$p_{FD} = \frac{1}{\gamma} \ln\left[1 + \frac{e^{\gamma\left(p_A + 2\sigma_A + \frac{(n+1)}{n}(H - \sigma_o)\left(\frac{D_o}{D_1}\right)^{2n}\right)}}{3n} \cdot \left\{\frac{U_1 \eta_o \gamma}{x_1 \tan^2\alpha} + e^{-\gamma p_A} - e^{-\gamma(p_A + \sigma_1 + \sigma_A)}\right\}\right.$$

$$\cdot \left\{ \sum_{j=o}^{\infty} \frac{(-1)^j \left(\frac{\gamma(H - \sigma_o)(n+1)}{n} \right)^j \cdot \left(\frac{D_o}{D_1} \right)^{2nj}}{\left(\frac{2\gamma H - 3}{2n} + j \right) \lfloor j} \cdot (1 - R^{-3/2 - \gamma H - nj}) \right\} \right]$$

.... 40**.

Thus equation 41 (of section 4.63) including redundant work becomes

$$(p_A + \sigma_A + \sigma_p - p_3) = \int_o^{\epsilon_3} \sigma d\epsilon + p_{FD} \qquad 41^{**}.$$

where $\epsilon_3 = \ln R + 2 \ln \left(\frac{D_1}{D_o} \right) + \frac{4}{3} \tan \alpha/2$

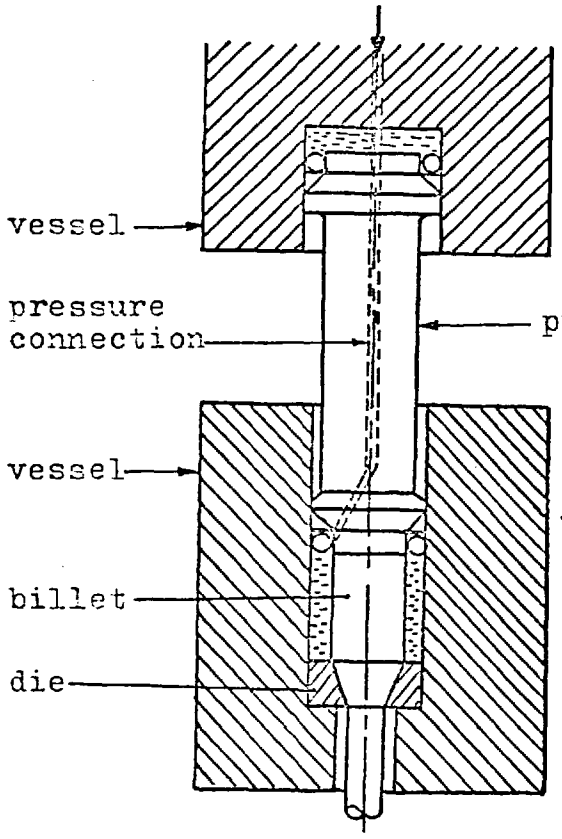

FIG.1 Proportional billet augmented hydrostatic extrusion

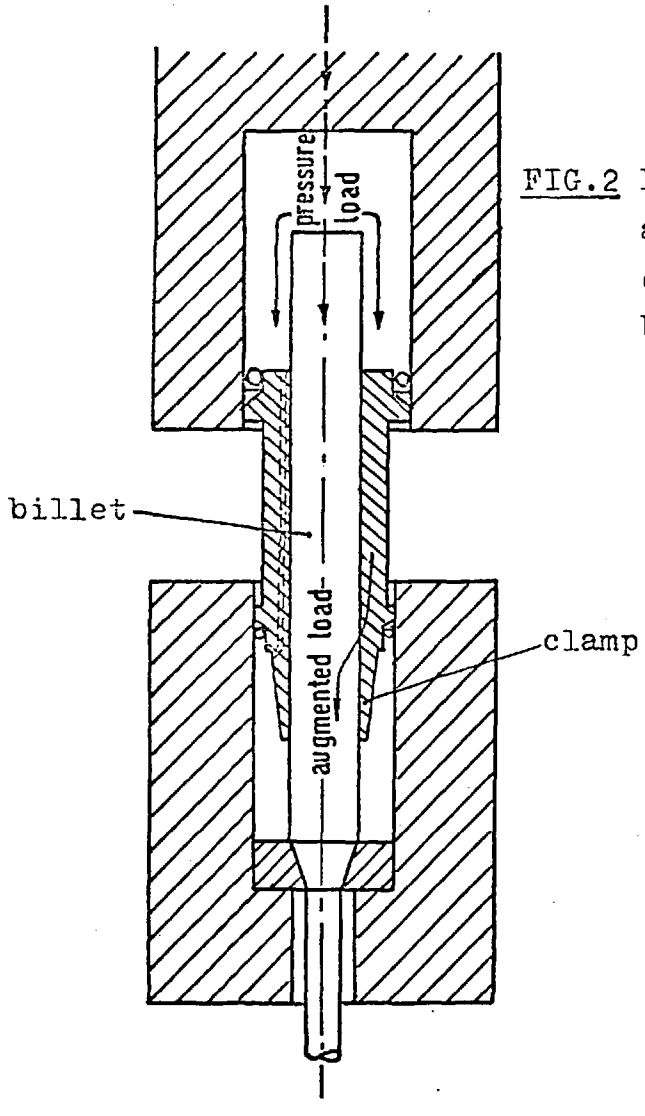

FIG.2 Proportional billet augmented hydrostatic extrusion of long bars

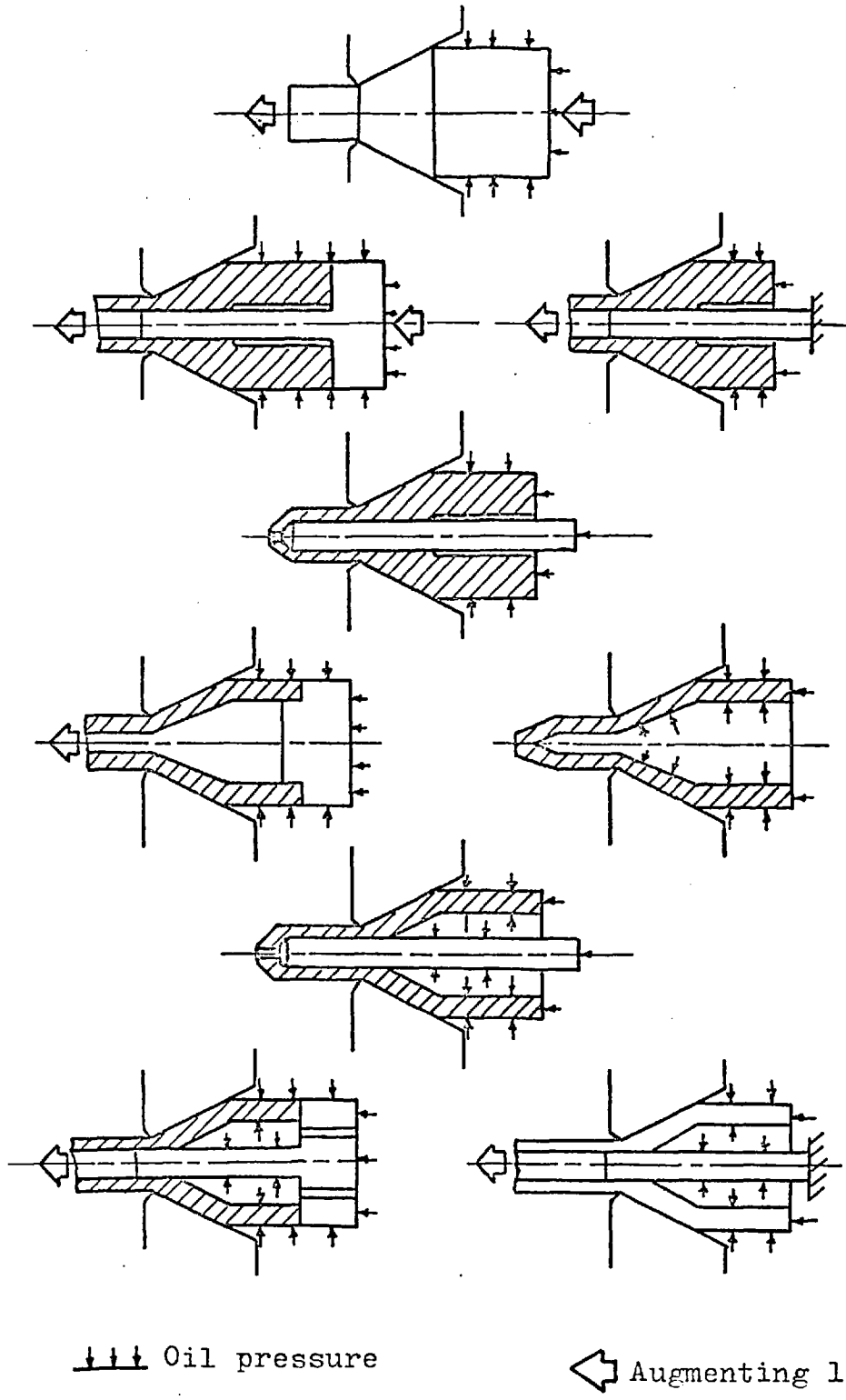

FIG.3 Methods of forming bar and tube by augmented hydrostatic extrusion

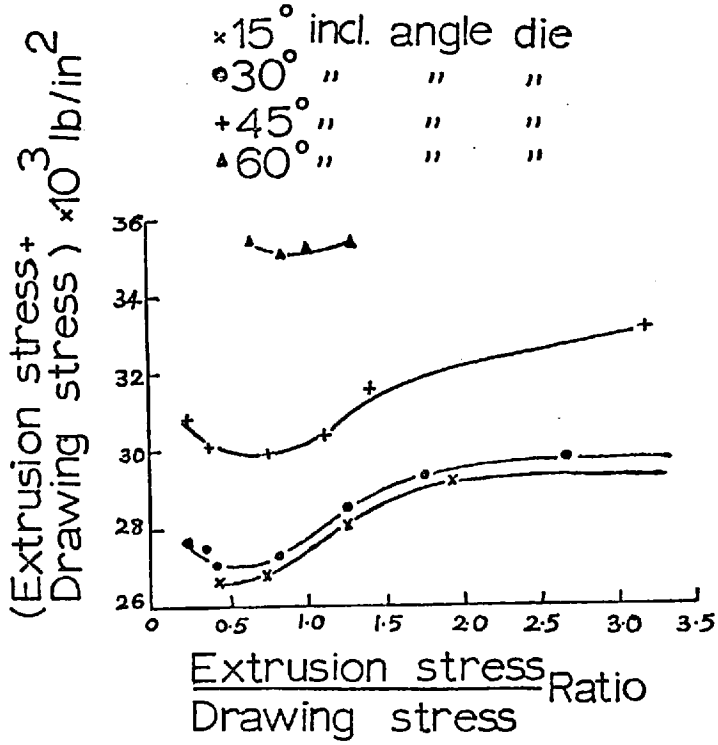

FIG.4 Extrusion pressure plus augmenting stress versus extrusion pressure/augmenting stress ratio in product augmentation

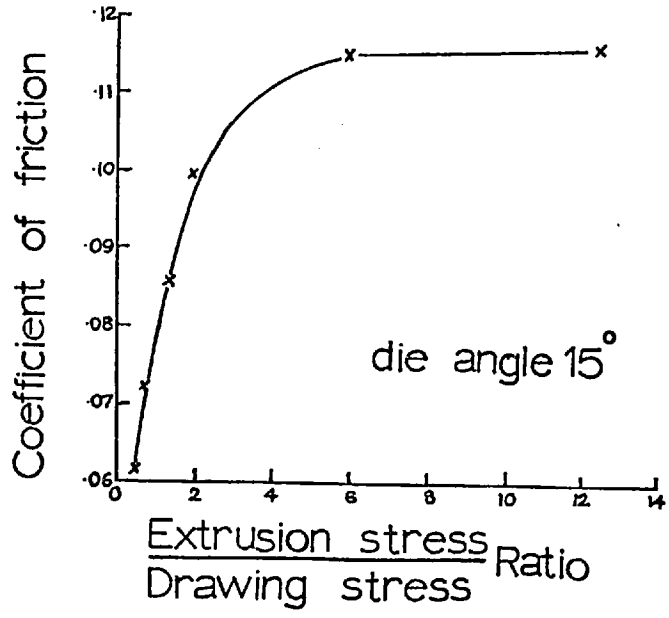

FIG.5 Coefficient of friction versus extrusion pressure/augmenting stress ratio in product augmentation

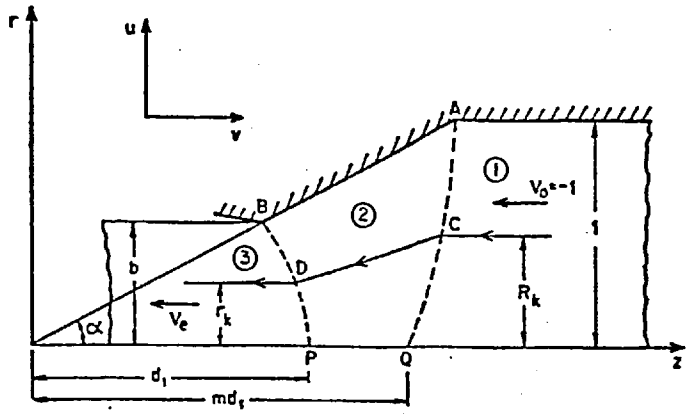

a. Basic flow pattern

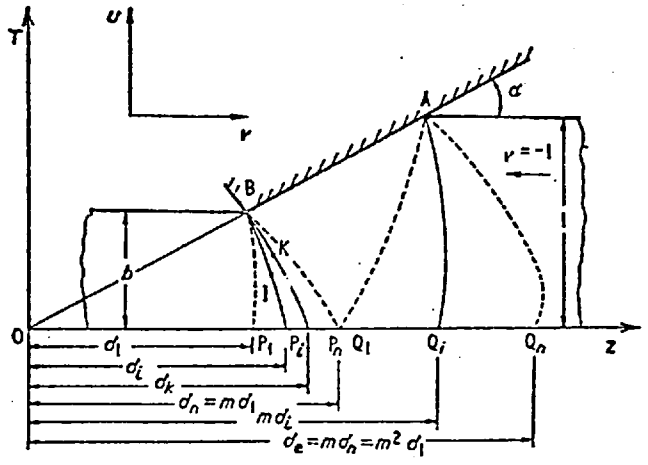

b. Superposition of basic flow patterns

FIG.6 Superposition of basic velocity patterns in axi-symmetric extrusion

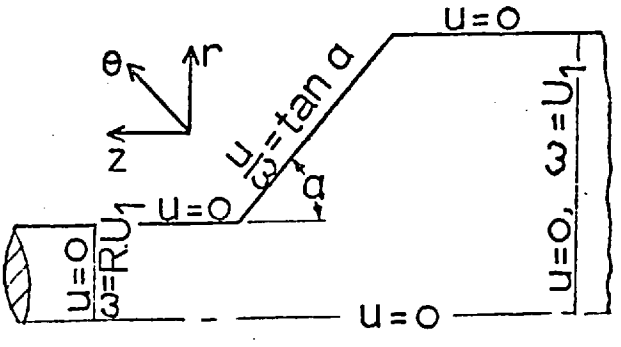

a. Velocity boundary conditions

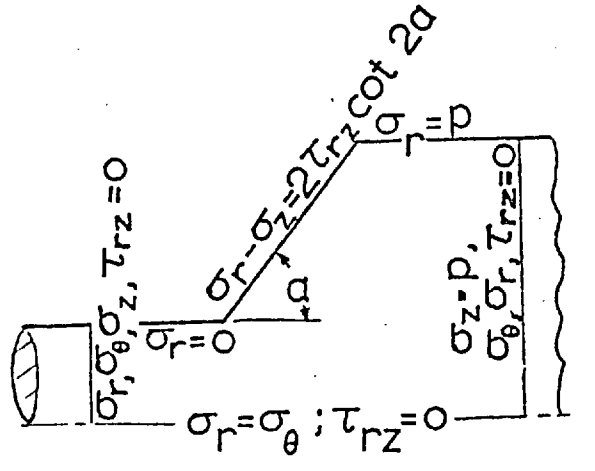

b. Stress boundary conditions (smooth die)

FIG.7 Boundary conditions for frictionless axi-symmetric extrusion

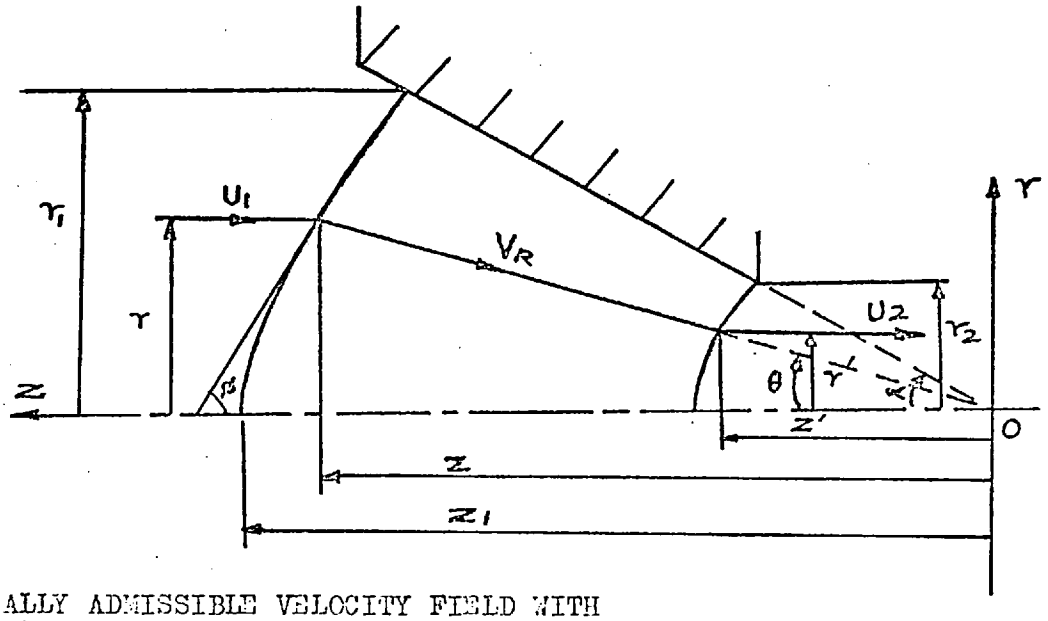

KINEMATICALLY ADMISSIBLE VELOCITY FIELD WITH PARABOLIC BOUNDARIES

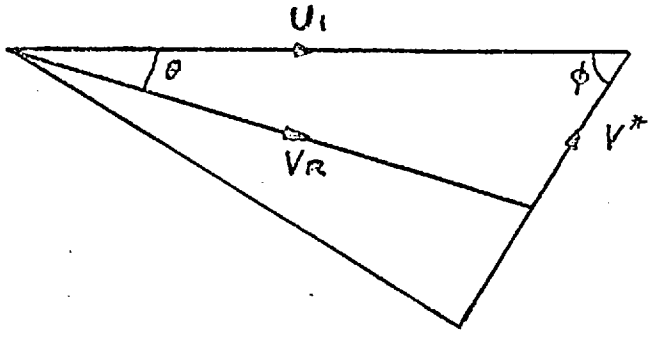

VELOCITY TRIANGLE

FIG.8 Kinematically admissible velocity field with parabolic boundaries in axi-symmetric extrusion

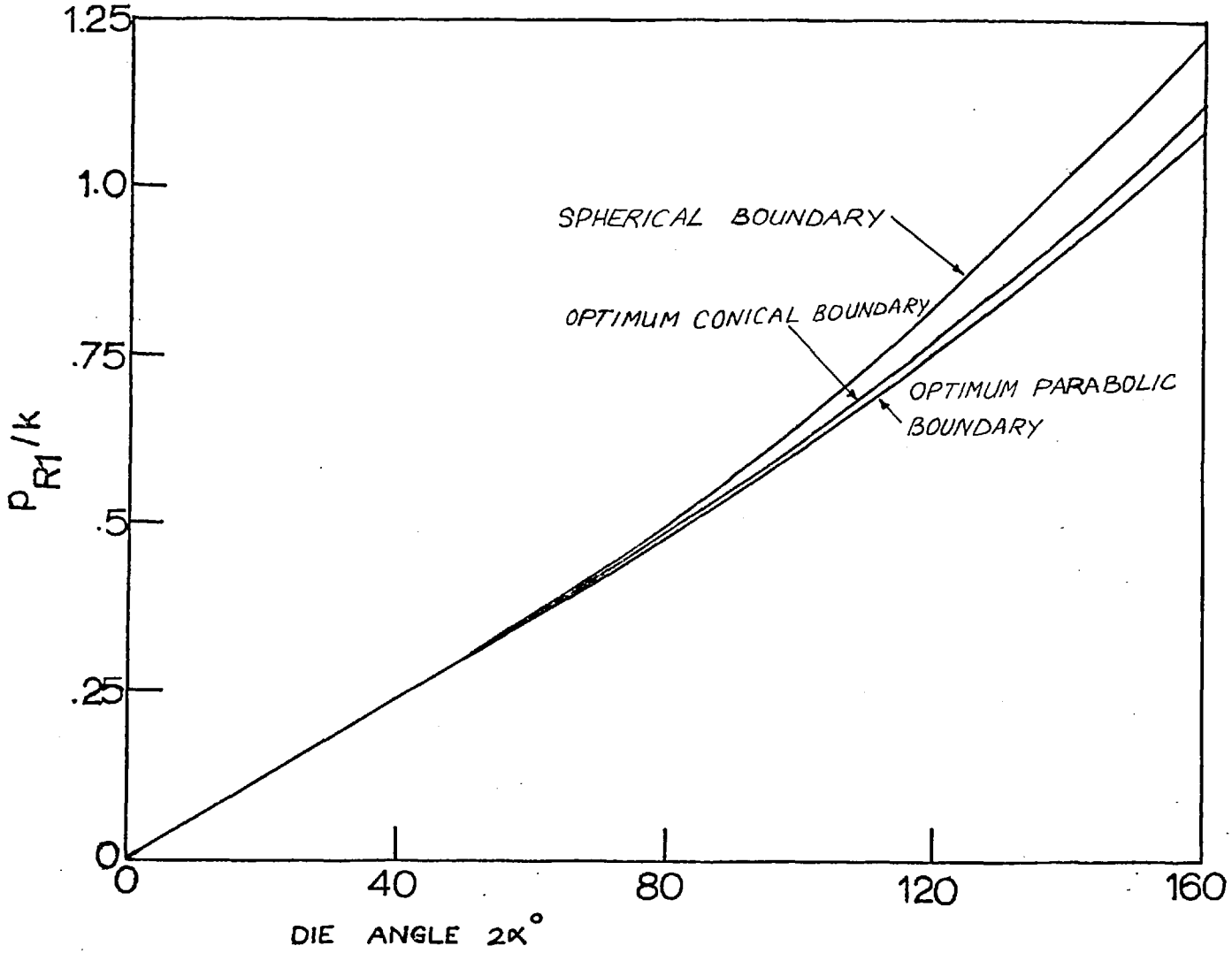

FIG.9 p_{R1}/k versus die angle for various boundaries

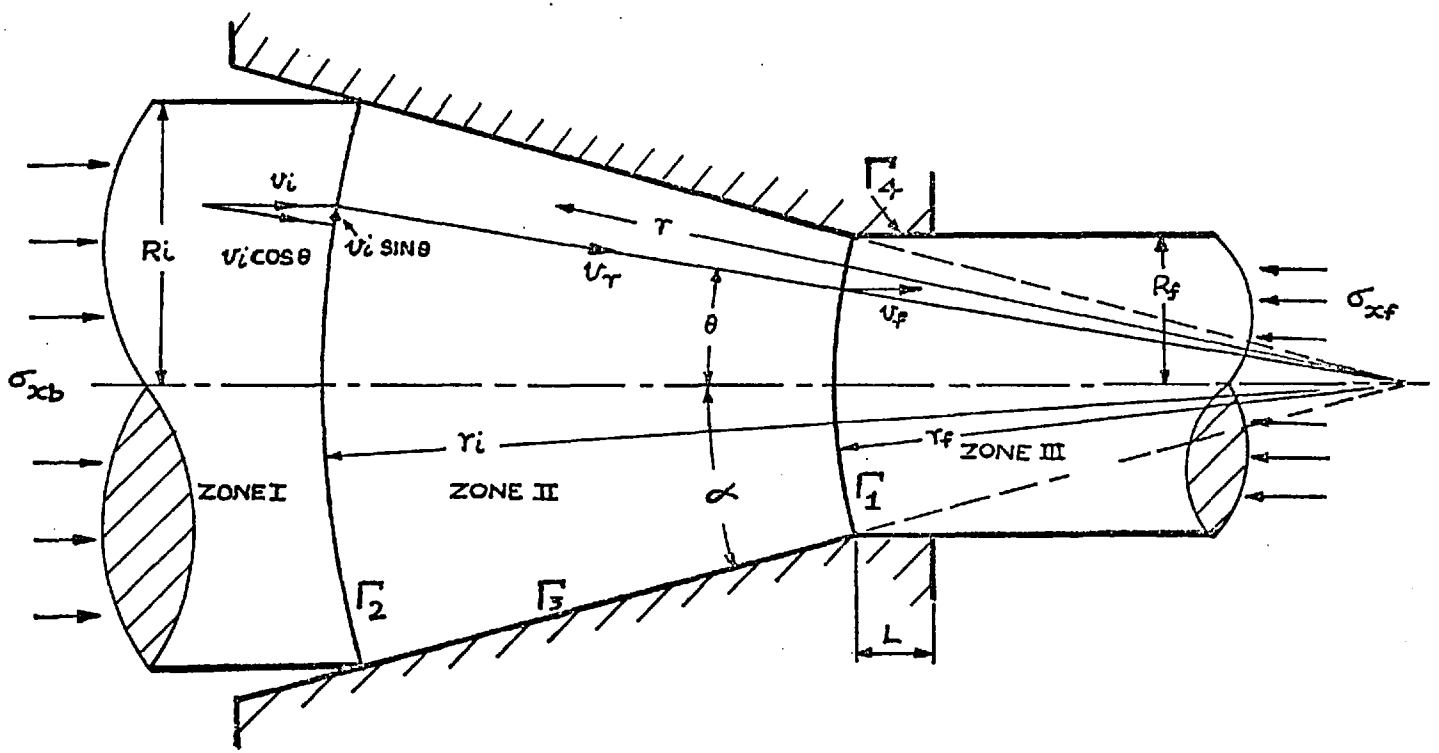

FIG.10 Admissible velocity field with spherical boundaries for upper bound solution (Section 4.3)

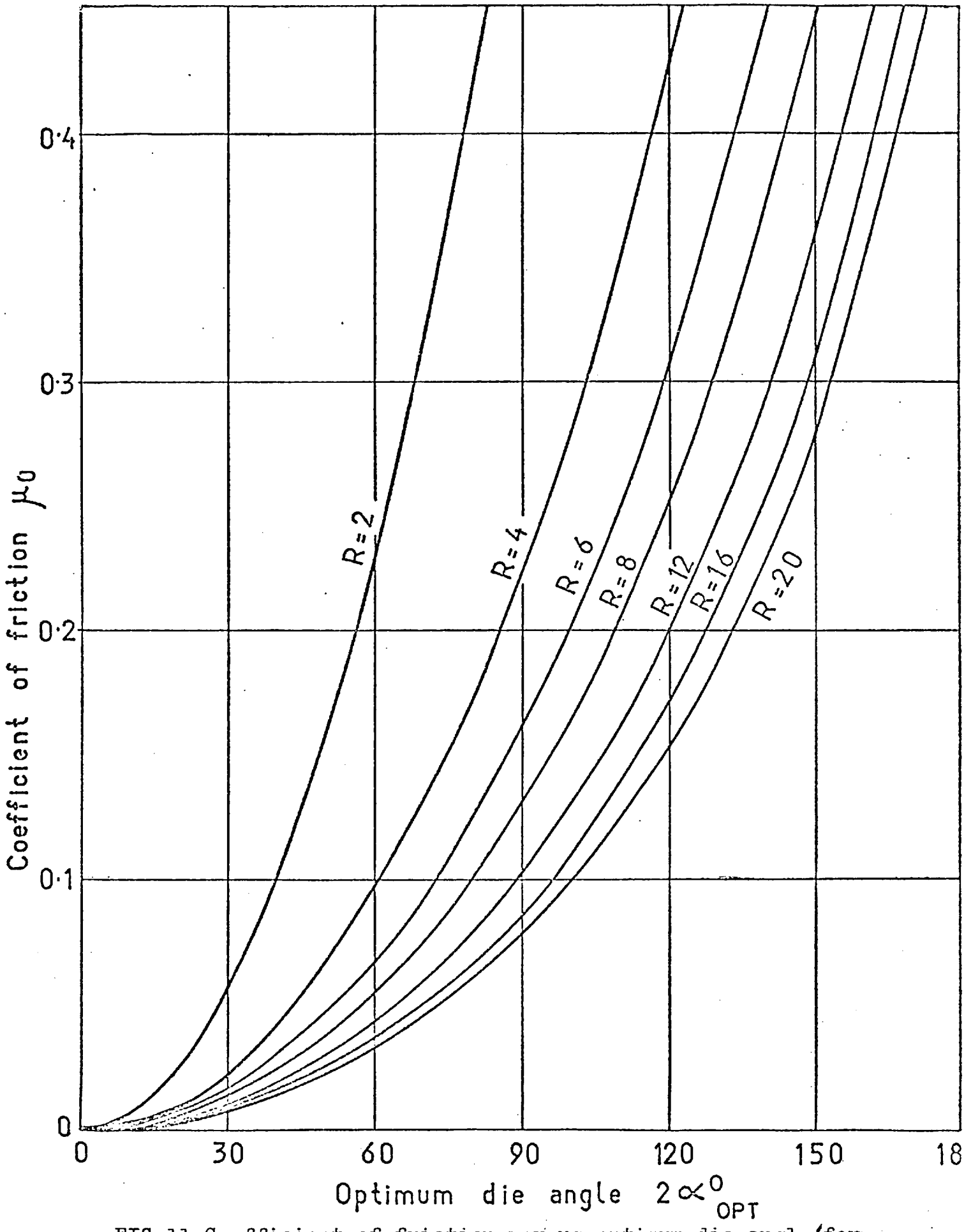

FIG.11 Coefficient of friction versus optimum die angle (for various extrusion ratios) in simple hydrostatic extrusion

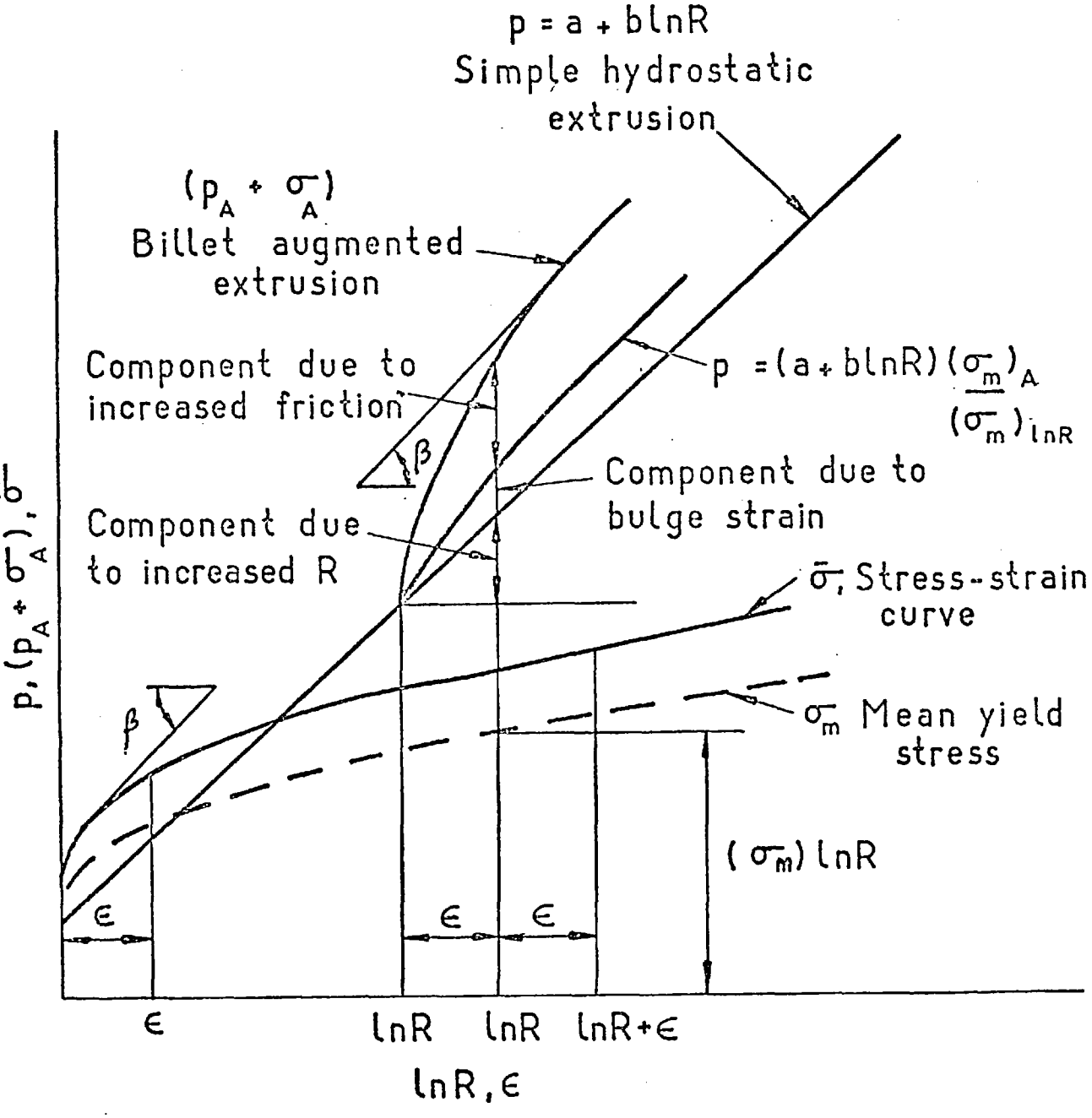

FIG.12 Derivation of coefficient of friction in billet augmented hydrostatic extrusion from total extrusion pressure versus lnR curve

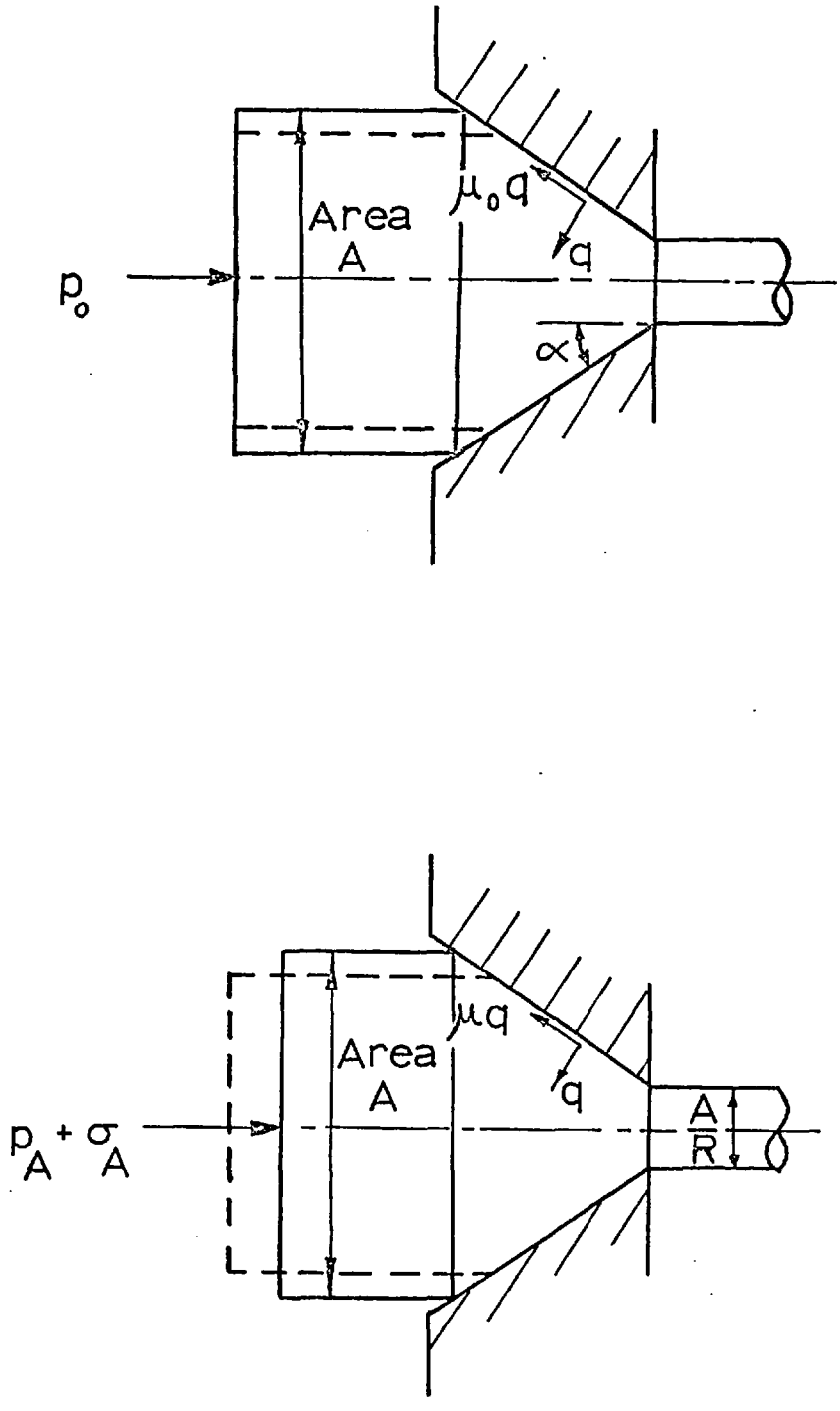

FIG.13 Models used in the estimation of the coefficient of friction in billet augmented hydrostatic extrusion

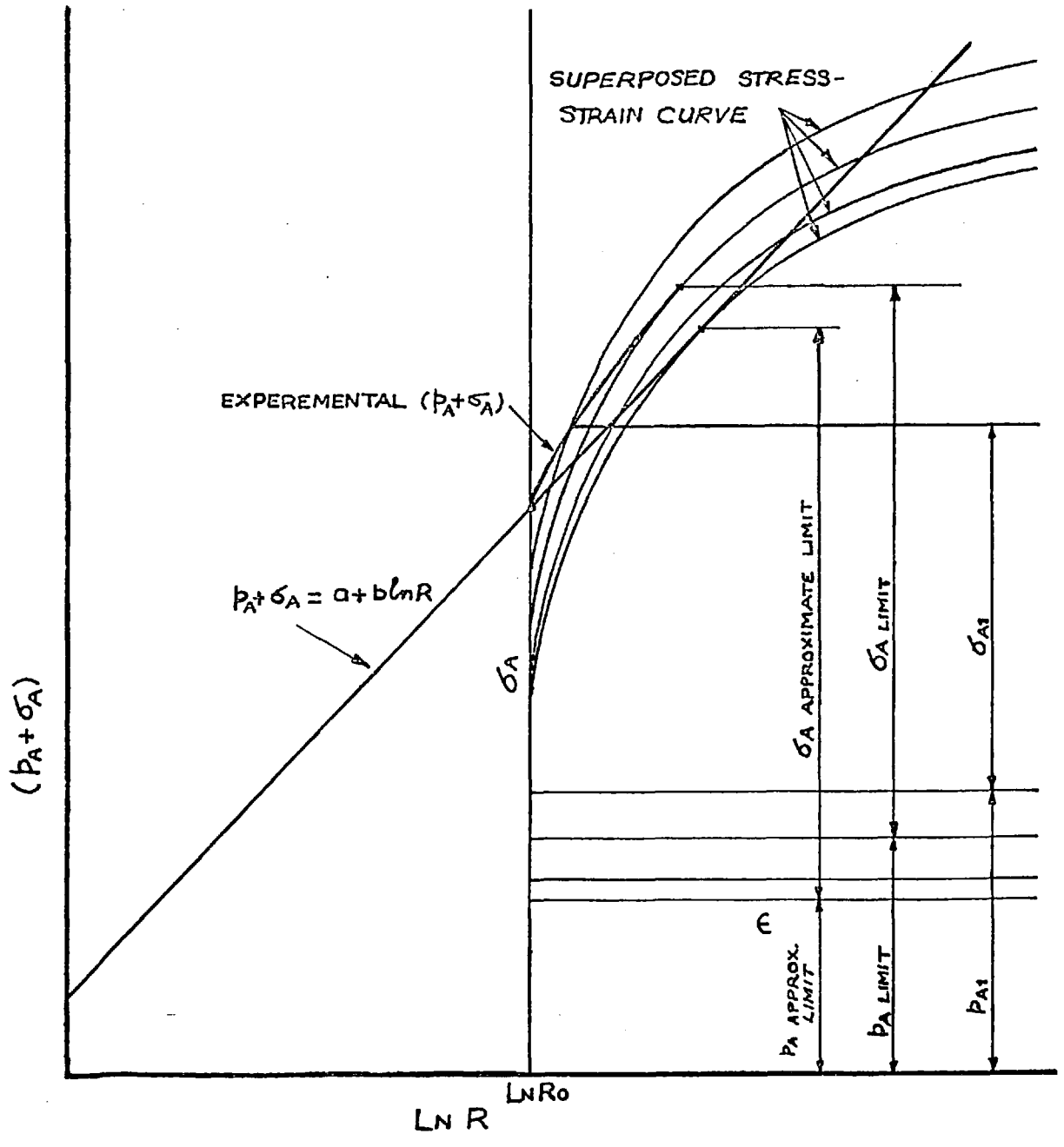

FIG.14 A construction for obtaining the limit of bulging in billet augmented hydrostatic extrusion by extrapolation using the experimental results

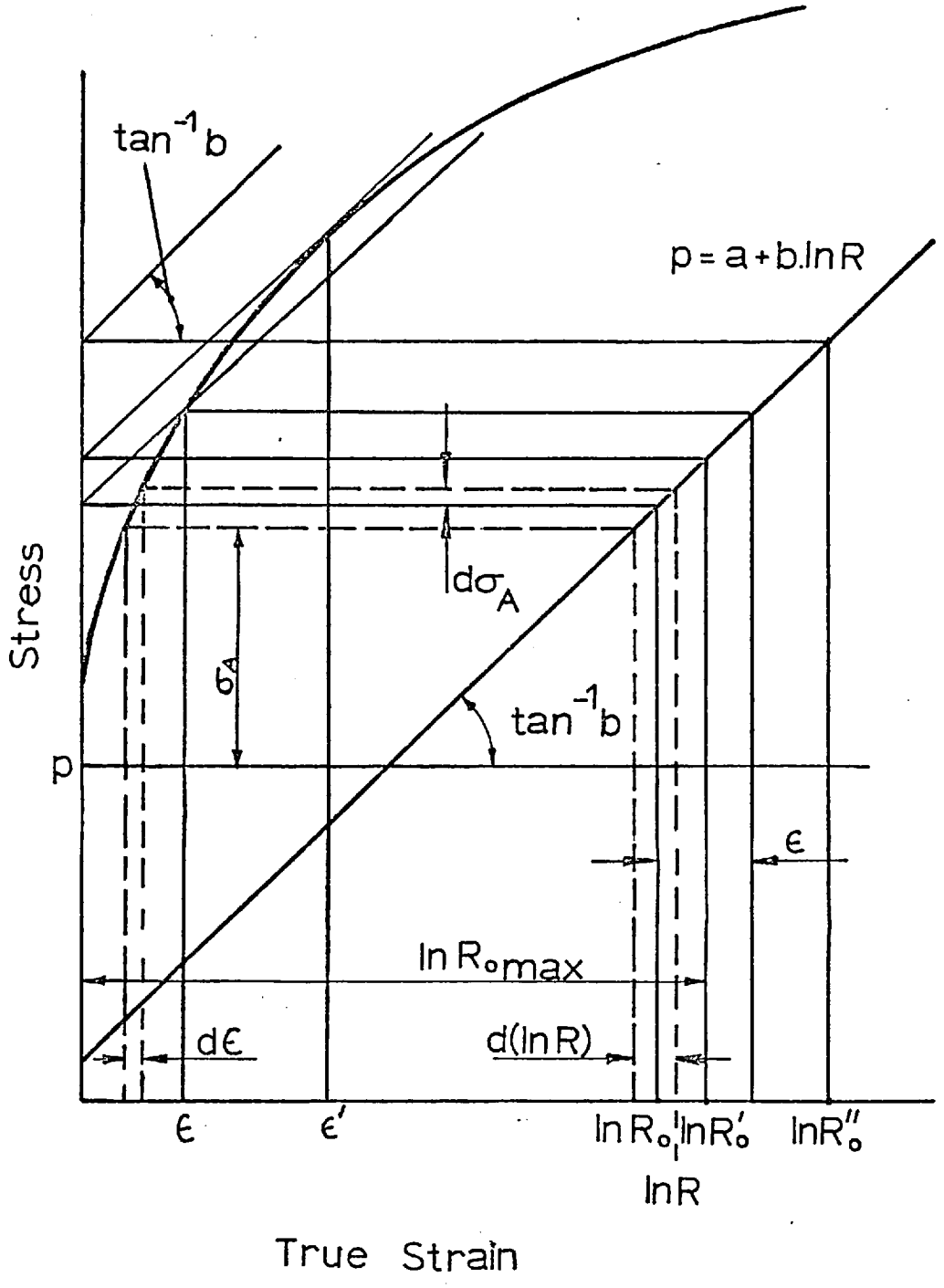

FIG.15 A construction for obtaining the approximate limit of bulging using the equation p = a + blnR and the stress strain curve

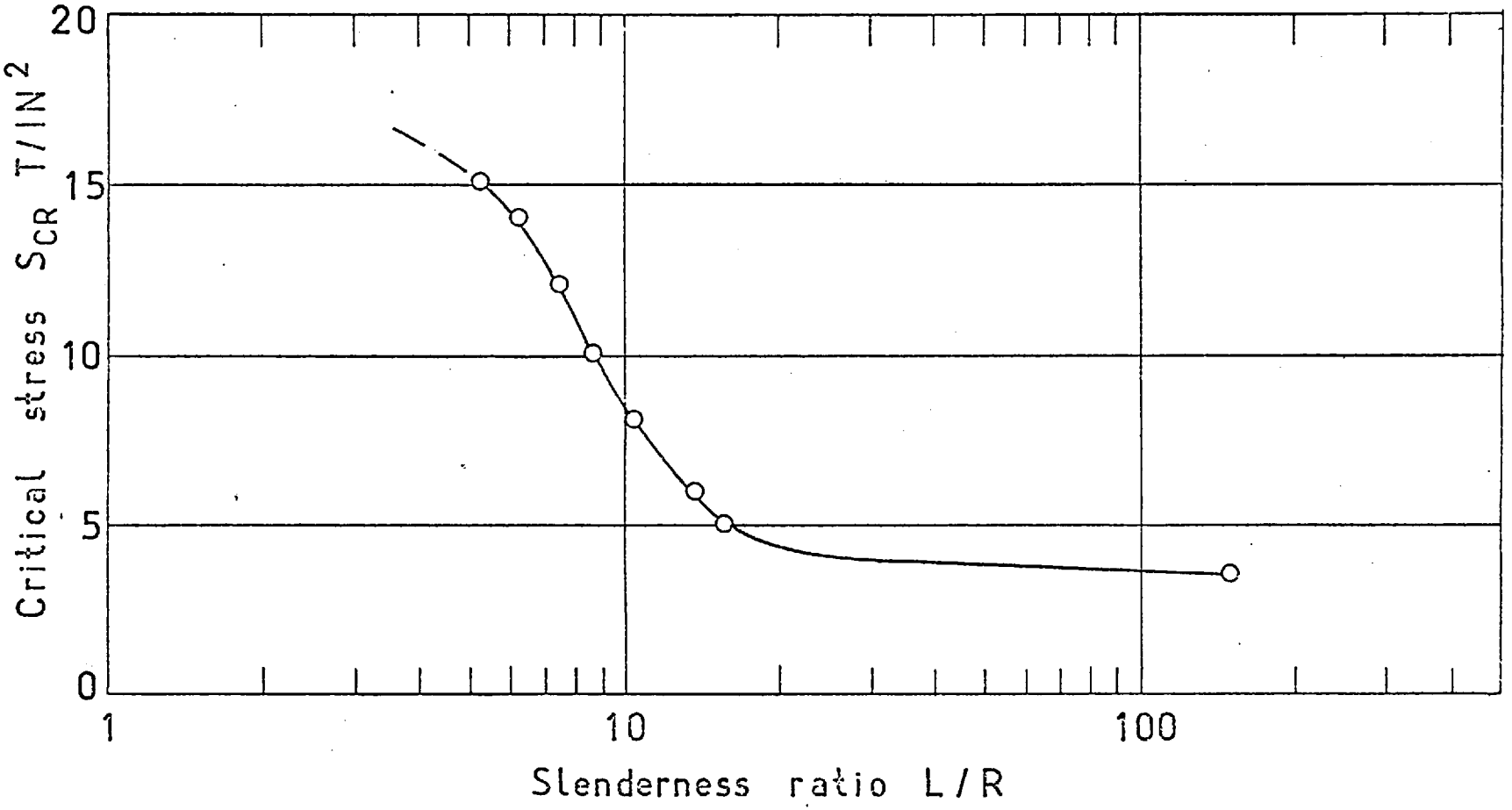

FIG.16a

Critical buckling stress versus slenderness ratio for annealed copper billets

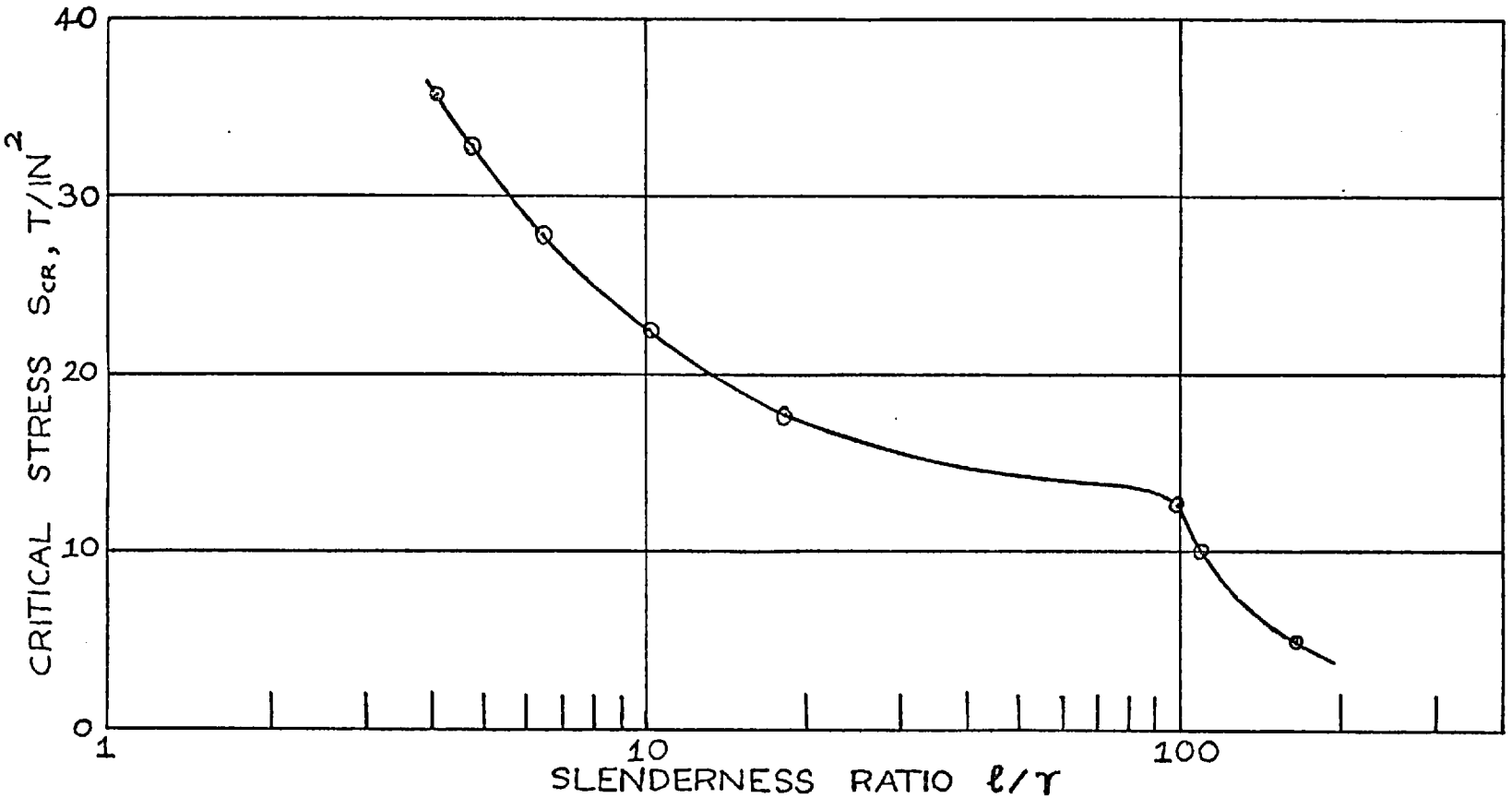

FIG.16b Critical buckling stress versus slenderness ratio for annealed Mild Steel billets

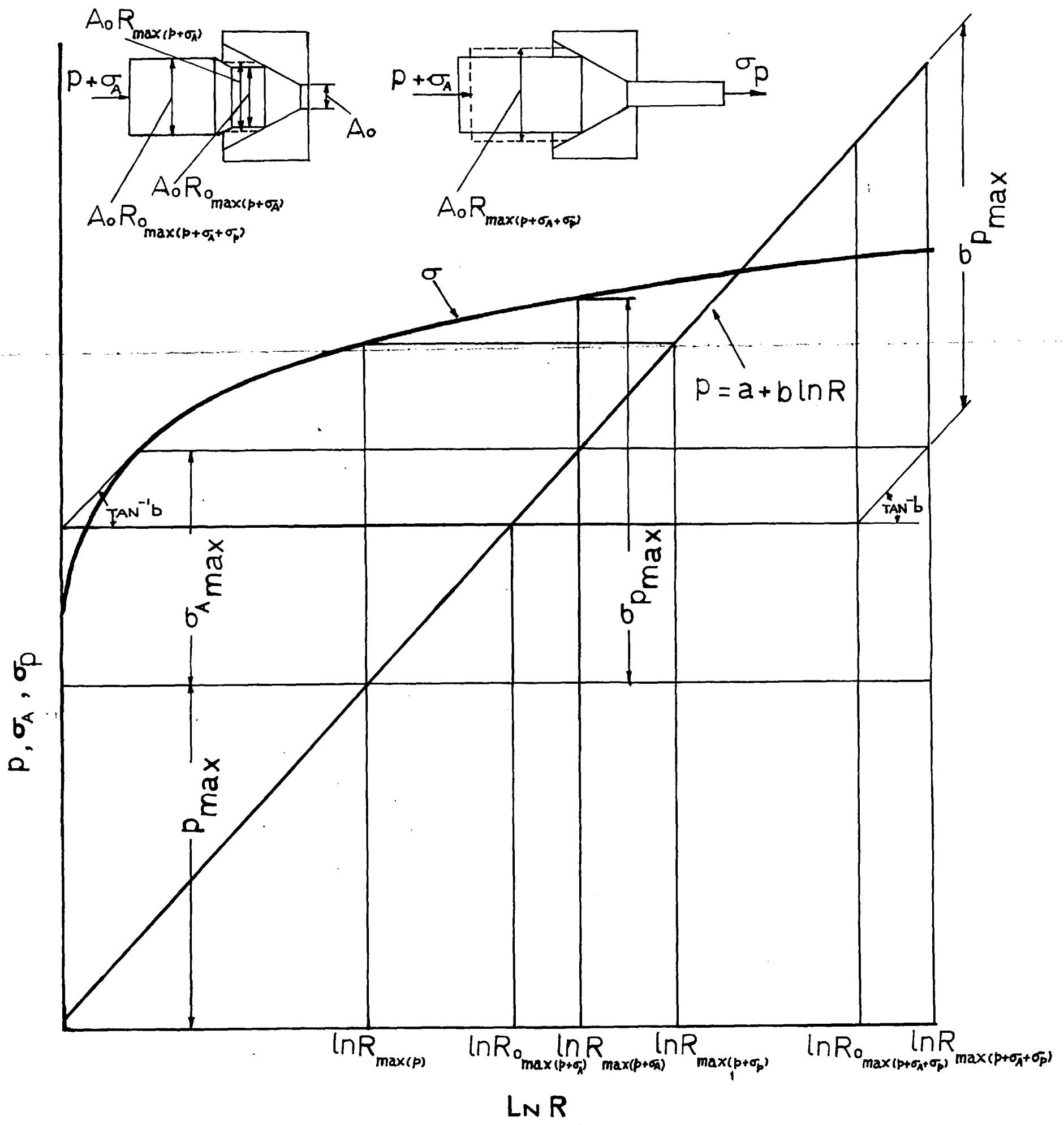

FIG.17 A construction for obtaining the maximum extrusion ratio achievable in product and billet augmented hydrostatic extrusion

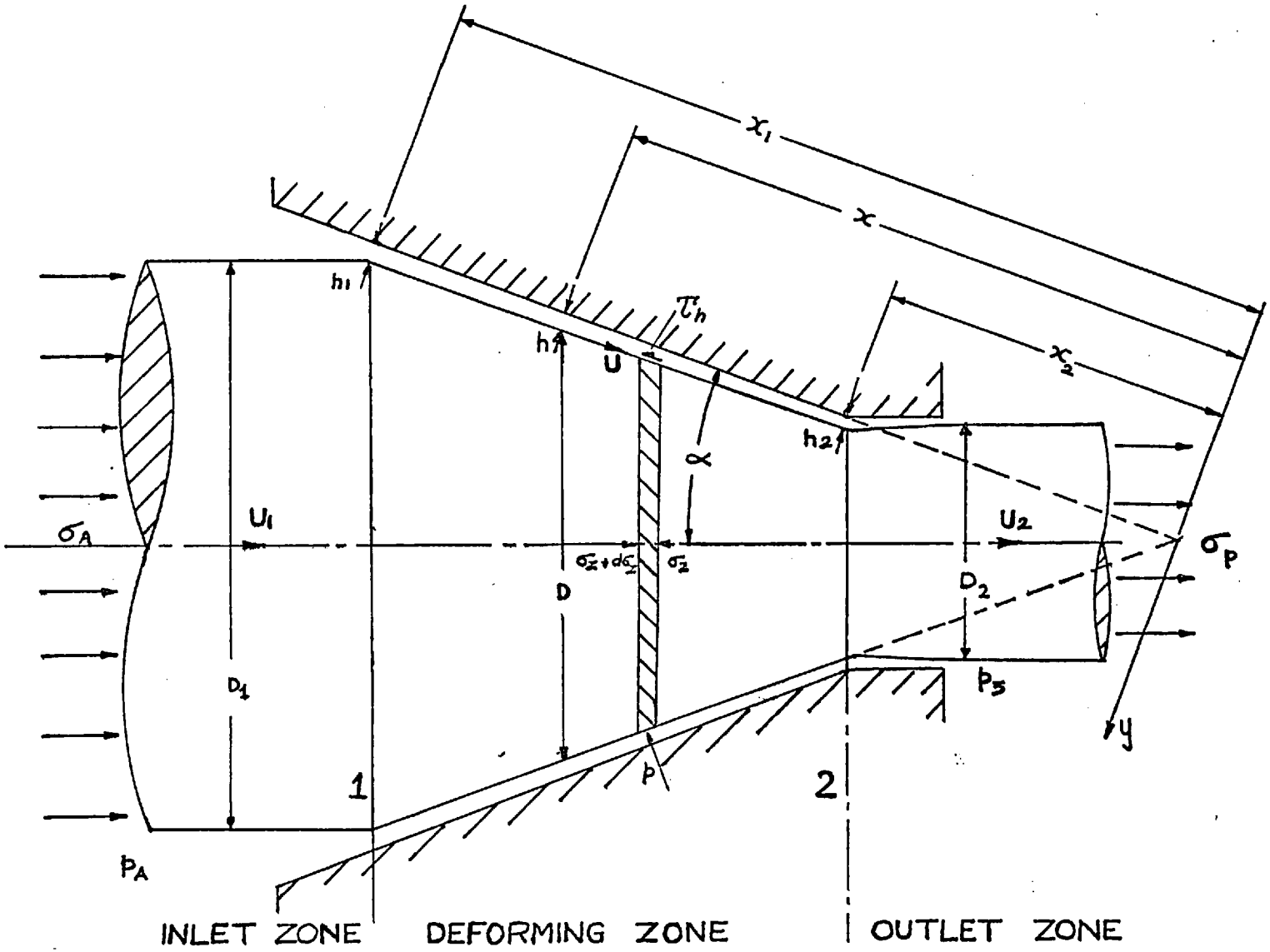
x_1
x
x_2
h_1
h
h_2
τ_h
U
α
σ_A
U_1
U_2
$\sigma_x + d\sigma_x$
σ_x
σ_p
D
D_2
D_1
p_3
p_A
p
1
2
y
INLET ZONE
DEFORMING ZONE
OUTLET ZONE

FIG. 18

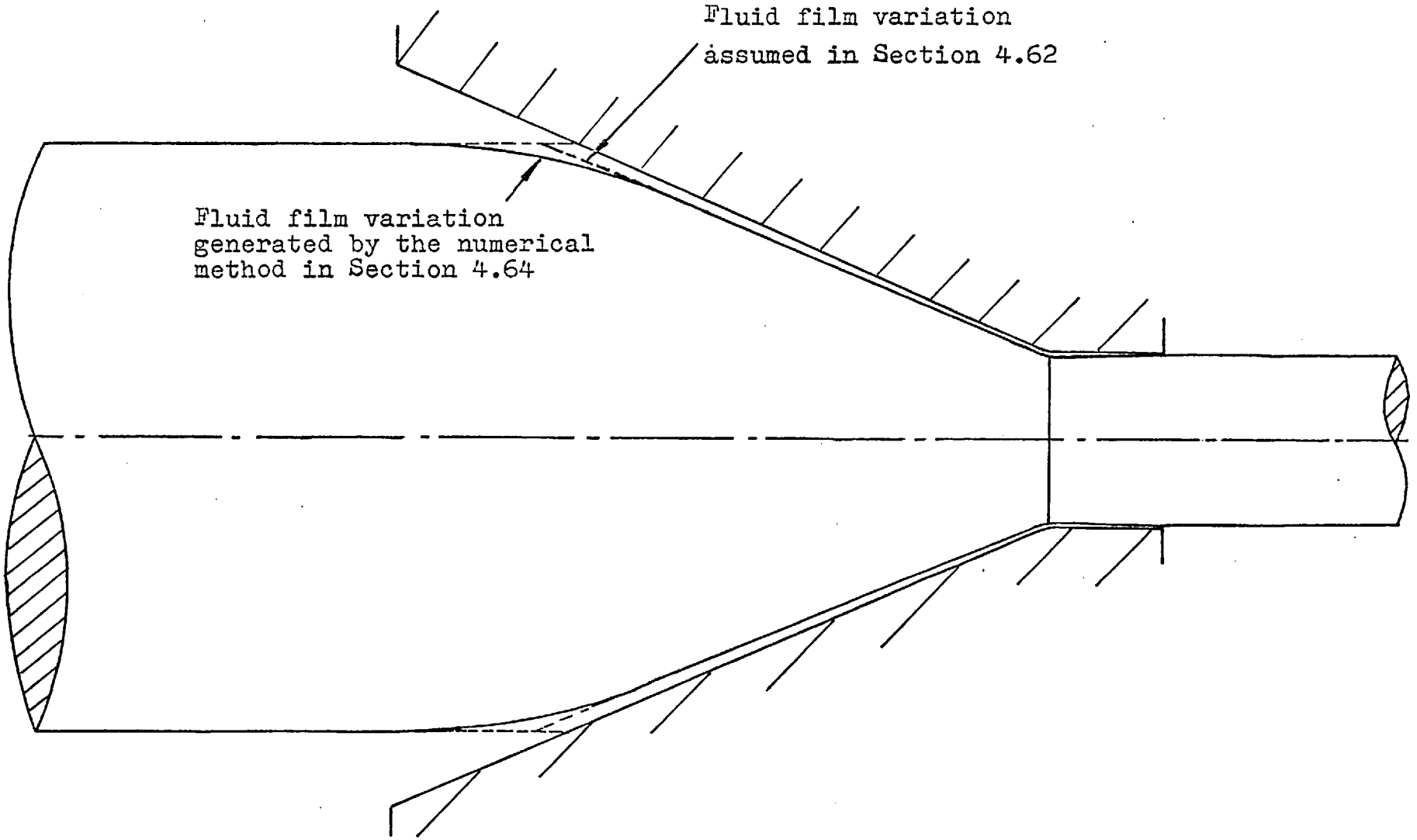

FIG.19 Deformation of the billet in the inlet zone in hydrostatic extrusion with hydrodynamic lubrication for a work-hardening material

MATERIAL: VITAL X

HARDEN TO 62 - 64 RC

GRIND ALL OVER

REMOVE SHARP CORNERS

ALL DIMENSIONS IN INCHES

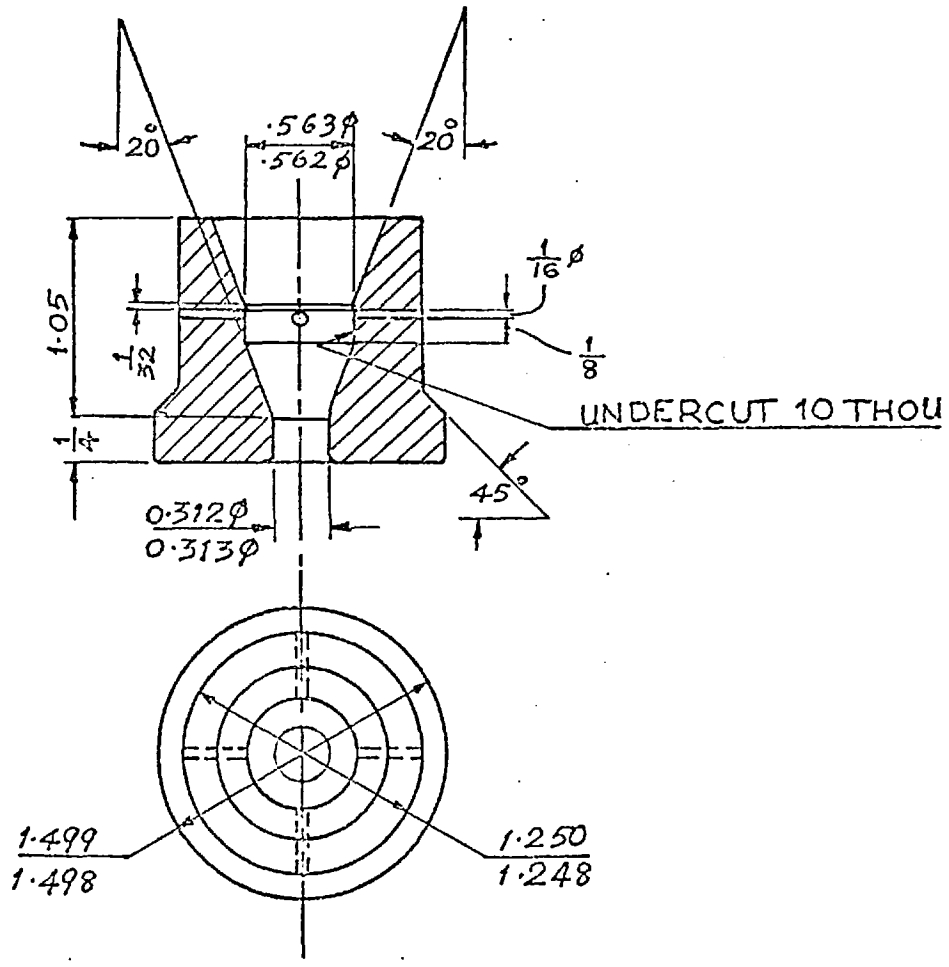

DOUBLE REDUCTION DIE

FIG. 20

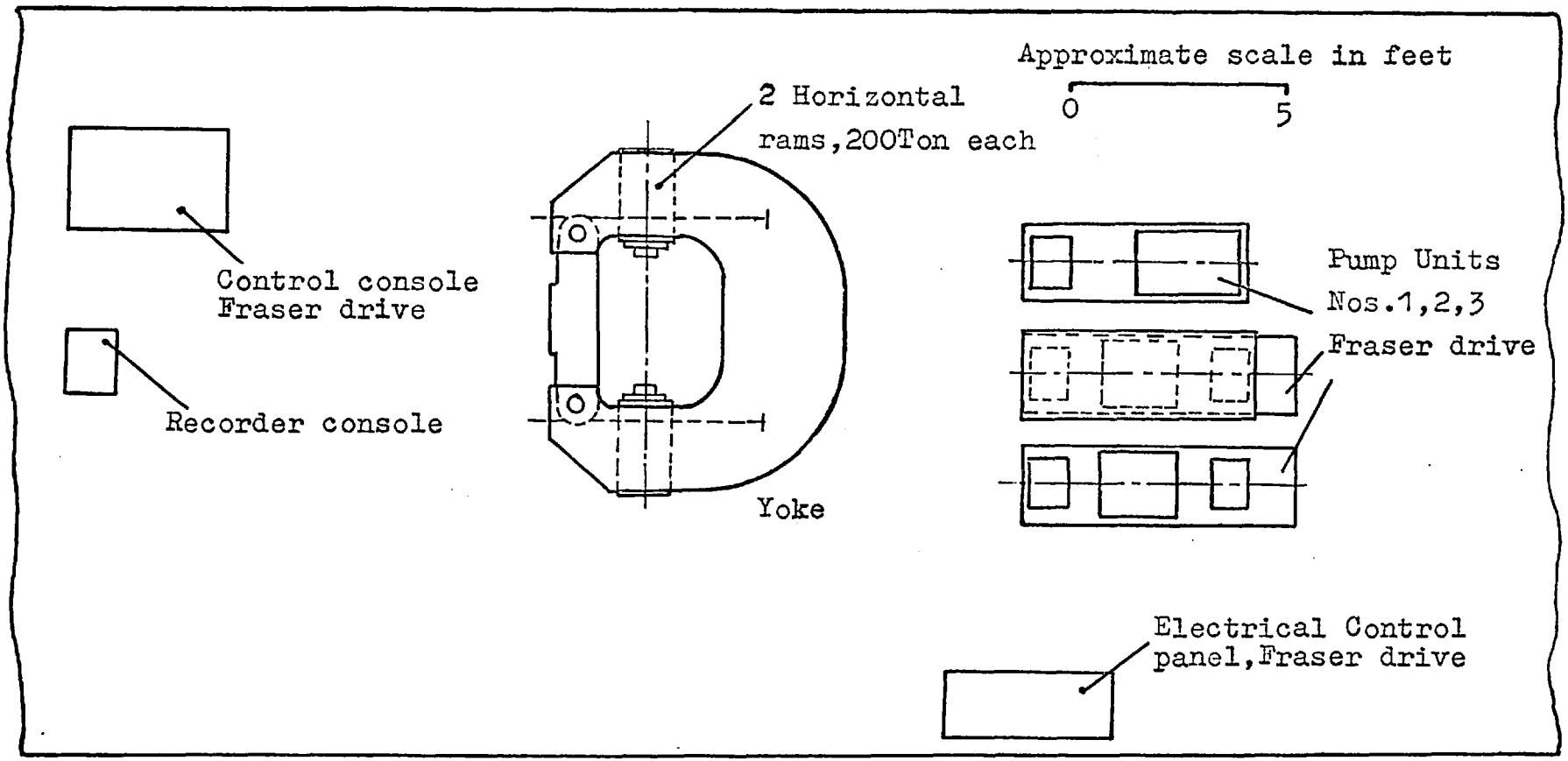

FIG.21 A plan drawing of the yoke,Fraser hydraulic drive and the controls

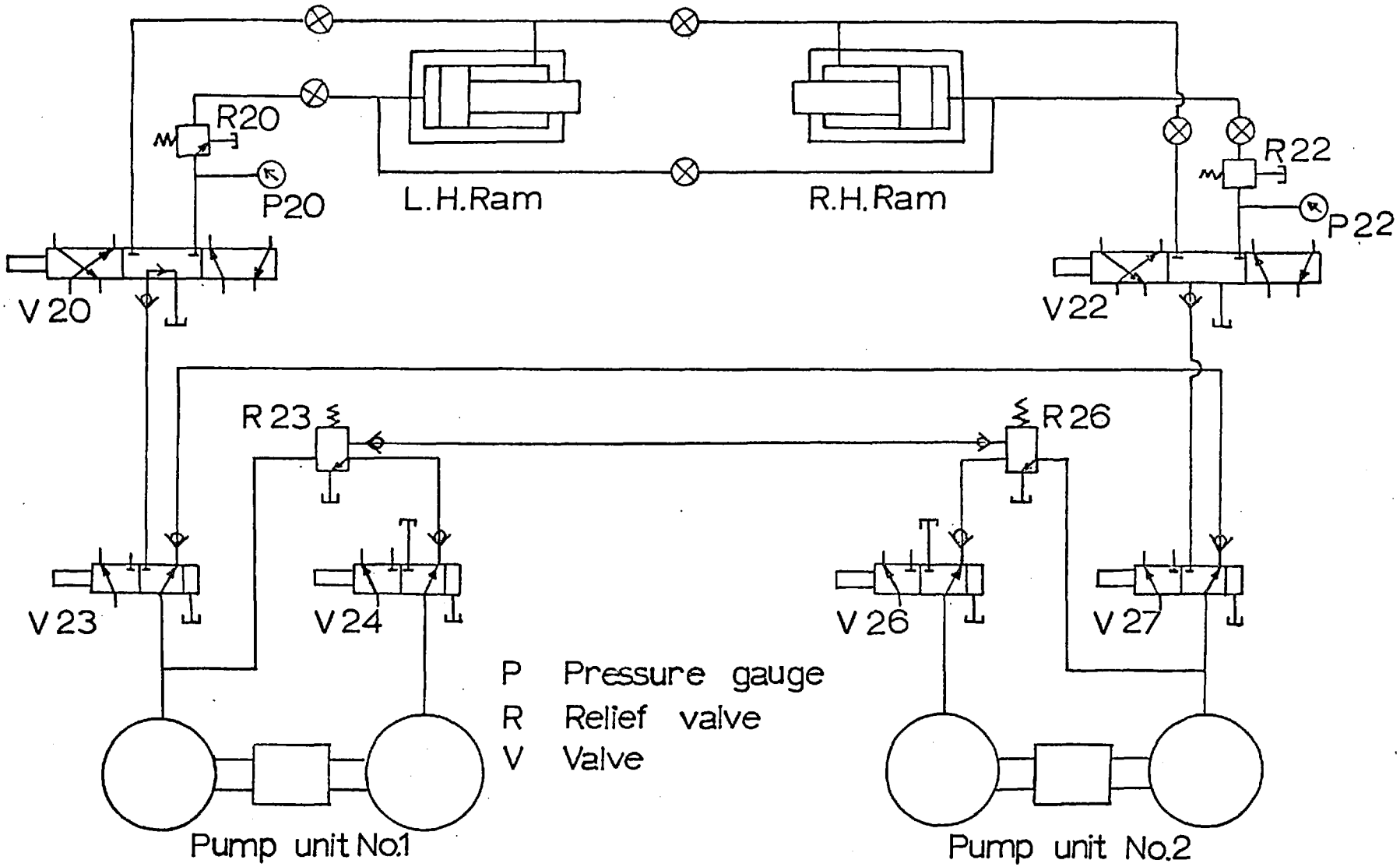

FIG. 22 A flow diagram of the 'Fraser' hydraulic drive

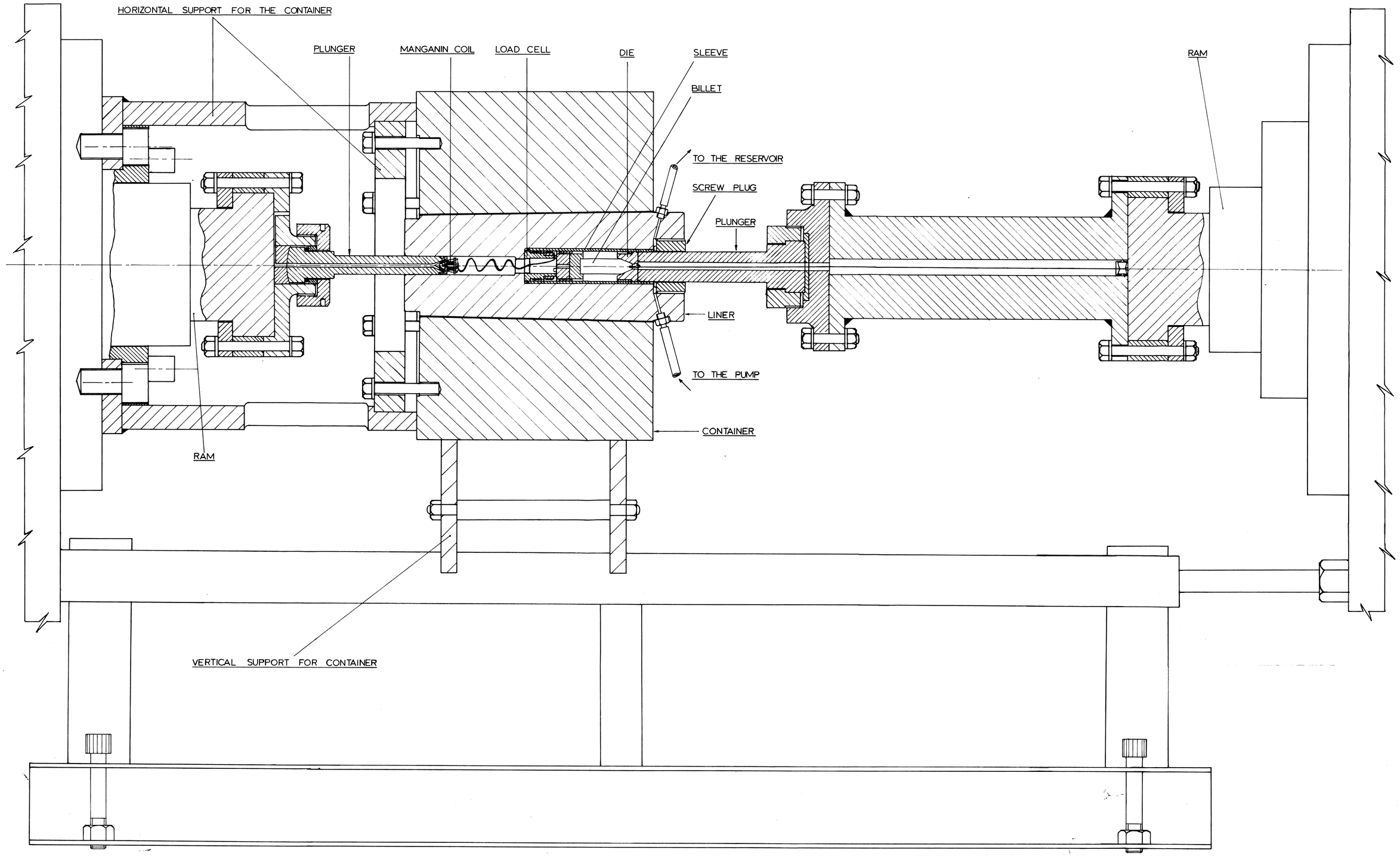

AUGMENTED HYDROSTATIC EXTRUSION

FIG. 23

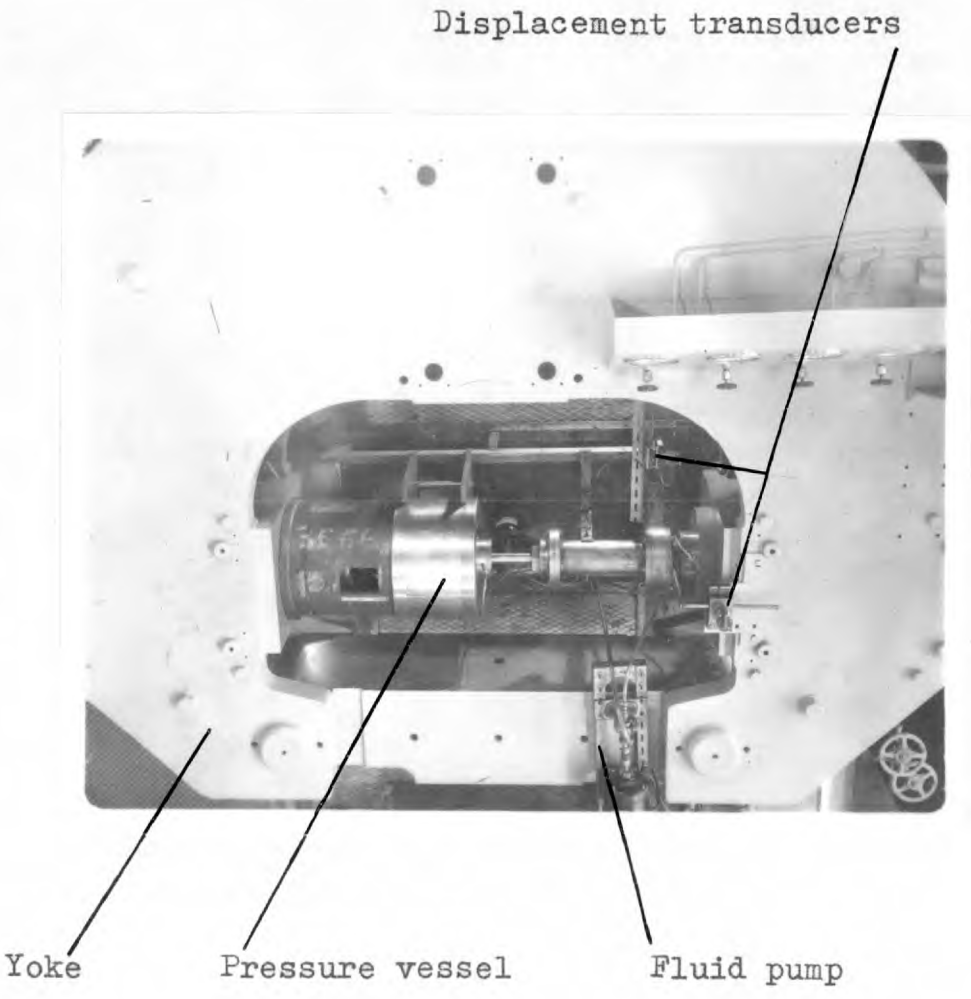

FIG.24 Photograph of the yoke and the hydrostatic extrusion sub-press

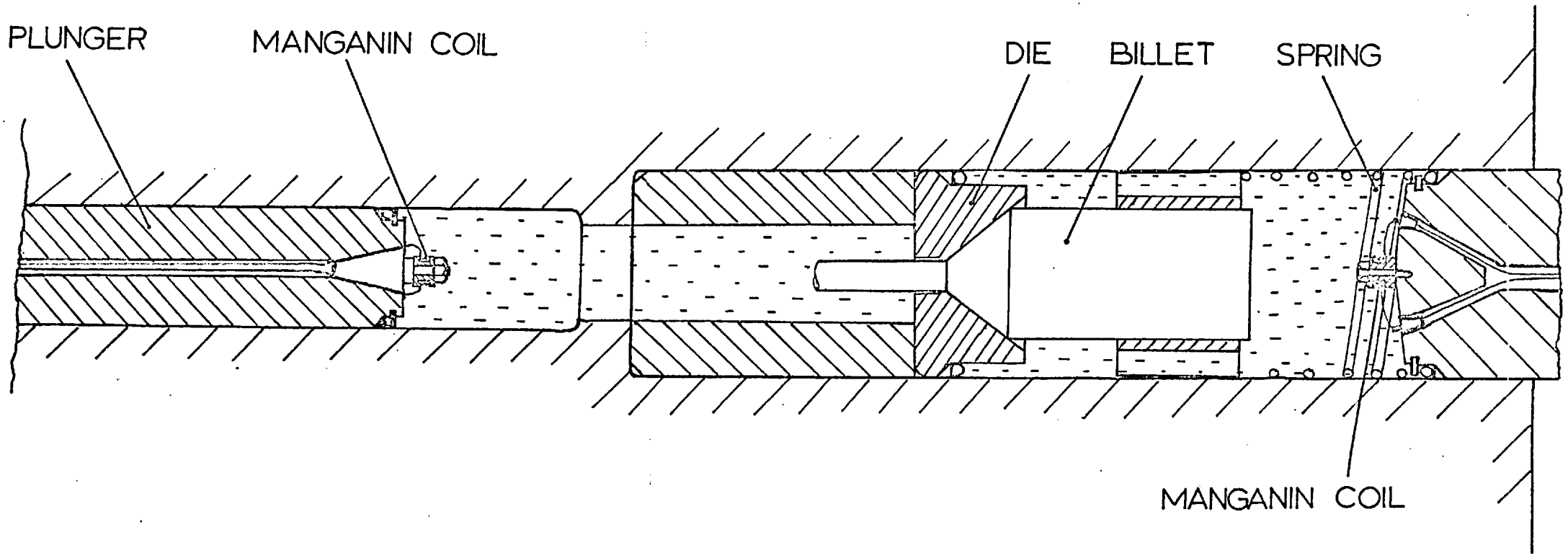

FLUID-TO-FLUID EXTRUSION

FIG.25

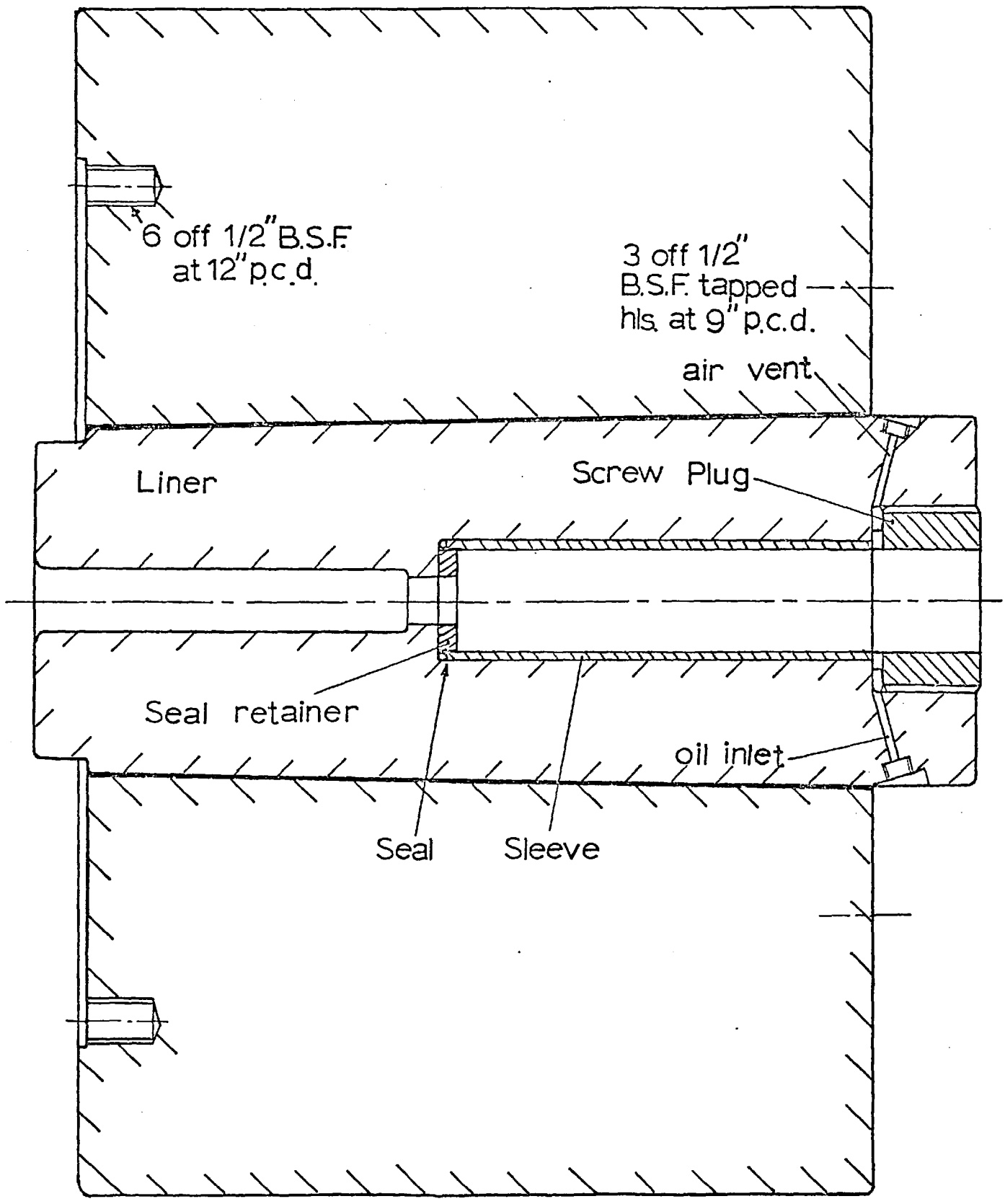

Fig.26 Container

Scale 1/2 Full Size

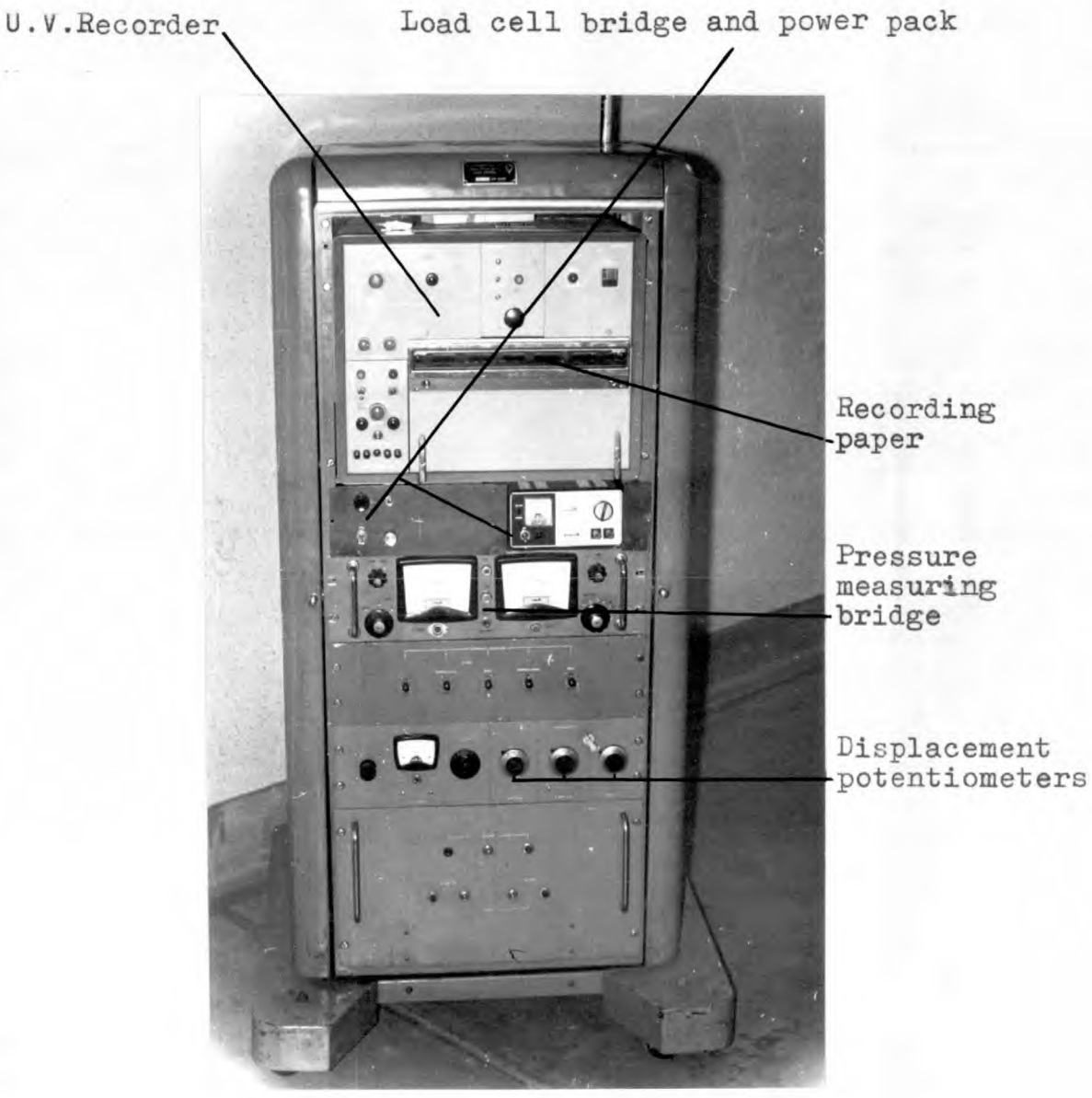

FIG.27 Recorder console

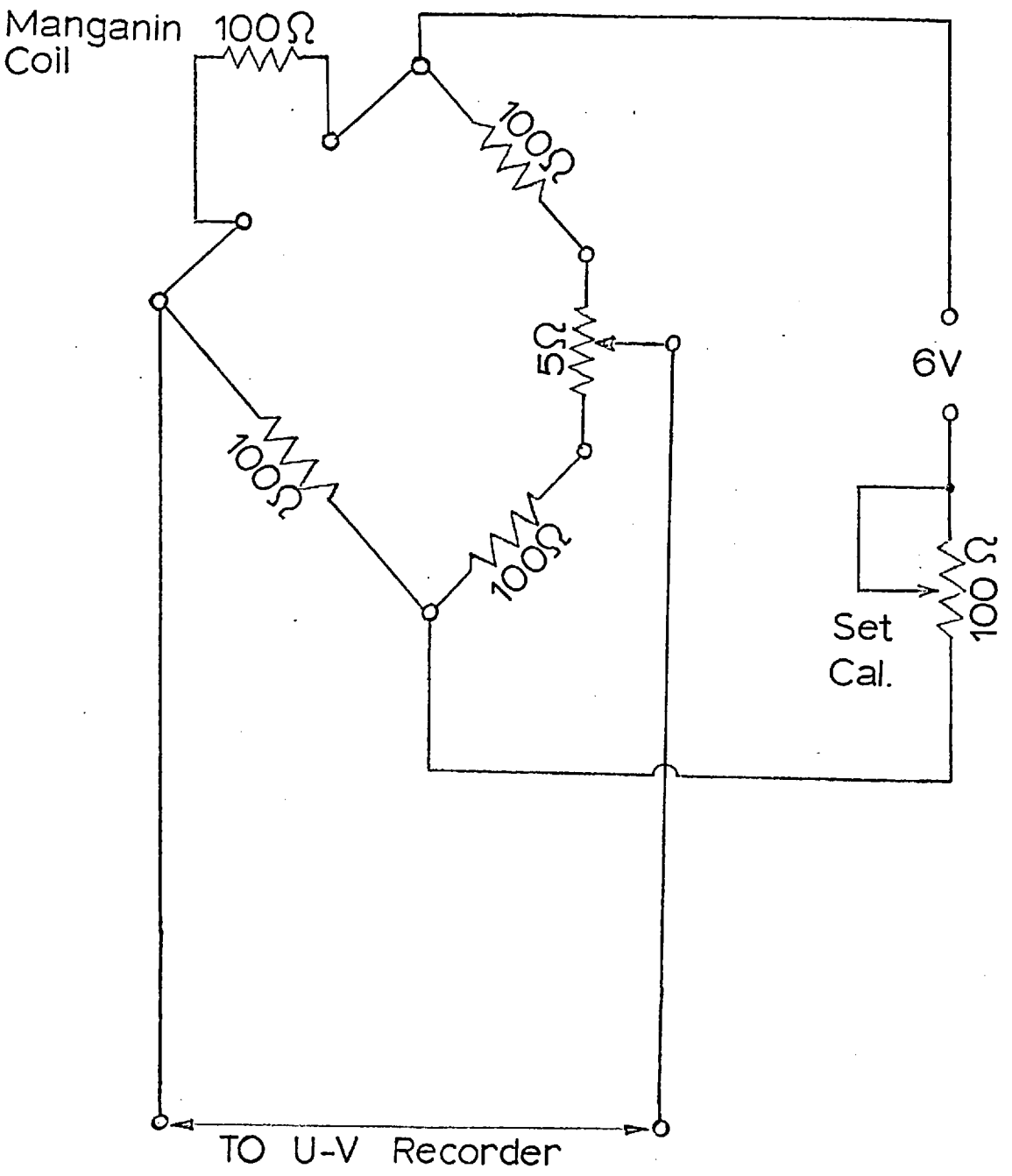

FIG.28

Wheatstone bridge circuit for pressure measurement

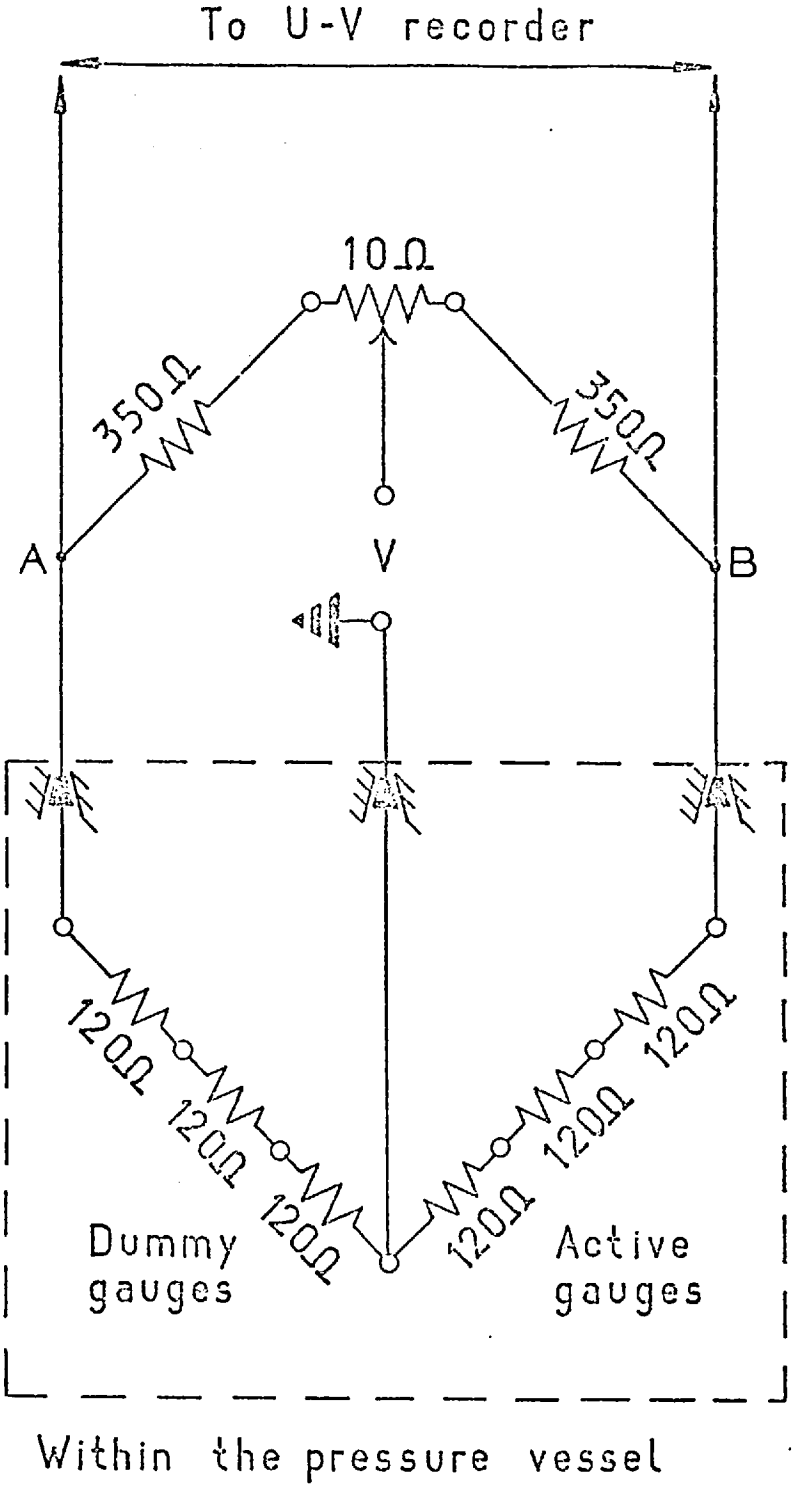

FIG.29

Wheatstone bridge circuit for augmenting load measurement

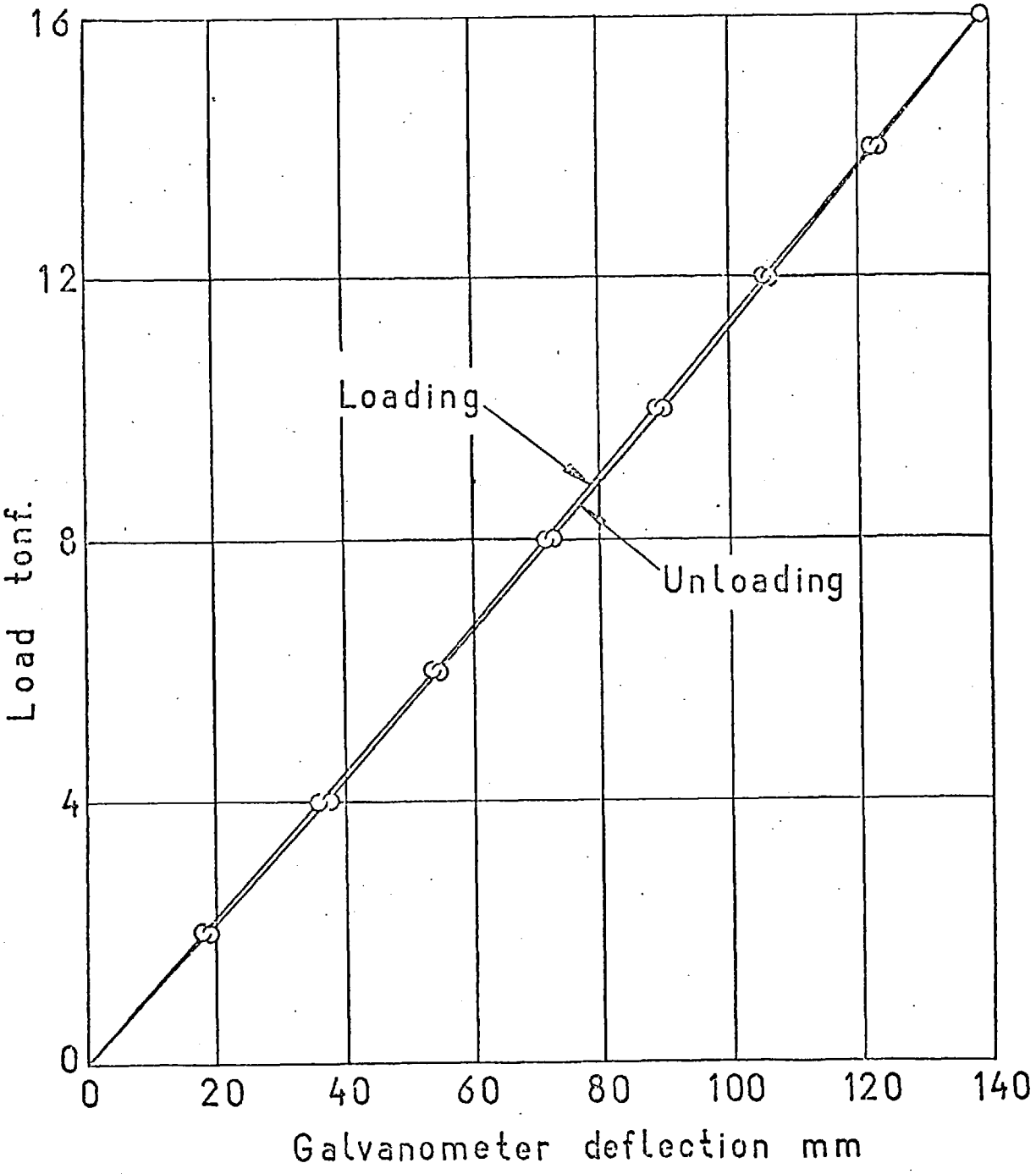

FIG.30a

Calibration curve for the 0-30Ton load cell

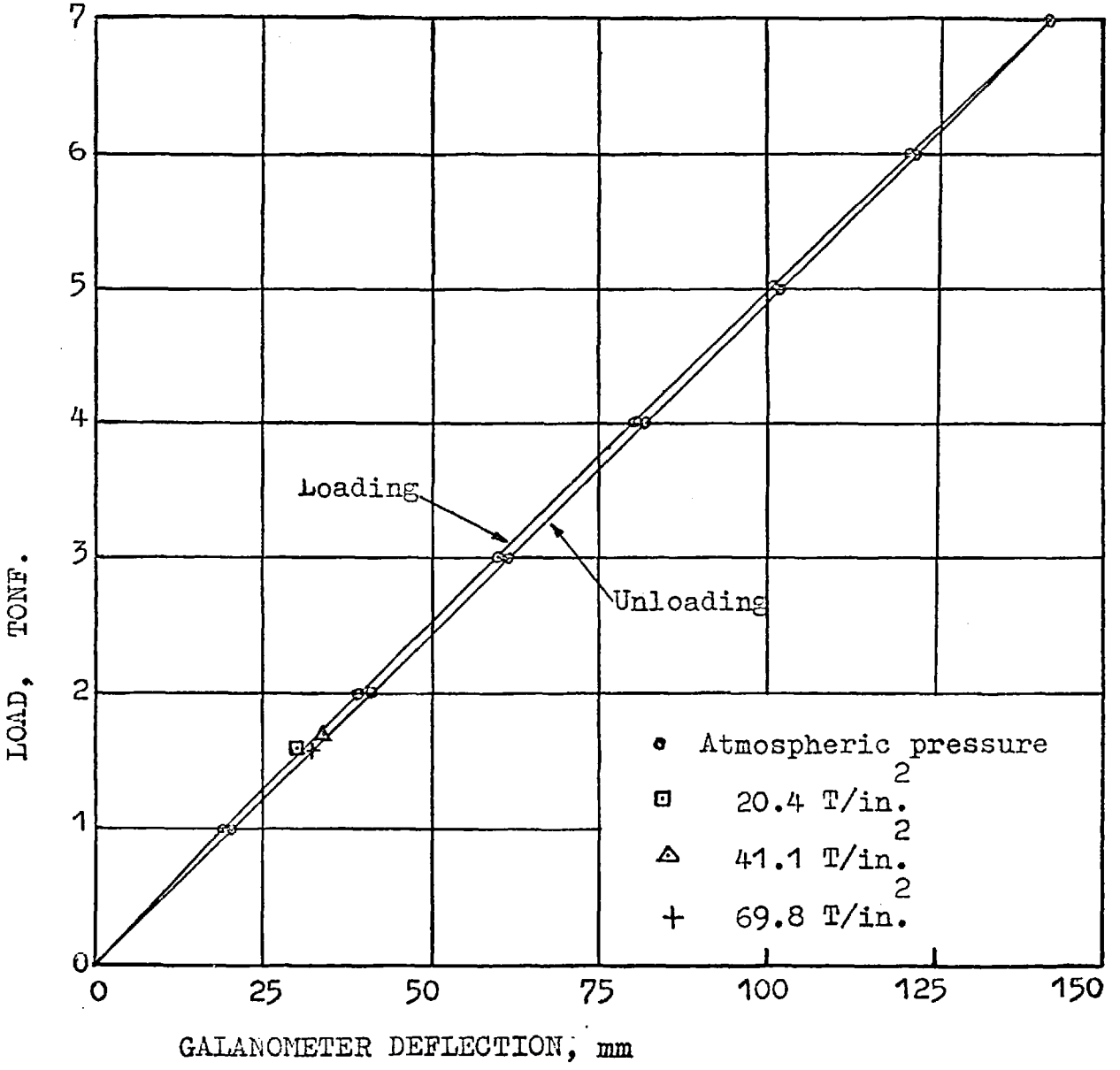

FIG.30b Calibration curve for the 0-7 Ton load cell

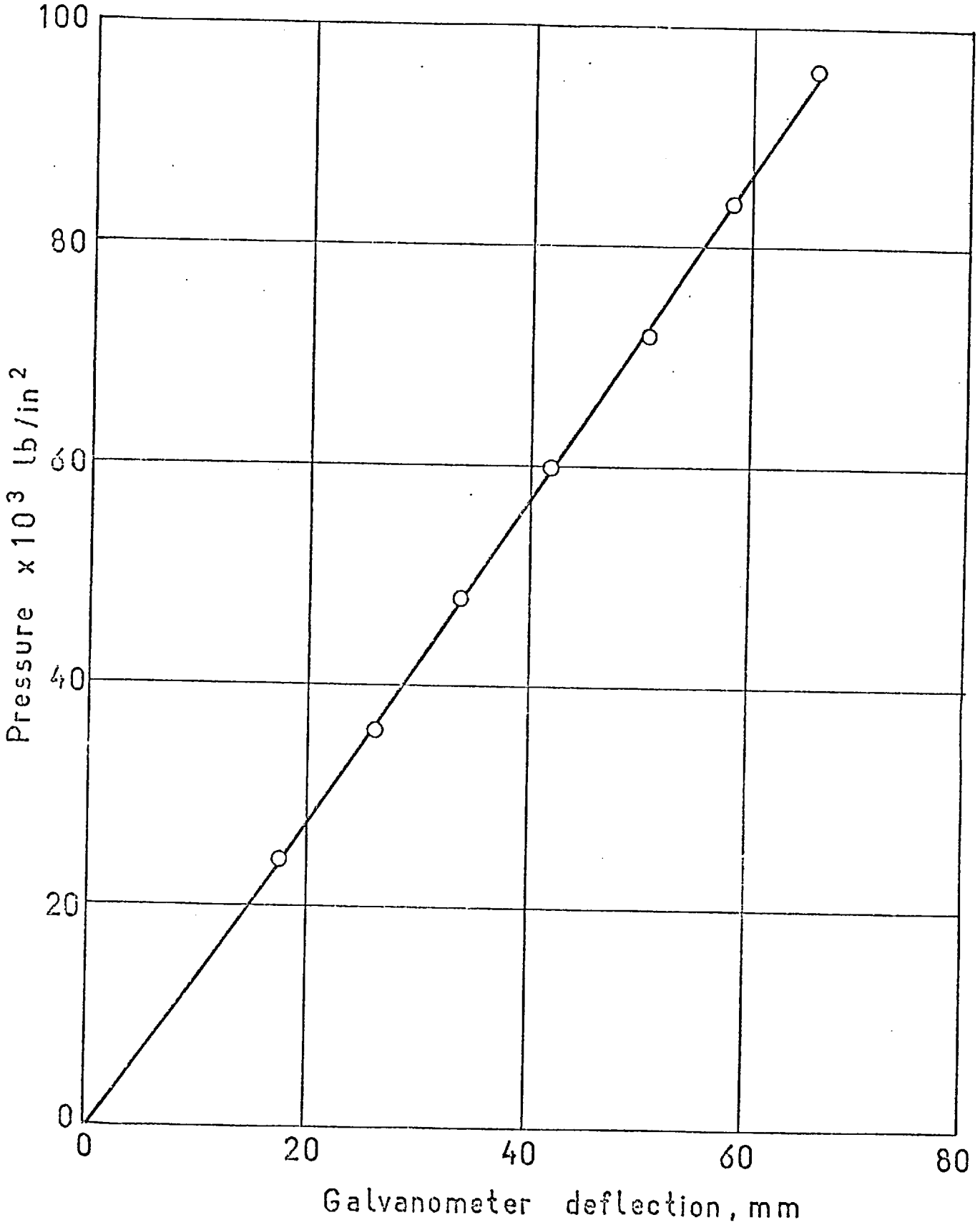

FIG.31a

Calibration curve for manganin coil 1

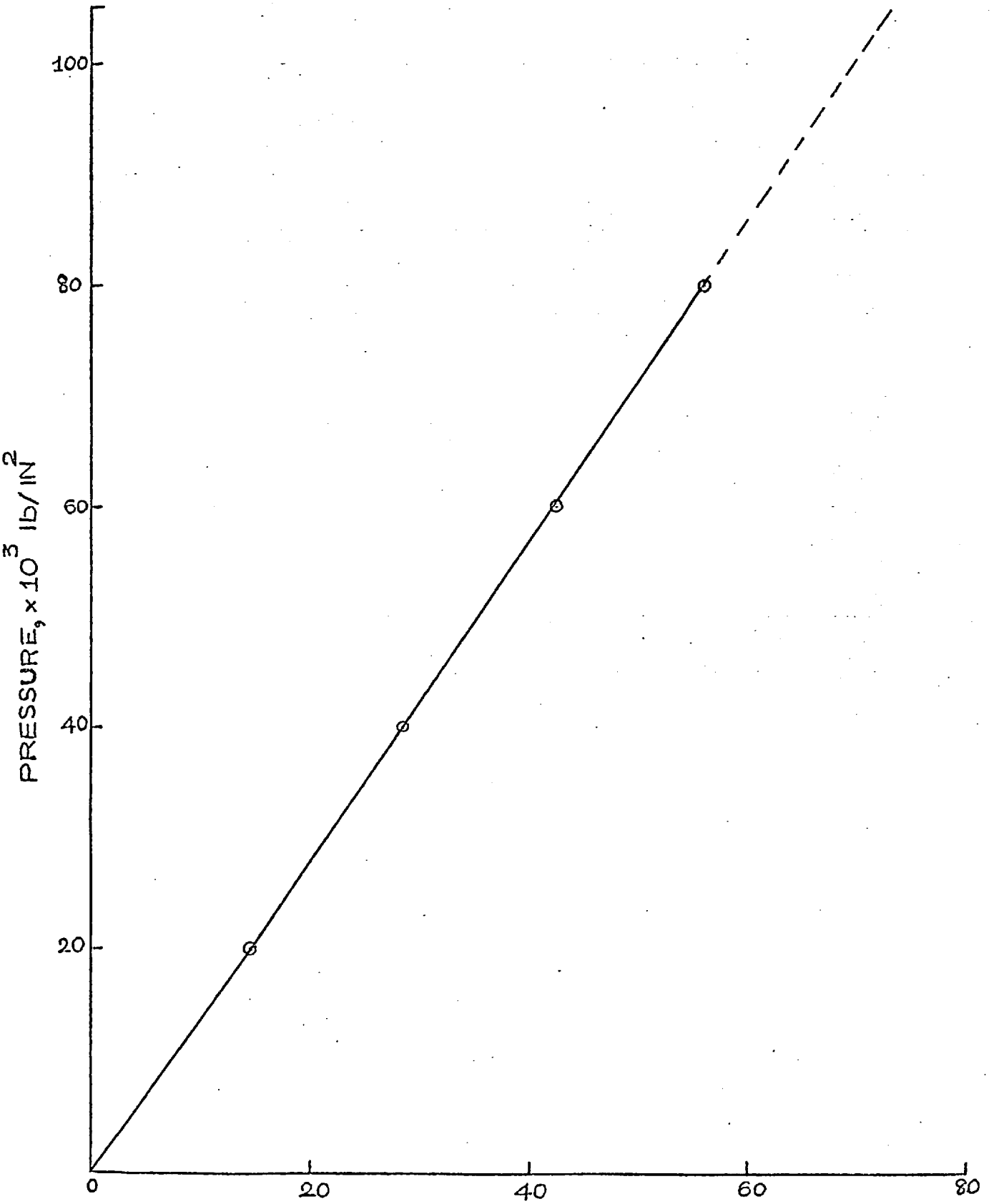

FIG.31b

Calibration curve for manganin coil 2

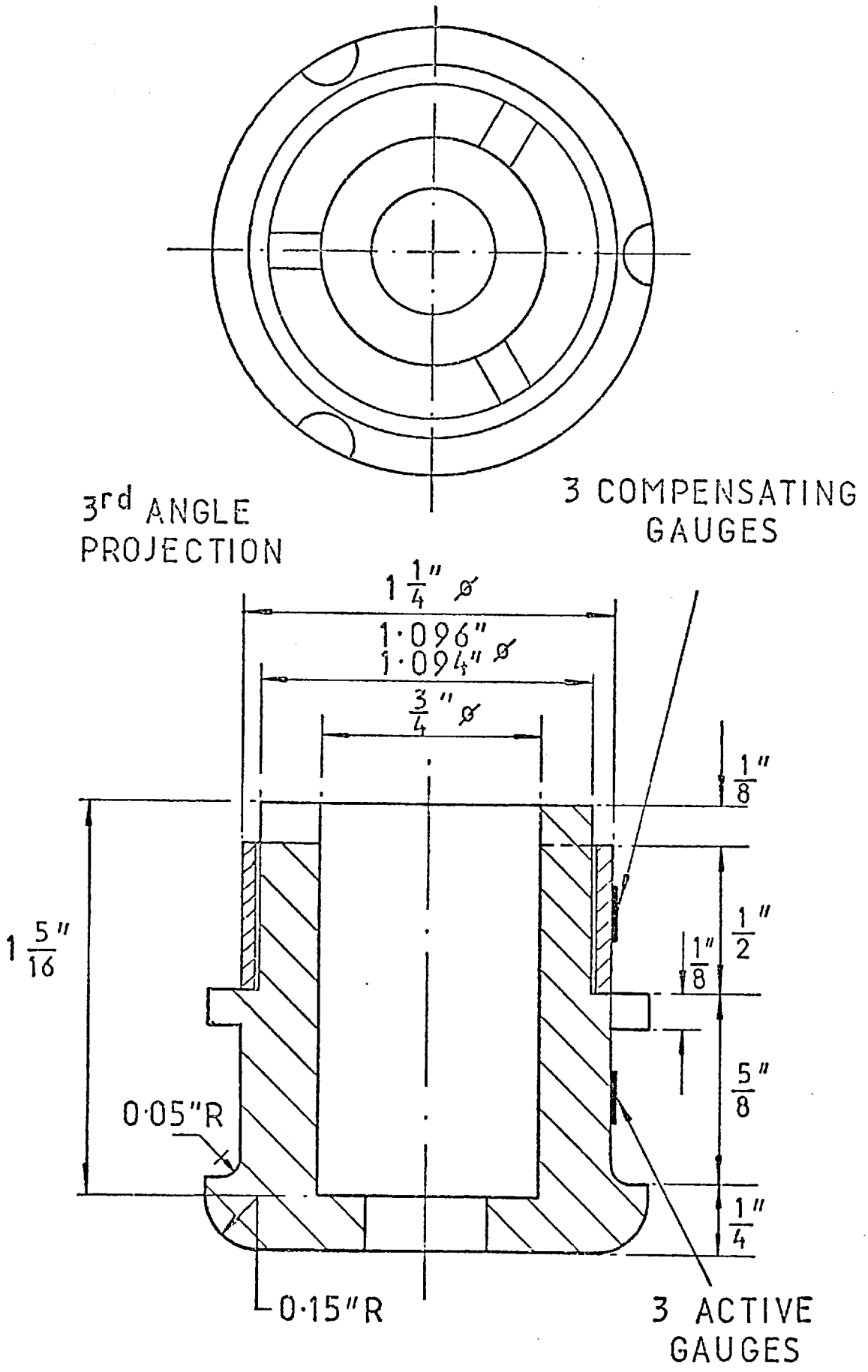

Fig.32a LOAD CELL 0-30TONS

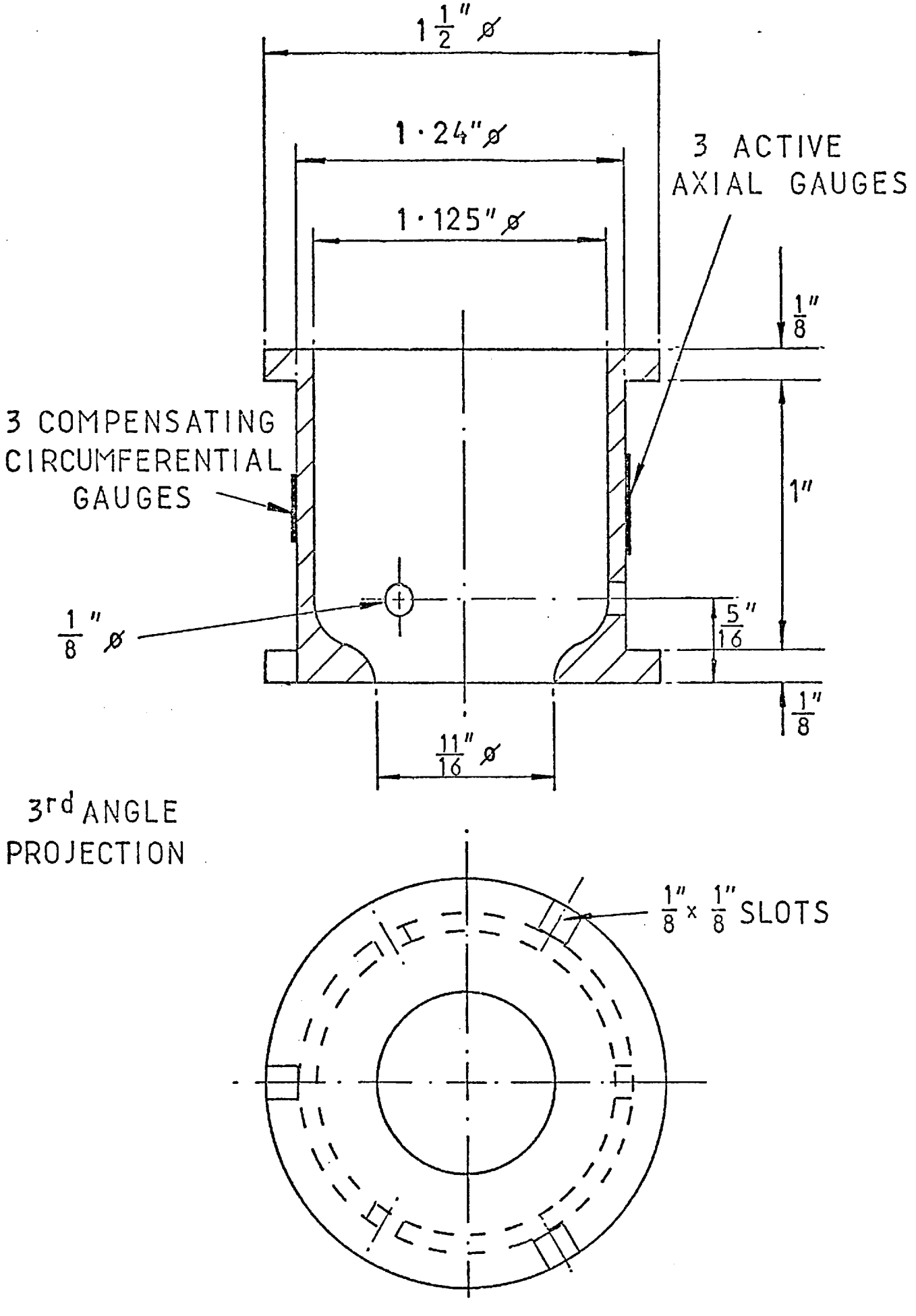

Fig.32b - LOAD CELL 0-7 TONS

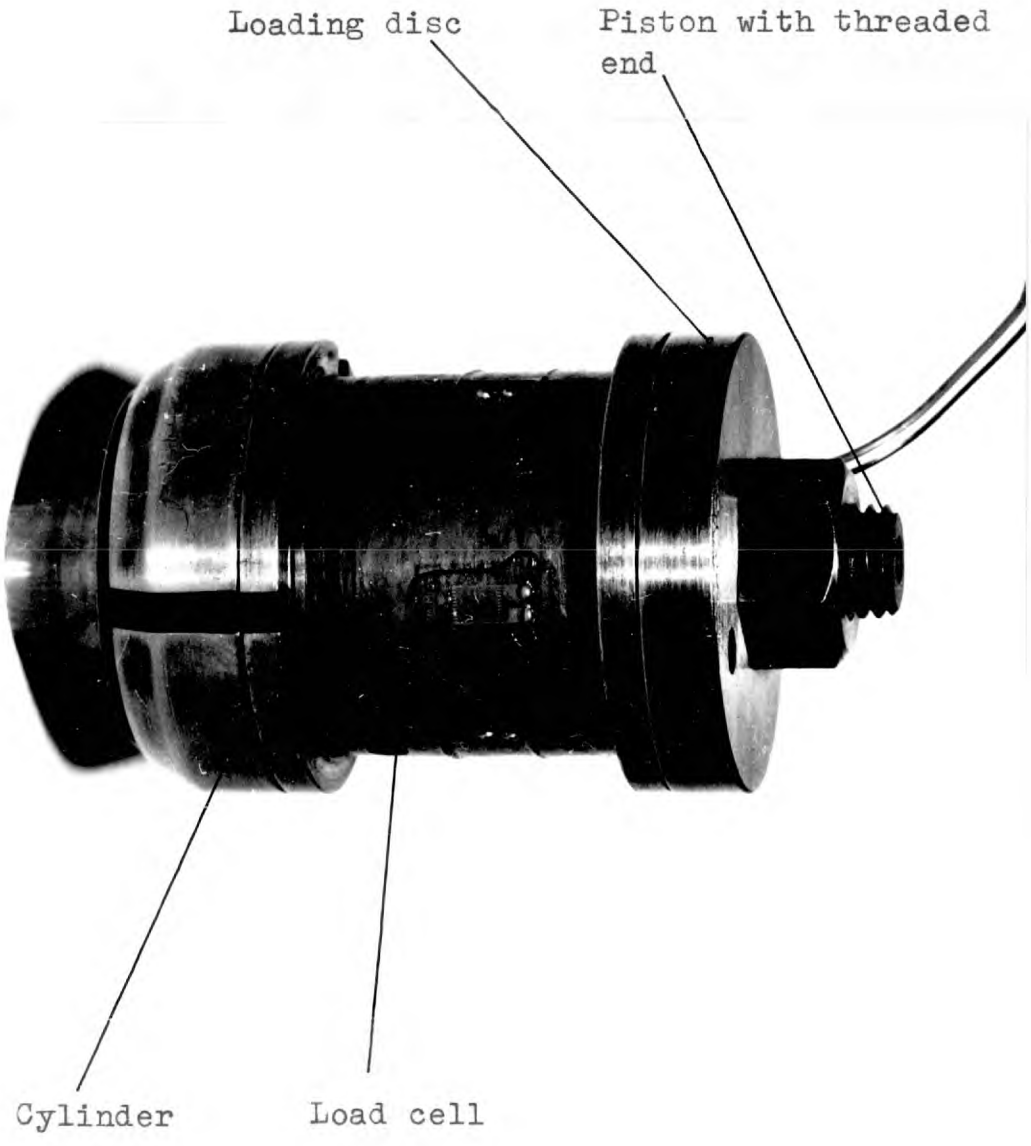

FIG.33 Loading device for calibration of the load cell under pressure

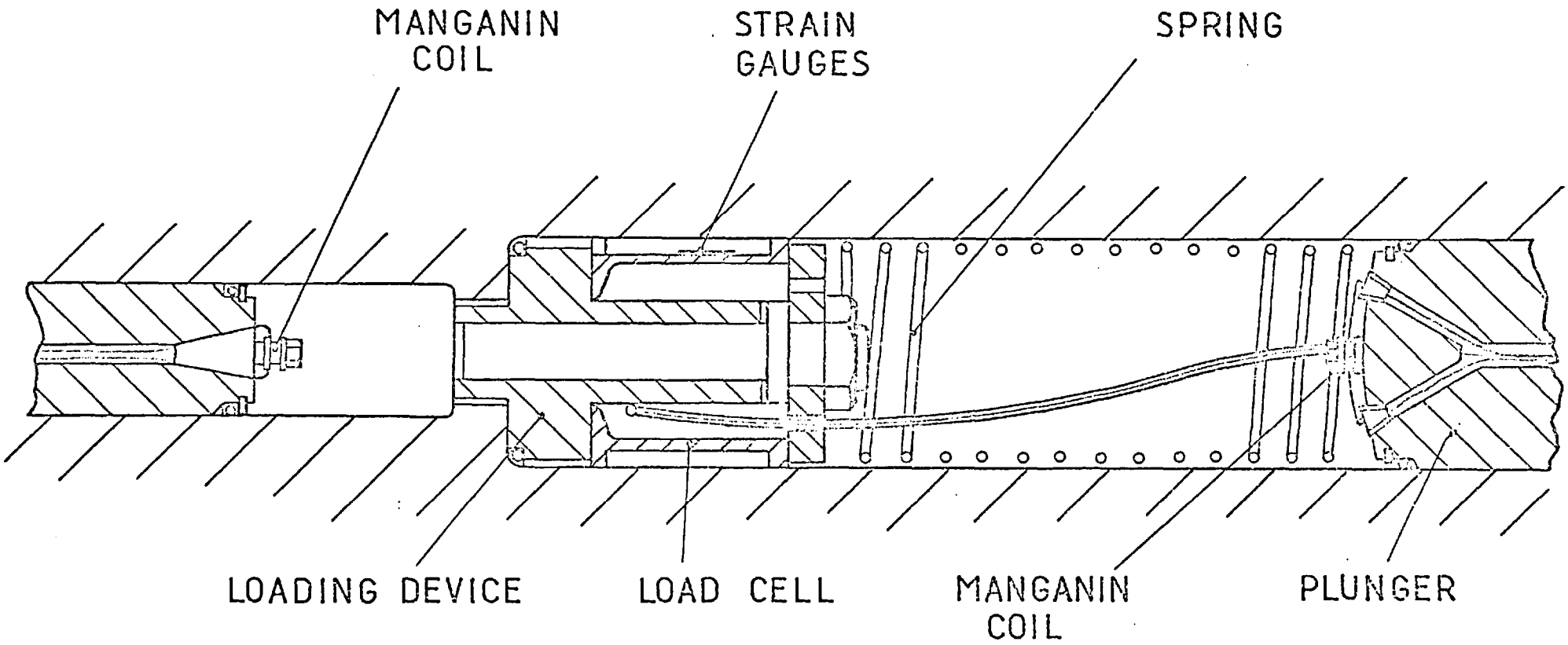

FIG.34

Arrangement of the tooling for calibration of the load cell under pressure

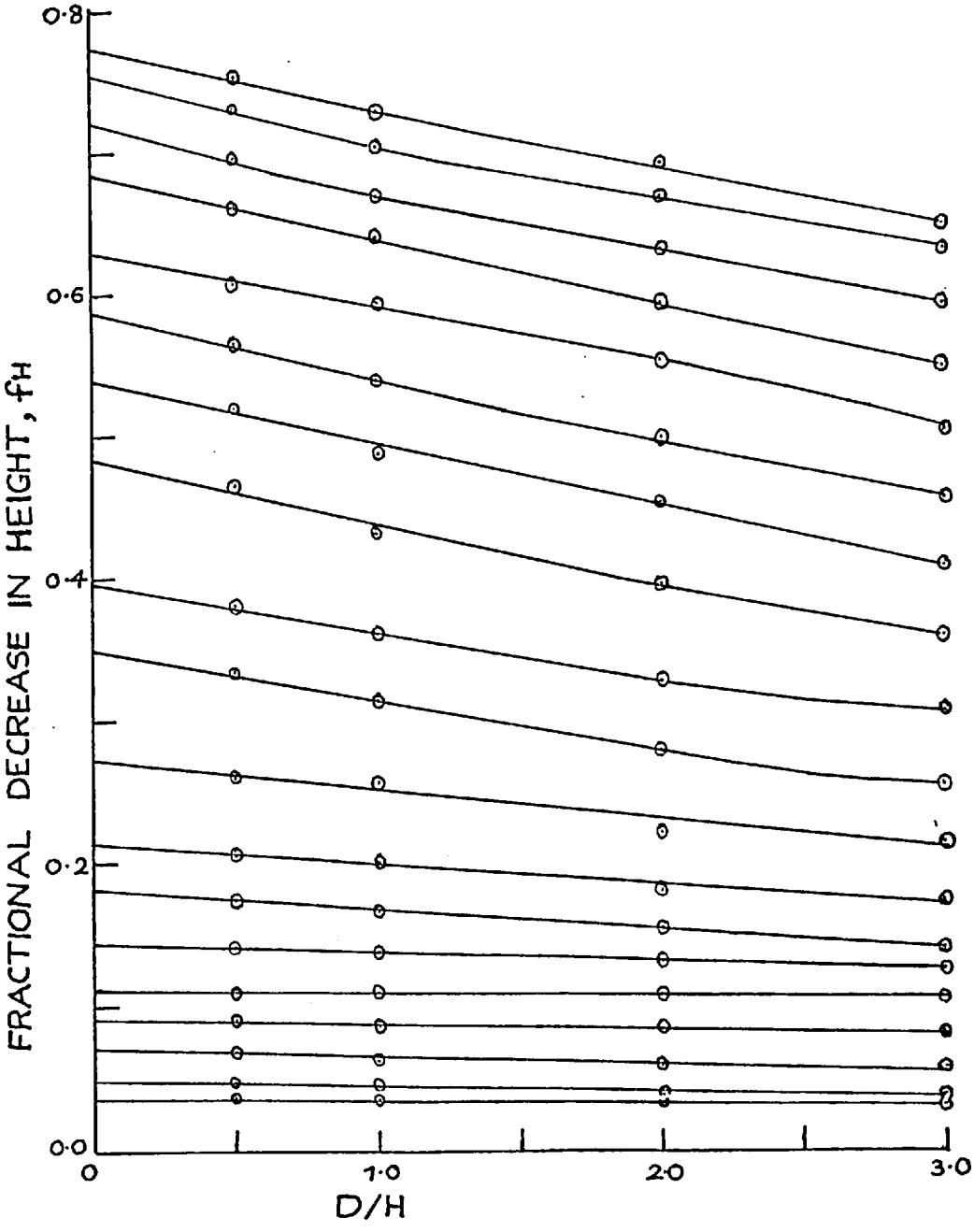

FIG.35a Extrapolation to d/h = 0 to obtain the fractional in height (to determine the stress-strain curve for copper)

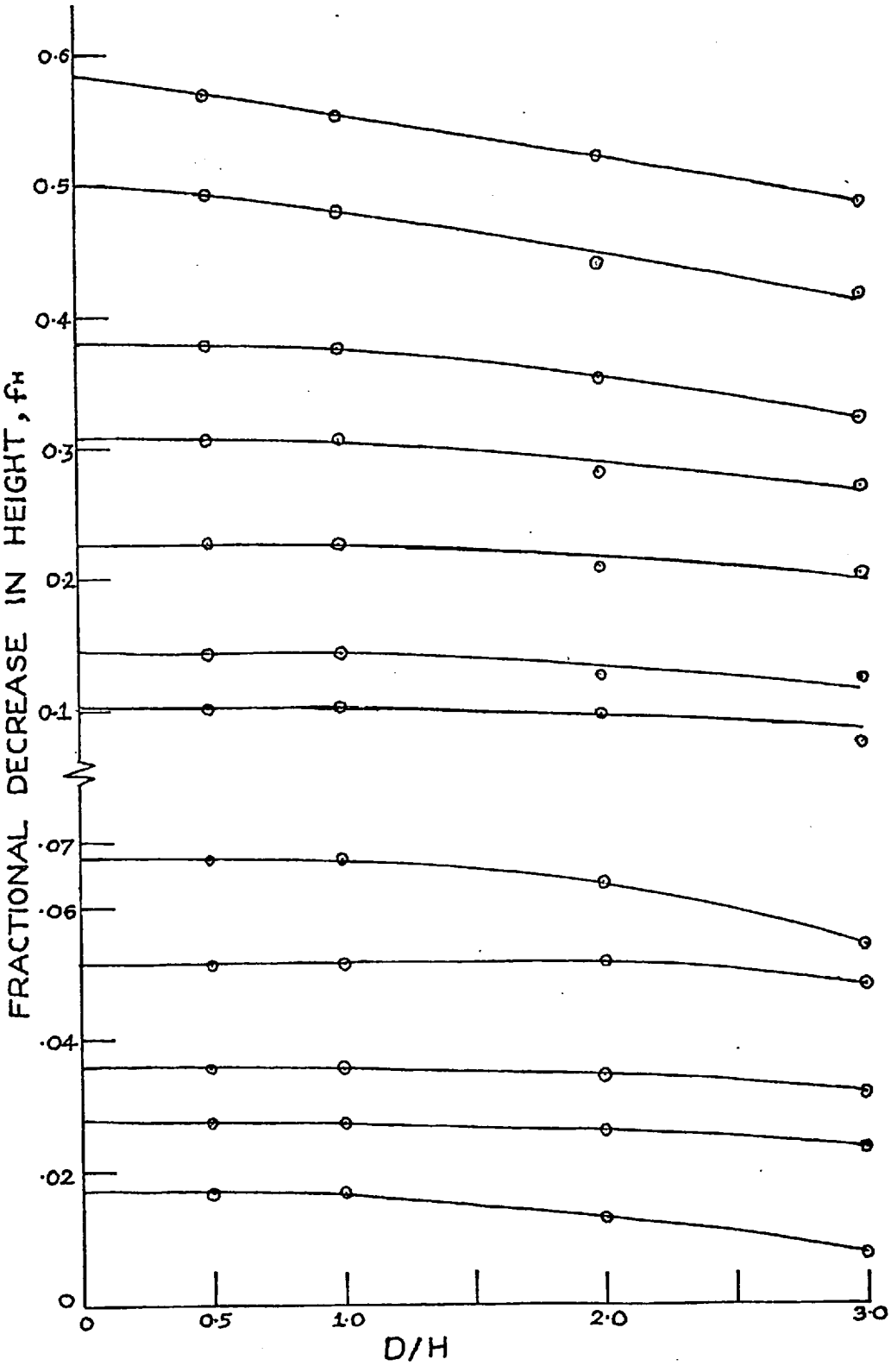

FIG.35b Extrapolation to d/h = 0 to obtain the fractional decrease in height (to obtain the stress-strain curve for mild steel)

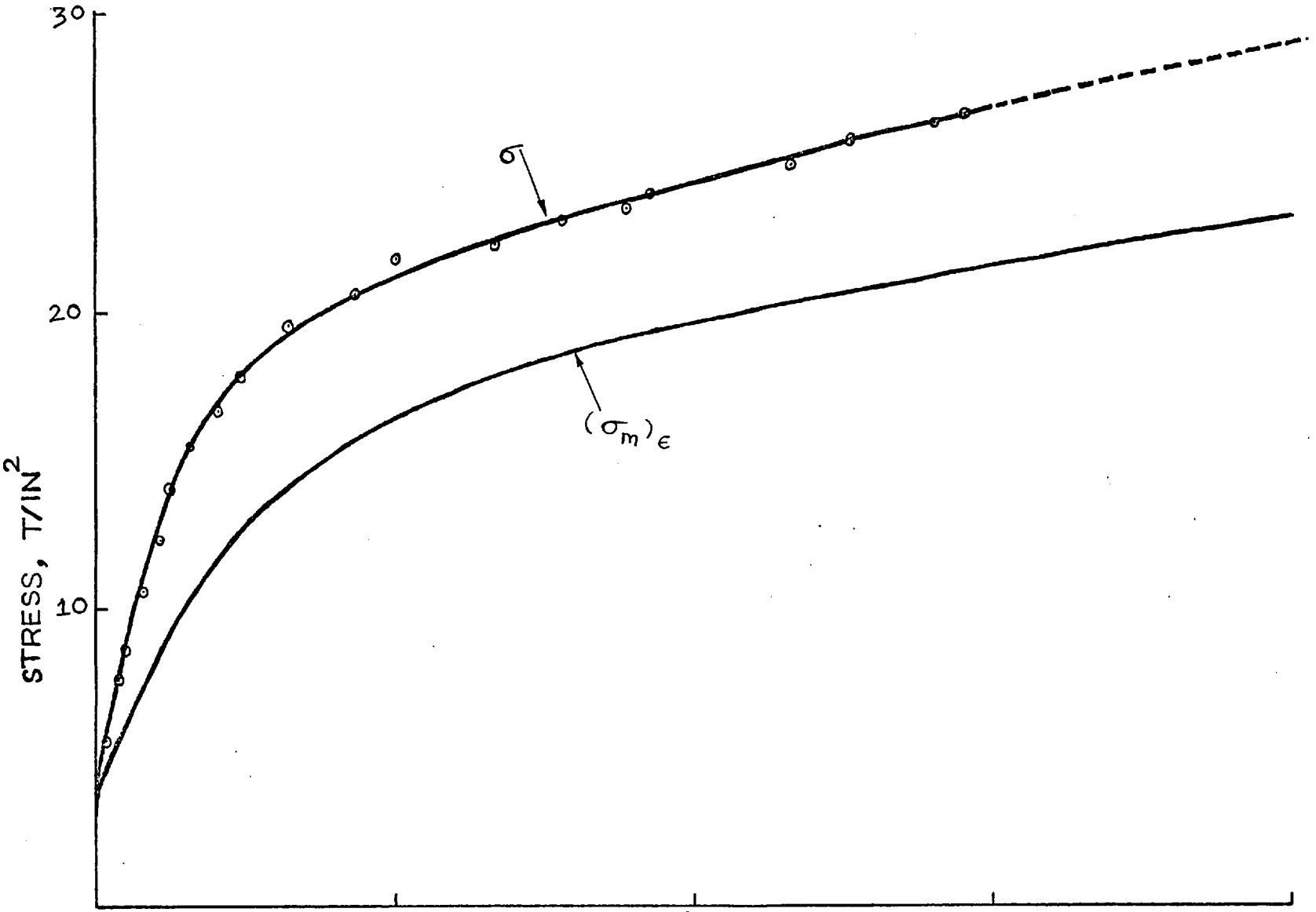

FIG.36a-STRESS STRAIN CURVE FOR COPPER (ANNEALED)

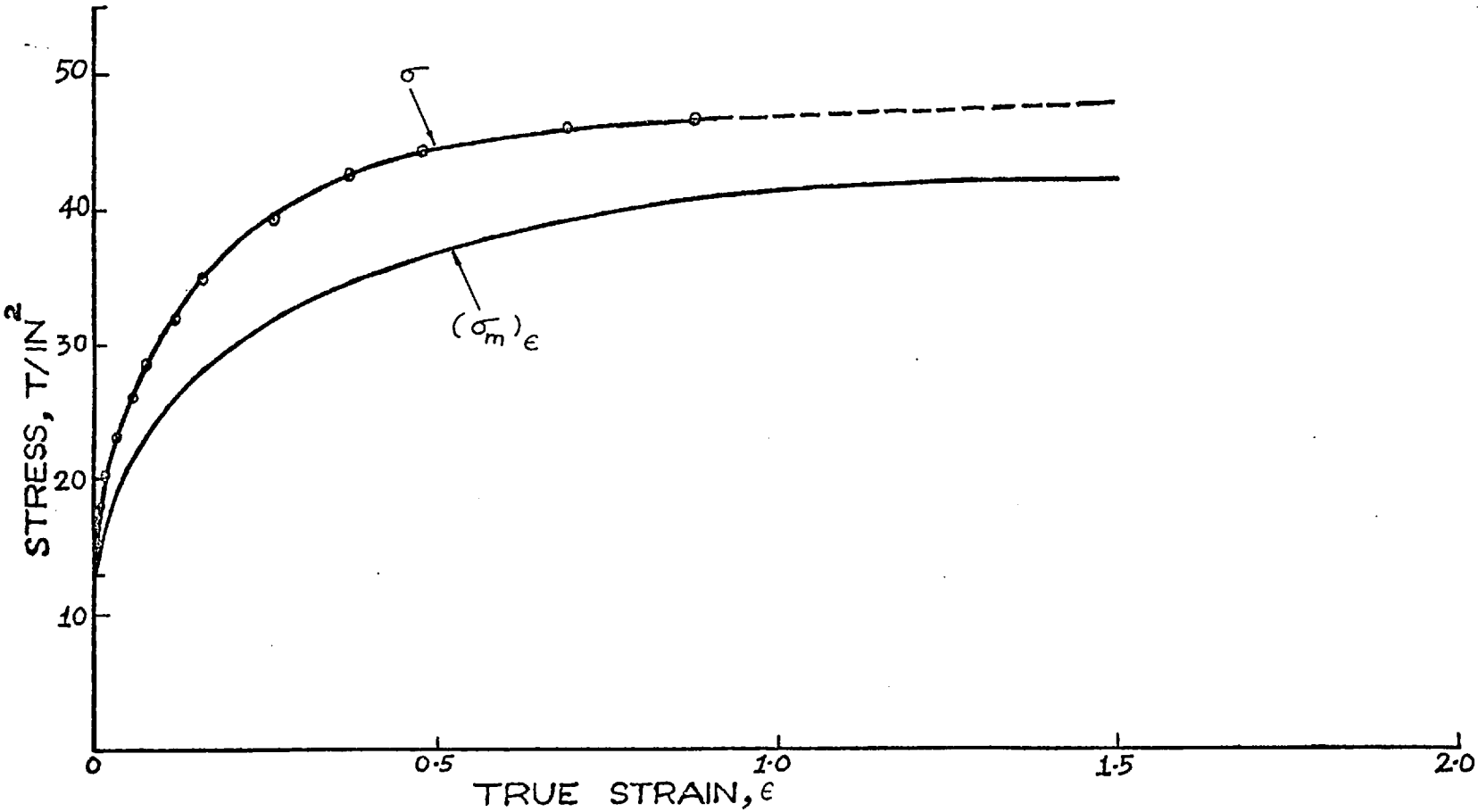

FIG.36b-STRESS STRAIN CURVE FOR MILD STEEL

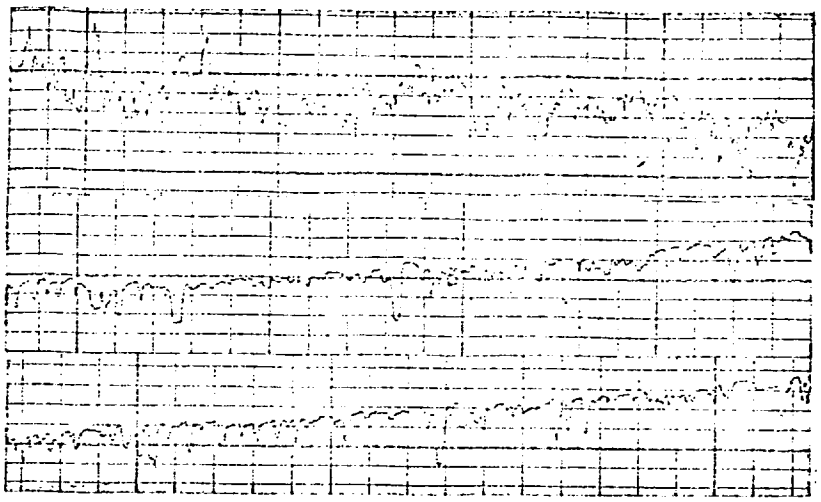

$2\alpha = 40^{\circ}$

(a)

(b)

(c)

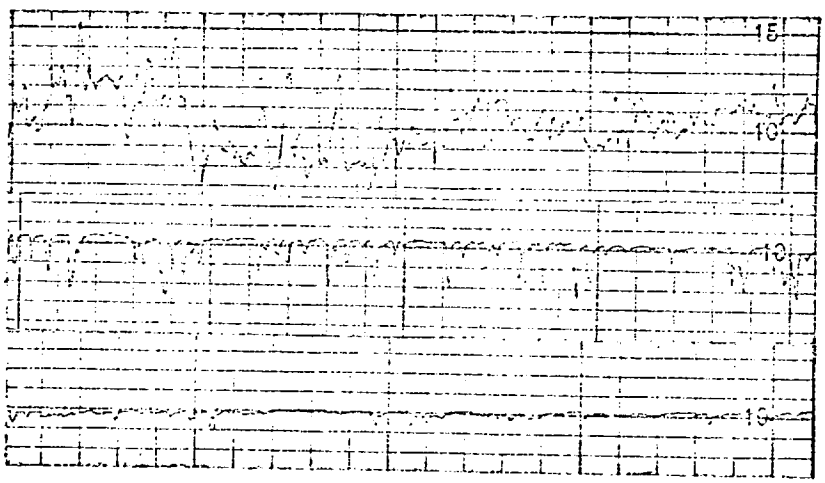

$2\alpha = 60^{\circ}$

(a)

(b)

(c)

Fig.37

Copper
R=2·5

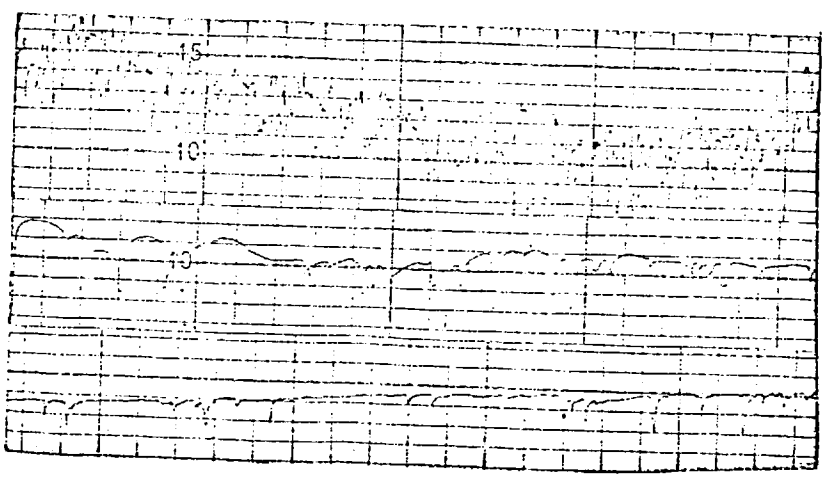

$2\alpha = 90^{\circ}$

(a)

(b)

(c)

(a)- Axial surface profile of billet.

(b)- " " " " deformation zone.

(c)- " " " " product

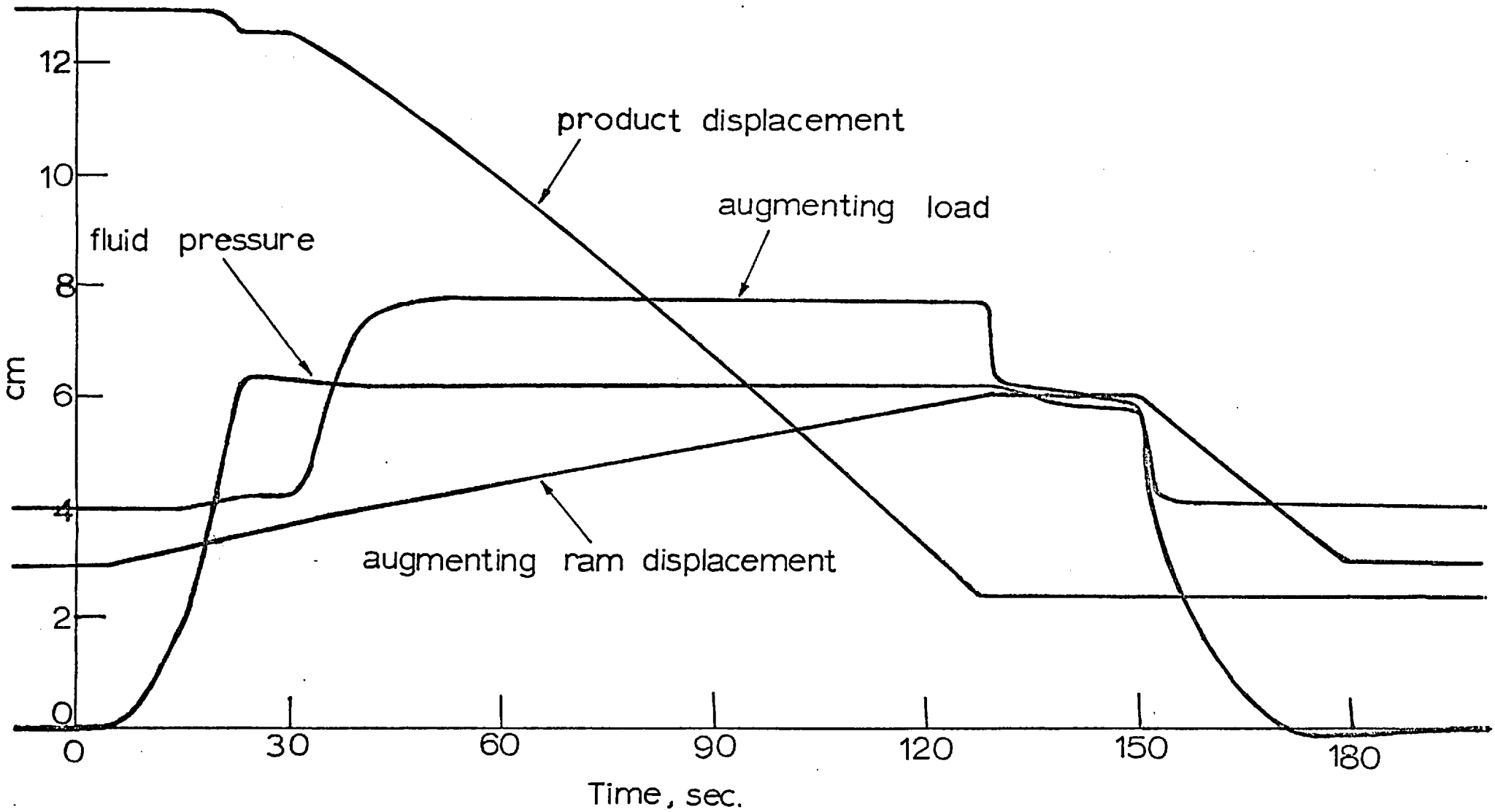

FIG.38 A typical record of the quantities measured in billet augmented hydrostatic extrusion

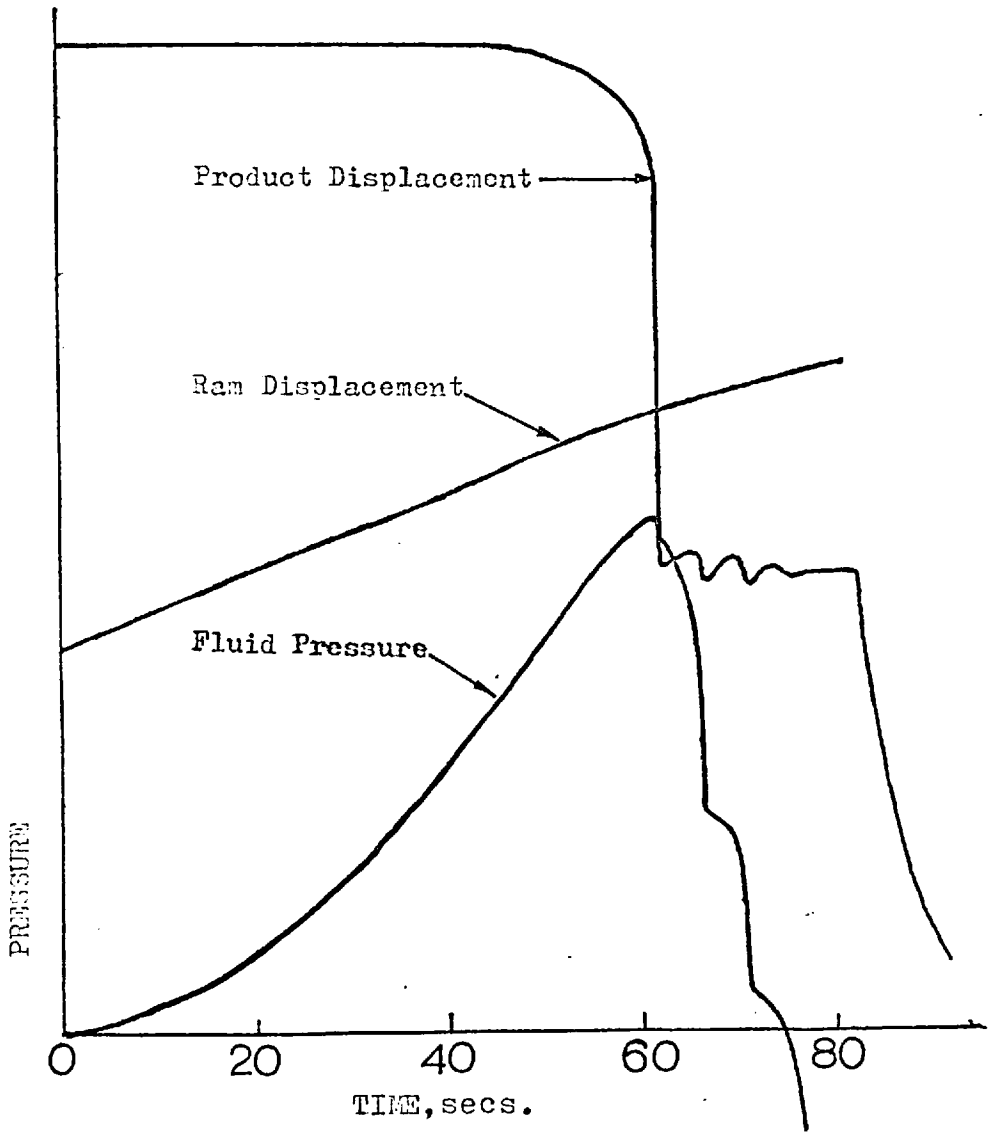

FIG.39 A record showing the fluid pressure, product displacement and ram displacement in a 'stick-slip' mode of simple hydrostatic extrusion

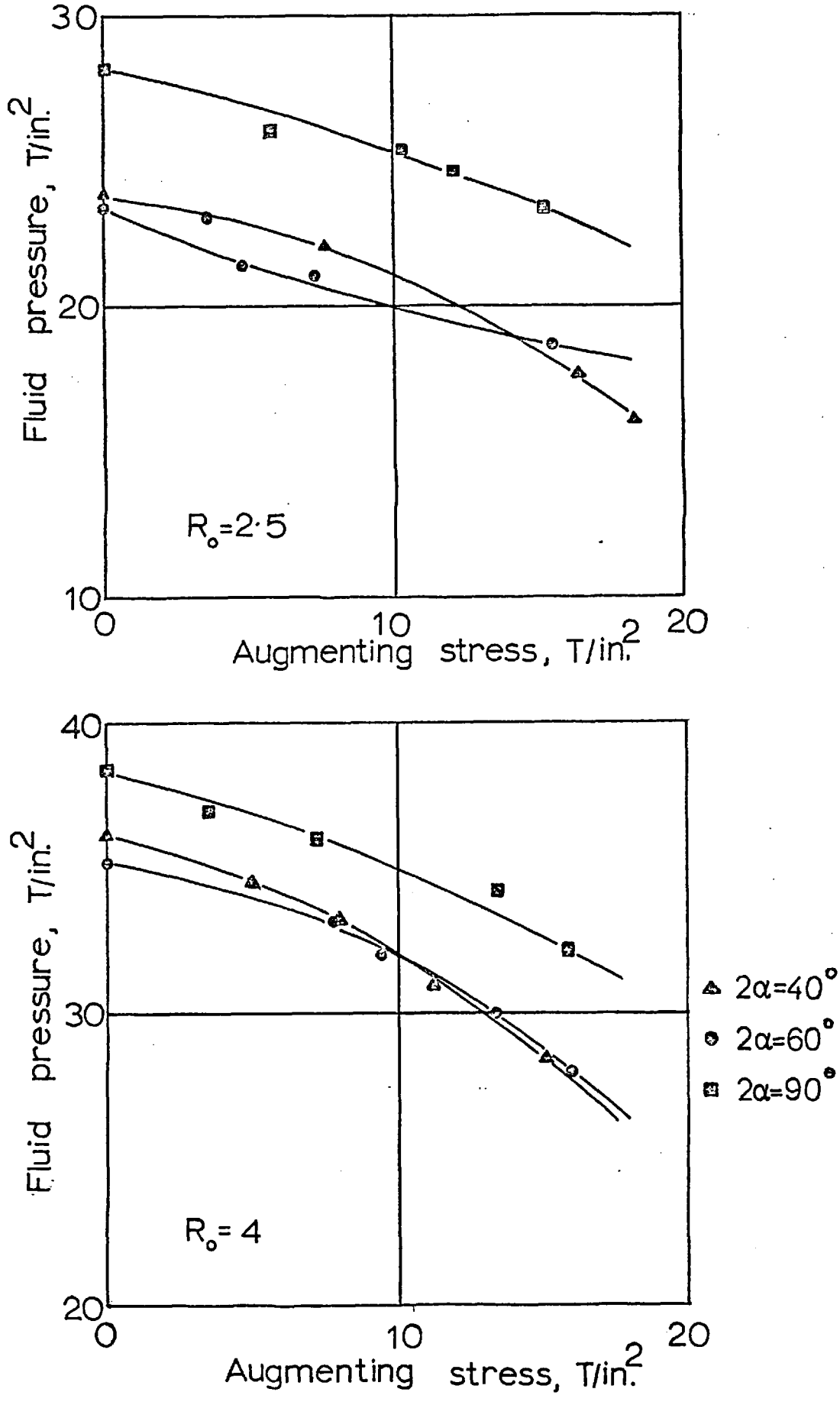

FIG.40 Augmenting stress versus fluid pressure for copper billets with extrusion ratios of 2.5 and 4 for different die angles

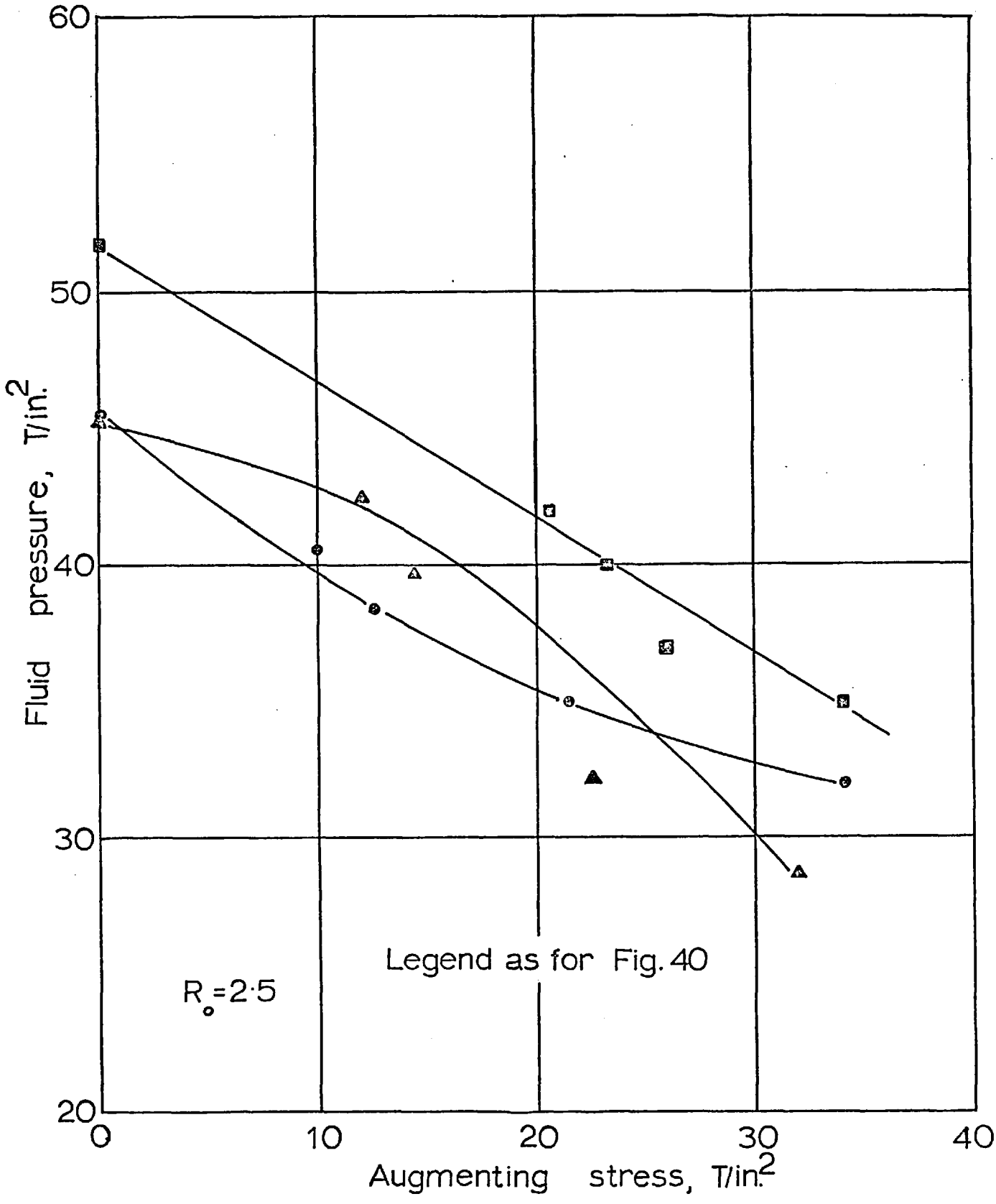

FIG. 41 Augmenting stress versus fluid pressure for mild steel billets with an extrusion ratio of 2.5(R_o) for different die angles

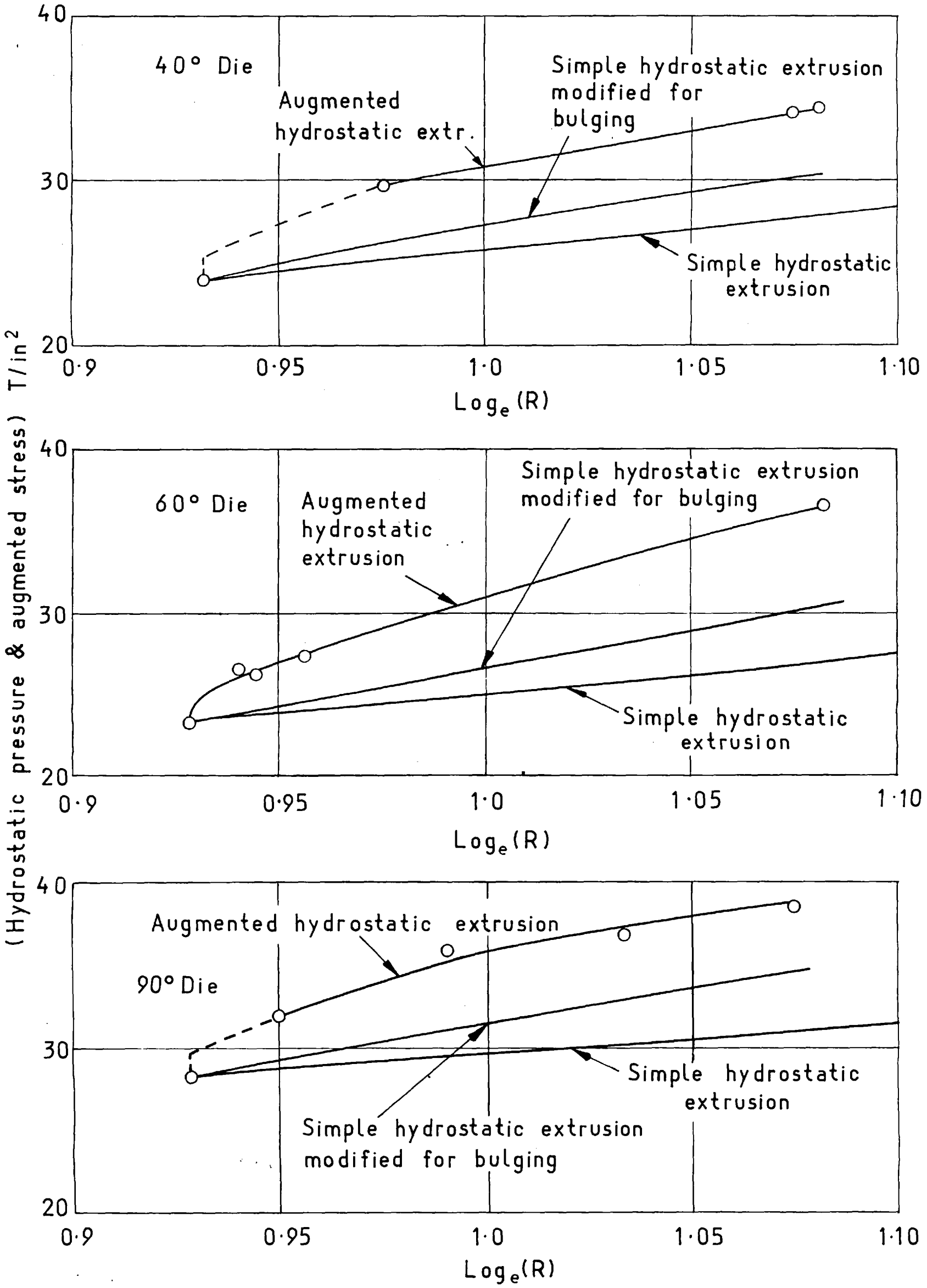

FIG.42 Total extrusion pressure($p_A+\sigma_A$) versus ln R for Copper billets with R_o=2.5

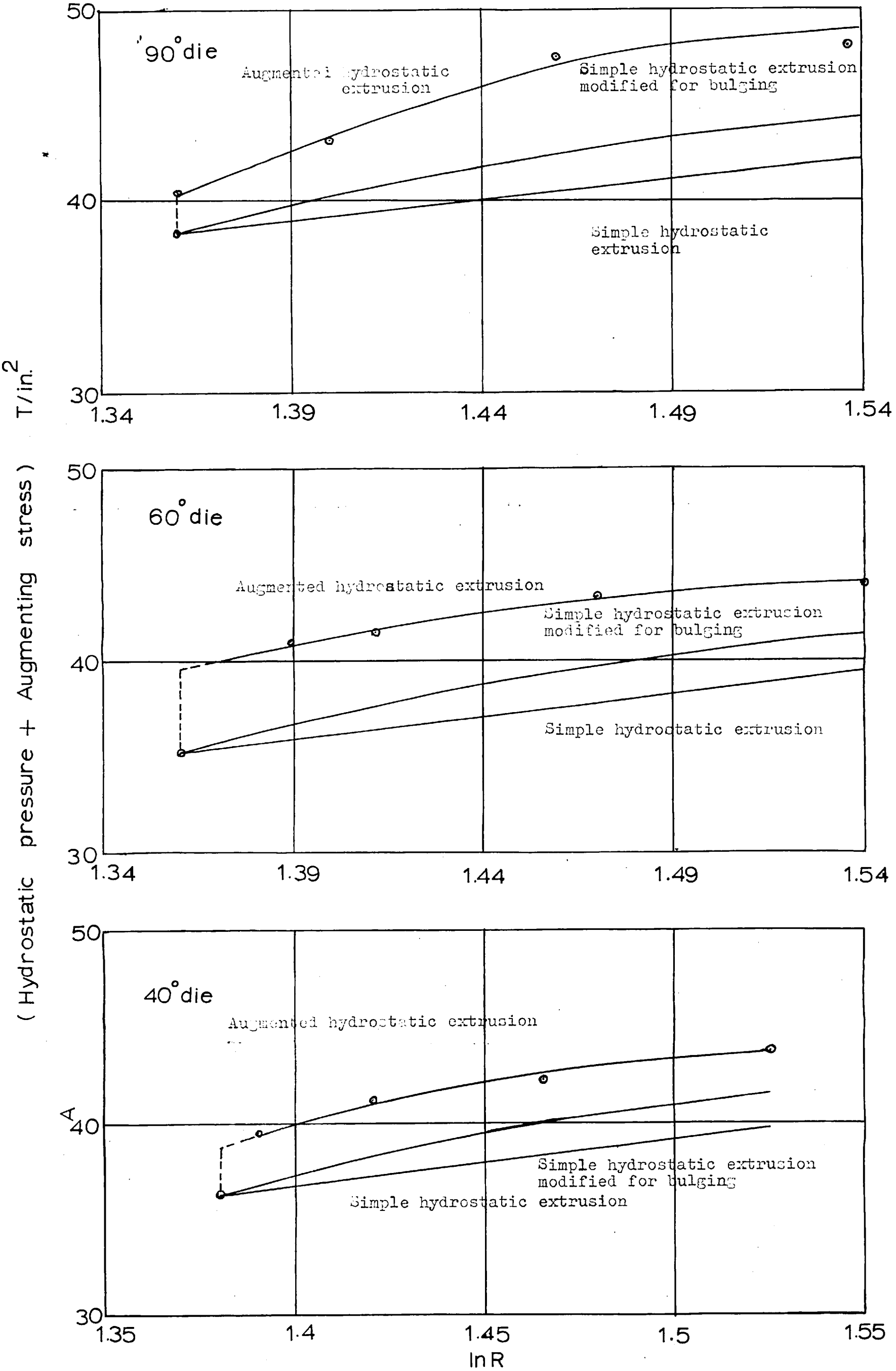

FIG.43 Total extrusion pressure($p + \sigma$) versus ln R for Copper with R_o=4

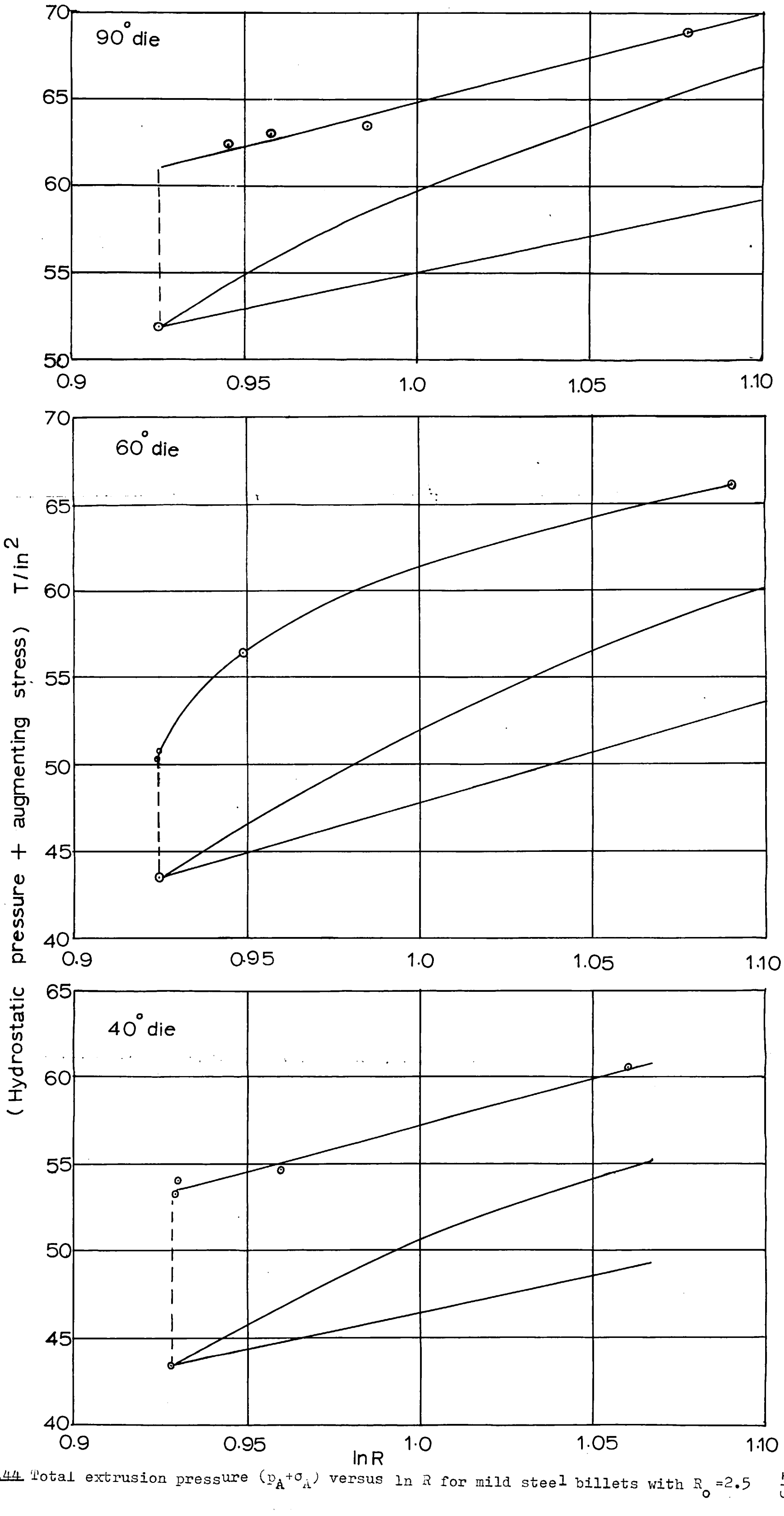

FIG.44 Total extrusion pressure ($p_A+\sigma_A$) versus ln R for mild steel billets with R_o =2.5

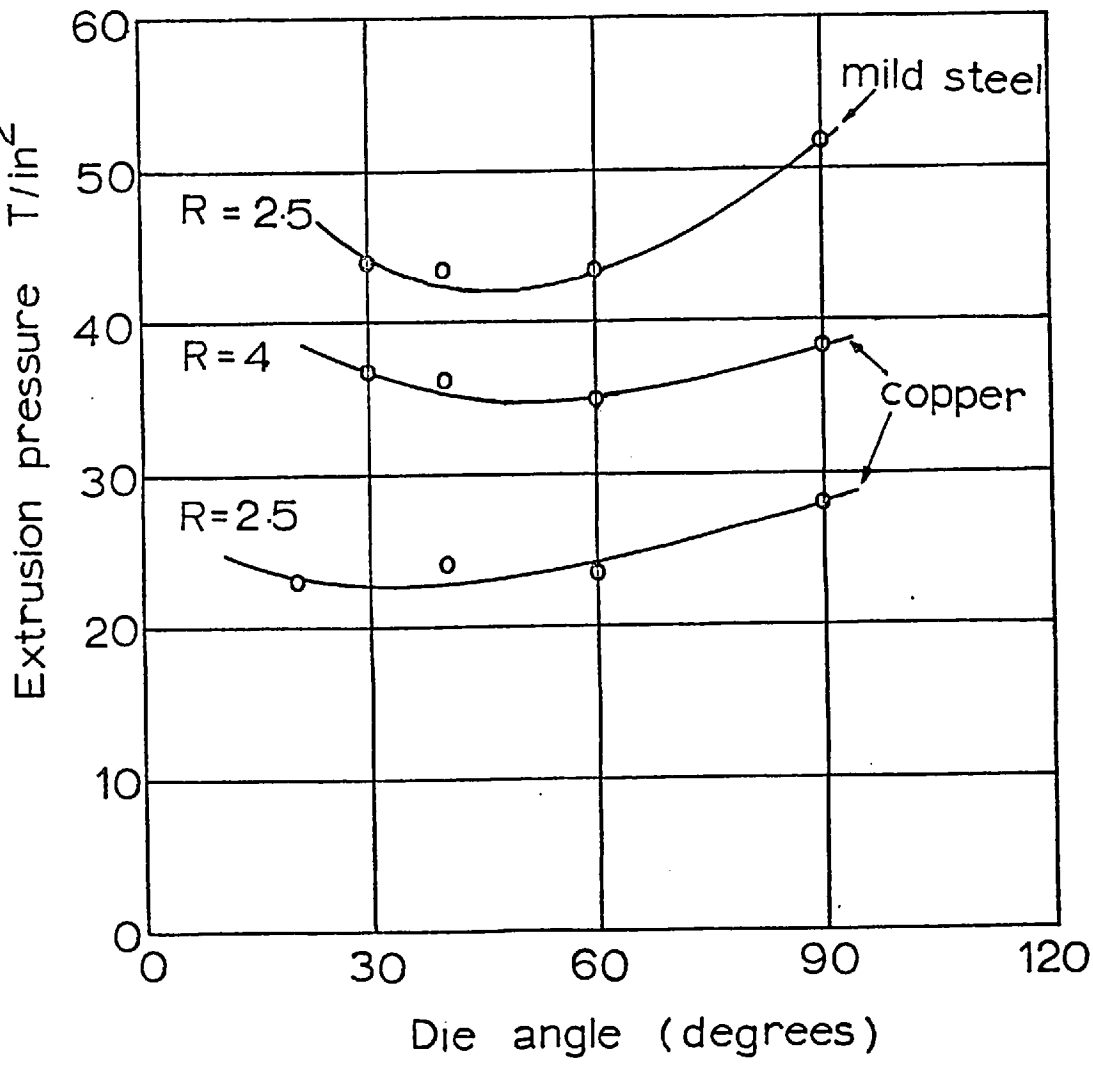

FIG.45 Simple hydrostatic extrusion pressure versus die angle for copper (R = 2.5,4) and mild steel (R = 2.5)

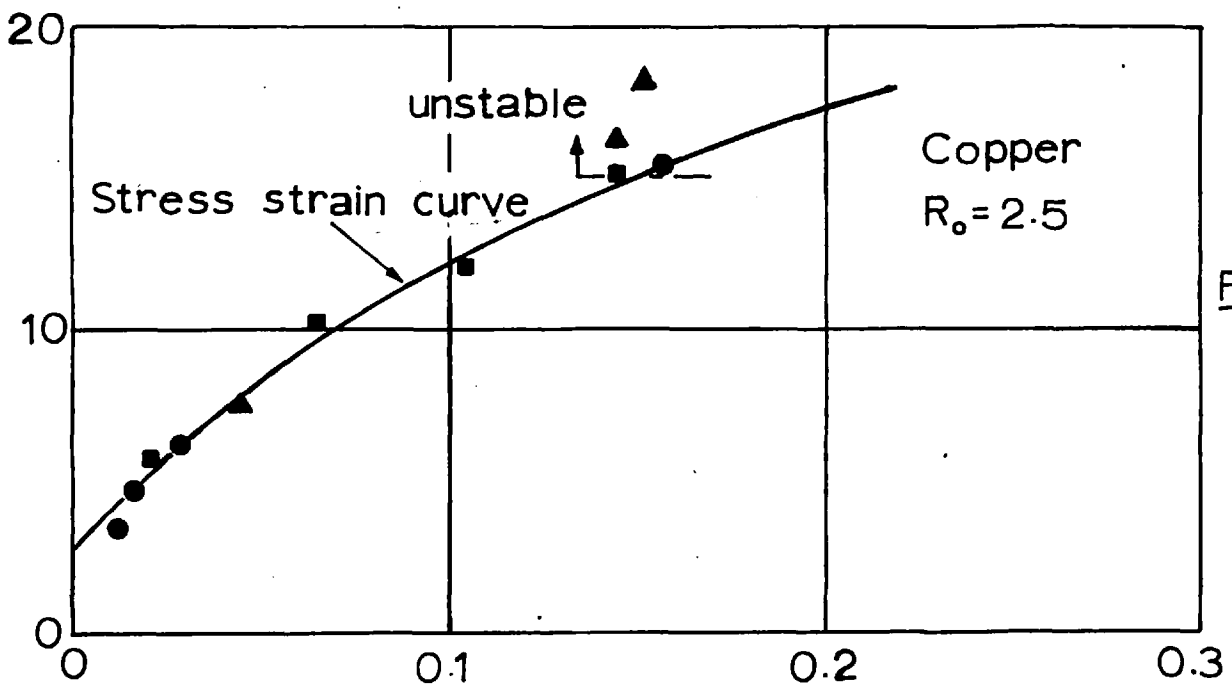

FIG. 46

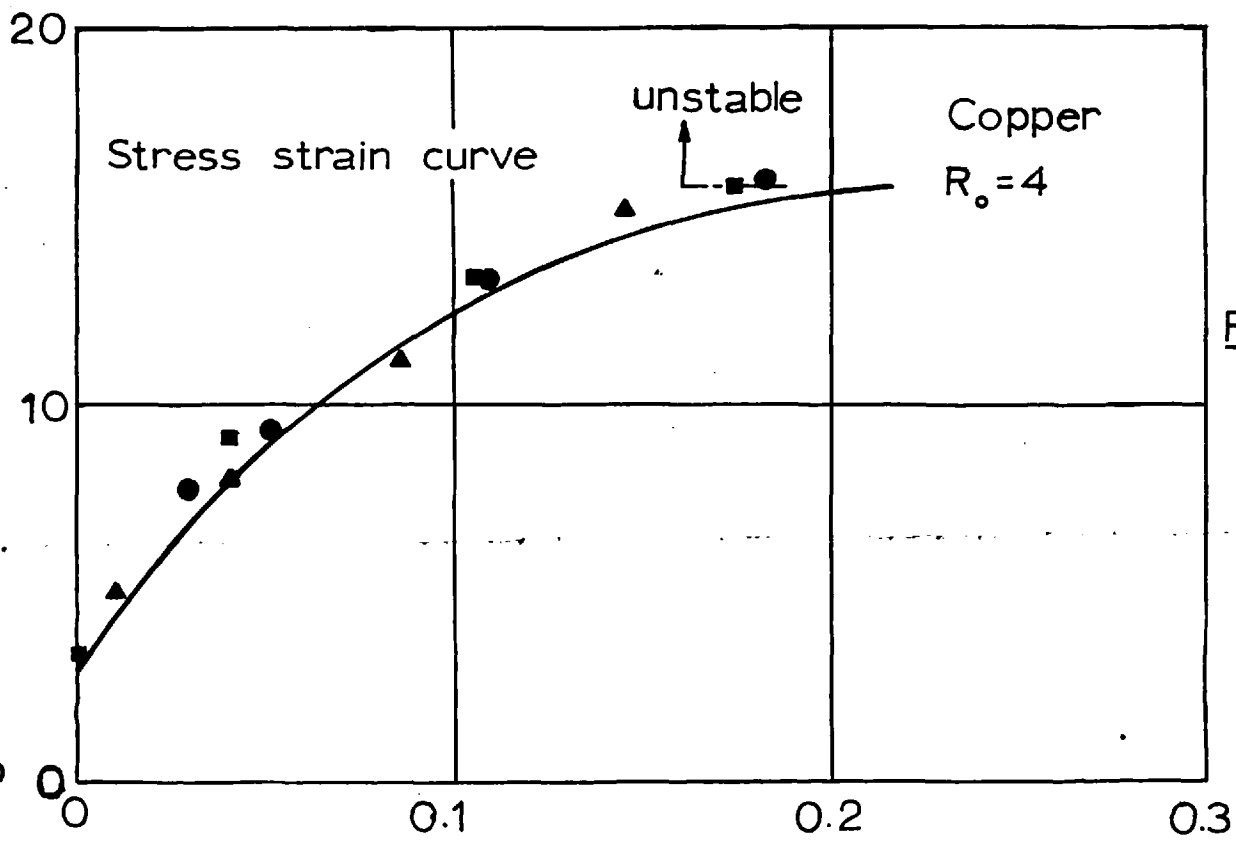

FIG. 47

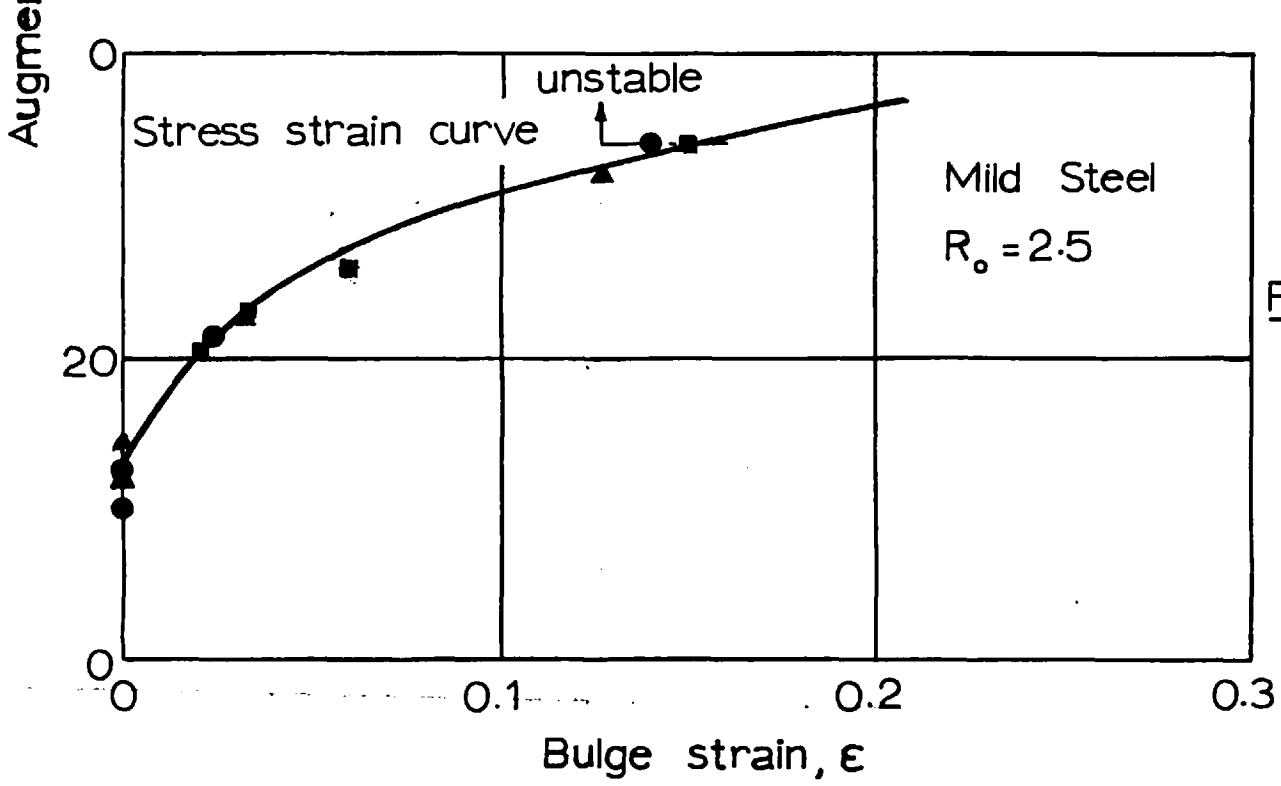

FIG. 48

Augmenting stress versus bulge strain for copper and mild steel billets

▲------- 40° included die angle
●------- 60° included die angle
■ ------- 90° included die angle

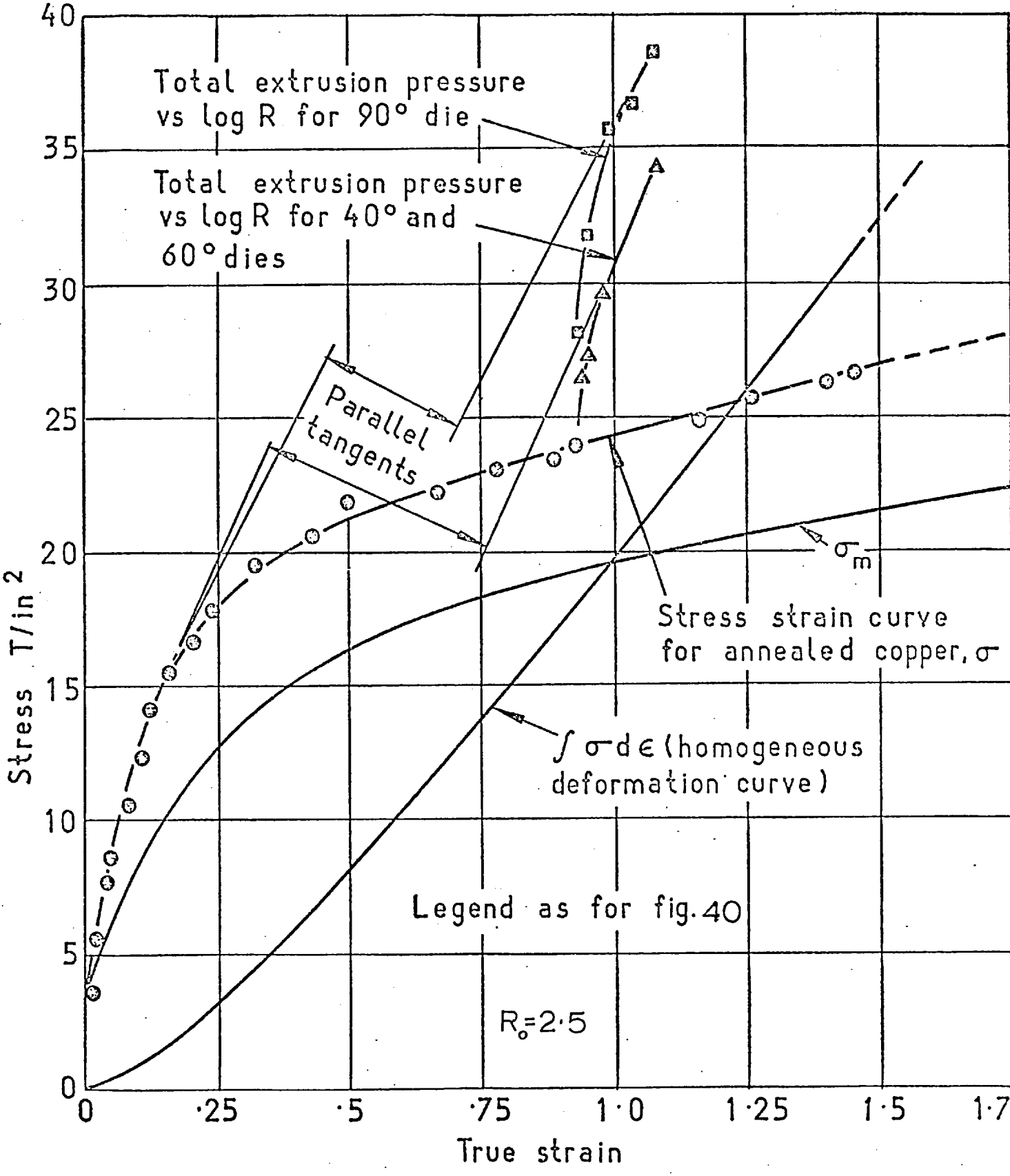

FIG.49

Diagram showing the derivation of the bulging limit for copper billets from experimental results

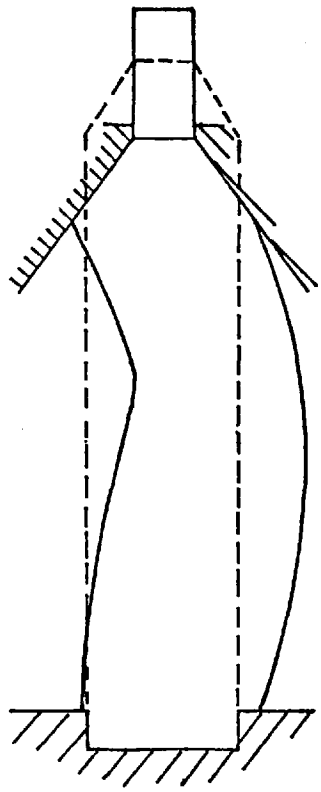

A MODE OF BUCKLING OF THE BILLET

Fig.50

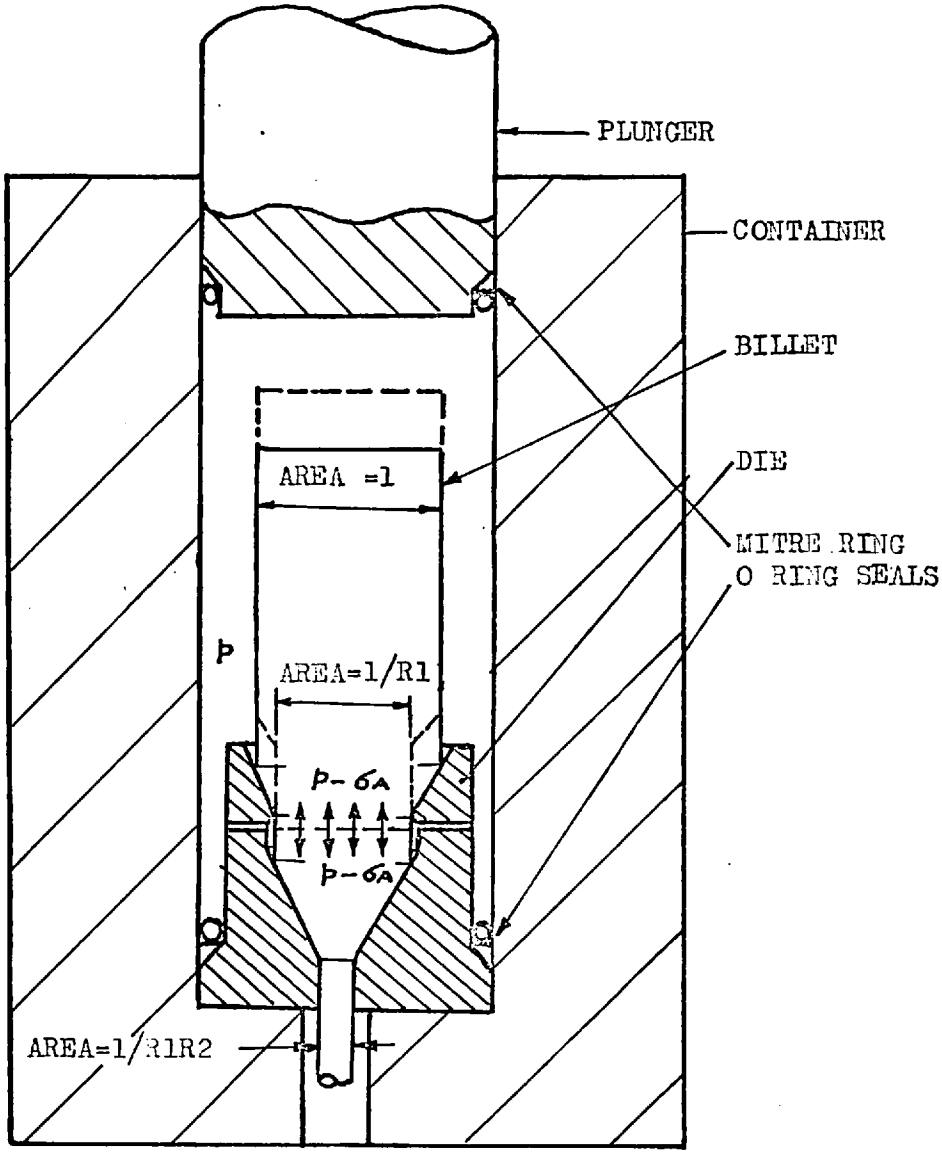

SCHEMATIC DIAGRAM SHOWING THE DOUBLE REDUCTION DIE IN HYDROSTATIC EXTRUSION

FIG. 51

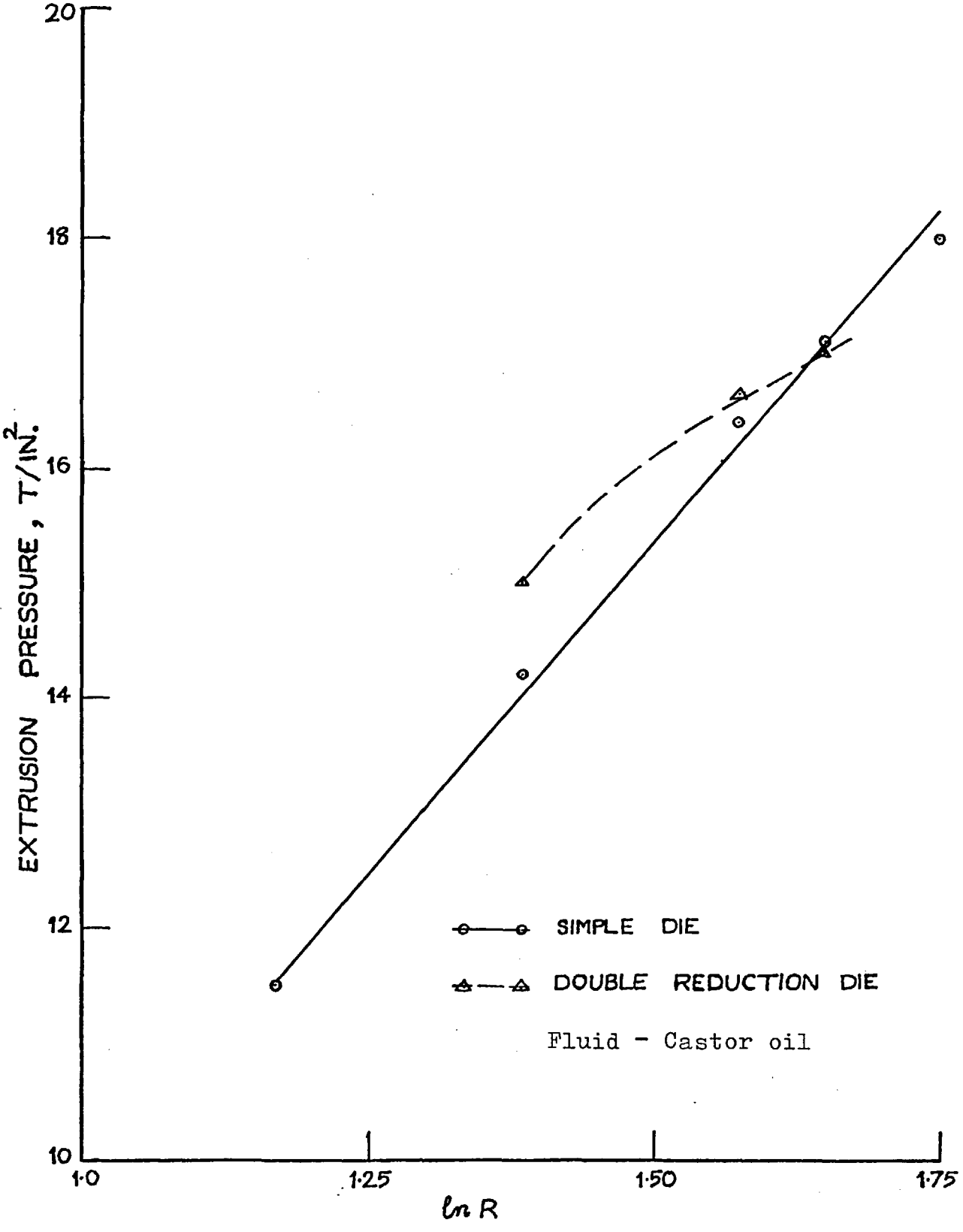

FIG.52a Double reduction die results with aluminium billets; extrusion pressure versus ln R1R2

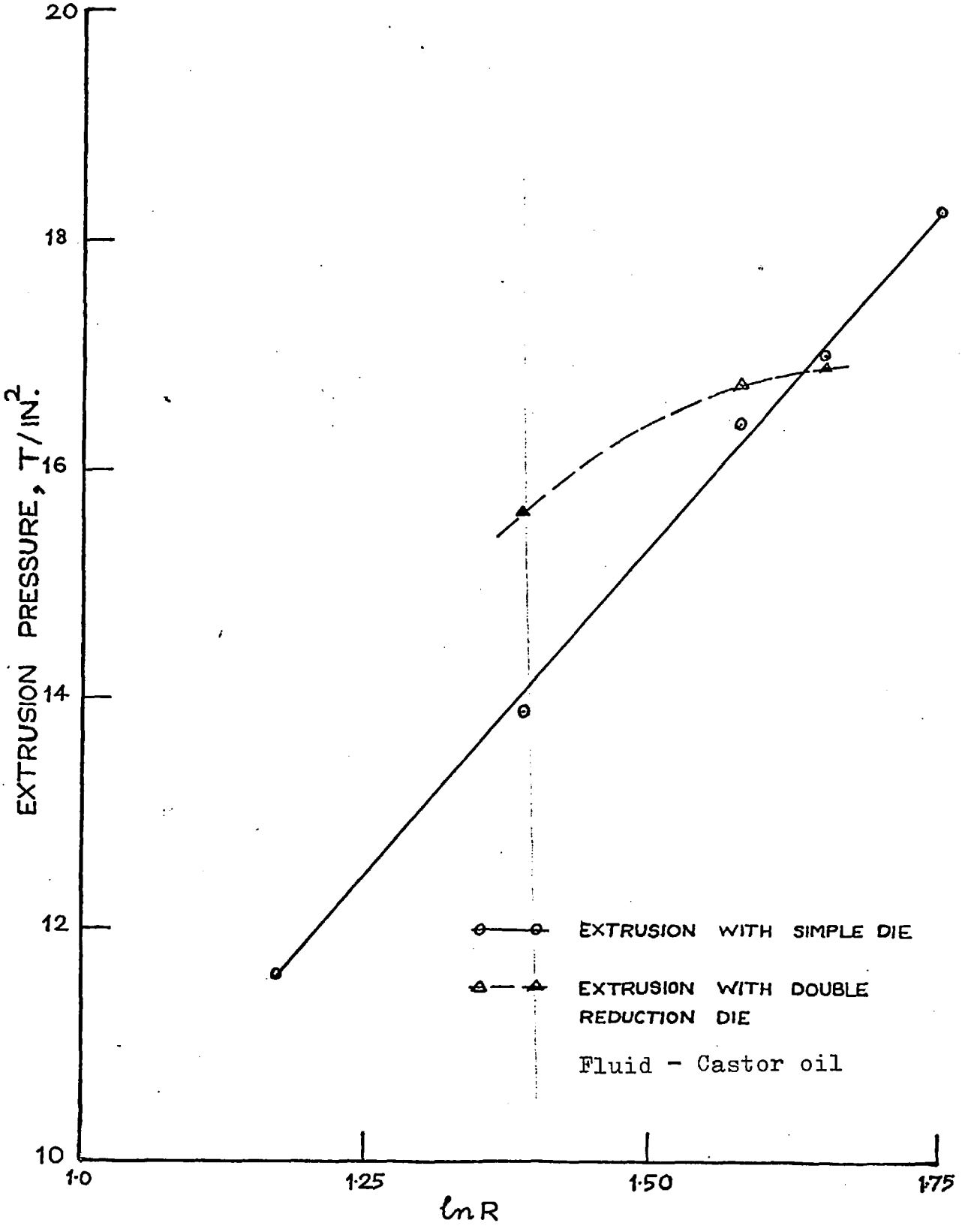

FIG.52b Double reduction die results with aluminium billets; extrusion pressure versus ln R1R2

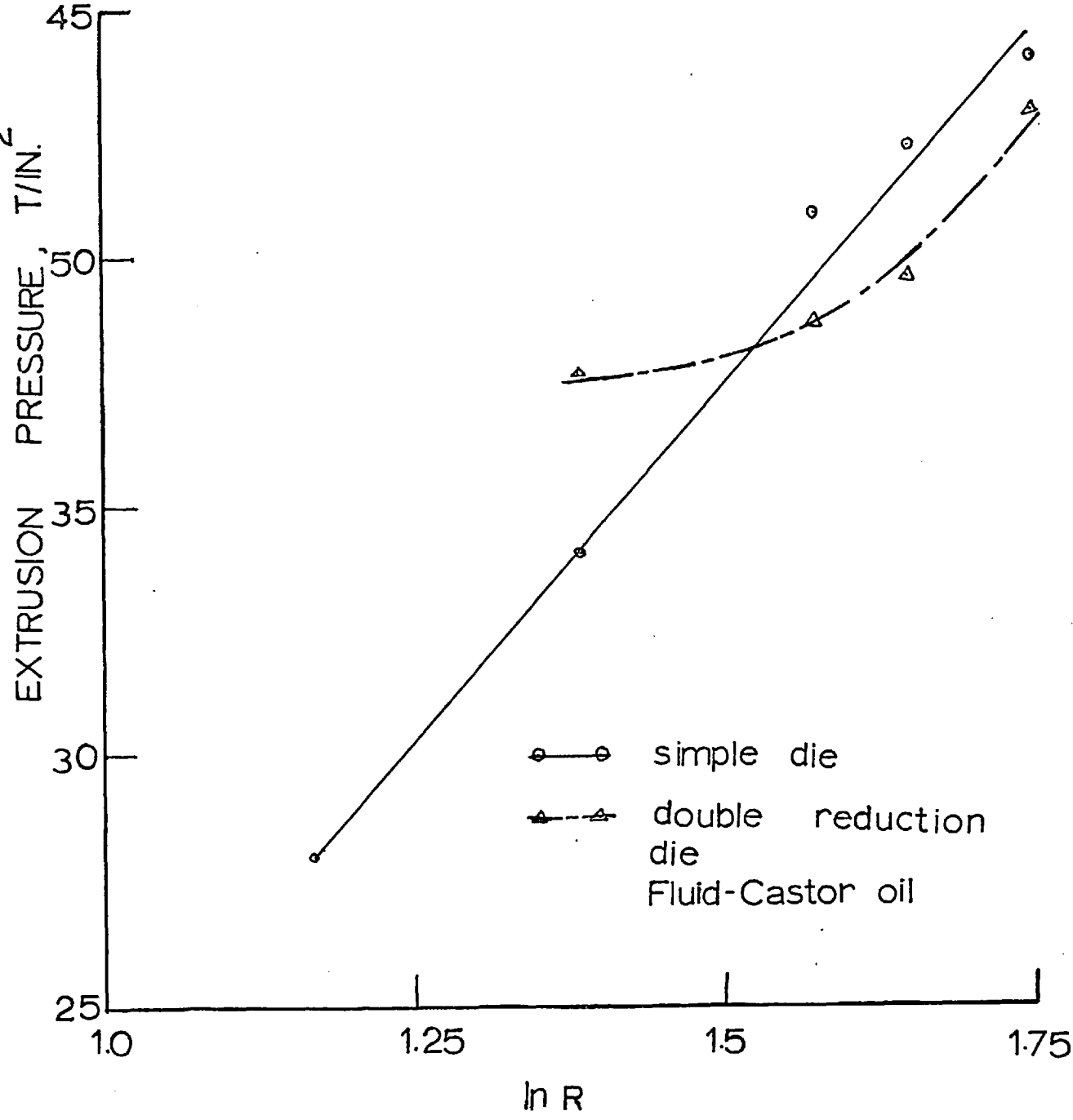

FIG.53a Double reduction die results with copper billets; extrusion pressure versus ln R1R2

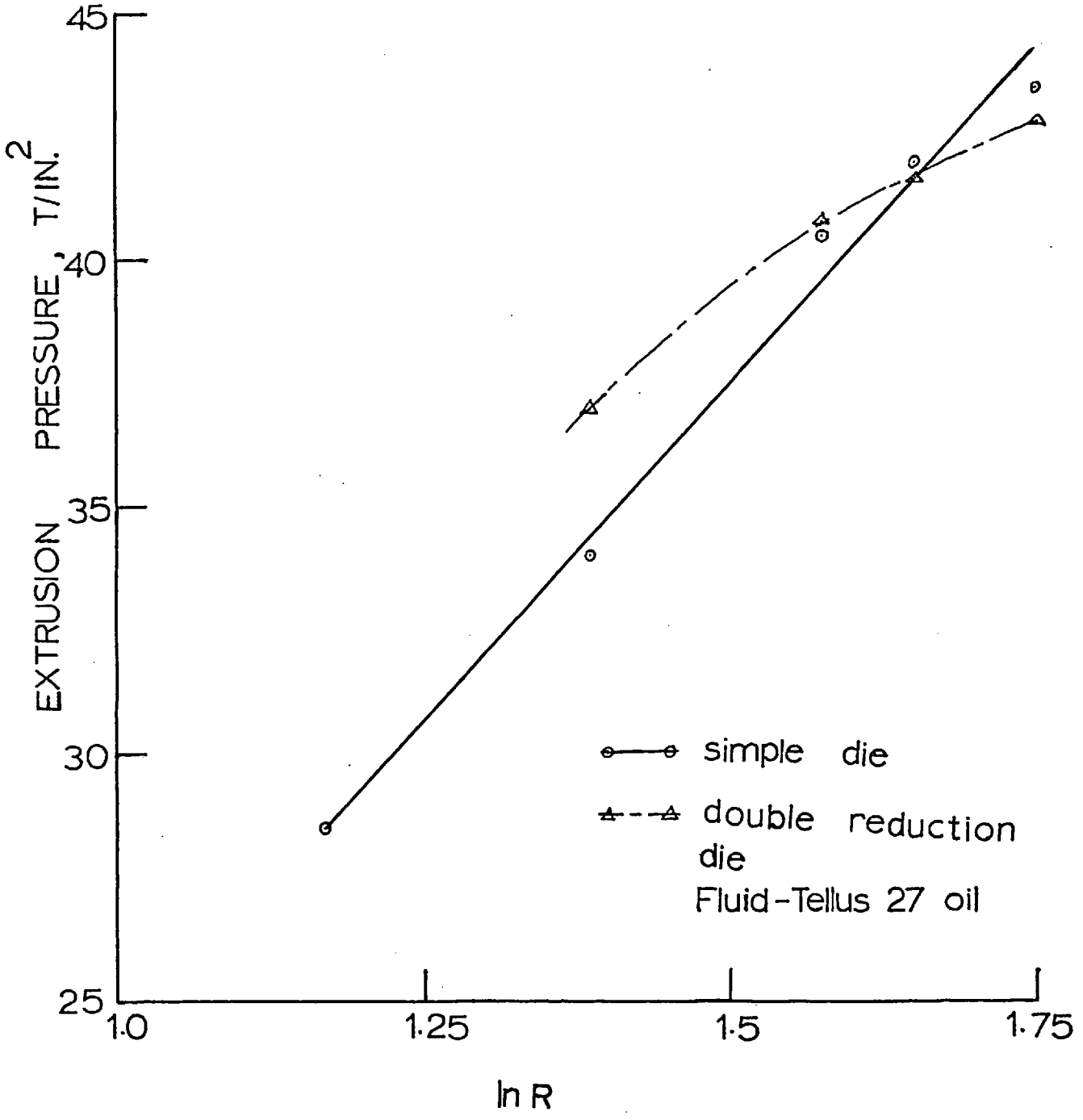

FIG.53b Double reduction die results with copper billets; extrusion pressure versus ln R1R2

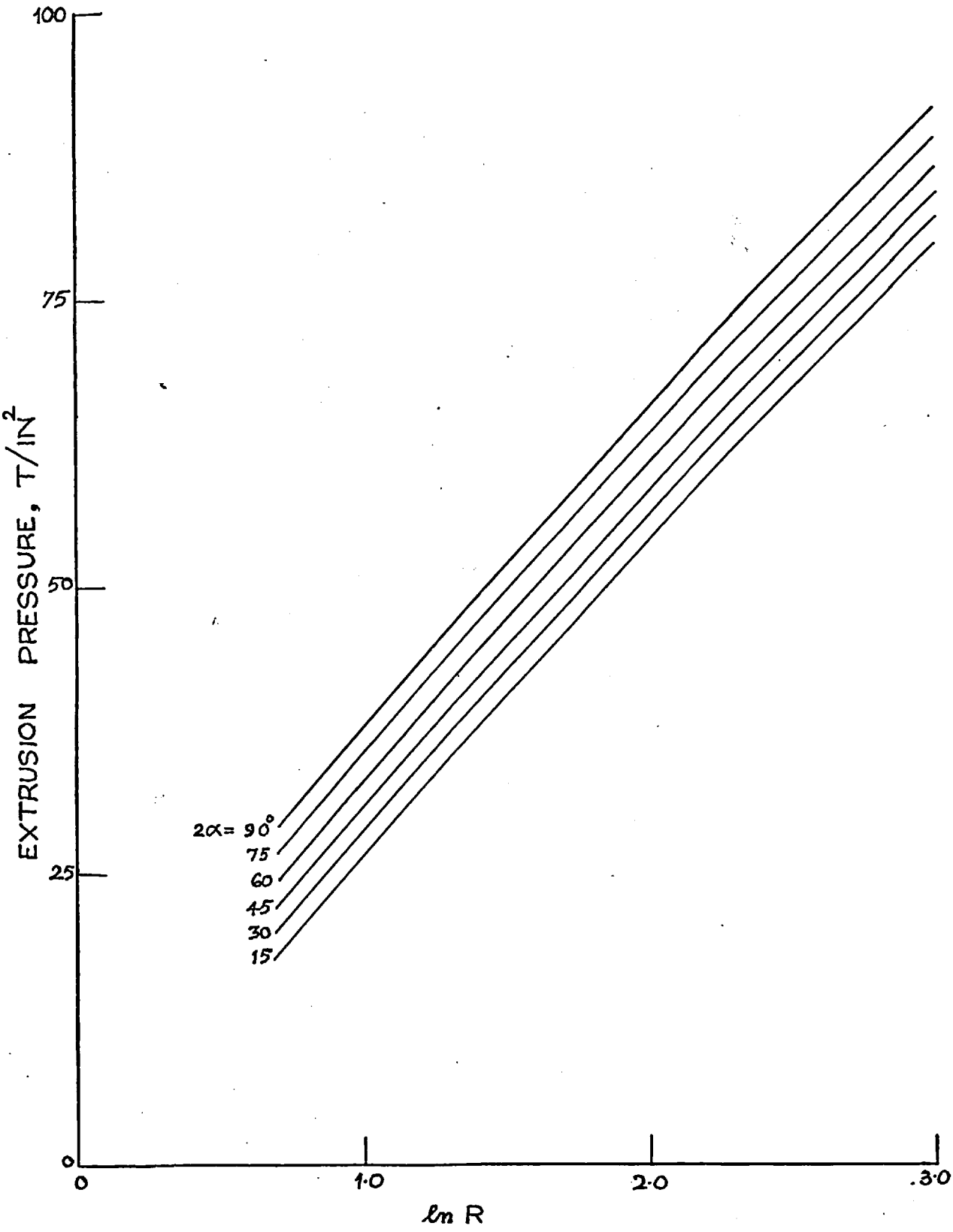

FIG.54 Simple hydrostatic extrusion pressure versus ln R curves for various die angles(copper billets)calculated by the hydrodynamic theory for a work-hardening material

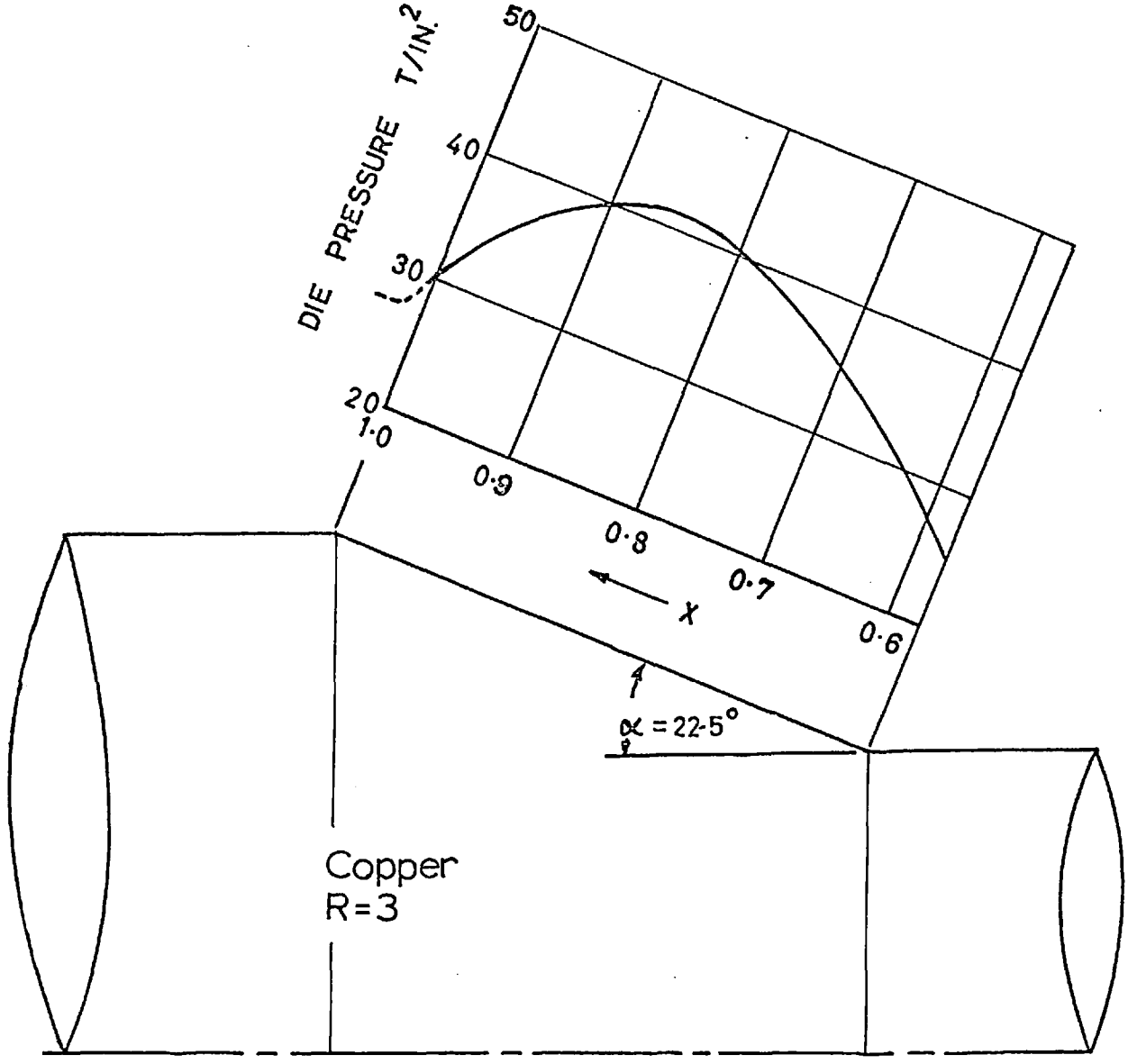

Fig.55 Theoretical pressure distribution along the die by the theory of hydrodynamic lubrication (Work-hardening material analysis).

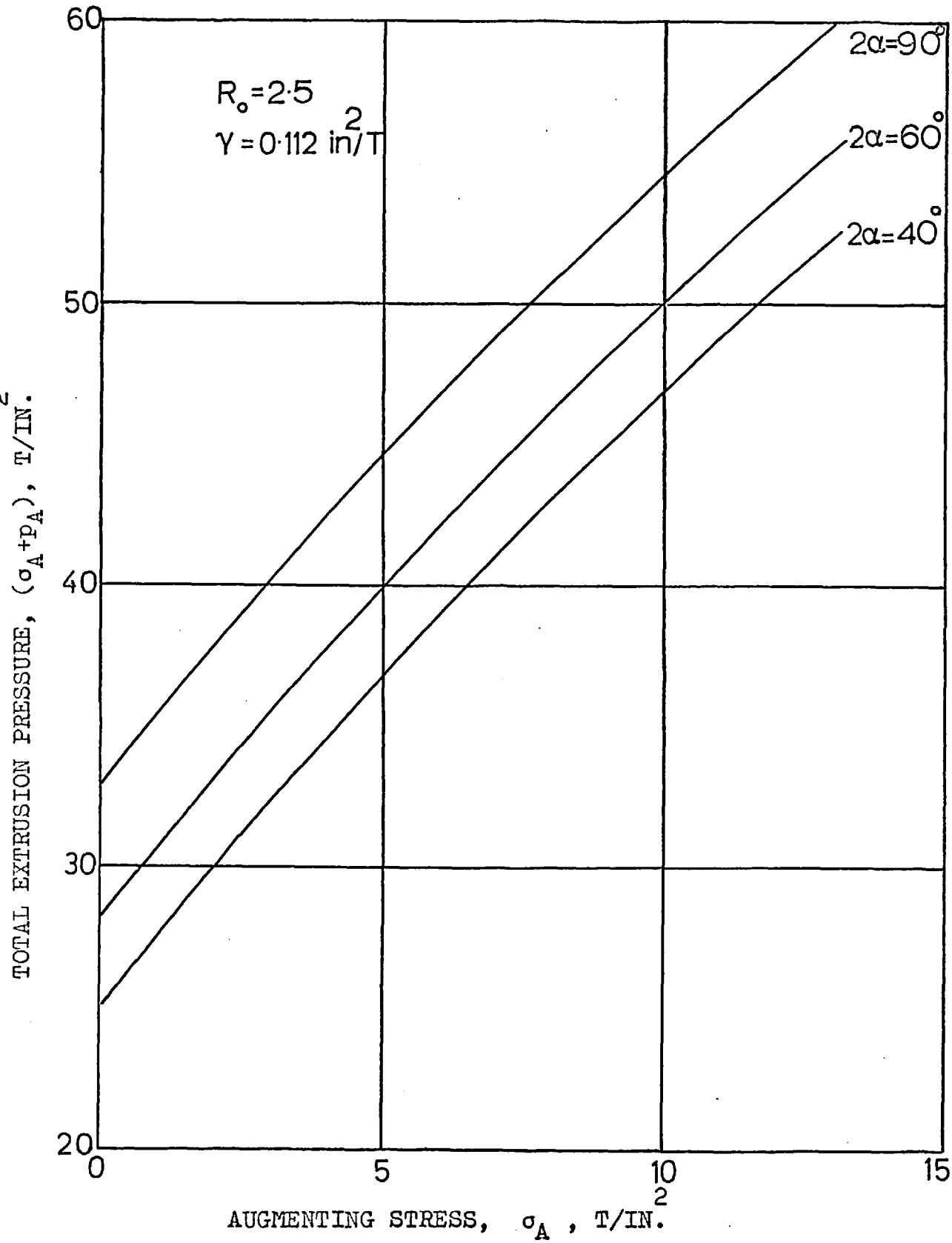

FIG.56 Variation of $(\sigma_A + p_A)$ versus σ_A calculated by the work-hardening theory of hydrodynamic lubrication for copper billets with an extrusion ratio of 2.5

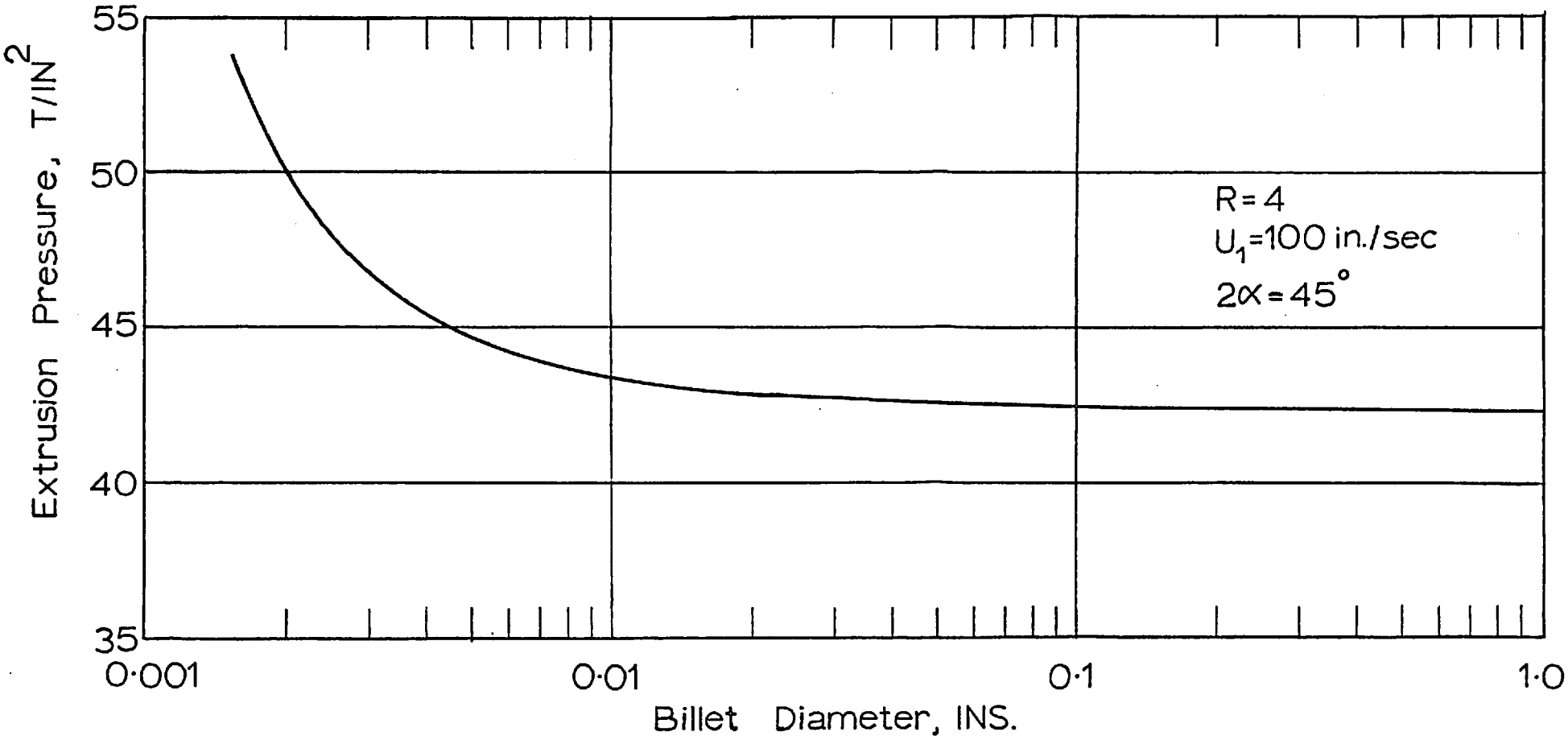

Fig.57 The variation of simple hydrostatic extrusion pressure with the size of the billet calculated using the work-hardening theory of hydrodynamic lubrication for copper

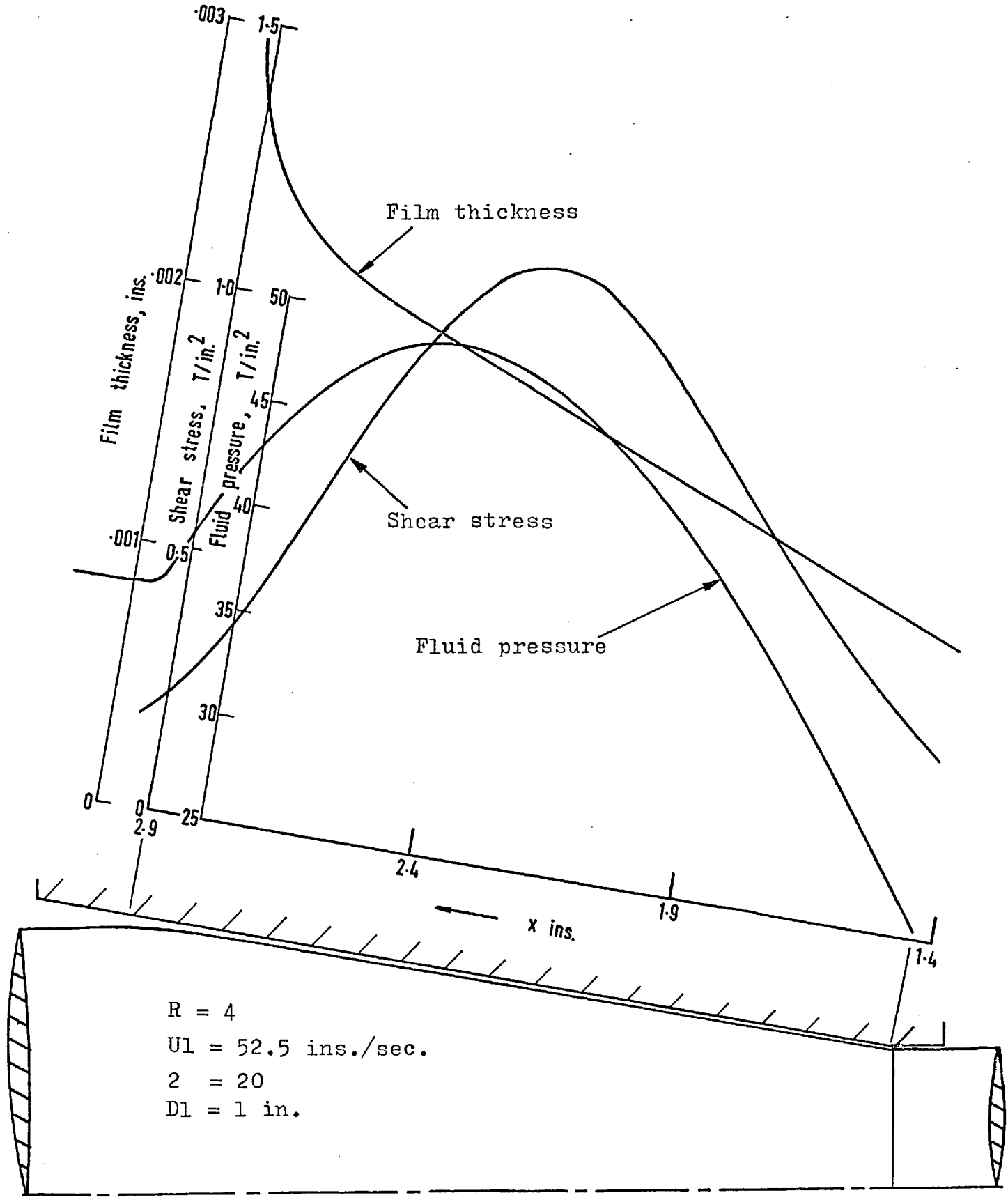

FIG.58 The fluid pressure, film thickness and shear stress variation along the die for copper billet calculated by the numerical method

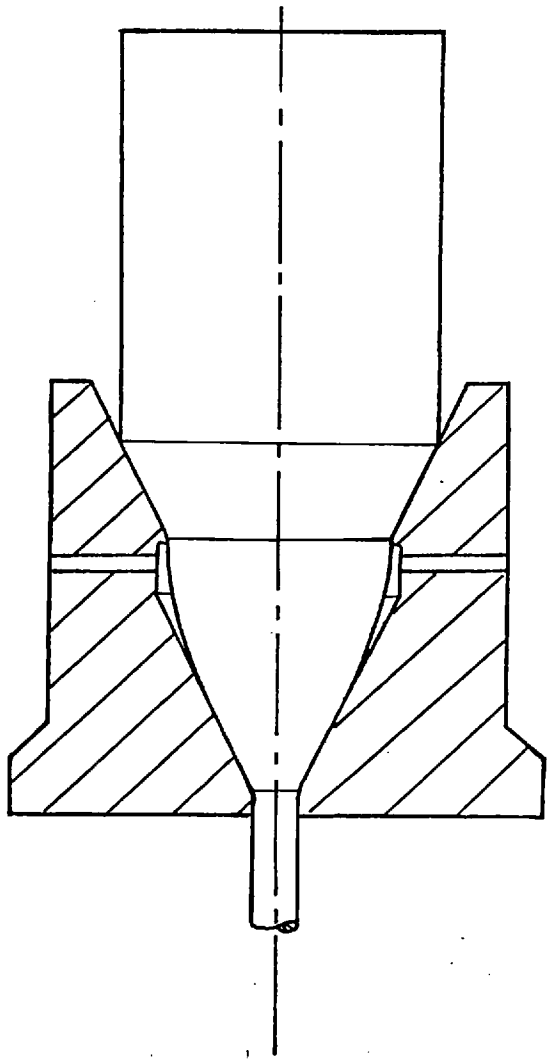

FIG.59 Curving in of the billet in the second reduction of the double reduction die

TABLE 1 Dimensionless redundant work p_{R1}/k and semi-die angle α.

Semi-die Angle α^{o}	Dimensionless Redundant Work, P_{R1}/k		
	$(\frac{\alpha}{\sin^2\alpha} - \cot\alpha)$ *	$\frac{4}{3}\tan\alpha/2$ +	Optimum Parabolic Boundary
0	0	0	0
10	.117	.117	.117
20	.237	.236	.235
30	.362	.358	.356
45	.571	.553	.546
60	.819	.770	.755
65	.915	.849	.831
70	1.020	.933	.910
75	1.135	1.023	.993
80	1.221	1.112	1.081

* Spherical Boundary with apex of the die cone as centre

+ Optimum Conical Boundary

TABLE 2 Critical buckling stress S_{CR} and slenderness ratio l/r for copper

S_{CR} (T/in^2)	ℓ/r
3.5	150
5	15.4
6	13.5
8	10.5
10	8.65
12	7.45
14	6.23
15	5.26

TABLE 3 Critical buckling stress S_{CR} and slenderness ratio l/r for mild steel

S_{CR}	l/r
5	163
10	115
13	101
18	18.5
23	10.4
28	6.35
33	4.67
36	4.05

TABLE (4) COOK AND LARKE TEST FOR COPPER (ANNEALED)

LOAD, P in tons	HEIGHT OF SPECIMEN, H INCHES				FRACTIONAL DECREASE IN HEIGHT fH					STRESS, $\sigma = \frac{4(1-fH)\ P}{\pi\ d_o^2}$ T/in^2	STRAIN, $\epsilon = \ln(\frac{1}{1-fH})$
	h_o=1.502	h_o=0.750	h_o=0.377	h_o=0.253	$d_o/h_o=\frac{1}{2}$	$d_o/h_o=1$	$d_o/h_o=2$	$d_o/h_o=3$	$d_o/h_o=0$*		
1.5	1.490	0.744	0.374	0.251	0.008	0.008	0.008	0.008	0.008	3.40	0.008
2.5	1.471	0.735	0.370	0.249	0.021	0.020	0.019	0.016	0.021	5.54	0.021
3.5	1.445	0.722	0.364	0.245	0.038	0.037	0.035	0.032	0.0390	7.61	0.040
4.0	1.430	0.715	0.362	0.243	0.0480	0.047	0.040	0.040	0.050	8.60	0.052
5.0	1.396	0.702	0.354	0.238	0.071	0.064	0.061	0.059	0.073	10.50	0.077
6.0	1.364	0.684	0.345	0.232	0.092	0.088	0.085	0.083	0.093	12.35	0.107
7.0	1.335	0.665	0.335	0.226	0.111	0.113	0.111	0.107	0.114	14.05	0.121
8.0	1.287	0.645	0.327	0.221	0.143	0.140	0.133	0.127	0.145	15.5	0.157
10.0	1.190	0.598	0.308	0.209	0.208	0.203	0.183	0.174	0.215	17.8	0.243
12.0	1.109	0.556	0.293	0.198	0.262	0.259	0.223	0.217	0.275	19.70	0.322
14.0	0.996	0.514	0.271	0.188	0.337	0.315	0.281	0.257	0.350	20.60	0.432
16.0	0.928	0.477	0.253	0.175	0.383	0.364	0.329	0.308	0.395	21.90	0.496
19.0	0.802	0.425	0.227	0.162	0.467	0.434	0.398	0.360	0.485	22.20	0.665
22.0	0.718	0.382	0.206	0.149	0.522	0.491	0.454	0.411	0.538	23.0	0.773
25.0	0.650	0.344	0.189	0.137	0.568	0.541	0.499	0.458	0.587	23.4	0.885
30.0	0.586	0.304	0.168	0.125	0.611	0.595	0.555	0.506	0.633	24.1	1.005
35.0	0.508	0.268	0.153	0.114	0.663	0.643	0.595	0.550	0.685	24.9	1.155
40.0	0.445	0.247	0.139	0.102	0.697	0.670	0.633	0.596	0.715	25.8	1.257
50.0	0.369	0.202	0.112	0.089	0.756	0.731	0.695	0.648	0.765	26.6	1.45

d_o = original diameter = 0.751 ins., h_o = original height of specimen.

* extrapolated from the plots of d_o/h_o -vs. fH.

TABLE (5) COOK AND LARKE TEST FOR MILD STEEL (ANNEALED)

LOAD, P $*10^3$ lbf	HEIGHT OF SPECIMEN, H INCHES				FRACTIONAL DECREASE IN HEIGHT fH					STRESS, $\sigma = \frac{4(1-fH)}{\pi} \frac{P}{d_o^2} \frac{1}{2240}$ T/in^2	STRAIN, $\epsilon = \ln(\frac{1}{1-fH})$
	h_o=1.500	h_o=0.750	h_o=0.375	h_o=0.248	$d_o/h_o=\frac{1}{2}$	d_o/h_o=1	d_o/h_o=2	d_o/h_o=3	d_o/h_o=0*		
14.00	1.4995	0.7495	0.375	0.248	–	–	–	–	–	–	–
16.00	1.499	0.749	0.3745	0.248	0.0007	–	–	–	–	–	–
18.00	1.4985	0.748	0.374	0.2475	0.001	–	–	–	–	18.35	0.001
20.02	1.474	0.737	0.370	0.246	0.0174	0.0173	0.0133	0.008	0.0174	20.25	0.0174
22.02	1.458	0.7285	0.365	0.242	0.028	0.028	0.027	0.024	0.028	21.8	0.028
24.00	1.446	0.7225	0.362	0.240	0.036	0.036	0.035	0.032	0.036	23.1	0.037
27.45	1.422	0.7095	0.3555	0.236	0.053	0.053	0.052	0.048	0.053	26.6	0.052
30.00	1.400	0.699	0.351	0.2345	0.067	0.067	0.064	0.054	0.067	28.6	0.0686
35.00	1.3485	0.6725	0.3385	0.2295	0.101	0.101	0.097	0.074	0.101	32.0	0.116
40.00	1.2815	0.6415	0.3275	0.2170	0.145	0.144	0.127	0.124	0.145	34.9	0.157
50.00	1.157	0.578	0.297	0.1975	0.229	0.229	0.208	0.202	0.229	39.3	0.260
60.00	1.0385	0.517	0.269	0.1805	0.308	0.308	0.283	0.270	0.308	42.4	0.369
70.00	0.932	0.467	0.2425	0.1675	0.379	0.377	0.353	0.322	0.380	44.25	0.479
90.00	0.7575	0.3895	0.210	0.144	0.495	0.482	0.440	0.416	0.500	45.9	0.693
110.00	0.643	0.3345	0.179	0.1265	0.571	0.555	0.523	0.486	0.585	46.5	0.879

d_o = original diameter = 0.746 ins.; h_o = original height of specimen.

* extrapolated from the plots of d_o/h_o vs. fH.

Table 6a. Billet augmented hydrostatic extrusion results

Material: Commercially pure copper annealed at 610°C for 1 hr.

2α = 40° = die angle

Product dia. = 0.313"

R_o, original extrusion ratio = 2.54

Hydrostatic fluid pressure F_A (T/in^2)	24	22.1	17.7	16.0
Augmenting load, F_A (Tonf)	-	1.57	3.73	4.15*
Dia. of residual billet, D (ins)	0.499	0.510	0.536	0.538
Augmenting stress, σ_A (T/in^2)	-	7.65	16.4	18.3*
Effective extrusion ratio, R	2.54	2.65	2.93	2.95
ln R	.932	.975	1.075	1.081
Bulge strain) $\varepsilon = \ln \frac{R}{R_o}$	0	0.044	0.143	0.149
Total extrusion pressure, $(\sigma_A + p)_A$, (T/in^2)	24	29.75	34.1	34.3*

* Unstable, still increasing.

Table 6b. Billet augmented hydrostatic extrusion results

Material: Commercially pure copper annealed at 610°C for 1 hr.

2α = 60° = die angle

Product dia. = 0.313"

R_o, original extrusion ratio = 2.53

Hydrostatic fluid pressure p_A (T/in^2)	23.4	23.1	21.4	21.1	18.7
Augmenting load, F_A (Tonf)	-	0.7	0.95	1.25	3.5*
Dia. of residual billet, D (ins)	.498	.501	.502	.505	.539
Augmenting stress, σ_A (T/in^2)	-	3.55	4.8	6.3	15.5*
Effective extrusion ratio, R	2.53	2.56	2.57	2.60	2.95
ln R	0.928	0.940	0.944	0.956	1.082
Bulge)) $\varepsilon = \ln \frac{R}{R_o}$ Strain)	0	0.012	0.016	0.028	0.154
Total extrusion pressure, $(\sigma_A + p)_A$ (T/in^2)	23.4	26.65	26.2	27.4	34.2*

* Unstable, still increasing.

Table 6c. Billet augmented hydrostatic extrusion results

Material: Commercially pure copper annealed at 610°C for 1 hr.

$2\alpha = 90°$ = die angle

Product dia. = 0.313"

Hydrostatic fluid pressure p_A (T/in^2)	28.2	26.1	25.5	24.7	23.4
Augmenting load, F_A (Tonf)	-	1.15	2.10	2.6	3.4*
Dia. of residual billet, D (ins)	.498	.503	.514	.525	.536
Augmenting stress, σ_A (T/in^2)	-	5.75	10.25	12.1	15.2*
Effective extrusion ratio, R	2.53	2.58	2.69	2.81	2.93
ln R	.928	.949	.990	1.033	1.074
Bulge) strain) $\varepsilon = \ln \frac{R}{R_o}$	0	0.02	0.064	.104	.144
Total extrusion pressure (T/in^2) $(\sigma_A + p_A)$	28.2	31.8	35.8	36.8	38.6*

* Unstable, still increasing.

TABLE 7a Billet augmented hydrostatic extrusion results

Material: Commercially pure copper annealed at 610° for 1 hr.

$2\alpha = 40^{\circ}$ = die angle

R_o = original extrusion ratio = 3.97

Product dia. = 0.313"

Hydrostatic fluid pressure p_A (T/in^2)	36.3	34.5	33.2	31	28.5
Augmenting load, F_A (Tonf)	-	1.58	2.55	3.73	5.38
Dia. of residual billet, D (ins)	.624	.627	.636	.651	.671
Augmenting stress, σ_A (T/in^2)	-	5.0	8.0	11.2	15.2
Effective extrusion ratio, R	3.97	4.01	4.14	4.33	4.60
ln R	1.38	1.39	1.42	1.465	1.525
Bulge Strain $\epsilon = \ln \frac{R}{R_o}$	-	0.0096	0.040	0.085	0.145
Total extrusion pressure ($\sigma_A + p_A$), (T/in^2)	36.3	39.5	41.2	42.2	43.7

TABLE 7b Billet augmented hydrostatic extrusion results

Material: Commercially pure copper annealed at 610° for 1 hr.

$2\alpha = 60^{\circ}$ = die angle

R_o = original extrusion ratio = 3.97

Product dia. = 0.313"

Hydrostatic fluid pressure p_A (T/in^2)	35.2	33.2	32.0	30	28
Augmenting load, F_A (Tonf)	-	2.45	3.03	4.55	5.85*
Dia. of residual billet, D (ins)	.624	.633	.640	.658	.684
Augmenting stress, σ_A (T/in^2)	-	7.8	9.4	13.4	16
Effective extrusion ratio, R	3.97	4.09	4.19	4.42	4.77
ln R	1.38	1.409	1.431	1.49	1.56
Bulge Strain $\}\epsilon = \ln \frac{R}{R_o}$	-	.029	.051	.109	.182
Total extrusion pressure ($\sigma_A + p_A$), (T/in^2)	35.1	41.0	41.4	43.4	44

* Unstable still increasing

TABLE 7c Billet augmented hydrostatic extrusion results

Material: Commercially pure copper annealed at 610° for 1 hr.

$2\alpha = 90^{\circ}$ = die angle

R_o = original extrusion ratio = 3.97

Product dia. = 0.313"

Hydrostatic fluid pressure p_A (T/in^2)	38.4	37.0	36.0	34.2	32.3
Augmenting load, F_A (Tonf)	-	1.065	2.29	4.53	5.74
Dia. of residual billet, D (ins)	.624	.624	.636	.656	.680
Augmenting stress, σ_A (T/in^2)	-	3.5	7.2	13.4	15.8
Effective extrusion ratio, R	3.97	3.97	4.13	4.39	4.73
ln R	1.38	1.38	1.42	1.48	1.554
Bulge Strain $\varepsilon = \ln \frac{R}{R_o}$	-	0	0.040	0.105	.174
Total extrusion pressure ($\sigma_A + p_A$), (T/in^2)	38.4	40.5	43.2	47.6	48.1

TABLE 8a Billet augmented hydrostatic extrusion results

Material: Mild Steel annealed at 900°C for 1 hr.

$2\alpha = 40^{\circ}$ = die angle

R_o = original extrusion ratio = 2.53

Product dia. = 0.313"

Hydrostatic fluid pressure p_A (T/in^2)	43.4	41.4	39.6	32.2	28.6
Augmenting load, F_A (Tonf)	-	2.34	2.81	4.52	7.06
Dia. of residual billet, D (ins)	.498	.498	.498	.506	.530
Augmenting stress, σ_A (T/in^2)	-	12.0	14.4	22.5	32
Effective extrusion ratio, R	2.53	2.53	2.53	2.61	2.87
ln R	.928	.928	.928	.960	1.055
Bulge Strain $\}\varepsilon = \ln \frac{R}{R_o}$	-	0	0	.032	.127
Total extrusion pressure ($\sigma_A + p_A$), (T/in^2)	43.4	53.4	54	54.7	60.6

TABLE 8b Billet augmented hydrostatic extrusion results

Material: Mild Steel annealed at 900°C for 1 hr.

$2\alpha = 60^{\circ}$ = die angle

R_o = original extrusion ratio = 2.52

Product dia. = 0.313"

Hydrostatic fluid pressure p_A (T/in^2)	43.5	40.6	38.4	35.0	32.0
Augmenting load, F_A (Tonf)	-	1.95	2.43	4.26	7.6*
Dia. of residual billet, D (ins)	-	.497	.497	.503	.533
Augmenting stress, σ_A (T/in^2)	-	10.0	12.5	21.5	34.1
Effective extrusion ratio, R	2.52	2.52	2.52	2.58	2.90
ln R	.925	.925	.925	.949	1.09
Bulge Strain $\}\varepsilon = \ln \frac{R}{R_o}$	-	0	0	.024	.140
Total extrusion pressure ($\sigma_A + p_A$), (T/in^2)	43.5	50.6	50.9	56.5	66.1

* Bulged and buckled still increasing

TABLE 8c Billet augmented hydrostatic extrusion results

Material: Mild Steel annealed at 900° for 1 hr.

$2\alpha = 90^{\circ}$ = die angle

R_o = original extrusion ratio = 2.52

Product dia. = 0.313"

Hydrostatic fluid pressure p_A (T/in^2)	51.8	42	40	37.5	35.0
Augmenting load, F_A (Tonf)	-	4.05	4.62	5.35	7.68*
Dia. of residual billet, D (ins)	.497	.502	.505	.512	.536
Augmenting stress, σ_A (T/in^2)	-	20.5	23.1	26.0	34.0
Effective extrusion ratio, R	2.52	2.375	2.615	2.675	2.93
ln R	.925	.945	.957	.985	1.078
Bulge Strain $\varepsilon = \ln \frac{R}{R_o}$	-	.02	.032	.06	.15
Total extrusion pressure ($\sigma_A + p_A$), (T/in^2)	51.8	62.5	63.1	63.5	69.0

* Still increasing

TABLE 9 Simple hydrostatic extrusion pressure for copper with R = 5.75

Extrusion pressure, T/in.^{2}	$2\alpha^o$
45.2	40
44.4	60
46.3	90

TABLE 10 Simple hydrostatic extrusion pressure for mild steel with R = 4.

Extrusion pressure, T/in.^{2}	$2\alpha^o$
62.2	40
69.5	60
72.4	90

TABLE 11 Coefficient of friction in simple and billet augmented hydrostatic extrusion of copper with R = 2.5

2α = 40°		2α = 60°		2α = 90°	
σ_A (T/in^2)	μ	σ_A (T/in^2)	μ	σ_A (T/in^2)	μ
0	0.0390	0	0.0390	0	0.0390
7.65	0.0922	3.55	0.1036	5.75	0.129
16.4	0.0910	4.8	0.0940	10.25	0.195
18.3	0.0910	6.3	0.1046	12.1	0.164
		15.5	0.113	15.2	0.159

μ_o = 0.0390 corresponding to $2\alpha_{opt}$ = 30°

$2\alpha = 40$		$2\alpha = 60$		$2\alpha = 90$	
σ_A (T/in^2)	μ	σ_A (T/in^2)	μ	σ_A (T/in^2)	μ
0	.067	0	.067	0	.067
5.0	.098	7.8	.142	3.5	.126
8.0	.100	9.4	.129	7.2	.143
11.2	.092	13.4	.124	13.4	.195
15.2	.091	16.0	.108	15.8	.160

TABLE 12

(Copper, R = 4)

$2\alpha = 40$		$2\alpha = 60$		$2\alpha = 90$	
σ_A (T/in^2)	μ	σ_A (T/in^2)	μ	σ_A (T/in^2)	μ
0	.078	0	.078	0	.078
12	.191	10	.190	20.5	.240
14.4	.198	12.5	.192	23.1	.220
22.5	.162	21.5	.219	26.0	.170
32	.135	34.2	.151	34	.135

TABLE 13

(Mild Steel, R = 2.5)

TABLE 14 Bulging limits for annealed copper billets

$2\alpha^{o}$	Bulging limit, T/in^2			
	$R_o = 2.5$		$R_o = 4$	
	Extrapolation method	Thompson's method	Extrapolation method	Thompson's method
40	15.4	16.0	15.2	16.0
60	15.4	16.2	15.4	16.5
90	15.6	16.0	15.1	16.2

TABLE 15 Bulging limits for annealed mild steel billets

$2\alpha^{o}$	Bulging limit, T/in^2	
	$R_o = 2.5$	
	Extrapolation method	Thompson's method
40	33.0	34.3
60	33.5	34.6
90	33.2	33.9

TABLE 16

Material: Aluminium

Diameter of Billet	Overall Extrusion Ratio, R	ln R	Extrusion Pressure, T/in^2	
			Simple Die	Double Reduction Die
.562	3.22	1.17	11.5	-
.625	3.99	1.385	14.2	15
.688	4.83	1.575	16.4	16.65
.715	5.2	1.65	17.1	17
.750	5.74	1.75	18.0	Leakage at 14 T/in^2
Fluid: (a) Castor Oil				
.562	3.22	1.17	11.6	-
.625	3.98	1.385	13.9	15.65
.688	4.83	1.575	16.4	16.75
.715	5.19	1.65	17.15	17.0
.750	5.74	1.75	18.25	Leakage at 10 T/in^2

(b) Shell Tellus 27 Oil

TABLE 17

Material: Copper

Diameter of Billet	Overall Extrusion Ratio, R	ln R	Extrusion Pressure, T/in^2	
			Simple Die	Double Reduction Die
.562	3.22	1.17	28.0	-
.625	3.99	1.385	33.8	37.7
.687	4.83	1.575	40.9	38.4
.715	5.20	1.65	42.2	39.6
.749	5.74	1.75	44	42.9
Fluid: (a) Castor Oil				
.562	3.22	1.17	28.5	-
.624	3.98	1.38	34.0	37.0
.687	4.83	1.575	40.5	40.8
.713	5.19	1.65	42.0	41.7
.750	5.74	1.75	43.5	42.8

(b) Shell Tellus 27 Oil

TABLE 18 Results of the double reduction die experiments with cast aluminium alloy

(a) Fluid: Tellus 27 oil

Diameter of Billet	Overall Extrusion Ratio, R	ln R	Extrusion pressure, T/in.^{2}	
			Simple Die	Double Reduction Die
0.624	3.97	1.384	51.5	52.0
0.687	4.82	1.573	53.8	55.0

(b) Fluid: Castor oil

Diameter of Billet	Overall Extrusion Ratio, R	ln R	Extrusion pressure, T/in.^{2}	
			Simple Die	Double Reduction Die
0.624	3.97	1.384	51.0	51.6
0.684	4.82	1.573	53.5	54.8